ENHANCED COGNITIVE RADIO WITH ENERGY HARVESTING AND NON-ORTHOGONAL MULTIPLE ACCESS

Sultangali Arzykulov

A thesis submitted in partial fulfillment of the requirement of Nazarbayev University for the degree of Doctor of Philosophy

April 2019

Declaration

I declare that the research contained in this thesis, unless otherwise formally indicated within the text, is the original work of the author. The thesis has not been previously submitted to this or any other university for a degree, and does not incorporate any material already submitted for a degree.

Signed:

Dated:

Abstract

The increasing demand for wireless applications is making radio spectrum scarce. Meantime, studies show that the assigned spectrum is not thoroughly utilized. The cognitive radio (CR) technology is proposed as a feasible key technology to solve issues related to the spectrum scarcity. CR can improve the spectrum utilization by reusing the unused spectrum occupied by licensed users. Introduction of CR networks produces two kinds of interference: interference from the CR network (secondary network) to the primary network (PN) and the interference among secondary users. All unwanted interference should be adequately managed in order not to jeopardize the performance of the PN and at the same time improve the performance of CR systems. Interference alignment (IA) is a promising technique that can efficiently manage interference. One of the aims of this thesis is to mitigate the interference by deploying multiple antennas at both transmitter and receiver sides in order to improve the performance of CR networks.

The rapid growth of data-hungry wireless applications is forcing us to perform energy harvesting (EH) from external power sources for the next-generation of wireless communication systems. Especially, CR networks, where receiver nodes need advanced hardware to process a large amount of data, require higher energy consumption. Thus, another goal of the current thesis is to investigate simultaneous wireless information and power transfer (SWIPT) in CR networks in the presence of intra- and inter-network interference over various channel state conditions.

Firstly, a cooperative CR network is investigated over the general $\alpha-\mu$ fading channel. The contribution of this study is mainly described by the exact closed-form expression for the outage probability (OP) of secondary users, which clearly shows how the outage saturation paradigm appears when the interference level at primary receiver is applied.

Secondly, the proposed cooperative CR is extended by applying multiple-input multiple out (MIMO) antennas and an IA technique to deal with intra- and inter-network interference. The negative effect of interference at both primary and secondary receivers is mitigated by using precoding and interference suppression beamforming matrices. The management of interference at primary receivers allows secondary transmitters to increase the transmit power level. Moreover, the instantaneous capacity performance is assessed for the same CR system by applying two EH methods, i.e., time-switching (TS) and power-splitting (PS). Then, the optimal values of TS and PS portions are determined for different channel state information (CSI) scenarios. In addition, the effect of imperfect CSI on bit error rate and capacity performance is provided.

Finally, we jointly study a cooperative CR and non-orthogonal multiple access (NOMA), where we derive closed-form expressions for the OP of NOMA secondary destination users for detect-and-forward and amplify-and-forward relaying techniques. Furthermore, power allocation factors for different distances of secondary NOMA users are found to satisfy OP fairness for all users. In addition, the proposed CR-NOMA network model is further studied with enabled SWIPT technology.

Acknowledgments

First and above all, I thank the Almighty for giving me the strength and patience to work through all these years.

My greatest appreciations go to my supervisor - Professor Theodoros A. TSIFTSIS. Thank him for introducing me into the research realm of wireless communications, the patient guidance, encouragement and advice he has provided throughout my Ph.D. study. He has taught me the methodology to carry out the research and to present the research works as clearly as possible. It was a great privilege and honor to work and study under his guidance.

My heartfelt thanks also go to my supervisor - Associate Professor Behrouz MAHAM, co-supervisor - Assistant Professor Refik C. KIZILIRMAK and external supervisor - Assistant Professor Mohamed M. ABDALLAH who cared about my work so much and responded to my questions and queries so promptly. I feel extremely lucky to have them as supervisors.

I want to express my deep gratitude to Assistant Professor Galymzhan NAURYZBAYEV for all his help from the beginning of my studies, for generously giving his time to offer me valuable comments toward improving my work and for being a good friend.

I would also like to take this opportunity to thank Professor Mohamed-Slim ALOUINI and Associate Professor Mohammad S. HASHMI - my viva examiners, for their very helpful comments and suggestions.

I am also very grateful to Professor Mohammad S. OBAIDAT, who has given me valuable support and who had a word of encouragement during my Ph.D. studies.

Some special words of gratitude go to Director of Ph.D. Studies Associate Professor Luis R. Rojas-SOLÓRZANO for his suggestions throughout my research and dealing with the bureaucracies of doing a Ph.D.

I would like to thank all my Ph.D. colleagues, with whom I have shared moments of deep anxiety but also of big excitement. Their presence was very important in a process that is often felt as tremendously solitaire. I would also like to thank all my friends for accepting nothing less than excellence from me.

I am extremely grateful to my parents for their love, prayers, caring and sacrifices for educating and preparing me for my future. I am very much thankful to my wife and my sons for their love, understanding and continuing support to complete this research work. Also, I express my thanks to my sisters and brothers for their support and valuable prayers. To you, I owe the deepest and most sincere thanks.

Finally, my thanks go to all the people who have supported me to complete the research work directly or indirectly.

Sultangali ARZYKULOV

Preface

Mr. Sultangali ARZYKULOV received the B.Sc. (Hons.) degree in radio engineering, electronics and telecommunications from Kazakh National Technical University named after K. I. Satpayev, Almaty, Kazakhstan, in June 2010. He received M.Sc. degree in communication engineering from the University of Manchester in September 2013. From 2010 to 2011, he worked as a network engineer in JSC "Kazakhtelecom", and then as a teaching assistant at Nazarbayev University from 2014 to 2018. Since September 2015, he has been pursuing his Ph.D. degree in Science, Engineering and Technology with a research focus on cognitive radio, multi-user MIMO systems, interference mitigation, wireless energy harvesting, non-orthogonal multiple access and millimeter wave communications

Main Supervisors

The topic of the current thesis was proposed by Prof. Theodoros A. TSIFTSIS, who was the main supervisor from September 2015 to March 2018. He left Nazarbayev University in March 2018 and his position as the main supervisor was taken by Dr. Behrouz MAHAM who was also in the initial team of the Ph.D. supervisory committee. This change was made for typical reasons due to the Ph.D. Program regulations of Nazarbayev University.

Contents

List of Figures

List of Tables

List of Abbreviations

1G	First Generation
3GPP	Third Generation Partnership Project
4G	Fourth Generation
5G	Fifth Generation
AF	Amplify-and-Forward
AWGN	Additive White Gaussian Noise
BF	Beamforming
BPSK	Binary Phase Shift Keying
CDF	Cumulative Distribution Function
CDMA	Code Division Multiple Access
CF	Compress-and-Forward
CR	Cognitive Radio
CRN	Cognitive Relaying Network
CSI	Channel State Information
DF	Decode-and-Forward
DoF	Degrees of Freedom
DSA	Dynamic Spectrum Access
EH	Energy Harvesting
FCC	Federal Communications Commission
FDMA	Frequency-Division Multiple Access
i.i.d.	Independent and Identically Distributed
i.n.i.d.	Independent But Not Necessarily Identically Distributed
IA	Interference Alignment
ID	Information Decoding
IoT	Internet of Things
IT	Information Transfer
ITC	Interference Temperature Constraint
LDS	Low Density Spreading
LPMA	Lattice Partition Multiple Access
LTE	Long Term Evolution
MA	Multiple Access
MGF	Moment Generating Function

MIMO	Multiple-Input Multiple-Output
MPA	Message Passing Algorithm
MUST	Multiple User Superposition Transmission
NOMA	Non-Orthogonal Multiple Access
Ofcom	Office of Communications
OFDMA	Orthogonal Frequency Division Multiple Access
OMA	Orthogonal Multiple Access
OF	Outage Fairness
OP	Outage Probability
PA	Power Allocation
PDF	Probability Density Function
PDMA	Pattern Division Multiple Access
PN	Primary Network
PS	Power-Splitting
PSR	Power-Splitting Relaying
PU	Primary User
QoS	Quality of Service
RF	Radio Frequency
RV	Random Variable
SCMA	Sparse Code Multiple Access
SER	Symbol Error Rate
SIC	Successive Interference Cancellation
SINR	Signal-to-Interference-plus-Noise Ratio
SN	Secondary Network
SNR	Signal-to-Noise Ratio
SR	Selective Relaying
SU	Secondary User
SWIPT	Simultaneous Wireless Information and Power Transfer
TDMA	Time-Division Multiple Access
TS	Time-Switching
TSR	Time-Switching Relaying
WBAN	Wireless Body Area Network
WEH	Wireless Energy Harvesting
WiFi	Wireless Fidelity
WiMax	Worldwide Interoperability for Microwave Access
WPT	Wireless Power Transfer

List of Symbols

$(\cdot)^{[\iota]}$	Time slot index
$(\cdot)^{\dagger}$	Hermitian transpose of a matrix
$\mathcal{CN}(a,b)$	Complex normal distribution with a mean and b variance
$f_X(x)$	Probability density function of random variable X
$F_X(x)$	Cumulative distribution function of random variable X
$\Gamma(\cdot)$	Gamma function
$\Gamma(a,b)$	Upper incomplete gamma function
$\gamma_{\text{inc}}(a,b)$	Lower incomplete gamma function
$\mathbb{E}(\cdot)$	Statistical expectation operator
h_{ji}	Channel gain between nodes j and i
$P_{(\cdot)}$	Transmit power at the secondary transmitter
$\bar{P}_{(\cdot)}$	Maximum allowed transmit power at the secondary transmitter
I	Interference temperature constraint
σ^2	Noise power at the receive node
ξ	Predefined SNR threshold
$K_1(\cdot)$	Modified Bessel function of the second kind of order 1
$\mathcal{R}_{\text{th}}$	Predefined rate threshold
$\min(a,b)$	Function that finds minimum between a and b
$\mathcal{M}_{\gamma}(-g)$	Moment generating function
$\mathbf{x}$	Lower bold case denotes vector
$\mathbf{X}$	Upper bold case denotes matrix
$\mathbf{H}$	MIMO channel
$\mathbf{I}$	Identity matrix
$\text{tr}(\mathbf{X})$	Trace of a matrix
$\lvert x\rvert$	Absolute value of x
$\lVert\mathbf{x}\rVert$	Euclidean norm of $\mathbf{x}$
$\mathbb{V}(\cdot)$	Variance operator
$\mathbb{C}^{N\times M}$	Space of complex $N \times M$ matrices
$\text{span}(\mathbf{X})$	Vector space spanned by the column vectors
$\text{eig}\,(\mathbf{X})$	Eigenvectors of $\mathbf{X}$
$d_{m,n}$	Distance between nodes m and n

τ	Path-loss coefficient
$\mathbf{V}$	Precoding BF matrix
$\mathbf{U}$	Interference suppression matrix
f	Number of data streams
T_j	Primary transmitter j
n	AWGN noise
ρ	Nominal transmit SNR
α	Time fraction of the TS
θ	Power fraction of the PS
$Q(x)$	Gaussian-Q function
$\alpha_{(\cdot)}$	NOMA power allocation factor at the source
$\beta_{(\cdot)}$	NOMA power allocation factor at the relay
D	Secondary Destination
G	Amplification factor at the relay
PR	Primary receiver
S	Secondary Source
R	Secondary Relay

DEDICATED WITH EXTREME AFFECTION AND GRATITUDE TO

my parents Mr. Ussenbatyr ARZYKULOV and Mrs. Zhantore ARZYKULOVA
my brothers NURZHAN and RAKHYMZHAN
my sisters NURGUL, MARZHAN and YERKEZHAN
my wife DINARA and my sons
DAMIR and ARSEN

Chapter 1

Introduction

1.1 Modern Wireless Systems

Wireless communication is the technology that has certainly changed the lives of human beings. Nowadays, many applications establish their broadcasting using wireless communication concept. The range of those applications varies from highly commercialized satellite and mobile communication networks to amateur radio communications, from regularly practiced Wi-Fi systems to rarely used deep-space networks, from fully infrastructure-based radio/television networks to non-infrastructure ad-hoc systems. The number of wireless applications will be increased dramatically in the future due to the high demand for the wireless medium.

1.2 Motivation

The radio frequency (RF) spectrum, an irreplaceable carrier underlying the wireless communication system, is conditionally assigned to a particular wireless application for independent use by regulatory authorities, such as the Federal Communications Commission (FCC) in the United States, the Office of Communications (Ofcom) in the UK and Ministry of Information and Communication of the Republic of Kazakhstan. Nowadays, the radio spectrum is becoming increasingly scarce due to the fact that more and more devices become wireless and occupy more RF spectrum. Meantime, studies show that some spectrum bands are left without being fully utilized [1]. The research works on the measurement of spectrum usage showed that up to 85% of the spectrum in some frequency bands below 3 GHz are not utilized [3]. The imbalance between the likely spectrum deficit and possible inadequate spectrum utilization inspired the innovative paradigm shift in access to the spectrum by permitting dynamic spectrum sharing and reuse, which is called as dynamic spectrum access (DSA) [4]. The most prominent candidate technology for the DSA is Cognitive Radio (CR), which is able to sense the environment and adapt its operating parameters dynamically. Hence, CR can coexist with existing systems (primary

systems) autonomously in a non-intrusive fashion [1]. Doing so, CR is a promising technology that can significantly improve the spectrum usage by reusing the spectrum that belongs to primary systems [5].

One of the major impairments in wireless communications is interference, which appears due to the broadcast and superposition nature of wireless medium. In the meaning of CR systems, interference problems are an extremely serious issue due to the following two main aspects. On the one hand, CR adheres to the fundamental premise of not creating any harmful interference to the primary system. On the other hand, the efficiency of CR can be limited by interference coming from either primary or other secondary CR nodes (secondary users). Hence, the problems associated with interference in CR networks deserve a thorough and extensive study, which is one of the main focuses of the thesis.

The eventual fate of mobile communication is expected to be completely different from what we experience today. Ultra top-notch videos and better wide-screen resolutions in mobile devices are forcing us either to look for better sustainable power sources or to perform energy harvesting (EH) from external power sources for the next-generation of wireless communication systems. Especially, CR networks, where receiver nodes need advanced hardware to process a large amount of information data, require higher energy consumption. Thus, another focus of the thesis is to investigate EH in CR networks in the presence of intra- and inter-network interference.

The fast increase in the demand for the mobile Internet has propelled 1000-fold data traffic boost by 2020 for the fifth generation (5G) mobile communication networks. In addition, 5G networks need to maintain massive connectivity of devices to meet the requirement for low-cost devices, low latency, and various service types due to the rapid development of the Internet of Things (IoT). Henceforth, such explosive data traffic delivers even more key challenges to efficiently handle the wireless spectrum. So far, non-orthogonal multiple access (NOMA) has been proposed as a potential candidate technology for 5G [6], which not only efficiently utilize the wireless spectrum as CR but also expected to increase the system throughput and support massive connectivity. Therefore, to further improve the performance of 5G networks, the application of NOMA to CR networks seems to be very crucial. Therefore, one more aim of the thesis is to examine a synergy between these two advanced communication techniques considering embedded EH techniques in the presence of interference.

1.3 Key Contributions

The main contributions of the current thesis are briefly summarized as follows:

- We model a cooperative underlay CR system where a primary receiver applies interference temperature model to secondary transmit nodes. The end-to-end closed-form expressions for the outage performance of secondary users are provided over the generalized $\alpha-\mu$ fading distribution, which includes various other distributions, i.e., Rayleigh, Gamma, Exponential, Nakagami-m, etc. The impact of interference temperature on the outage performance and symbol error rate of the secondary network is investigated.

- Further, the proposed cooperative underlay CR is studied by applying multiple antennas and interference managing techniques to deal with intra- and inter-network interference. We apply precoding and interference suppression beamforming matrices to mitigate the negative effect of interference at primary and secondary receivers. The management of interference at primary receivers allows secondary transmitters to increase the transmit power level. Closed-form expressions for the outage performance of primary and secondary networks are determined.

- The performance of CR relaying networks is investigated by applying EH at the secondary relay node. EH methods are studied under imperfect channel conditions. Moreover, the instantaneous capacity performance is assessed for both methods. In addition, some useful insights into how the channel state information quality impacts on capacity performance are also provided.

- The synergy of cooperative underlay CR and NOMA is studied in terms of the outage performance of NOMA users by applying relaying protocols over Rayleigh and Nakagami-m fading channels. We find power allocation factors for NOMA secondary users to guarantee outage fairness among NOMA users. Moreover, considering the effect of the imperfect CSI on the outage performance, we derive a general closed-form solution for the outage probability when the number of secondary NOMA nodes is extended to K users. Finally, EH-enabled CR-NOMA is investigated in terms of the outage and EH performance.

1.4 List of Publications

The work presented in this thesis has led to the following publications:

Published and Accepted Papers

Journal Papers

- S. Arzykulov, G. Nauryzbayev, T. A. Tsiftsis, and M. Abdallah, "On the Performance of Wireless Powered Cognitive Relay Network with Interference Alignment," *IEEE Transactions on Communications*, vol. 66, no. 9, pp. 3825-3836, September 2018.

- S. Arzykulov, T. A. Tsiftsis, G. Nauryzbayev, and M. Abdallah, "Outage Performance of Cooperative Underlay CR-NOMA with Imperfect CSI," *IEEE Communications Letters*, vol. 23, no. 1, pp. 176-179, January 2019.

- S. Arzykulov, G. Nauryzbayev, and T. A. Tsiftsis, "Underlay Cognitive Relaying System over $\alpha - \mu$ Fading Channels," *IEEE Communications Letters*, vol. 21, no. 1, pp. 216-219, January 2017.

Conference Papers

- S. Arzykulov, T.A. Tsiftsis, G. Nauryzbayev, and M. Abdallah, "Outage Performance of Underlay CR-NOMA Networks with Detect-and-Forward Relaying," *2018 IEEE Global Communications Conference (GLOBECOM)*, Abu Dhabi, United Arab Emirates, 2018, pp. 1-6.

- S. Arzykulov, G. Nauryzbayev, T.A. Tsiftsis, and M. Abdallah, "On the Capacity of Wireless Powered Cognitive Relay Network with Interference Alignment," *GLOBECOM 2017 - 2017 IEEE Global Communications Conference*, Singapore, 2017, pp. 1-6.

- S. Arzykulov, G. Nauryzbayev, T.A. Tsiftsis, and M. Abdallah, "On the BER performance of Wireless Powered Cognitive Relay Network with Interference Alignment," in *2017 IEEE 28th Annual International Symposium on Personal, Indoor, and Mobile Radio Communications (PIMRC)*, Montreal, QC, 2017, pp. 1-5.

- S. Arzykulov, T.A. Tsiftsis, G. Nauryzbayev, and M. Abdallah, "Outage Performance of Underlay CR-NOMA Networks," *2018 10th International Conference on Wireless Communications and Signal Processing (WCSP)*, Hangzhou, 2018, pp. 1-6.

- G. Nauryzbayev, S. Arzykulov, T.A. Tsiftsis, and M. Abdallah, "Performance of Cooperative Underlay CR-NOMA Networks over Nakagami-m Channels," *2018 IEEE International Conference on Communications Workshops (ICC Workshops)*, Kansas City, MO, 2018, pp. 1-6.

- G. Nauryzbayev, S. Arzykulov, E. Alsusa, and T. A. Tsiftsis, "An Alignment-based Interference Cancellation Scheme for Network-MIMO Systems," *2016 10th International Conference on Signal Processing and Communication Systems (ICSPCS)*, Gold Coast, QLD, 2016, pp. 1-5.

- G. Nauryzbayev, S. Arzykulov, E. Alsusa, and T. A. Tsiftsis, "A Closed-form Solution to Implement Interference Alignment and Cancellation Scheme for the MIMO Three-user X-channel Model," *2016 10th International Conference on Signal Processing and Communication Systems (ICSPCS)*, Gold Coast, QLD, 2016, pp. 1-6.

Submitted Papers

Journal Papers

- S. Arzykulov, G. Nauryzbayev, T. A. Tsiftsis, B. Maham, and M. Abdallah, "On the Outage Performance of Relaying CR-NOMA," *IEEE Transactions on Cognitive Communications and Networking*, April 2019.

- S. Arzykulov, G. Nauryzbayev, T. A. Tsiftsis, and B. Maham, "Outage of AF-based Underlay CR-NOMA Networks," *IEEE Transactions on Vehicular Technology*, January 2019.

- S. Arzykulov, G. Nauryzbayev, T. A. Tsiftsis, and B. Maham, "New Results on the Outage for CR-NOMA Relaying Systems," *IEEE Access*, March 2019.

Conference Papers

- S. Arzykulov, G. Nauryzbayev, T.A. Tsiftsis, B. Maham, and K. M. Rabie, "Wireless Powered Cognitive Relay Networks: Outage Analysis," *IEEE International Symposium on Personal, Indoor and Mobile Radio Communications*, Istanbul, Turkey, September 2019.

- G. Nauryzbayev, S. Arzykulov, and K. M. Rabie, "Underlay CR-NOMA Relaying Networks over Generalized Fading Channels," *IEEE Global Communications Conference (Globecom)*, Waikoloa, HI, USA, December 2019.

- N. Miridakis, S. Arzykulov, T. A. Tsiftsis, G. Yang, and G. Nauryzbayev, "Green CR-NOMA: A New Interweave Energy Harvesting Transmission Scheme for Secondary Access," *16th International Symposium on Wireless Communication Systems*, Oulu, Finland, August 2019.

- A. U. Makarfi, K. M. Rabie, R. Kharel, O. S. Badarneh, G. Nauryzbayev, X. Li, S. Arzykulov, and O. Kaiwartya, "Performance Analysis of SWIPT Networks over Composite Fading Channels," *IEEE Global Communications Conference (Globecom)*, Waikoloa, HI, USA, December 2019.

1.5 Thesis Organization

The thesis consists of seven chapters. Chapter 1 is the introduction, which provides an overview of the research, motivations and contributions. The following chapters are organized as the next.

Chapter 2 presents a literature review on the relevant background for the research work presented in this thesis. We first provide an introduction to the concepts of the CR with its main three paradigms. Then, some review on using multiple antennas in CR networks are provided. Moreover, different types of interference involved in CR networks are analyzed, and an interference managing technique named interference alignment is proposed as a novel approach to deal with interference. In the end, we review works where the improvement in the performance of the CR networks by applying wireless energy harvesting and NOMA techniques is shown.

Chapter 3 starts with some introduction of relaying networks in the CR systems. Then, a system model of a dual-hop CR with interference temperature constraints at a primary receiver is presented. The end-to-end outage probability (OP) for the secondary network is derived for Rayleigh and general $\alpha - \mu$ fading channels. Moreover, evaluation of the symbol error rate is derived for the proposed system model. Furthermore, in the numerical part, the correctness of the derived analytical results are validated through extensive Monte Carlo simulations.

In Chapter 4, we investigate a dual-hop decode-and-forward wireless powered cognitive relaying network with interference alignment over Rayleigh fading channels. We assume a secondary relay node to be energy-constrained which needs to harvest energy from both information and interference signals. By applying beamforming matrices to primary and secondary networks, the performance metrics such as the OP, capacity and bit error rate are studied under perfect and imperfect channel state information scenarios for both power-splitting relaying and time-switching relaying protocols. Moreover, the Chapter studies the optimal network performance by calculating the optimal energy harvesting time-switching and power-splitting coefficients. Finally, closed-form expressions for the OP of primary and secondary users are derived which are validated through Monte Carlo simulations.

Chapter 5 focuses on a downlink dual-hop CR-NOMA model with an imposed interference constraint at the primary receiver. The chapter considers several different

scenarios for the proposed system model. First, it proposes a system model with two NOMA secondary destination users, where only one secondary transmit node is limited by maximum transmit power. We derive the OP for the considered system model applying decode-and-forward (DF) and amplify-and-forward (AF) relaying methods over Rayleigh and Nakagami-m fading channels. Then, by considering the effect of imperfect CSI on the system performance, we derive a general closed-form solution for the OP when the number of secondary NOMA users is extended to K users. In addition, the OP for the scenario where both source and relay are restricted by the maximum transmit power is studied. Furthermore, in order to obtain fairness between NOMA users, the power allocation factors are optimized depending on the distance between secondary users. Finally, the obtained OP performance for cooperative NOMA compared to that for conventional cooperative OMA to show the supremacy of the former.

Chapter 6 studies the OP of the dual-hop underlay CR network consisted of a secondary relay node with energy harvesting and two NOMA secondary destination users. Moreover, the optimal power allocation factors are found for different distances of NOMA users in order to satisfy OP fairness for both secondary destination users. Additionally, the proposed CR-NOMA is compared with conventional CR multiple access in terms of the OP.

Finally, Chapter 7 concludes the thesis and discusses related future works.

Chapter 2

Literature Review

2.1 Radio Spectrum

In recent years, wireless communication networks have obtained significant popularity due to its convenient untethered connectivity and mobile access. However, the radio spectrum in wireless communication networks is a naturally limited resource. Traditionally, spectrum regulators adopt the fixed spectrum access technique in order to support various wireless services and applications, where each spectrum band is assigned to one or several dedicated users. As a result of doing this, only the delegated, a.k.a. licensed, users get access to communicate over the allotted spectrum band, while other unlicensed users do not have rights to use that spectrum, even if the spectrum is not used by licensed users. The recent fast-growing demand on wireless communications systems has resulted in the fact that most of the available spectrum bands have fully been occupied, which leads to the spectrum scarcity issue. Moreover, the increase of the different wireless services, i.e., voice, web, multimedia, etc., has triggered the overcrowding of spectrum usage, which has consequently brought forth the low quality of service (QoS) for wireless network users [5]. Fig. 2.1 shows the radio spectrum allocation in the USA, where it illustrates that the radio spectrum has been entirely reserved by different wireless applications. From the figure, one can judge that the spectrum is too limited to support additional wireless applications. However, due to the high demand for wireless communications, the spectrum needs to be further utilized by newly emerging wireless networks. For example, over the last three decades, the need for extra bandwidth (radio spectrum) of cellular communication systems has increased exponentially while evolving from the voice-oriented first generation (1G) to the multimedia-rich fourth generation (4G). Despite the widely observed spectrum deficiency, spectrum measures reveal a surprising fact on the spectrum utilization. Thus, the recent studies have affirmed that some licensed spectrum bands, namely, amateur radio, television bands, etc., are mostly not been utilized leaving large spectral holes [7, 8] due to the fixed spectrum allocation and the independent usage of the spectrum band. Hence, more dynamic and flexible spectrum utilization methods are required to avoid the scarce problem in the wireless networks.

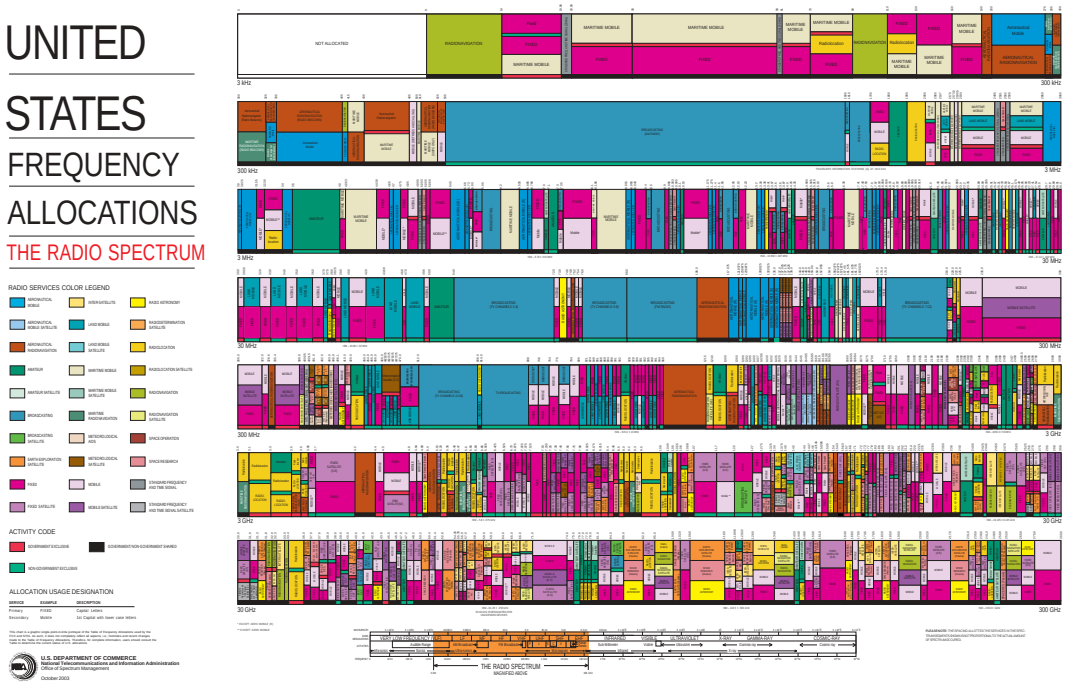

Figure 2.1. The radio spectrum allocations in the USA [1].

2.2 Cognitive Radio Technology

Recently, the FCC has offered CR networks as a feasible key technology to solve the issue related to spectrum scarcity. The concept of CR was first proposed in 1999 by Joseph Mitola III [9, 10]. Cognition implies that the radio learns from its environment and modifies its operating parameters based on the gained information. Hence, the CR concept lies in allowing permission to unlicensed users, named as secondary users (SUs), to broadcast in a licensed spectrum only if licensed users, named primary users (PUs), are not affected by the harmful interference coming from SUs [5]. In point of fact, there are specific policies for unlicensed users to opportunistically utilize the unoccupied licensed spectrum bands developed by the FCC [11]. Fig. 2.2 illustrates an example of the CR network, where PUs coexist with SUs. A secondary network base station coordinates SUs to be in the keep-out radius of the PUs. Thus, the SUs are urged not to use the licensed channel to keep their interference caused to PUs at a tolerable level [4].

CR quickly gained importance in research areas, as it provides more intelligent and optimized networks. The CR cycle is presented in Fig. 2.3, where it summarizes the main stages of the CR process. The cognitive cycle provides intellectual adaptation through learning and information exchange between various objects in the network. The CR cycle consists of six basic elements:

- **Environment:** It involves any object in the surrounding environment that might

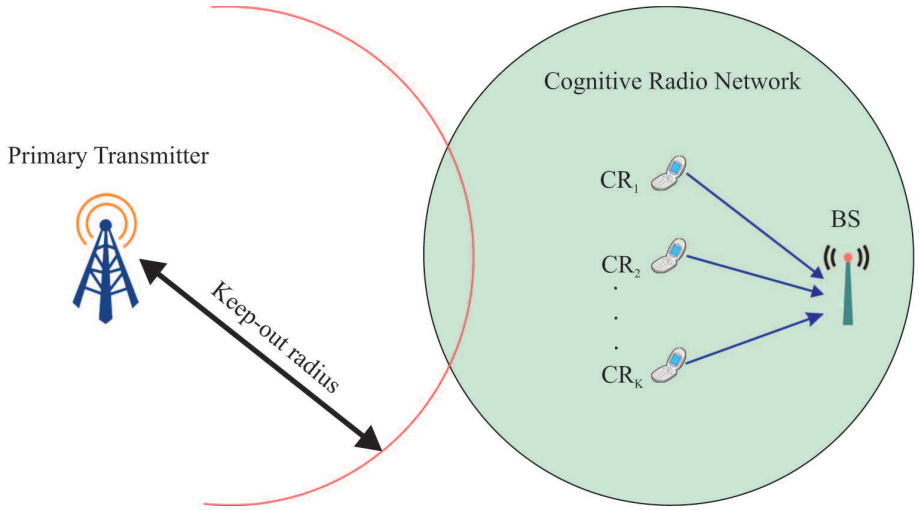

Figure 2.2. Cognitive radio network.

change the network condition, e.g., physical channels, neighbor users, obstacles, different climate conditions, etc.

- **Sense:** Various CR objects are intelligent to sense and monitor the spectrum bands, physically distributed channel parameters, levels of interference, and position of SUs and PUs.
- **Plan:** CR first makes a plan and assesses this plan before decisions are made.
- **Decide:** Decision is knowledge- and learning-based, where the decision-making process optimizes the resources of the system.
- **Act**: Depending on the decisions made, the SUs will act on the environment-based, which can be within a series of operations, e.g., the media access, packets routing, resource allocations and transmission scheme modifications.
- **Learn:** Learning is considered to be a prime part in the CR cycle. During this process, CR devices monitor all information related to network conditions and the environment using an obtained knowledge and a learning tool. Doing so, the system can learn from current and prior operations, expect future behavior and use all the obtained knowledge to intelligently plan and make a decision.

2.2.1 Cognitive Radio Paradigms

There are main three CR paradigms such as interweave, underlay, and overlay [5, 12]. The interweave is the simplest paradigm, however, it was originally what motivated the initiation of CR. In the interweave CR (See Fig. 2.4a), the SUs can opportunistically

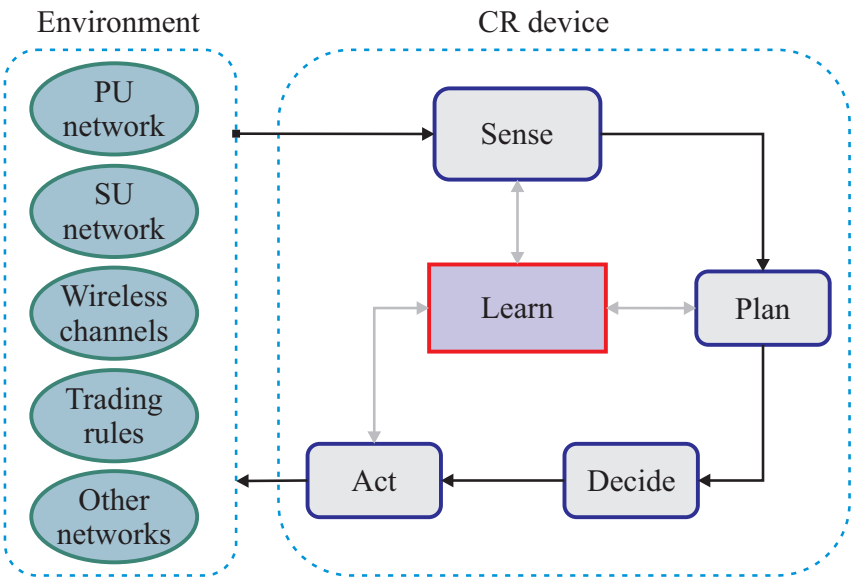

Figure 2.3. The Cognitive radio cycle.

access free primary network (PN) channels by detecting spectrum holes (unoccupied frequency bands). Hence, the SUs do not have to co-exist with the PUs. Not similar to the interweave, in underlay CR as shown in Fig. 2.4b, the SUs can simultaneously start their broadcasting along with the PUs by conditioning that the SUs should not cause harmful interference to primary receiver nodes [13]. Therefore, the SUs will be able to broadcast across PN frequency bands with restricted maximum transmit power in order to not exceed the primary receivers' noise floor. Hence, the underlay approach does not need to sense the spectrum to get access to transmission, which is the main benefit of this paradigm. Yet, the SUs are required to reduce their transmit power in order to not disturb the PN, which can force the SN to use short-distance communications. The overlay CR paradigm, similar to the underlay approach, can coexist with the PUs. But, the SUs need to assist to the PUs and should have entire information about signals of PUs (i.e., the message and codebook). Thus, the SUs can coexist with the PUs by not being restricted with the maximum transmit power level. As it is assumed that CR has information about the message and the codebook of the PUs, the SUs can use this knowledge to eliminate the interference from the PUs by applying methods such as dirty paper coding. In addition, the SUs assist to transfer the primary transmitter messages to the dedicated PN destinations, which helps to compensate for the interference caused to the PUs [5]. The main disadvantage of the overlay approach is that the SUs need to have full knowledge of the PU signal and to obtain that may be impractical since it is necessary to use the considerable coordination between multiple PUs and SUs.

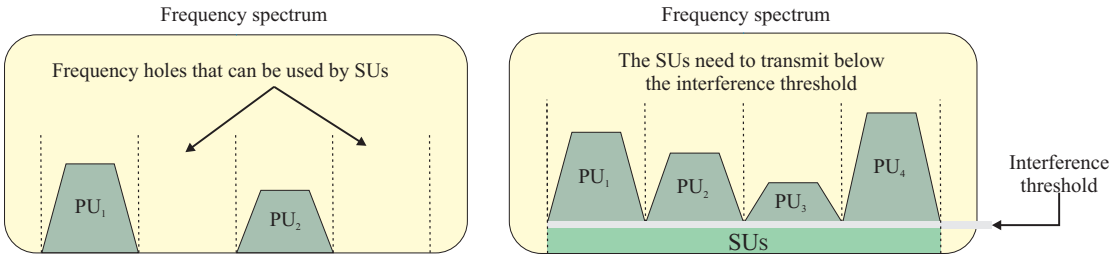

(a) Interweave. **(b)** Underlay.

Figure 2.4. Cognitive radio paradigms.

2.2.2 Multiple Input Multiple Output (MIMO)

Wireless channel is a complex and time-varying medium, which causes challenges to propagated signals. The signal transmitted through the wireless channel reaches the receiving node through a number of different paths (multipath). The multipath is the result of scattering and reflection of radiated energy from objects, e.g., trees, hills, buildings, etc. Each path has a different signal amplitude, an angle of arrival and a time-varying path delay. As a result, multipath propagation can cause destructive interference and deteriorate the wireless channel link quality, which leads to low level received signal amplitude. In digital communication systems, such as the wireless Internet, this can lead to a decrease in the data transfer rate and an increase in the number of errors. As a solution for this issue, the pioneering works in [14] and [15] showed that deploying multiple antennas together with the transmission of several signals at the source and destination can eliminate the issue induced by the multipath propagation, and can even take advantage of this effect. Hence, by employing multiple-input multiple-output (MIMO) antennas, the spectral efficiency in wireless communication networks can be increased linearly with the number of antennas. Thus, MIMO is recognized as an important technical invention, which can serve as a promising solution for the ever-increasing demand for high data rates in future wireless communications.

MIMO system provides the main two performance gains such as the *spatial diversity gain* and the *spatial multiplexing gain* [16]. Broadcasting and/or receiving replicated data symbols over various antennas cause space diversity, which helps to reduce the possibility of a transmission failure due to the fact that some symbol replica may experience deep fades, whereas others may not. Moreover, it has been admittedly proven that the ergodic channel capacity of a spatial multiplexing MIMO system increases linearly with the number of independent parallel spatial channels supported by the MIMO system, which is known as the *degrees of freedom* (DoF) [15]. Given its potential, MIMO has been adopted in next-generation WiFi, WiMax, *Long Term Evolution* (LTE), 4G and other cellular network standards.

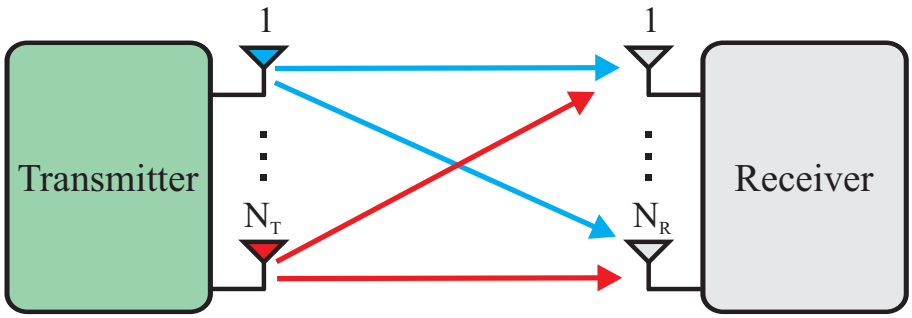

Figure 2.5. The MIMO network with N_T transmit and N_R receive antennas.

Multi-antennas can be utilized to achieve many desirable functions for wireless transmissions, such as folded capacity increase without bandwidth expansion [15, 17, 18], a dramatic enhancement of transmission reliability via space-time coding [19], and effective co-channel interference suppression for multiuser transmissions [20]. All these benefits of MIMO techniques can be also applied to CR networks to further improve the performance of PNs and SNs [21]. Generally speaking, multi-antennas can be used to allocate transmit dimensions in space and hence provide the secondary transmitter in a CR network more DoF in space in addition to time and frequency so as to balance between maximizing its own transmit rate and minimizing the interference powers at the primary receivers.

2.2.3 Interference in Cognitive Radio Networks

Interference connected to CR systems can be divided into mainly two types, namely, intra-network interference and inter-network interference. When users within one network (either the PN or SN) cause self-interference to each other, it is considered as intra-network interference. Two types of intra-network interference are considered in CR systems: interference within PNs and SNs. However, when the mutual interference between the primary and secondary networks exists, it is considered as inter-network interference. The management of inter-network interference is more difficult as CR transmitters must strictly control their transmitted signals to assure that the PN's QoS is guaranteed. In addition to that, CR receivers need to efficiently manage the interference coming from the PN, thus, providing a valuable QoS for the receivers of the SN.

The interference caused by the SN to the PN is very crucial and needs to be at a tolerable level due to the CR principle. As a solution to this, a new interference metric has been proposed named interference temperature model [22]. Traditional interference controlling methods use mainly transmitter-centric approach, while the interference temperature model applies interference temperature limits and practices receiver-centric approach to handling interference at primary receivers. The interference temperature limit indicates

the maximum amount of tolerable interference at primary receivers. Therefore, if that interference limit is acceptable, SN users can get access to utilize the primary spectrum.

By introducing MIMO in CR networks, interference in the network becomes denser due to several replicas of the same transmitted signal, which makes the issue of interference in CR networks more challenging.

2.3 Interference Alignment

Traditionally, interference is handled by methods where each user is provided with a certain portion of wireless resources, i.e., time-division multiple access (TDMA) and frequency-division multiple access (FDMA) [23]. These traditional approaches use interference managing techniques, i.e., orthogonalization, which characterizes interference as a background noise and interference decoding [24], which mitigates unwanted interference.

For instance, in TDMA, each user utilizes the whole available frequency band in certain allocated time slots. In the case of FDMA, each user communicates over various portions of a frequency band depending on the users' priority. These methods allow users to utilize part of wireless resources without interference which makes these techniques achieve lower capacity performance compare to that of interference networks. All of these traditional methods are rather suboptimal for general multi-source networks. Recently, a new interference managing technique named interference alignment (IA) has been proposed by Cadambe and Jafar in [25]. IA is a linear precoding technique that attempts to align interfering signals in time, frequency, or space. The key idea is that users coordinate their transmissions, using linear precoding, such that the interference signal lies in a reduced dimensional subspace at each receiver. In MIMO networks, IA uses the spatial dimension offered by multiple antennas for alignment. Hence, IA is considered to be an emerging technique in the interference management, the basic concept of which is to remove interference at a receiver's end in order to achieve effective capacity at the high SNR [26, 27]. Moreover, IA technique can design the transmit policies such that the interference can be aligned at all receivers. For instance, for N user pairs, the IA technique achieves a sum throughput on the order of $\frac{N}{2}$ interference free links [23, 28]. In other words, each user in the network can effectively get half the system capacity.

Mainly three types of IA have been studied in the literature, which can be attained in frequency, time or space dimensions [29, 30]. The most popular among them is the space dimensional IA technique, which applicable with MIMO antennas [31]. The fundamental idea of MIMO IA lies on eliminating all interference in the detection through the proper allocation of both the signal and interference into orthogonal subspaces. In the IA network, each node should be equipped with a sufficient number of antennas in order to

perfectly remove all interference [32]. Hence, the required number of antennas at every node to make the issue of IA solvable is calculated by a feasibility condition [33]. IA has found its wide use in different types of wireless network topologies by being an excellent technique in eliminating interference [29]. The idea of IA has been successfully applied to different network models, i.e., MIMO interference channels [33], cellular downlink and uplink [34, 35], X-networks [25], two-way communication networks [36], blind alignment [37], index coding networks [38] and multicast / compound networks [39], etc. The survey of IA can be found in [40–43]. The fundamental aspects of IA were given in [40], while the practical challenges in applying IA and potential future directions were discussed in [23]. The current research works on IA was studied in [41] with an antenna selection and multiuser diversity techniques. Furthermore, [42] reviewed IA in the interference channel with the features of DoF and imperfect channel state information (CSI). Moreover, a more extensive survey of IA research works was presented in [43], where the authors discussed some research problems and open challenges. As it is discussed above, IA is applicable to various wireless networks, namely cellular networks, device-to-device networks, CR network, etc. From here, IA can be said to be a comprehensive technique which can be applied in many multi-user networks to manage interference.

In Chapter 3, interference temperature model to investigate CR system performance over various wireless fading channels is studied, while, in Chapter 4, we will evaluate the performance of interference channels and study how to efficiently manage intra- and inter-network interference by applying IA methods in order to guarantee the QoS for both PNs and SNs.

2.4 Wireless Energy Harvesting

The future mobile communication will be totally different from its current version. Nowadays demand for high-quality videos and better screen resolutions from mobile users forces researchers to seek out better sustainable power sources or to execute wireless EH in the upcoming wireless networks. Recently, to deal with this issue, a simultaneous wireless information and power transfer (SWIPT) technique has been developed [44], where the same RF signal is used to deliver both energy and intended information. In the upcoming mobile generations, the SWIPT technology can be of primary importance with its energy and information transmission that can be adopted in various modern communications systems [45, 46]. The main three benefits of the SWIPT technology can be described by follows. First of all, the lifetime of SWIPT adopted wireless nodes can be prolonged by harvesting energy from ambient signals. Second, the transmission efficiency of the SWIPT method is better compare with that of the conventional time-division multiplexing mechanism due to simultaneous power and information transmission in the prior

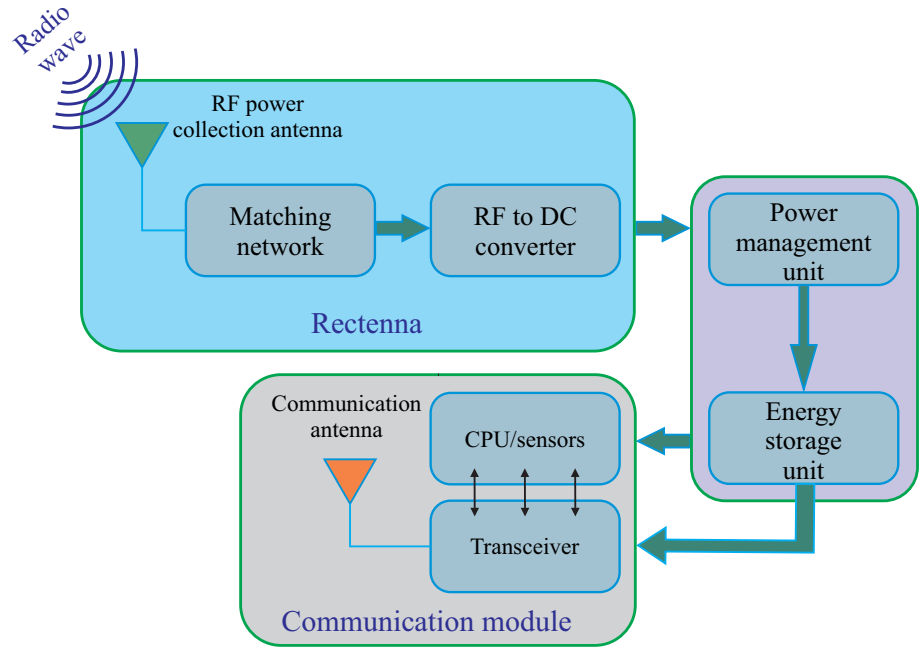

Figure 2.6. A transceiver with energy harvesting module.

method. The last gain is the fact that, in SWIPT, the interference is controlled and even can be used for EH purposes [41]. Fig. 2.6 illustrates a block diagram of a transceiver with an energy harvesting module. The wireless power receiver part consists of a receiving antenna, a matching network, an RF-DC rectifier, a power management unit and an energy storage unit (i.e., a rechargeable battery [47]). Then, after the energy storage unit is successfully charged, the power is provided to the central processing unit or transceiver to process information.

There are some review articles on EH and SWIPT [44, 45, 48–56]. A well-organized overview of SWIPT technology has been provided by the authors in [48], where recent advances and future challenges of the technology were presented. In [45], a survey on current studies in RF-EH networks was presented, which covered circuit designs, communication protocols and emerging operation designs for various EH systems. Furthermore, the authors in [50] have discussed smart antenna technologies applied in SWIPT adopted MIMO networks with the basics of SWIPT and receiver architectures. The above-mentioned survey works have contributed important insights into the foundational features of EH and SWIPT technologies as well as provided some recommendations. A review based on SWIPT from both the technical and theoretical perspectives was presented by the authors in [51]. The work has started with surveying of various kinds of SWIPT scenarios with their challenging problems. Furthermore, by presenting performance improvement through derived results, the authors suggested using massive MIMO

technology in order to obtain better performance in the SWIPT technique. The recent advances of EH and wireless power transfer (WPT) in terms of signal processing, information/communication theory and wireless networking were summarized in [52]. Moreover, a comprehensive survey of EH in full-duplex CR systems in perspective of architectures and related case studies were presented in [53]. The authors in [54] have discussed existing solutions for implementing WPT such as a static charger scheduling, a wireless charger deployment and a mobile charger dispatch. In addition, the authors in [54] have reviewed open problems and practical challenges in adopting wireless charging. The survey work on exploiting interference for wireless EH systems was introduced in [55], where the authors presented a classification of wireless EH systems which utilize interference. The work introduced current advances on an antenna dimension, a receiver architecture, a network topology and an interference management. Fundamental aspects of the energy scheduling and properties of various power sources in EH systems were presented in [57], while, the authors in [56] discussed fundamental limits of EH systems and it was concluded that, in EH networks, each transmitted symbol is instantaneously constrained by the energy available in the battery. Finally, works in [44] and [58] have illustrated overview based on the policies of EH and WPT in wireless sensor networks. The author in [44] concluded that RF EH is mostly suitable for small-sized battery-powered sensors which can be used in wireless body area networks (WBANs), future smart buildings, etc.

In Chapter 4, we study the EH performance of CR networks with MIMO antennas in the presence of interference. Saying so, we demonstrate how interference can be used as an EH source instead of just being canceled.

2.5 Non-Orthogonal Multiple Access (NOMA)

NOMA is another spectrum scarcity resolving technology, which has recently received much attention in wireless communications as being a promising candidate for upcoming 5G networks [59]. Each user in NOMA can utilize the whole available resources such as time or frequency, which results in better spectrum efficiency [60, 61]. There are various multiple access (MA) techniques for 5G networks have been introduced by academia and industry, e.g., sparse code multiple access (SCMA) [62, 63], low density spreading (LDS) [64], pattern division multiple access (PDMA) [65, 66], lattice partition multiple access (LPMA) [67] and power-domain NOMA [68–71]. All above-mentioned techniques adopt the same fundamental idea, where more than one user use all available orthogonal resource block such as a frequency channel, a time slot, a spreading code or an orthogonal spatial DoF, etc. In traditional orthogonal multiple access (OMA) methods, e.g., orthogonal frequency division multiple access (OFDMA) and TDMA, each user is served in an individual orthogonal resource block. Those OMA techniques are inefficient

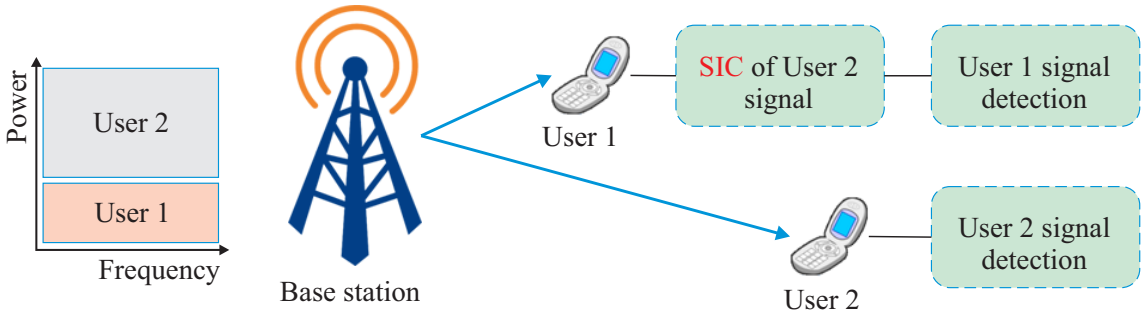

Figure 2.7. An example of a power-domain NOMA for two users.

as, despite some users' poor channel conditions, each user is solely allocated with one of the scarce bandwidth resources for fairness purposes. Certainly, inefficient use of resources for poorer users negatively impacts on the spectrum efficiency and throughput of the overall system. On the other hand, the NOMA technique guarantees that users with weak and strong channel conditions can get simultaneous access to the whole available resources, i.e., time, frequency or code. As a consequence, by guarantying the users' fairness, the system throughput of NOMA can be significantly larger than that of OMA [72]. Academic and industrial research works have proved that the NOMA technique can obtain better spectral efficiency gain compared to conventional OMA techniques. Apart from this, it has demonstrated that NOMA can effectively support massive connectivity, which is a vital criterion for the IoT [73, 74].

Despite the fact that the application of NOMA in wireless networks is novel, related concepts have been considered in information theory for a long period. Saying so, fundamental components of NOMA, i.e., successive interference cancellation (SIC), superposition coding and the message passing algorithm (MPA), have already been introduced at the beginning of this century [75, 76]. However, removing orthogonality which is the principle idea of NOMA, had not been practiced in the prior generations of cellular networks. In this context, it is noted that the conception of NOMA is quite different from that of code division multiple access (CDMA). Indeed, CDMA is basically based on the idea that users are separated using the differences between their spreading codes, while NOMA serves several users with the same code. Therefore, in CDMA, the chip rate should be much higher than the supported data rate. For example, to obtain the data rate of 10 Gbps, the requirement for the chip rate can be several hundred Gbps, which is tough to execute with practical equipment.

NOMA is compatible with existing and future wireless systems. Therefore, NOMA can be integrated with traditional OMA techniques such as OFDMA and TDMA [77]. Due to this ability, downlink NOMA has been adopted in the 3GPP LTE which is called multiple user superposition transmission (MUST) [78]. Especially, an application of the NOMA principle assures that two users can be served at the same time within the same

OFDMA subcarrier. Thus, the LTE resource blocks remain unchanged.

The most popular type of NOMA is the power-domain NOMA [69], where transmitters broadcast a superimposed signal to all receivers by serving them simultaneously with different power levels depending on their QoS or channel conditions [68], i.e., users with better channel conditions are allocated with less transmit power, while users with worse channel conditions are assigned with higher transmit power to obtain user fairness (Fig. 2.7). Then, receiver nodes with better channel qualities apply the SIC to decode messages of users with weak channel qualities before decoding their own ones[1] [71] . The performance of NOMA in a cellular downlink scenario with randomly deployed users was investigated in [69], where it was concluded that NOMA performs better than a conventional OMA in terms of the ergodic sum rate. However, it was also deduced that the OP of NOMA crucially depends on the appropriate choice of the power allocation (PA) factors. Authors in [68] studied the OP of NOMA with randomly distributed users as well, but with partial CSI. The analytical results there also showed the outperformance of NOMA. Moreover, the NOMA scheme was studied from a fairness standpoint in [79], where PA techniques were investigated to ensure fairness for downlink users.

2.5.1 Cognitive Radio NOMA

Recently, an advance of NOMA technique has also been applied into CR systems. The synergy of these promising technologies can significantly decrease the complexity of the power allocation design and surely support the QoS requirements of users [80–84]. For instance, the authors in [85] applied the NOMA policy to large-scale underlay CR networks to improve the connectivity of SNs. Not similar to conventional NOMA wireless networks, in CR-NOMA systems, the power of the superimposed signals need to be constrained in order to not exceed interference level at the PN. Related work has been studied in [86], where the secondary NOMA transmitters supported two functions: the first is to deliver information to SN's receivers, the second is to act as a relay helping the PN's receivers. Moreover, underlay CR-NOMA networks were studied in [85], where a secondary source transmits superimposed NOMA messages to the SUs. The results revealed that careful design of the target data rates and PA factors enhances the performance of NOMA users compared to OMA ones. The advantage of cooperative communications has also been applied in CR-NOMA networks [87], [88]. For instance, the authors in [87] studied the application of NOMA to achieve the superposition transmission for an unicast PU and multicast SUs, where the SN provides a cooperation between PUs in order to compensate the access to the primary spectrum, whereas, the same system model was studied in [84], where the direct connection along with the relay channel is considered.

[1]For the sake of brevity, hereafter, the appearance of NOMA in the text assumes power-domain NOMA.

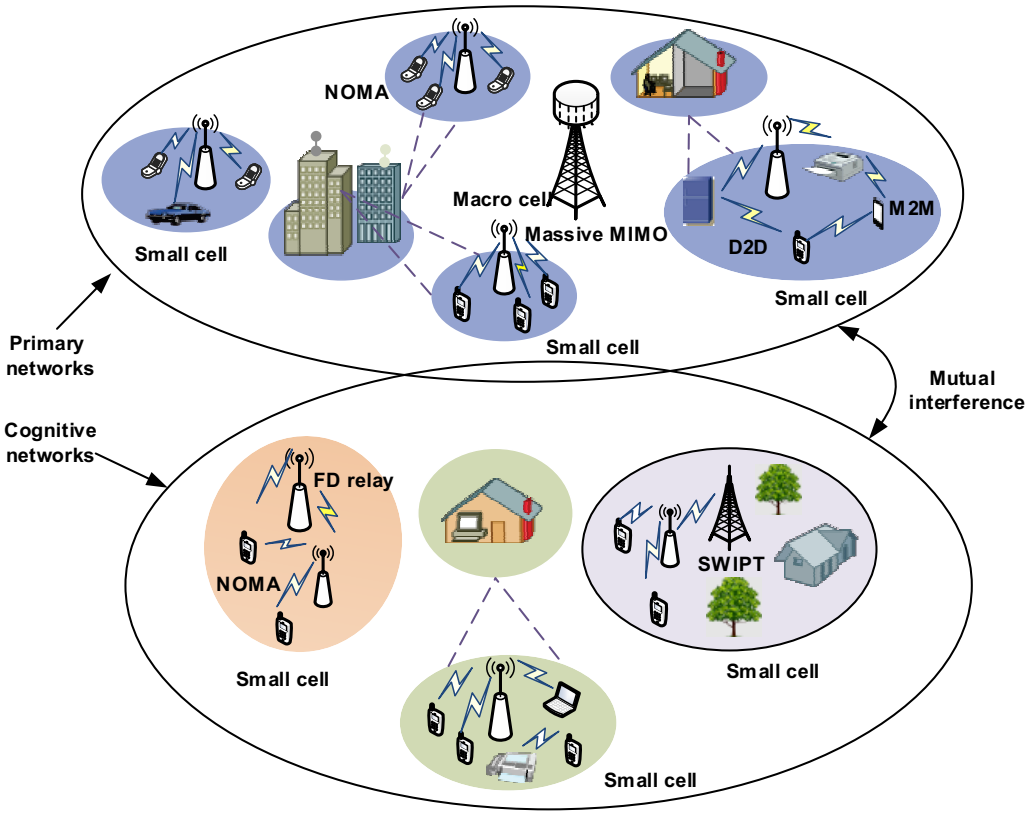

Figure 2.8. An illustration of CR-NOMA [2].

The authors in [88] proposed a novel cooperative multicast CR-NOMA scheme, where a two-stage cooperative strategy was devised to enhance fairness of SUs.

Chapter 3

Cognitive Relaying Networks

In this Chapter, a dual-hop detect-and-forward cognitive relaying system with interference temperature constraints over the general $\alpha-\mu$ fading channel is studied. The contribution of this Chapter is mainly described by the exact closed-form expression for the OP. Moreover, the symbol error rate calculation is derived for the proposed system model. Furthermore, the correctness of the derived analytical results is validated through Monte-Carlo simulations which show how the outage saturation paradigm appears when the interference level at the primary receiver is constrained. Finally, it is revealed that the system performs better when higher interference constraint is applied.

3.1 Introduction

3.1.1 Cooperative Communication

The large demand for mobile access and advances in wireless hardware technology have caused tremendous progress in wireless communication networks over the past decades. In previous years, many attempts to attain reliable and high data-rate communication over the wireless channels have been failed because of different wireless channel characteristics such as shadowing, multi-path fading, and path loss effects. Due to these effects, the wireless channel quality varies in space, time, and frequency. Therefore, techniques used in traditional wireline communications are not always suitable for wireless channels. One of the techniques to overcome such an issue is a transmit/receive diversity technique, where a *diversity gain* can be achieved in space, time or frequency domains. With a good knowledge of CSI, more resources such as power, time, and frequency can be allocated to users with stronger CSI and users with unreliable channels are allocated with fewer resources. Yet while CSI is not available, one can implement space-frequency or space-time resource allocation policies to improve the reliability of the network. Particularly, recent advances in MIMO antennas benefit in achieving spatial diversity gains in modern wireless networks [17, 89–92]. On the other hand, the cost and size of many wireless network applications, such as mobile phones, sensors, etc., are limited and installation of

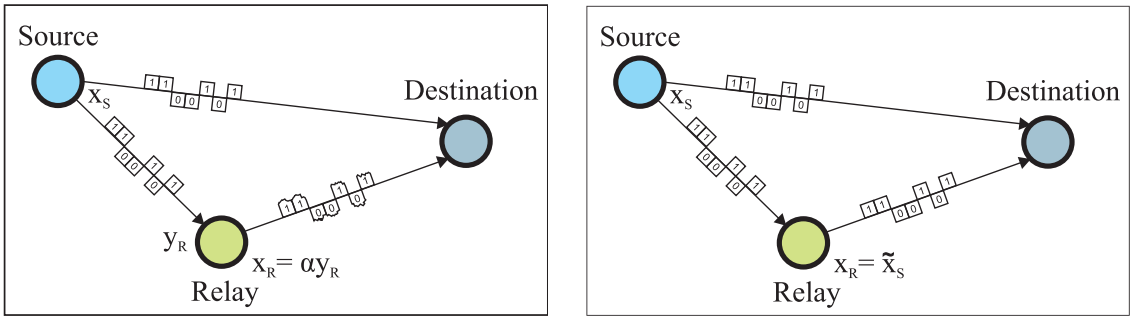

(a) Amplify-and-forward.

(b) Detect-and-forward.

Figure 3.1. The basic cooperative relaying schemes: amplify-and-forward and decode-and-forward.

multiple antennas on such devices can be impractical. In such a circumstance, a desirable and promising alternative technique can be when single antenna mobile users can cooperate with each other to build up a distributed antenna system to obtain spatial diversity gains. This method is called cooperative or relaying communications [93].

In cooperative communication systems, users help one another to relay their messages to a destination user [94–100]. On that basis, cooperative users can achieve spatial diversity gains by imitating a distributed antenna array of MIMO systems. Thus, due to wireless channel characteristics, different cooperative users experience various fading effects while relaying each others' data to the destination user, which consequently improves transmission reliability.

Many relaying techniques have been studied in the literature, namely, AF [101, 102], DF [101, 103], coded cooperation [104], selective relaying (SR) [105], compress-and-forward (CF) [105] and so on. All relaying techniques work in a half-duplex mode, which means that, at each time slot, only one user serves as a source node, whereas other users act as relay nodes to forward messages from the source to the destination. Depending on the system requirement, any cooperative user can act as either a source or a relay. Fig. 3.1 illustrates AF and DF relaying schemes, which are the most basic and widely adopted relaying schemes. In both schemes, in the 1^{st} time slot, the source transmits its data to both the destination and the relay. In the 2^{nd} time slot, while the AF relaying scheme is implemented, the received signal at the relay is amplified and forwarded to the destination. Then, the destination combines the both received signal from the source and the relay to increase the performance of the signal detection. If the DF relaying scheme is adopted, within the 2^{nd} time slot, the relay detects the received signal from the source and forwards a re-encoded message to the destination.

3.1.2 Cognitive Relaying Networks

CR is a promising technique that can utilize the wireless spectrum usage, the main idea of which is to allow SUs to broadcast in licensed frequency bands when no communication activity is required for PUs. The benefits of cooperative communications have also been applied in CR [106–110]. A relay network adopted to CR enhances the throughput and coverage area of the entire network [106]. In cognitive relaying networks (CRNs), the SN can obtain better throughput by implementing the main two approaches. The first one is while the PUs and the SUs cooperate with each other, whereas, in the second approach, the cooperation happens only among the SUs [107]. The authors in [108] compared the performance of licensed and unlicensed bands with that of the conventional relay network. The results showed that adopting cooperation in CR shows outstanding performance in wireless relay networks by reducing inter-cell interference. Another CRN studies [109] has developed the best relay selection technique in an underlay CRN, where obtained results showed that the CRN achieves the same full selection diversity order as traditional networks. Moreover, an increase in the number of relays resulted in a better OP compared to conventional relay networks. Furthermore, an underlay dual-hop DF CRN in Nakagami-m fading channels was studied in [110], where each relay demodulates the received signal and forwards it to the destination. The authors in [111] derived the OP of underlay CRN which operates in generalized-K and generalized-*gamma* distributions.

In the wireless medium, a large number of distributions exist that can well represent the statistics of the wireless channel. For example, the long-term signal variation can be described by the Log-normal distribution, while the short-term signal variation can be presented by various other distributions, i.e., Rice, Rayleigh, Hoyt, Weibull, and Nakagami-m. All studies in the literature of CRNs were mainly adopted Rayleigh, Rician and Nakagami-m fading channels, while neglecting other distributions such as Log-normal, Negative exponential, Weibull, etc. By motivated from the research above, the rest of this Chapter considers a study of CRNs over the general $\alpha - \mu$ distribution that fully embraces all the aforementioned channel distributions [112].

3.2 Contribution of the Chapter

The main contributions of this Chapter are as follows:

- The outage performance study is provided for a dual-hop underlay CR system, where the primary receiver applies the interference temperature model to secondary transmit nodes.

- Considering imposed transmit power constraint at the SN, the OP is derived in the closed form for the secondary source and relay nodes over Rayleigh fading distribution.
- The closed-form OP expressions further derived for the generalized $\alpha-\mu$ fading distribution, which includes various other distributions, i.e., Rayleigh, Gamma, Exponential, Nakagami-m, etc.
- Finally, all derived analytical results are validated through Monte-Carlo simulations. Moreover, the numerical part shows how the level of interference constraint impacts on the end-to-end outage and symbol error rate performance of the secondary destination node.

The remainder of this Chapter is organized as follows. The proposed system model for the underlay CRN is described in Section 3.3. The OP analysis for different fading distributions is presented in section 3.4, while numerical results are illustrated in Section 3.5. Finally, the Chapter is summarized in Section 3.6.

3.3 System Model

The underlay CRN model is considered as shown in Fig. 3.2, where PR, S, R and D represent the primary receiver, the secondary source, the secondary relay and the secondary destination, accordingly. Moreover, the corresponding channel gains between nodes are denoted by h_{SP}, h_{RP}, h_{SR} and h_{RD}. It is assumed that there is no direct link between S and D. Thus, we assume short-distance communication where R applies a DF relaying scheme to forward signal from S to D. Regarding the principle of the underlay CR paradigm, the secondary nodes can broadcast only if they do not cause harmful interference to PR. Hence, source and relay transmit power constraints are accordingly written by

$$P_S \leq \min\left(\frac{I}{|h_{SP}|^2},\ \bar{P}_S\right), \tag{3.1}$$

$$P_R \leq \min\left(\frac{I}{|h_{RP}|^2},\ \bar{P}_R\right), \tag{3.2}$$

where $\bar{P}_S$ and $\bar{P}_R$ are the maximum source and relay transmit power, respectively, and I is the interference temperature constraint (ITC), which is the maximum tolerable level of interference that PR can accept for a reliable PN communication. The transmission of the secondary network is executed in two time-slot periods. In the 1^{st} time slot, S transmits the signal to R with the average power P_S. Thus, the received signal at R can be written

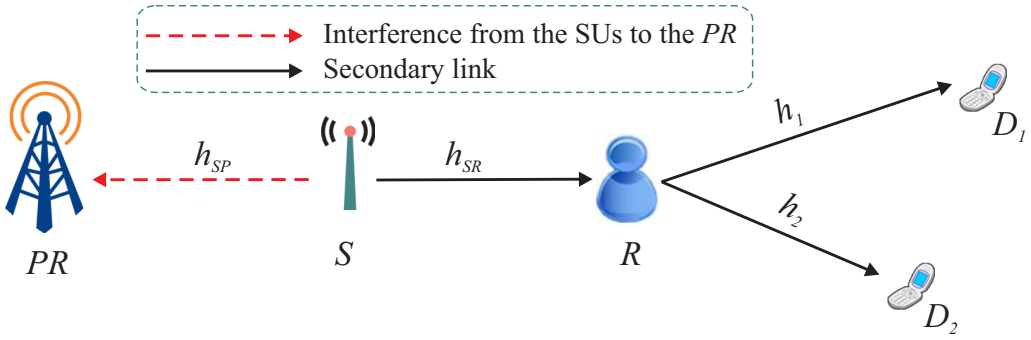

Figure 3.2. A system model for cooperative underlay CR network consisting of a secondary source, relay and destination.

as[1]

$$y_R = \sqrt{P_S} h_{SR} x_S + n_R, \tag{3.3}$$

where x_S , with $\mathbb{E}(|x_S|^2) = 1$, denotes the intended data to D and n_R denotes the additive white Gaussian noise (AWGN) term at R. Then, the received signal at R are fully decoded and re-encoded for the further transmission with the signal-to-noise ratio (SNR) of

$$\gamma_R = \frac{P_S |h_{SR}|^2}{\sigma_R^2}, \tag{3.4}$$

where σ_R^2 is the noise power at R. Hence, in the 2^{nd} time slot, R transmits a re-encoded version of the signal to D with an average power of P_R, which can be expressed by

$$y_D = \sqrt{P_R} |h_{RD}|^2 \tilde{x}_S + n_D, \tag{3.5}$$

where $\tilde{x}_S$ is the decoded message at R while n_D is the AWGN term at D. Then, D receives and estimates the original signal by the following SNR

$$\gamma_D = \frac{P_R |h_{RD}|^2}{\sigma_D^2}, \tag{3.6}$$

where σ_D^2 is the noise power at D. Therefore, the end-to-end instantaneous system capacity can be written as [109], [110]

$$C = \frac{1}{2} \min \left[\log_2 \left(1 + \min \left(\frac{I}{|h_{SP}|^2}, \bar{P}_S \right) \frac{|h_{SR}|^2}{\sigma_R^2} \right), \right. \\ \left. \log_2 \left(1 + \min \left(\frac{I}{|h_{RP}|^2}, \bar{P}_R \right) \frac{|h_{RD}|^2}{\sigma_D^2} \right) \right]. \tag{3.7}$$

[1]Thereafter, time index is omitted for brevity reasons.

The factor $\frac{1}{2}$ in (3.7) implies that the $S \rightarrow R \rightarrow D$ communication session requires two time slots.

3.4 Outage Probability Analysis

In wireless communication networks, the OP of a communication channel is the probability that an achievable rate is not supported because of variable channel capacity. Thus, an outage event can occur if the obtained SNR level is below than a predefined SNR threshold [113]. Now, by defining the probability of the instantaneous capacity in (3.7) is below than a predefined rate threshold $\mathcal{R}_{\text{th}}$, the OP of D can be written by followings

$$P_{\text{out}} = \Pr(C \leq \mathcal{R}_{\text{th}}). \tag{3.8}$$

Furthermore, the end-to-end OP of D can be further rewritten as follows

$$P_{\text{out}}(\xi) = \Pr\left[\min\left(\min\left(\frac{I}{|h_{SP}|^2},\ \bar{P}_S\right)\frac{|h_{SR}|^2}{\sigma_R^2},\ \min\left(\frac{I}{|h_{RP}|^2},\ \bar{P}_R\right)\frac{|h_{RD}|^2}{\sigma_D^2}\right) < \xi\right], \tag{3.9}$$

where $\xi = 2^{2\mathcal{R}_{\text{th}}} - 1$ is the corresponding threshold for the SNR. Now, we divide (3.9) into two terms to simplify the demonstration of the cumulative distribution functions (CDFs) of the system model as

$$\eth_S \triangleq \min\left(\frac{I}{|h_{SP}|^2},\ \bar{P}_S\right)\left(\frac{|h_{SR}|^2}{\sigma_R^2}\right) \tag{3.10}$$

and

$$\eth_R \triangleq \min\left(\frac{I}{|h_{RP}|^2},\ \bar{P}_R\right)\left(\frac{|h_{RD}|^2}{\sigma_D^2}\right). \tag{3.11}$$

Then, by substituting (3.10) and (3.11) into (3.9), also knowing the independence of the random variables (RVs) $\eth_S$ and $\eth_R$, the OP of D can be further rewritten as

$$\begin{aligned} P_{\text{out}}(\xi) &= \Pr\left(\min\left(\eth_S, \eth_R\right) \leq \xi\right) = 1 - \Pr\left(\min\left(\eth_S, \eth_R\right) > \xi\right) \\ &= 1 - \Pr(\eth_S > \xi)\Pr(\eth_R > \xi) = 1 - \left(1 - F_{\eth_S}(\xi)\right)\left(1 - F_{\eth_R}(\xi)\right) \\ &= F_{\eth_S}(\xi) + F_{\eth_R}(\xi) - F_{\eth_S}(\xi)F_{\eth_R}(\xi), \end{aligned} \tag{3.12}$$

where $F_{\eth_S}$ and $F_{\eth_R}$ represent the CDFs of the RVs $\eth_S$ and $\eth_R$, respectively. Now, we compute the CDF of $\eth_S$ by followings

$$F_{\eth_S}(\xi) = \Pr(\eth_S < \xi) = \Lambda + \Psi, \tag{3.13}$$

where

$$\Lambda = \Pr\left\{\frac{\bar{P}_S |h_{SR}|^2}{\sigma_R^2} < \xi,\ \bar{P}_S \leq \frac{I}{|h_{SP}|^2}\right\} = \Pr\left\{|h_{SR}|^2 < \frac{\xi\sigma_R^2}{\bar{P}_S},\ |h_{SP}|^2 \leq \frac{I}{\bar{P}_S}\right\}, \tag{3.14}$$

$$\Psi = \Pr\left\{\frac{|h_{SR}|^2 I}{|h_{SP}|^2\sigma_R^2} < \xi,\ \bar{P}_S > \frac{I}{|h_{SP}|^2}\right\} = \Pr\left\{\frac{|h_{SR}|^2}{|h_{SP}|^2} < \frac{\xi\sigma_R^2}{I},\ |h_{SP}|^2 > \frac{I}{\bar{P}_S}\right\}. \tag{3.15}$$

3.4.1 Outage Analysis for the Rayleigh Distribution

Here, we first derive an outage analysis assuming that all channels in the proposed system model experience an independent but not necessarily identically distributed (i.n.i.d.) Rayleigh block fading, i.e., the channels remain constant during every transmission block but vary independently between various blocks.

The probability density function (PDF) of the Rayleigh distribution is written as [114]

$$f_X(x) = \frac{x}{\sigma^2} e^{\frac{-x^2}{2\sigma^2}},\ x \geq 0, \tag{3.16}$$

where σ denotes the scale parameter of the distribution. Hence, the CDF of the distribution can be expressed as

$$F_X(x) = 1 - e^{\frac{-x^2}{2\sigma^2}},\ x \in [0, \infty). \tag{3.17}$$

Definition Assume that X is a continuous RV with generic PDF $f_X(x)$ which is defined over the support $n_1 < x < n_2$ and $Y = g(X)$ be an invertible function of X with inverse function $X = s(Y)$. Hence, by applying the "*change of variable*" technique [115], the PDF of Y can be written by

$$f_Y(y) = f_X\left(s(y)\right)|s'(y)|, \tag{3.18}$$

which can be defined over the support $g(n_1) < y < g(n_2)$.

As it mentioned before each channel between nodes, i.e., $h_{(m)},\ \forall m \in \{SP, RP, SR, RD\}$, is i.n.i.d. with zero mean and unit variance. Therefore, using (3.18), $|h_{(m)}|^2,\ \forall m \in$

$\{SP, RP, SR, RD\}$, follows exponential distribution [116], which PDF and CDF can be respectively derived as

$$f_Y(y) = \begin{cases} \lambda e^{-\lambda y}, & y \geq 0, \\ 0, & y < 0 \end{cases} \tag{3.19}$$

and

$$F_Y(y) = \begin{cases} 1 - e^{-\lambda y}, & y \geq 0, \\ 0, & y < 0, \end{cases} \tag{3.20}$$

where $\lambda = \frac{1}{2\sigma^2}$.

Proposition 1 The closed-form OP expression of D for the Rayleigh distribution can be written as

$$P_{\text{out}}(\xi) = 1 - \left(e^{-\frac{\lambda\xi\sigma_R^2}{P_S}} - \frac{\xi\sigma_R^2 e^{-\frac{\lambda\left(I+\xi\sigma_R^2\right)}{P_S}}}{I+\xi\sigma_R^2} \right) \left(e^{-\frac{\lambda\xi\sigma_D^2}{P_R}} - \frac{\xi\sigma_D^2 e^{-\frac{\lambda\left(I+\xi\sigma_D^2\right)}{P_R}}}{I+\xi\sigma_D^2} \right). \tag{3.21}$$

Proof: See Appendix A.1 for details. ■

3.4.2 The $\alpha-\mu$ Distribution

The $\alpha - \mu$ distribution is a general fading distribution that can introduce the Gamma, Rayleigh, Exponential, Weibull, one-sided Gaussian, and Nakagami-m [117]. Saying so, the $\alpha - \mu$ distribution can be turned into the Weibull distribution by inserting $\mu = 1$. Hence, from the Weibull distribution, setting $\alpha = 1$ and $\alpha = 2$, the negative exponential and the Rayleigh distributions can be obtained, accordingly. Furthermore, from the $\alpha - \mu$ distribution, the Nakagami-m distribution results when $\alpha = 2$. Then, from the Nakagami-m distribution by setting $\mu = 1$ and $\mu = \frac{1}{2}$, the Rayleigh and the one-sided Gaussian distributions can be obtained, respectively.

3.4.2.1 Outage Analysis for the $\alpha-\mu$ Distribution

The $\alpha-\mu$ distribution is the most appropriate fading distribution that can describe the small-scale fading channels [112, 118]. The PDF of the $\alpha-\mu$ fading signal with an envelope *r* can be written as [119, 120]

$$p(r)_{\alpha-\mu} = \frac{\alpha\mu^{\mu} r^{\alpha\mu-1}}{\hat{r}^{\alpha\mu}\Gamma(\mu)} e^{\frac{-\mu r^{\alpha}}{\hat{r}^{\alpha}}}, \tag{3.22}$$

where $\alpha > 0$ is an arbitrary parameter, $\hat{r}$ stands for α-root mean value which is equal to $\hat{r} = \sqrt[\alpha]{\mathbb{E}\left(r^{\alpha}\right)}$, $\mathbb{E}(\cdot)$ is the expected value, and $\Gamma(\cdot)$ is the Gamma function defined as $\Gamma(s) \triangleq \int_0^{\infty} t^{s-1}e^{-t}\mathrm{d}t$ [121]. Also, $\mu \geq \frac{1}{2}$ is the inverse of normalized variance of r^{α} given by

$$\mu = \mathbb{E}^2(r^{\alpha})/\mathbb{E}(r^{2\alpha}) - \mathbb{E}^2(r^{\alpha}). \tag{3.23}$$

The PDF, $f_{\gamma}(\gamma)$, and the CDF, $F_{\gamma}(\gamma)$, of the SNR can be expressed as [113]

$$f_{\gamma}(\gamma) = \frac{\alpha\mu^{\mu}\gamma^{(\alpha\mu/2)-1}}{2\bar{\gamma}^{\alpha\mu/2}\Gamma(\mu)}e^{-\mu\left(\frac{\gamma}{\bar{\gamma}}\right)^{\alpha/2}} \tag{3.24}$$

and

$$F_{\gamma}(\gamma) = \frac{\gamma_{\text{inc}}\left(\mu, \mu\left(\frac{\gamma_{\text{th}}}{\bar{\gamma}}\right)^{\alpha/2}\right)}{\Gamma(\mu)}, \tag{3.25}$$

respectively, where $\gamma_{\text{inc}}(s,x) = \int_0^x t^{s-1}e^{-t}\mathrm{d}t$ is the lower incomplete gamma function [121].

Proposition 2 The closed-form expression for the CDFs $F_{\eth_S}$ and $F_{\eth_R}$ of D for the $\alpha-\mu$ distribution can be respectively written as

$$\begin{aligned} F_{\eth_S}(\xi) =& \frac{\Gamma\left(\mu_{SR}, \mu_{SR}\left(\frac{\xi\sigma_R^2}{\bar{\gamma}\bar{P}_S}\right)^{\frac{\alpha_{SR}}{2}}\right)}{\Gamma(\mu_{SR})}\frac{\Gamma\left(\mu_{SP}, \mu_{SP}\left(\frac{I}{\bar{\gamma}\bar{P}_S}\right)^{\frac{\alpha_{SP}}{2}}\right)}{\Gamma(\mu_{SP})} \\ &+ \frac{\Gamma\left(\mu_{SP}, \mu_{SP}\left(\frac{I}{\bar{\gamma}\bar{P}_S}\right)^{\frac{\alpha_{SP}}{2}}\right)}{\Gamma(\mu_{SP})} - \frac{\mu_{SP}^{\mu_{SP}}}{\Gamma\left(\mu_{SP}\bar{\gamma}^{\alpha_{SP}\mu_{SP}/2}\right)} \\ &\times \sum_{i=0}^{\mu_{SR}-1}\left[\frac{\left(\mu_{SR}\left(\frac{\xi\sigma_R^2}{\bar{\gamma}I}\right)^{\frac{\alpha_{SR}}{2}}\right)^i}{i!\left(\frac{\mu_{SP}}{\bar{\gamma}^{\alpha_{SP}/2}} + \mu_{SR}\left(\frac{\xi\sigma_R^2}{\bar{\gamma}I}\right)^{\frac{\alpha_{SR}}{2}}\right)^{\mu_{SP}+i}}\right. \\ &\left.\times\, \Gamma\left(\mu_{SP}+i, \left(\frac{I}{\bar{P}_S}\right)^{\frac{\alpha_{SR}}{2}}\left(\frac{\mu_{SP}}{\bar{\gamma}^{\alpha_{SP}/2}} + \mu_{SR}\left(\frac{\xi\sigma_R^2}{\bar{\gamma}I}\right)^{\frac{\alpha_{SR}}{2}}\right)\right)\right] \end{aligned} \tag{3.26}$$

and

$$F_{\Theta_R}(\xi) = \frac{\Gamma\left(\mu_{RD}, \mu_{RD}\left(\frac{\xi\sigma_D^2}{\bar{\gamma}\bar{P}_R}\right)^{\frac{\alpha_{RD}}{2}}\right)}{\Gamma(\mu_{RD})} \frac{\Gamma\left(\mu_{RP}, \mu_{RP}\left(\frac{I}{\bar{\gamma}\bar{P}_R}\right)^{\frac{\alpha_{RP}}{2}}\right)}{\Gamma(\mu_{RP})} + \frac{\Gamma\left(\mu_{RP}, \mu_{RP}\left(\frac{I}{\bar{\gamma}\bar{P}_R}\right)^{\frac{\alpha_{RP}}{2}}\right)}{\Gamma(\mu_{RP})} - \frac{\mu_{RP}^{\mu_{RP}}}{\Gamma\left(\mu_{RP}\bar{\gamma}^{\alpha_{RP}\mu_{RP}/2}\right)} \times \sum_{i=0}^{\mu_{RD}-1} \left[\frac{\left(\mu_{RD}\left(\frac{\xi\sigma_D^2}{\bar{\gamma}I}\right)^{\frac{\alpha_{RD}}{2}}\right)^i}{i!\left(\frac{\mu_{RP}}{\bar{\gamma}^{\alpha_{RP}/2}} + \mu_{RD}\left(\frac{\xi\sigma_D^2}{\bar{\gamma}I}\right)^{\frac{\alpha_{RD}}{2}}\right)^{\mu_{RP}+i}} \times \Gamma\left(\mu_{RP}+i, \left(\frac{I}{\bar{P}_R}\right)^{\frac{\alpha_{RD}}{2}}\left(\frac{\mu_{RP}}{\bar{\gamma}^{\alpha_{RP}/2}} + \mu_{RD}\left(\frac{\xi\sigma_D^2}{\bar{\gamma}I}\right)^{\frac{\alpha_{RD}}{2}}\right)\right)\right]. \tag{3.27}$$

Proof: See Appendix A.2 for details. ■

Finally, the closed-form OP expression of D for the $\alpha-\mu$ distribution can be derived by inserting (3.26) and (3.27) into (3.12).

The impact of the ITC on the OP can be explained by the next example. As it is indicated in the literature [109,110], an increase of the transmit power of S and R saturates the OP of the destination user. That occurs because the transmit power, with respect to $\min\left(I/|h|^2,\ \bar{P}\right)$, will be equal to $(I/|h|^2)$ as $P \to \infty$, i.e., a fixed I will control the maximum transmitted power from S and R. Therefore, if the value of I increases it allows S and R to transmit at higher power levels, which further results in an improvement of the OP performance. The importance of I can be shown by another example when $I \to 0$. In that case, $F_{\Theta_S}(\xi) = F_{\Theta_R}(\xi) \approx 1$ which comes to $P_{\text{out}}(\xi) \approx 1$. Hence, PR cannot tolerate any interference from the SN transmitters when $I \to 0$, which means that a communication in the SN is unavailable.

3.4.3 Symbol Error Rate Analysis

The symbol error rate (SER) for binary phase shift keying (BPSK), in traditional wireless communications, can be written as [122]

$$SER = \frac{1}{\pi}\int_0^{\pi/2} \mathcal{M}_\gamma\left(-\frac{g_{psk}}{\sin^2(\theta)}\right) \mathrm{d}\theta, \tag{3.28}$$

where $g_{psk} = \sin^2(\pi/M)$ denotes a constant value which equals to unity for BPSK while $\mathcal{M}_\gamma(-g)$ indicates the moment generating function (MGF) of the obtained SNR which

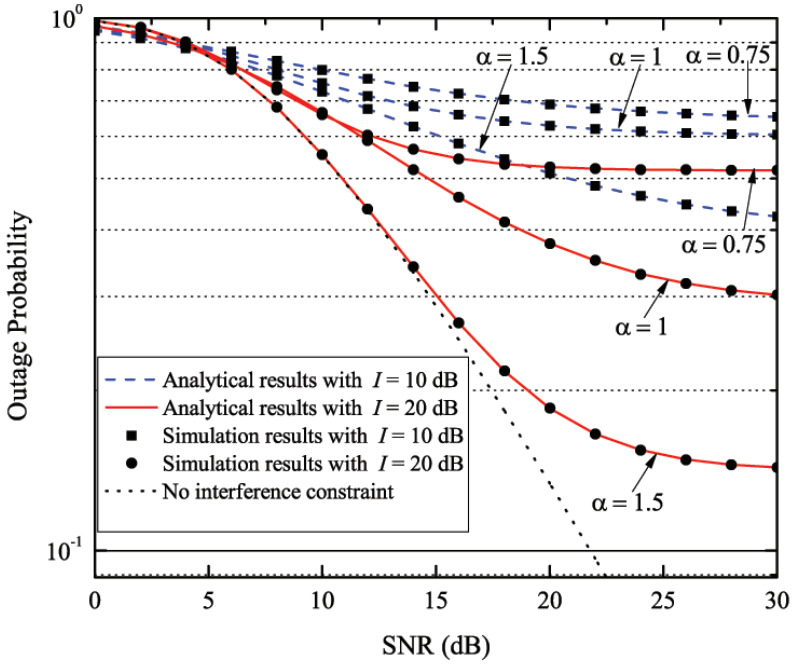

Figure 3.3. The OP versus SNR performance for various ITC over the Weibull distribution.

can be written as

$$\mathcal{M}_{\gamma}(-g) = \int_{0}^{\infty} f_{\gamma}(x) e^{-gx} \mathrm{d}x. \tag{3.29}$$

Thus, to evaluate the SER, the PDF of (3.12) should be substituted into (3.29). Hence, by using the derived MGF in (3.28), the SER can be calculated numerically.

3.5 Numerical Results and Discussion

This section discusses the OP and SER performance of the proposed system model for different cases of the $\alpha - \mu$ distribution.

Fig. 3.3 illustrates the results when the Weibull distribution ($\mu = 1$) is adopted. The comparison is made among various values of α while the ITC is taken as 10 dB and 20 dB. Moreover, ξ is set to be equal to 5 dB. The simulated results validate the analytical ones by shown perfect match. The results show that the best performance of the system is attained when no ITC is implemented by PR. Furthermore, when $\alpha = 1.5$, the system obtains better performance compared with the case when lower values of α are set. For instance, when $I = 20$ dB, the system with parameters of $\alpha = 1.5$ and $\alpha = 0.75$ obtains the OP of 0.6 at 10 dB and 12 dB, accordingly. From these results, we can observe the impact of the arbitrary fading parameter on the OP. In addition, it is shown that the curve of the OP starts saturating when the value of the transmit SNR approaches to that of I.

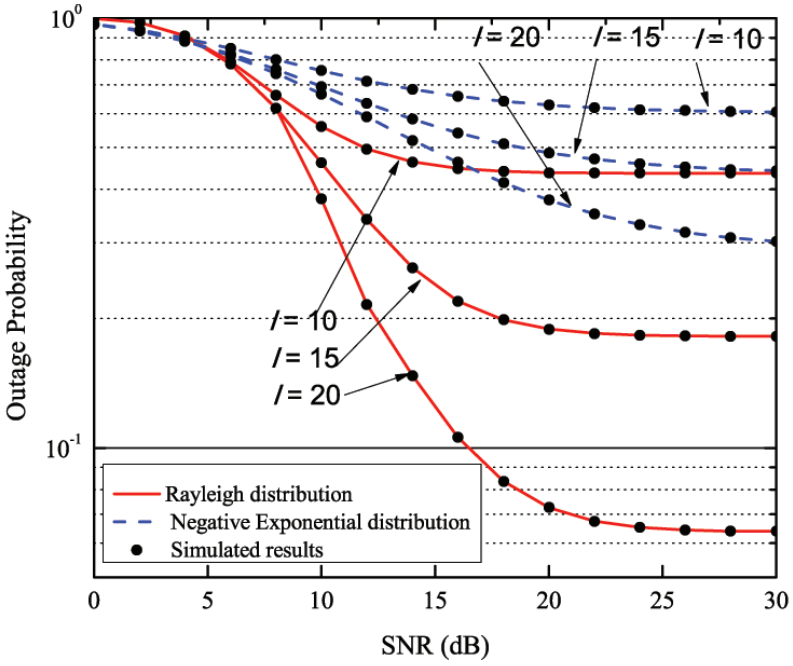

Figure 3.4. The OP versus SNR performance for different ITC over Rayleigh and Negative Exponential distributions.

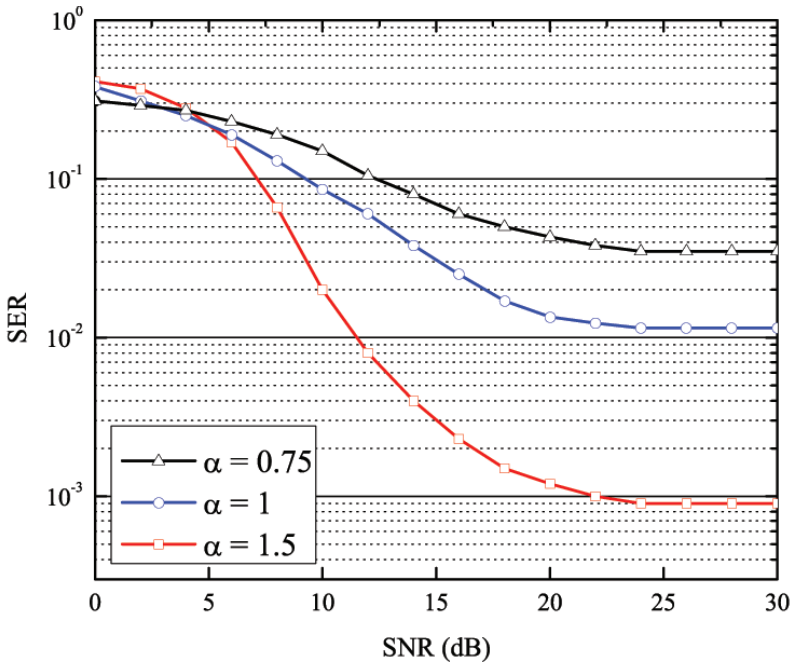

Figure 3.5. The SER versus SNR performance over the Weibull distribution when $I = 20$ dB.

This can be explained by the fact that, due to the ITC, the secondary transmit nodes can not broadcast at a higher power level than $I/|h|^2$.

Fig. 3.4 demonstrates the OP depicted for the Rayleigh distribution with $\alpha = 2$ and $\mu = 1$ as well as for the Negative Exponential distribution with $\alpha = 2$ and $\mu = 1/2$ when

various ITC values are implemented. From the figure, it is clearly seen that the Rayleigh distribution channel characteristics demonstrate better OP compared with the Negative Exponential one. For example, when $I = 20$ dB and the transmit SNR equals to 10 dB, the former obtains the OP of 0.2 while the latter achieves the OP of 0.7.

In Fig. 3.5, the SER given in (3.28) when the channel follows the Weibull distribution is depicted with $I = 20$ dB. In general, it is noted that networks with larger values of α achieve much better performance compared to that of lower values of α. Indicatively, the network with $\alpha = 1.5$ attains the SER of 0.1 at about transmit SNR of 6.5 dB, while, when $\alpha = 1$ and $\alpha = 0.75$, the same SER can be obtained at about 9.5 dB and 12.5 dB, respectively. Finally, it is noticed from all SER results that the system obtains better SER performance in higher transmit SNRs. However, curves of the SER start saturating while transmit SNR tends to the value of I.

3.6 Chapter Summary

This Chapter introduced the $\alpha-\mu$ distribution in the dual-hop CRN where secondary transmit nodes were constrained from the maximum transmit power due to the underlay CR concept. The $\alpha-\mu$ is a general distribution that includes several others distributions, i.e., Rayleigh, Gamma (and its discrete versions Erlang and central Chi-squared), Exponential, Nakagami-m (and its discrete version Chi), One-sided Gaussian, and Weibull. Based on the dual-hop CRN model proposed here, the analytical results for the OP were obtained in closed forms. Moreover, the impact of the ITC on the system outage and SER performance were investigated. From the derived results, it was observed that the ITC degrades the outage and SER performances which can be seen from the outage saturation. It was also revealed that the lower values of I degrade the OP performance of the system. In addition, the correctness of the derived results was validated by the Monte-Carlo simulations, where the perfect match between simulation and analytical results were obtained.

For the contribution of this Chapter, we can indicate that the statistics of those distributions that are special cases of the $\alpha-\mu$ distribution can be obtained directly from the formulations developed here by simply reducing these formulations into the respective particular case. It is worth to mention that even the $\alpha-\mu$ distribution has one more parameter than Weibull or Nakagami-m distributions, it does not pose any additional mathematical difficulty. Hence, the $\alpha-\mu$ distribution is suitable to adjust to field data by representing many other distributions in its special cases.

Chapter 4

Wireless Powered CRN with Interference Alignment

This Chapter studies a dual-hop DF wireless powered CRN with IA over Rayleigh fading channels. The energy-constrained secondary relay node harvests energy from both information and interference signals. Then, the secondary relay uses the harvested energy to forward the information signal from the secondary source to destination node. By applying beamforming matrices to the PNs and SNs, the performance metrics such as the OP, capacity and the bit error rate are studied under perfect and imperfect channel state information scenarios for both power-splitting relaying and time-switching relaying protocols. Moreover, the optimal network performance is achieved by calculating the optimal energy harvesting time-switching and power-splitting coefficients. Finally, closed-form OP expressions of primary and secondary users are derived. Monte-Carlo simulations are used to corroborate the analytical results, which show that the power-splitting relaying technique performs better than time-switching relaying in the proposed system model.

4.1 Introduction

4.1.1 Wireless Powered CRNs with IA

It was clearly explained in the previous chapters that SUs in CR systems can communicate in the licensed spectrum using three approaches, i.e., interweave, underlay and overlay [5]. These approaches impose some restrictions on their operation modes which, in turn, may degrade the performance of SUs. For instance, in the case of the underlay CR, the PUs impose the ITC to the SUs to guarantee the tolerable interference level at primary receivers (PRs). However, by employing the IA technique [25, 123–126], the interference caused by the SUs in wireless multi-user CR systems can be managed without imposing any ITC to the SUs. Furthermore, the advances of EH can be applied in CR systems [127] as CR nodes are mostly battery-powered devices which need to recharge or replace their batteries periodically.

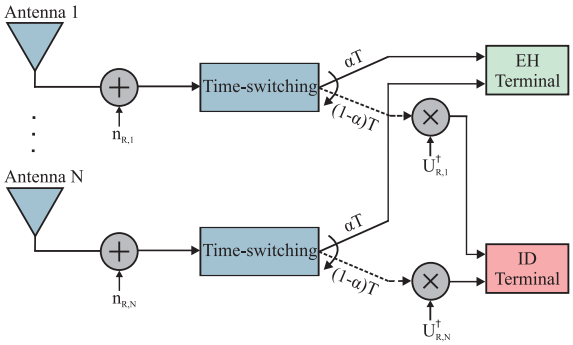

(a) Time-switching mode.

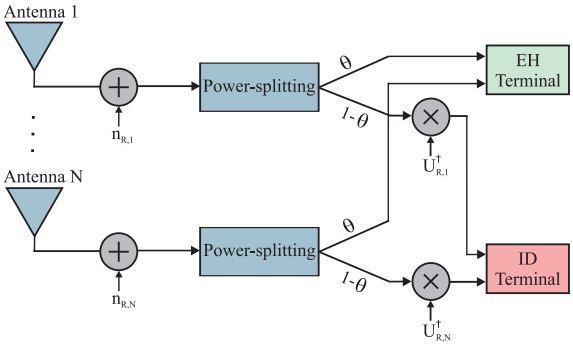

(b) Power-splitting mode.

Figure 4.1. Time-switching and power-splitting energy harvesting modes.

The underlay CR with embedded IA technique was studied in [116, 128–130]. The authors in [128] employed IA in CR to gain frequency domain diversity at the PUs to increase the throughput of the SN. A cancellation algorithm for a practical IA was developed in [130], where the authors studied the interference management at the PUs and the DoF optimization of the SUs. In [129], the authors presented the DoF region in a MIMO CR with a cooperative relay and embedded IA algorithm.

There are main two EH approaches in CR systems, i.e, time-switching (TS) and power-splitting (PS) protocols [131]. In the TS method (see Fig. 4.1a), the receiver switches between EH and information decoding (ID) modes over time [127]. In the PS method (see Fig. 4.1b), at the receiver's end, the received power is divided into two fractions: one is devoted for EH, whereas the rest is dedicated to ID purposes [127]. There are many research works related to SWIPT networks in the literature [50, 127, 132–138]. In [134], the authors proposed a joint study of IA and SWIPT in MIMO networks, where the performance improvement of the SWIPT network by dynamically selecting users as either EH or ID terminals was illustrated. The performance of the EH method in cooperative relaying networks, where a power-limited relay harvests energy to assist the source to deliver the signal to the destination, was investigated in [127, 133, 135, 139–141]. Lately, CR systems with the ability of EH have received significant attention [136, 137, 142]. The authors in [136] studied an optimal spectrum sensing policy for the EH-based CR systems

which maximizes the expected total throughput under energy causality and collision constraints. In the proposed system model, secondary nodes harvest the energy from PUs' transmissions within the TS mode. In [116], a novel SWIPT scheme to optimize wireless energy harvesting (WEH) and information transfer (IT) performance in symmetric IA networks were introduced. In all the aforementioned works, the authors assumed perfect CSI which is impractical due to the presence of channel estimation errors [143]. Thus, research works in [143] and [144] investigated the performance of the EH-based overlay CR under the imperfect CSI scenario. The authors in [143] studied the joint optimization of the PS ratio selection and power control, whereas, in [144], joint resource allocation and admission control schemes with several SUs were studied.

4.1.2 Practical Implementation

IA embedded systems may face some several challenging problems in a practical implementation, i.e., CSI acquisition, CSI overhead signaling and degradation of the system performance at low SNRs. These challenges were studied in [145–147]. The authors in [145] proposed an adaptive transmission scheme which considerably reduces the error probability and produces robustness to the CSI uncertainty. In addition, in [146], the authors presented a sequential antenna switching IA scheme that reduces the computational complexity and CSI-feedback overhead. Moreover, a low complexity algorithm for CSI feedback was developed in [147], which allows reducing feedback dimension while maintaining the IA feasibility. Furthermore, the authors in [146, 148] improved the IA network performance at low SNR values., while a MIMO-based orthogonal frequency division multiplexing interference network was initially studied practically in [149], where channel gains measured using a flexible software-defined radio were consistent with theoretical and simulation results. In [150], a transmit antenna selection was introduced in order to increase the sum-rate performance of the IA-based MIMO network, where authors verified the practical feasibility of the system through practical implementation. These studies have demonstrated a significant move to the IA implementation in practice. Hence, IA techniques can be efficiently coupled with CR and EH since both latter techniques have been already used in practical systems [151–153].

4.1.3 Motivation

Nowadays, numerous techniques are considered to be a candidate that can be executed in the 5G communication networks. The main conditions required for the 5G candidates are higher spectral and energy efficiency, lower end-to-end latency, more connected nodes, etc. [154]. Therefore, IA-embedded networks can improve the spectral efficiency by mitigating interference while the CRNs can utilize unused spectrum bands to connect more

nodes. In addition, 5G networks can be more energy efficient using RF SWIPT with different EH protocols. Hence, a joint study of the CR, IA and EH techniques could contribute a thorough insight into how the next generation communication networks should be designed. Despite a large number of research works on the CR, IA and SWIPT, all of them have been studied separately. In other words, in the literature, each of these techniques has been studied separately from the other two technologies. For example, recent IA advances were ignored in CR or SWIPT systems [50, 80, 132]. Moreover, the interference in IA networks was just removed instead of being employed for EH goals in [116, 129]. In addition, the SN's performance was suffered from the limited transmit power due to the applied ITC from the PRs in underlay CR systems, while the interference at PRs might be managed through IA [136, 155]. Hence, the main aim of this Chapter is to investigate IA-based underlay CR systems with the EH-enabled relay over Rayleigh fading channels in the case of the perfect and the imperfect CSI.

4.2 Contribution of the Chapter

Main contributions are as follows:

- The performance of the PRs and the EH-based relay in the TS and PS modes under the interference presence is investigated. Moreover, precoding and interference suppression beamforming (BF) matrices are applied to mitigate the negative effect of interference at primary and secondary receivers. The management of interference allows avoiding ITC implementation at the PRs, which consequently gives a possibility to increase the power level at the secondary transmitters.

- The instantaneous capacity performance is assessed for the PUs and SUs in the TS and PS methods. In addition, the optimal values of TS and PS portions are determined for different CSI scenarios. From the obtained results, PS relaying (PSR) shows better performance than the TS relaying (TSR). Then, some useful insights into how the CSI quality impacts on BER and capacity performance for the TS and PS-based systems are provided.

- Closed-form OP expressions of the PUs and the SU are determined. Moreover, Monte-Carlo simulations for the OP are consistent with the analytical results showing that the performance of the PSR mode outperforms that of the TSR system for secondary destinations, while, for the PRs in the 1^{st} time slot, the OP of the TSR outperforms that of the PSR.

The remainder of the Chapter is organized as the next. The system model with employed IA for perfect and imperfect CSI scenarios is described in Section 4.3, while the

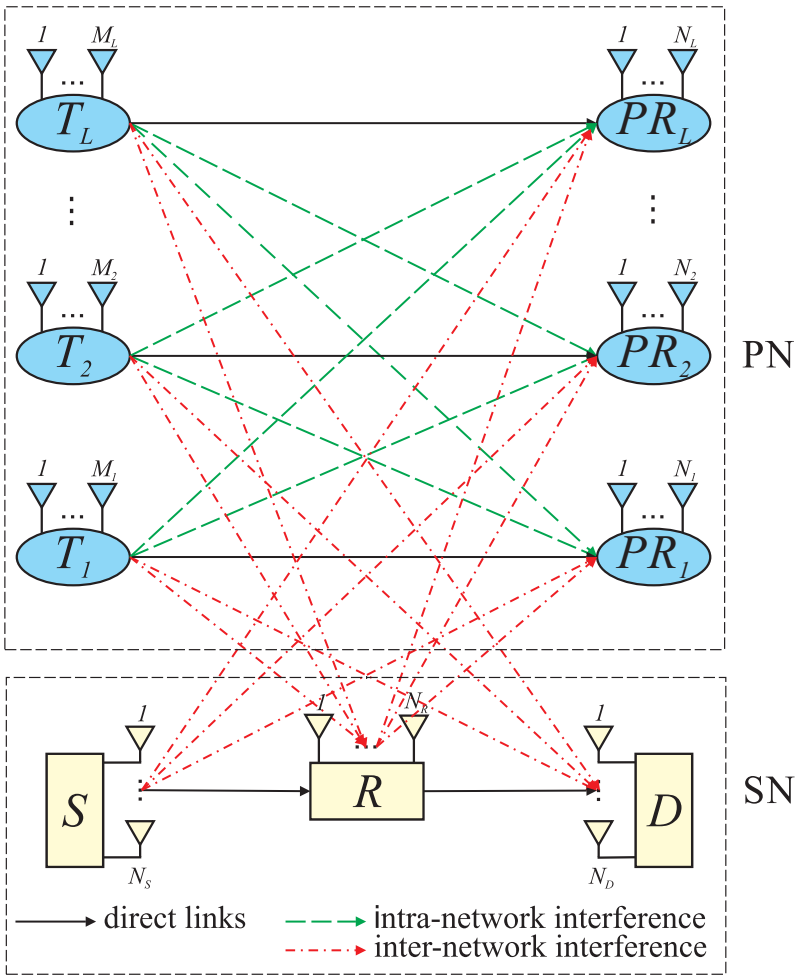

Figure 4.2. The IA- and EH-based CRN with L PUs and one SN sharing the spectrum simultaneously.

study of TSR and PSR protocols with instantaneous capacity derivations are presented in Sections 4.4 and 4.5, respectively. Section 4.6 derives the OP expressions of the PUs and the SUs. Numerical results are presented and discussed in Section 4.7. Finally, the Chapter is concluded in Section 4.8.

Notation: Vectors and matrices are denoted by lowercase and uppercase bold symbols, e.g., $\mathbf{x}$ and $\mathbf{X}$, respectively, while $\mathbf{I}$ represents the identity matrix. The superscripts $(\cdot)^{\dagger}$ and $(\cdot)^{[\iota]}$ stand for the Hermitian transpose and time slot index, accordingly. $\mathrm{tr}(\mathbf{X})$ calculates the trace of $\mathbf{X}$. $\|\mathbf{x}\|$ and $|x|$ denote the Euclidean norm of $\mathbf{x}$ and the absolute value of x, respectively. $\mathbb{E}(\cdot)$ and $\mathbb{V}(\cdot)$ are the expectation and variance operators, respectively. $\mathbb{C}^{N\times M}$ is the space of complex $N \times M$ matrices. $\mathcal{CN}(a, b)$ denotes the complex normal distribution with a mean and b variance. Finally, $\mathrm{span}(\mathbf{X})$ and $\mathrm{eig}\,(\mathbf{X})$ denote the vector space spanned by the column vectors and the eigenvectors of $\mathbf{X}$, accordingly.

4.3 System Model

The proposed system model is shown in Fig. 4.2, where a MIMO CRN consisting of one SN and L PU-pairs is presented. Each primary transmitter T_i, $i \in \{1, 2, ..., L\}$, communicates to its corresponding receiver PR_j, $j \in \{1, 2, ..., L\}$, by causing interference to the other PRs and SUs. The SN consists of S, R and D. An energy-constrained R can scavenge the energy from the desired and interfering signals. It is assumed that R utilizes all the harvested energy at each EH time interval to maintain the S-D communication within the half-duplex DF relaying. Other nodes than R, i.e., T_i, PR_j S and D are assumed to be provided with external power sources. It is also assumed that all nodes support MIMO antennas, where each appropriate channel remains constant through a transmission time slot ι, with $\iota \in \{1, 2\}$, and varies independently in every time period.

In the PN, the intra-network channels between T_i and PR_j are denoted by $\mathbf{H}_{j,i}^{[\iota]} \in \mathbb{C}^{N_j \times M_i}$, $\forall i, j \in \{1, 2, ..., L\}$, where PR_j and T_i nodes are deployed with N_j and M_i antennas, respectively. In the SN, channels between S-R and R-D transmission links are described by $\mathbf{H}_{R,S} \in \mathbb{C}^{N_R \times N_S}$ and $\mathbf{H}_{D,R} \in \mathbb{C}^{N_D \times N_R}$, accordingly. N_S, N_R and N_D denote the numbers of antennas at S, R and D, respectively. Inter-network interference channels are denoted by $\mathbf{H}_{j,R} \in \mathbb{C}^{N_j \times N_R}$, $\mathbf{H}_{j,S} \in \mathbb{C}^{N_j \times N_S}$ and $\mathbf{H}_{R,i} \in \mathbb{C}^{N_R \times M_i}$. Moreover, every channel link can be characterized by the corresponding distance and the path loss exponent[1], i.e., $d_{m,n}$ and $\tau_{m,n}$, $\forall n \in \mathcal{A} = \{1, 2, ..., L, S, R\}$ and $\forall m \in \mathcal{B} = \{1, 2, ..., L, R, D\}$. Each entry of $\mathbf{H}$ is assumed to be an i.n.i.d. Rayleigh block fading modeled as $\mathcal{CN}(0, 1)$.

It is assumed that a global CSI is available at each node[2]. Each transmit node l with the power of P_l employs a precoding BF matrix $\mathbf{V}_l \in \mathbb{C}^{(M_l \text{ or } N_l) \times f_l}$, with $\text{tr}\{\mathbf{V}_l \mathbf{V}_l^{\dagger}\} = 1$, $\forall l \in \mathcal{A}$, where f_l is the number of data streams that is sent from the corresponding transmit node. Furthermore, every receiver employs the interference suppression matrix $\mathbf{U}_m \in \mathbb{C}^{N_m \times f_m}$, $\forall m \in \mathcal{B}$, where f_m denotes the number of data streams. Thus, PR_j, within the time slot ι, obtains the following signal

$$\mathbf{y}_j^{[\iota]} = \underbrace{\sum_{i=1, i \neq j}^{L} \sqrt{\frac{P_i}{d_{j,i}^{\tau_{j,i}}}} \mathbf{U}_j^{[\iota]\dagger} \mathbf{H}_{j,i}^{[\iota]} \mathbf{V}_i^{[\iota]} \mathbf{s}_i + F^{[\iota]}}_{\text{interference from PN and SN}} + \tilde{\mathbf{n}}_j^{[\iota]} + \underbrace{\sqrt{\frac{P_j}{d_{j,j}^{\tau_{j,j}}}} \mathbf{U}_j^{[\iota]\dagger} \mathbf{H}_{j,j}^{[\iota]} \mathbf{V}_j^{[\iota]} \mathbf{s}_j}_{\text{desired signal}}, \tag{4.1}$$

[1] In wireless communications, the power attenuation increases logarithmically with the distance between the transmitter and the receiver [156].

[2] In different works in the literature, it is common to accept that any primary node exploits pilot signals which can be systematically transmitted to maintain the channel estimation and synchronization [157, §12.3.1], [158]. Saying so, each secondary node is able to attain own channel estimation between the primary/secondary transmitters and itself, by the condition that the secondary node participates in this training process.

where $\tilde{\mathbf{n}}_j^{[\iota]} = \mathbf{U}_j^{[\iota]\dagger}\mathbf{n}_j^{[\iota]}$ denotes the AWGN vector with the effective zero mean at the output of the beamformer, with $\mathbb{E}\{\tilde{\mathbf{n}}_j^{[\iota]}\tilde{\mathbf{n}}_j^{[\iota]\dagger}\} = \sigma_{\tilde{n}_j}^2\mathbf{I}$. Moreover, $\mathbb{E}\{\mathbf{s}_l\mathbf{s}_l^\dagger\} = \mathbf{I}$, with $\forall l \in \mathcal{A}$, where the $\mathbf{s}_l$ vector contains symbols of the desired constellation taken from i.i.d. Gaussian input signaling. Thus, all transmit nodes satisfy the average power constraint by meeting all the aforementioned conditions. Then, interference caused by the SN to PR_j denotes as

$$F^{[\iota]} = \begin{cases} \sqrt{\frac{P_S}{d_{j,S}^{\tau_{j,S}}}}\mathbf{U}_j^{[1]\dagger}\mathbf{H}_{j,S}\mathbf{V}_S\mathbf{s}_S, \text{ if } \iota = 1, \\ \sqrt{\frac{P_R}{d_{j,R}^{\tau_{j,R}}}}\mathbf{U}_j^{[2]\dagger}\mathbf{H}_{j,R}\mathbf{V}_R\mathbf{s}_R, \text{ if } \iota = 2. \end{cases} \tag{4.2}$$

Within 1^{st} time slot of the relaying process, R receives the following signal

$$\mathbf{y}_R = \underbrace{\frac{\sqrt{P_S}\mathbf{U}_R^\dagger\mathbf{H}_{R,S}\mathbf{V}_S\mathbf{s}_S}{\sqrt{d_{R,S}^{\tau_{R,S}}}}}_{\text{desired signal}} + \underbrace{\sum_{i=1}^{L}\frac{\sqrt{P_i}\mathbf{U}_R^\dagger\mathbf{H}_{R,i}\mathbf{V}_i^{[1]}\mathbf{s}_i}{\sqrt{d_{R,i}^{\tau_{R,i}}}}}_{\text{interference from PN}} + \tilde{\mathbf{n}}_R, \tag{4.3}$$

where $\tilde{\mathbf{n}}_R = \mathbf{U}_R^\dagger\mathbf{n}_R$ denotes the effective AWGN noise at R after the applied interference suppression BF matrices.

Furthermore, R decodes the desired signal $\mathbf{s}_S$ and forwards it to D. Thus, the received signal at D can be written as

$$\mathbf{y}_D = \underbrace{\frac{\sqrt{P_R}\mathbf{U}_D^\dagger\mathbf{H}_{D,R}\mathbf{V}_R\hat{\mathbf{s}}_S}{\sqrt{d_{D,R}^{\tau_{D,R}}}}}_{\text{desired signal}} + \underbrace{\sum_{i=1}^{L}\frac{\sqrt{P_i}\mathbf{U}_D^\dagger\mathbf{H}_{D,i}\mathbf{V}_i^{[2]}\mathbf{s}_i}{\sqrt{d_{D,i}^{\tau_{D,i}}}}}_{\text{interference from PN}} + \tilde{\mathbf{n}}_D, \tag{4.4}$$

where $\hat{\mathbf{s}}_S$ stands for decoded signal at R while $\tilde{\mathbf{n}}_D = \mathbf{U}_D^\dagger\mathbf{n}_D$ denotes the effective AWGN noise at D.

All the interference at receivers can be perfectly managed when IA is feasible. Therefore, to cancel those interference, the following conditions should be satisfied at PR_j [125]

$$\mathbf{U}_j^{[\iota]\dagger}\mathbf{H}_{j,i}^{[\iota]}\mathbf{V}_i^{[\iota]} = \mathbf{0}, \ \forall i,j \in \{1,2,...,L\} \text{ and } \forall i \neq j, \tag{4.5a}$$

$$\mathbf{U}_j^{[\iota]\dagger}\mathbf{W}^{[\iota]} = \mathbf{0}, \text{ where } \mathbf{W}^{[\iota]} = \begin{cases} \mathbf{H}_{j,S}\mathbf{V}_S, \text{ if } \iota = 1, \\ \mathbf{H}_{j,R}\mathbf{V}_R, \text{ if } \iota = 2, \end{cases} \tag{4.5b}$$

$$\text{rank}\left(\mathbf{U}_j^{[\iota]\dagger}\mathbf{H}_{j,j}^{[\iota]}\mathbf{V}_j^{[\iota]}\right) = f_j, \ \forall j \in \{1,2,...,L\}, \tag{4.5c}$$

and at R and D as

$$\mathbf{U}_R^{\dagger}\mathbf{H}_{R,i}\mathbf{V}_i^{[1]} = \mathbf{0},\ \forall i \in \{1, 2, ..., L\}, \tag{4.6a}$$

$$\text{rank}\left(\mathbf{U}_R^{\dagger}\mathbf{H}_{R,S}\mathbf{V}_S\right) = f_S,\ \text{and} \tag{4.6b}$$

$$\mathbf{U}_D^{\dagger}\mathbf{H}_{D,i}\mathbf{V}_i^{[2]} = \mathbf{0},\ \forall i \in \{1, 2, ..., L\}, \tag{4.6c}$$

$$\text{rank}\left(\mathbf{U}_D^{\dagger}\mathbf{H}_{D,R}\mathbf{V}_R\right) = f_D,\ \text{respectively}. \tag{4.6d}$$

When the conditions given in (4.5) are met, there is no need for PR_j to apply the ITC to the SN. Hence, the secondary transmit nodes can broadcast with any available power level [116].

This Chapter concentrates on SWIPT instead of a DoF similarly as in [116] and [134]. Thus, each transmitter is assumed to broadcast only one data stream f_l, $\forall l \in \mathcal{A}$, to the dedicated user. Hence, the BF matrices can be replaced by the corresponding vectors. Moreover, as symmetric networks are considered, all nodes are assumed to have the same antenna parameters, i.e., $M_i = N_S = M$, $N_j = N_R = N_D = N$. Therefore, due to the IA feasibility analysis, the largest number of user pairs in the proposed system should satisfy the following condition [116]

$$L + 1 \leq M + N - 1. \tag{4.7}$$

In this chapter, the QoS of PR_j is considered as the service of the PUs in a high priority. The transmission rate can directly reflect the variability of PUs' QoS, so a rate threshold $\mathcal{R}_{\text{th}}^j$ is defined according to the QoS requirement of PR_j. Hence, the QoS of PR_j can be satisfied if $\mathcal{R}^j \geq \mathcal{R}_{\text{th}}^j$, which means that SUs can not transmit over the licensed band unless the mentioned condition is satisfied.

4.3.1 Imperfect CSI

An assumption of the perfect CSI is highly idealistic in practice. Thus, this Chapter examines the effect of imperfect CSI on the IA cancellation at the receiving node. The CSI mismatch can be described by [125]

$$\hat{\mathbf{H}} = \mathbf{H} + \mathbf{E}, \tag{4.8}$$

where $\hat{\mathbf{H}}$ is the observed mismatched channel, $\mathbf{H} \sim \mathcal{CN}(0, \mathbf{I})$ stands for the real channel matrix and $\mathbf{E}$ denotes the inaccuracy degree in the estimated CSI which is independent from $\mathbf{H}$. The $\mathbf{E}$ can be described, considering the nominal transmit SNR ρ, as $\mathbf{E} \sim \mathcal{CN}(0, \lambda\mathbf{I})$ with $\lambda = \psi\rho^{-\kappa}$, where λ is an error variance which represents different acquisition scenarios for any constant values of $\kappa \geq 0$ and $\psi > 0$. Considering this

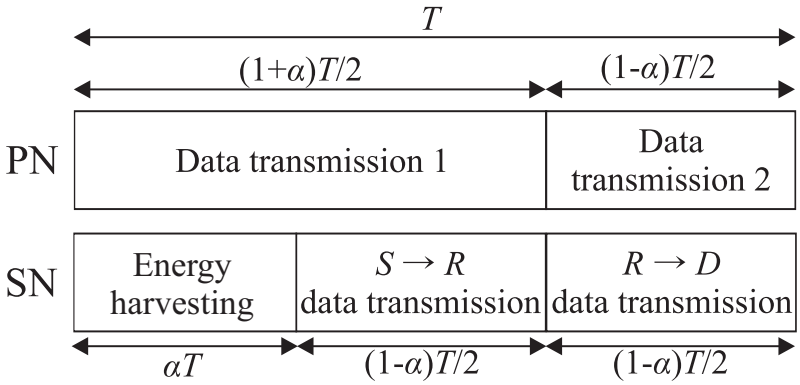

Figure 4.3. The time frame structure of the TSR.

model, the perfect CSI can be obtained when $\kappa \to \infty$ for $\rho > 1$. Hence, the real channel matrix, conditioning on $\hat{\mathbf{H}}$, can be written as [159]

$$\mathbf{H} = \frac{1}{1+\lambda}\hat{\mathbf{H}} + \tilde{\mathbf{H}}, \tag{4.9}$$

where $\tilde{\mathbf{H}} \sim \mathcal{CN}(0, \frac{\lambda}{1+\lambda}\mathbf{I})$ is independent of $\hat{\mathbf{H}}$.

4.4 Time-Switching Relaying

Fig. 4.3 depicts the TSR protocol, where the required time for the S-D information transmission is taken as T and the time fractions of αT, with $0 \leq \alpha \leq 1$, is allotted for EH, whereas the other two equal time proportions $(1-\alpha)T/2$ are allocated for the S-R and R-D data transmission sessions, accordingly [127]. In the case of the PN, T_i conveys its information to the respective receiver over time T, which can be divided into two time periods, i.e., $(1+\alpha)T/2$ and $(1-\alpha)T/2$, to align with the time structure of the SN. Due to the proposed TSR system model, within the EH time period, R receives the following signal

$$\mathbf{y}_R^{\text{EH}} = \sqrt{\frac{P_S}{d_{R,S}^{\tau_{R,S}}}}\mathbf{H}_{R,S}\mathbf{v}_S s_S + \sum_{i=1}^{L}\sqrt{\frac{P_i}{d_{R,i}^{\tau_{R,i}}}}\mathbf{H}_{R,i}\mathbf{v}_i^{[1]}s_i + \mathbf{n}_R. \tag{4.10}$$

Then, by neglecting the relatively small energy scavenged from the noise, the harvested energy at R can be written as [127]

$$E_H^{\text{TSR}} = \eta\alpha T\left(\frac{P_S\left\|\mathbf{H}_{R,S}\mathbf{v}_S\right\|^2}{d_{R,S}^{\tau_{R,S}}} + \sum_{i=1}^{L}\frac{P_i\left|\left|\mathbf{H}_{R,i}\mathbf{v}_i^{[1]}\right|\right|^2}{d_{R,i}^{\tau_{R,i}}}\right). \tag{4.11}$$

The relation between harvested energy and the relay transmit power can be written as

$$P_R^{\text{TSR}} = E_H^{\text{TSR}}/((1-\alpha)T/2). \tag{4.12}$$

Moreover, by assuming that all the harvested power is utilized for data transmission, we can rewrite the relay transmit power by using (4.11) as

$$P_R^{\text{TSR}} = \frac{2\alpha\eta}{1-\alpha}\left(\frac{P_S\,||\mathbf{H}_{R,S}\mathbf{v}_S||^2}{d_{R,S}^{\tau_{R,S}}} + \sum_{i=1}^{L}\frac{P_i\left|\left|\mathbf{H}_{R,i}\mathbf{v}_i^{[1]}\right|\right|^2}{d_{R,i}^{\tau_{R,i}}}\right), \tag{4.13}$$

where η denotes the EH conversion efficiency, with $0 < \eta < 1$. During the S-R data transmission phase, considering imperfect CSI in (4.9) and interference suppression vectors, the received information signal at R can be written as

$$\begin{aligned}
\mathbf{y}_R^{IT} =& \sqrt{\frac{P_S}{d_{R,S}^{\tau_{R,S}}}}\mathbf{u}_R^{\dagger}\left(\frac{1}{1+\lambda}\hat{\mathbf{H}}_{R,S}+\tilde{\mathbf{H}}_{R,S}\right)\mathbf{v}_S s_S \\
&+\sum_{i=1}^{L}\sqrt{\frac{P_i}{d_{R,i}^{\tau_{R,i}}}}\mathbf{u}_R^{\dagger}\left(\frac{1}{1+\lambda}\hat{\mathbf{H}}_{R,i}+\tilde{\mathbf{H}}_{R,i}\right)\mathbf{v}_i^{[1]}s_i+\tilde{\mathbf{n}}_R \\
=& \underbrace{\frac{1}{1+\lambda}\sqrt{\frac{P_S}{d_{R,S}^{\tau_{R,S}}}}\mathbf{u}_R^{\dagger}\hat{\mathbf{H}}_{R,S}\mathbf{v}_S s_S}_{\text{desired signal}} + \underbrace{\sqrt{\frac{P_S}{d_{R,S}^{\tau_{R,S}}}}\mathbf{u}_R^{\dagger}\tilde{\mathbf{H}}_{R,S}\mathbf{v}_S s_S}_{\text{CSI mismatch of desired signal}} \\
&+\underbrace{\frac{1}{1+\lambda}\sum_{i=1}^{L}\sqrt{\frac{P_i}{d_{R,i}^{\tau_{R,i}}}}\mathbf{u}_R^{\dagger}\hat{\mathbf{H}}_{R,i}\mathbf{v}_i^{[1]}s_i}_{\text{inter-network interference = 0}} + \underbrace{\sum_{i=1}^{L}\sqrt{\frac{P_i}{d_{R,i}^{\tau_{R,i}}}}\mathbf{u}_R^{\dagger}\tilde{\mathbf{H}}_{R,i}\mathbf{v}_i^{[1]}s_i}_{\text{inter-network interference due to CSI mismatch}} + \tilde{\mathbf{n}}_R.
\end{aligned} \tag{4.14}$$

The corresponding signal-to-interference-plus-noise ratio (SINR) at R, from (4.14), can be written as

$$\gamma_R = \frac{\frac{P_S}{d_{R,S}^{\tau_{R,S}}(1+\lambda)^2}||\mathbf{u}_R^{\dagger}\hat{\mathbf{H}}_{R,S}\mathbf{v}_S||^2}{\frac{P_S}{d_{R,S}^{\tau_{R,S}}}||\mathbf{u}_R^{\dagger}\tilde{\mathbf{H}}_{R,S}\mathbf{v}_S||^2 + I_{\text{PN}}^{\text{TSR}} + \sigma_{\tilde{n}_R}^2}, \tag{4.15}$$

where $\sigma_{\tilde{n}_R}^2$ is the noise power at R and interference from T_i is denoted by

$$I_{\text{PN}}^{\text{TSR}} = \sum_{i=1}^{L}\frac{P_i\left|\left|\mathbf{u}_R^{\dagger}\tilde{\mathbf{H}}_{R,i}\mathbf{v}_i^{[1]}\right|\right|^2}{d_{R,i}^{\tau_{R,i}}}. \tag{4.16}$$

Similar to (4.14), the signal received by D can be written as

$$\mathbf{y}_D = \underbrace{\frac{1}{1+\lambda}\sqrt{\frac{P_R^{\text{TSR}}}{d_{D,R}^{\tau_{D,R}}}}\mathbf{u}_D^{\dagger}\hat{\mathbf{H}}_{D,R}\mathbf{v}_R s_R}_{\text{desired signal}} + \underbrace{\sqrt{\frac{P_R^{\text{TSR}}}{d_{D,R}^{\tau_{D,R}}}}\mathbf{u}_D^{\dagger}\tilde{\mathbf{H}}_{D,R}\mathbf{v}_R s_R + \sum_{i=1}^{L}\sqrt{\frac{P_i}{d_{D,i}^{\tau_{D,i}}}}\mathbf{u}_D^{\dagger}\tilde{\mathbf{H}}_{D,i}\mathbf{v}_i^{[2]}s_i}_{\text{interference due to CSI mismatch}} + \tilde{\mathbf{n}}_D. \tag{4.17}$$

Further, the respective SINR at D can be written as

$$\gamma_D = \frac{\frac{P_R^{\text{TSR}}}{d_{D,R}^{\tau_{D,R}}(1+\lambda)^2}||\mathbf{u}_D^{\dagger}\hat{\mathbf{H}}_{D,R}\mathbf{v}_R||^2}{\frac{P_R^{\text{TSR}}}{d_{D,R}^{\tau_{D,R}}}||\mathbf{u}_D^{\dagger}\tilde{\mathbf{H}}_{D,R}\mathbf{v}_R||^2 + G_{\text{PN}} + \sigma_{\tilde{n}_D}^2}, \tag{4.18}$$

where $\sigma_{\tilde{n}_D}^2$ denotes the noise power at D and interference from T_i is denoted by

$$G_{\text{PN}} = \sum_{i=1}^{L}\frac{P_i||\mathbf{u}_D^{\dagger}\tilde{\mathbf{H}}_{D,i}\mathbf{v}_i^{[2]}||^2}{d_{D,i}^{\tau_{D,i}}}. \tag{4.19}$$

Furthermore, the SINR for PR_j is derived as

$$\gamma_j^{[\iota]} = \frac{P_j||\mathbf{u}_j^{[\iota]\dagger}\hat{\mathbf{H}}_{j,j}^{[\iota]}\mathbf{v}_j^{[\iota]}||^2}{d_{j,j}^{\tau_{j,j}}(1+\lambda)^2\left(A^{[\iota]} + B_{\text{TSR}}^{[\iota]} + \sigma_{\tilde{n}_j}^{[\iota]2}\right)}, \tag{4.20}$$

where the intra-network interference from another T_i due to the CSI mismatch is written as

$$A^{[\iota]} = \frac{P_j||\mathbf{u}_j^{[\iota]\dagger}\tilde{\mathbf{H}}_{j,j}^{[\iota]}\mathbf{v}_j^{[\iota]}||^2}{d_{j,j}^{\tau_{j,j}}} + \frac{P_i||\mathbf{u}_j^{[\iota]\dagger}\tilde{\mathbf{H}}_{j,i}^{[\iota]}\mathbf{v}_i^{[\iota]}||_{i\neq j}^2}{d_{j,i}^{\tau_{j,i}}}, \tag{4.21}$$

while the inter-network interference from SN is denoted by

$$B_{\text{TSR}}^{[\iota]} = \begin{cases} \frac{P_S}{d_{j,S}^{\tau_{j,S}}}||\mathbf{u}_j^{[1]\dagger}\tilde{\mathbf{H}}_{j,S}\mathbf{v}_S||^2, \text{ if } \iota = 1, \\ \frac{P_R^{\text{TSR}}}{d_{j,R}^{\tau_{j,R}}}||\mathbf{u}_j^{[2]\dagger}\tilde{\mathbf{H}}_{j,R}\mathbf{v}_R||^2, \text{ if } \iota = 2. \end{cases} \tag{4.22}$$

4.4.1 Capacity for TSR

The instantaneous capacity for PR_j can be written as [160]

$$\mathcal{C}_j = \log_2(1+\gamma_j), \tag{4.23}$$

where γ_j denotes the SINR of PR_j. Now, after substituting (4.20) into (4.23) and considering the exploited two-time slots, the instantaneous capacity for the P_j is derived as

$$\mathcal{C}_j^{\text{TSR}} = \sum_{\iota=1}^{2} J^{[\iota]} \log_2 \left(1 + \frac{\frac{P_j}{d_{j,j}^{\tau_{j,j}}(1+\lambda)^2} ||\mathbf{u}_j^{[\iota]\dagger} \hat{\mathbf{H}}_{j,j}^{[\iota]} \mathbf{v}_j^{[\iota]}||^2}{A^{[\iota]} + B_{\text{TSR}}^{[\iota]} + \sigma_{\tilde{n}_j}^{2\ [\iota]}} \right), \tag{4.24}$$

where $J^{[\iota]} = \begin{cases} \frac{1+\alpha}{2}, & \text{if } \iota = 1, \\ \frac{1-\alpha}{2}, & \text{if } \iota = 2. \end{cases}$

Moreover, the end-to-end instantaneous capacity for D can be calculated by the weakest channel between the S-R and R-D transmission channels, which can be written as

$$\mathcal{C}_D = \frac{1}{2} \log_2 \left(1 + \min\left(\gamma_R, \gamma_D\right)\right). \tag{4.25}$$

Hence, by using (4.15), (4.18) and (4.25), the instantaneous capacity expression in (4.25) can be rewritten for the TSR protocol as

$$\mathcal{C}_D^{\text{TSR}} = \frac{1-\alpha}{2} \log_2 \left[1 + \min \left(\frac{\frac{P_S}{d_{R,S}^{\tau_{R,S}}(1+\lambda)^2} ||\mathbf{u}_R^\dagger \hat{\mathbf{H}}_{R,S} \mathbf{v}_S||^2}{\frac{P_S}{d_{R,S}^{\tau_{R,S}}} ||\mathbf{u}_R^\dagger \tilde{\mathbf{H}}_{R,S} \mathbf{v}_S||^2 + I_{\text{PN}}^{\text{TSR}} + \sigma_{\tilde{n}_R}^2}, \right. \right.$$
$$\left. \left. \frac{\frac{P_R^{\text{TSR}}}{d_{D,R}^{\tau_{D,R}}(1+\lambda)^2} ||\mathbf{u}_D^\dagger \hat{\mathbf{H}}_{D,R} \mathbf{v}_R||^2}{\frac{P_R^{\text{TSR}}}{d_{D,R}^{\tau_{D,R}}} ||\mathbf{u}_D^\dagger \tilde{\mathbf{H}}_{D,R} \mathbf{v}_R||^2 + G_{\text{PN}} + \sigma_{\tilde{n}_D}^2} \right) \right]. \tag{4.26}$$

As the derivation of (4.26) is complicated, the instantaneous capacity can be assessed only numerically.

4.5 Power-Splitting Relaying

In the PSR protocol, the total time period of T is divided into two equal time fractions to support the S-R and R-D data transmissions [138] (see Fig. 4.4). During the first half of the time period, R utilizes a coefficient θ ($0 < \theta < 1$) to determine a part of the obtained signal power to harvest, while the remaining signal portion $(1-\theta)$ is used for the S-R data transmission purpose. Thus, within the EH time period, the obtained signal at R can be written as

$$\mathbf{y}_R^{\text{EH}} = \sqrt{\frac{\theta P_S}{d_{R,S}^{\tau_{R,S}}}} \mathbf{H}_{R,S} \mathbf{v}_S s_S + \sum_{i=1}^{L} \sqrt{\frac{\theta P_i}{d_{R,i}^{\tau_{R,i}}}} \mathbf{H}_{R,i} \mathbf{v}_i^{[1]} s_i + \sqrt{\theta} \mathbf{n}_R. \tag{4.27}$$

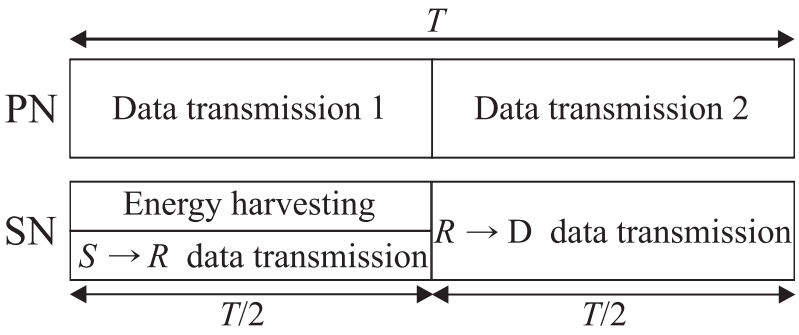

Figure 4.4. Time frame structure of the PSR.

Then, R harvests the following signal [127]

$$E_H^{\text{PSR}} = \frac{\eta\theta T}{2}\left(\frac{P_S\left|\left|\mathbf{H}_{R,S}\mathbf{v}_S\right|\right|^2}{d_{R,S}^{\tau_{R,S}}} + \sum_{i=1}^{L}\frac{P_i\left|\left|\mathbf{H}_{R,i}\mathbf{v}_i^{[1]}\right|\right|^2}{d_{R,i}^{\tau_{R,i}}}\right). \tag{4.28}$$

The relationship between the relay transmit power and the harvested energy for PSR protocol can be described by [127]

$$P_R^{\text{PSR}} = 2E_H^{\text{PSR}}/T. \tag{4.29}$$

Now, the transmit power at R can be rewritten as

$$P_R^{\text{PSR}} = \eta\theta\left(\frac{P_S\left|\left|\mathbf{H}_{R,S}\mathbf{v}_S\right|\right|^2}{d_{R,S}^{\tau_{R,S}}} + \sum_{i=1}^{L}\frac{P_i\left|\left|\mathbf{H}_{R,i}\mathbf{v}_i^{[1]}\right|\right|^2}{d_{R,i}^{\tau_{R,i}}}\right). \tag{4.30}$$

Furthermore, using (4.9) and applying interference suppression vector $\mathbf{u}_R$, the received signal at R is calculated by

$$\begin{aligned}\mathbf{y}_R^{IT} = &\underbrace{\frac{1}{1+\lambda}\sqrt{\frac{(1-\theta)P_S}{d_{R,S}^{\tau_{R,S}}}}\mathbf{u}_R^\dagger\hat{\mathbf{H}}_{R,S}\mathbf{v}_S s_S}_{\text{desired signal}} + \underbrace{\sqrt{\frac{(1-\theta)P_S}{d_{R,S}^{\tau_{R,S}}}}\mathbf{u}_R^\dagger\tilde{\mathbf{H}}_{R,S}\mathbf{v}_S s_S}_{\text{interference from } S \text{ due to CSI mismatch}} \\ &+ \underbrace{\sum_{i=1}^{L}\sqrt{\frac{(1-\theta)P_i}{d_{R,i}^{\tau_{R,i}}}}\mathbf{u}_R^\dagger\tilde{\mathbf{H}}_{R,i}\mathbf{v}_i^{[1]}s_i}_{\text{interference from PN due to CSI mismatch}} + \tilde{\mathbf{n}}_R.\end{aligned} \tag{4.31}$$

Hence, the corresponding SINR at R can be derived by

$$\gamma_R = \frac{\frac{P_S(1-\theta)}{d_{R,S}^{\tau_{R,S}}(1+\lambda)^2}\left|\left|\mathbf{u}_R^\dagger\hat{\mathbf{H}}_{R,S}\mathbf{v}_S\right|\right|^2}{\frac{P_S(1-\theta)}{d_{R,S}^{\tau_{R,S}}}\left|\left|\mathbf{u}_R^\dagger\tilde{\mathbf{H}}_{R,S}\mathbf{v}_S\right|\right|^2 + I_{\text{PN}}^{\text{PSR}} + \sigma_{\tilde{n}_R}^2}, \tag{4.32}$$

where interference from T_i is denoted by

$$I_{\text{PN}}^{\text{PSR}} = \sum_{i=1}^{L} \frac{(1-\theta)P_i||\mathbf{u}_R^{\dagger}\tilde{\mathbf{H}}_{R,i}\mathbf{v}_i^{[1]}||^2}{d_{R,i}^{\tau_{R,i}}}. \tag{4.33}$$

Further, D receives the following signal

$$\begin{aligned}\mathbf{y}_D = &\underbrace{\frac{1}{1+\lambda}\sqrt{\frac{P_R^{\text{PSR}}}{d_{D,R}^{\tau_{D,R}}}}\mathbf{u}_D^{\dagger}\hat{\mathbf{H}}_{D,R}\mathbf{v}_R s_R}_{\text{desired signal}} + \tilde{\mathbf{n}}_D \\ &+ \underbrace{\sqrt{\frac{P_R^{\text{PSR}}}{d_{D,R}^{\tau_{D,R}}}}\mathbf{u}_D^{\dagger}\tilde{\mathbf{H}}_{D,R}\mathbf{v}_R s_R + \sum_{i=1}^{L}\sqrt{\frac{P_i}{d_{D,i}^{\tau_{D,i}}}}\mathbf{u}_D^{\dagger}\tilde{\mathbf{H}}_{D,i}\mathbf{v}_i^{[2]}s_i}_{\text{interference due to CSI mismatch}}.\end{aligned} \tag{4.34}$$

Then, the corresponding SINR of D from (4.34) is calculated by

$$\gamma_D = \frac{\frac{P_R^{\text{PSR}}}{d_{D,R}^{\tau_{D,R}}(1+\lambda)^2}||\mathbf{u}_D^{\dagger}\hat{\mathbf{H}}_{D,R}\mathbf{v}_R||^2}{\frac{P_R^{\text{PSR}}}{d_{D,R}^{\tau_{D,R}}}||\mathbf{u}_D^{\dagger}\tilde{\mathbf{H}}_{D,R}\mathbf{v}_R||^2 + G_{\text{PN}} + \sigma_{\tilde{n}_D}^2}. \tag{4.35}$$

In the case of the PN, the SINR at PR_j can be as

$$\gamma_j^{[\iota]} = \frac{P_j||\mathbf{u}_j^{[\iota]\dagger}\hat{\mathbf{H}}_{j,j}^{[\iota]}\mathbf{v}_j^{[\iota]}||^2}{d_{j,j}^{\tau_{j,j}}(1+\lambda)^2\left(A^{[\iota]} + B_{\text{PSR}}^{[\iota]} + \sigma_{\tilde{n}_j}^{[\iota]2}\right)}, \tag{4.36}$$

where the interference from the SN is expressed as

$$B_{\text{PSR}}^{[\iota]} = \begin{cases} \frac{P_S}{d_{j,S}^{\tau_{j,S}}}||\mathbf{u}_j^{[1]\dagger}\tilde{\mathbf{H}}_{j,S}\mathbf{v}_S||^2, \text{ if } \iota = 1, \\ \frac{P_R^{\text{PSR}}}{d_{j,R}^{\tau_{j,R}}}||\mathbf{u}_j^{[2]\dagger}\tilde{\mathbf{H}}_{j,R}\mathbf{v}_R||^2, \text{ if } \iota = 2. \end{cases} \tag{4.37}$$

4.5.1 Capacity for PSR

The instantaneous capacity for PR_j can be written using (4.36) as

$$\mathcal{C}_j^{\text{PSR}} = \frac{1}{2}\sum_{\iota=1}^{2}\log_2\left(1 + \frac{\frac{P_j}{d_{j,j}^{\tau_{j,j}}(1+\lambda)^2}\left|\left|\mathbf{u}_j^{[\iota]\dagger}\hat{\mathbf{H}}_{j,j}^{[\iota]}\mathbf{v}_j^{[\iota]}\right|\right|^2}{A^{[\iota]} + B_{\text{PSR}}^{[\iota]} + \sigma_{\tilde{n}_j}^{[\iota]2}}\right). \tag{4.38}$$

Furthermore, using (4.25), (4.32) and (4.35), the instantaneous end-to-end capacity expression for D is derived by

$$\mathcal{C}_D^{\text{PSR}} = \frac{1}{2}\log_2\left[1+\min\left(\frac{\frac{P_S(1-\theta)}{d_{R,S}^{\tau_{R,S}}(1+\lambda)^2}||\mathbf{u}_R^\dagger\hat{\mathbf{H}}_{R,S}\mathbf{v}_S||^2}{\frac{P_S(1-\theta)}{d_{R,S}^{\tau_{R,S}}}||\mathbf{u}_R^\dagger\tilde{\mathbf{H}}_{R,S}\mathbf{v}_S||^2+I_{\text{PN}}^{\text{PSR}}+\sigma_{\tilde{n}_R}^2}, \frac{\frac{P_R^{\text{PSR}}}{d_{D,R}^{\tau_{D,R}}(1+\lambda)^2}||\mathbf{u}_D^\dagger\hat{\mathbf{H}}_{D,R}\mathbf{v}_R||^2}{\frac{P_R^{\text{PSR}}}{d_{D,R}^{\tau_{D,R}}}||\mathbf{u}_D^\dagger\tilde{\mathbf{H}}_{D,R}\mathbf{v}_R||^2+G_{\text{PN}}+\sigma_{\tilde{n}_D}^2}\right)\right]. \tag{4.39}$$

Similarly as in the TSR case, the average instantaneous capacity performance for the PSR protocol can be obtained numerically.

4.6 Outage Probability Analysis

4.6.1 Outage Probability of PSR

In wireless communications, the signal is considered to be in an outage if an obtained rate at a receiver is lower than a predefined rate threshold [161]. If the predefined rate threshold of PR_j is $\mathcal{R}_{\text{th}}^j$ (bits/s/Hz), then the OP of PR_j, for one data stream per user and considering the perfect CSI, can be expressed by

$$P_{\text{out}} = \Pr\left[\mathcal{C}_j^{\text{PSR}} < \mathcal{R}_{\text{th}}^j\right] \tag{4.40}$$

Hence, within time slot ι, the OP of PR_j is derived by

$$P_{\text{out}(j)}^{[\iota]} = \Pr\left[\frac{1}{2}\log_2\left(1+\frac{P_j|h_{j,j}^{[\iota]}|^2}{d_{j,j}^{\tau_{j,j}}\sigma_{\tilde{n}_j}^{[\iota]2}}\right) < \mathcal{R}_{\text{th}}^j\right], \tag{4.41}$$

where $h_{j,j}^{[\iota]} = \mathbf{u}_j^{[\iota]\dagger}\mathbf{H}_{j,j}^{[\iota]}\mathbf{v}_j^{[\iota]}$.

As it is assumed that each user has a single data stream, then $\mathbf{v}_j^{[\iota]}$ and $\mathbf{u}_j^{[\iota]}$, with $\forall\iota \in \{1,2\}$, $j \in \{1,2,...,L\}$, are i.n.i.d. unitary vectors which follow $\mathcal{CN}(0,1)$ and independent from $\mathbf{H}_{j,j}^{[\iota]}$. Thus, $h_{j,j}^{[\iota]} = \mathbf{u}_j^{[\iota]\dagger}\mathbf{H}_{j,j}^{[\iota]}\mathbf{v}_j^{[\iota]}$ also follows $\mathcal{CN}$(0,1) [116]. Moreover, the variance of $h_{j,j}^{[\iota]}$ can be described by

$$\mathbb{V}\left(\left|h_{j,j}^{[\iota]}\right|\right) = \mathbb{E}\left(\left|h_{j,j}^{[\iota]}\right|^2\right) - \mathbb{E}\left(\left|h_{j,j}^{[\iota]}\right|\right)^2. \tag{4.42}$$

From (4.42), it is easily can be derived that $\left|h_{j,j}^{[\iota]}\right|^2$ follows an exponential distribution with $\mathcal{CN}(1,1)$ [116].

Proposition 3 The closed-form OP expression for PR_j within time slot ι is written as

$$P_{\text{out}(j)}^{[\iota]} = 1 - \exp\left(-\frac{\xi^j d_{j,j}^{\tau_{j,j}} \sigma_{\tilde{n}_j}^{[\iota]2}}{P_j}\right), \tag{4.43}$$

where $\xi^j = 2^{2\mathcal{R}_{\text{th}}^j} - 1$ is the respective SNR threshold at PR_j.

Proof: See Appendix B.1 for details. ■

Now, regarding the SN where it has EH at R, the OP expression of D is derived, using (4.39) and (4.40), as

$$P_{\text{out}(D)} = \Pr\left[\frac{1}{2}\log_2\left(1 + \min(\gamma_R, \gamma_D)\right) < \mathcal{R}_{\text{th}}^D\right]. \tag{4.44}$$

Proposition 4 The closed-form OP expression for D is written as

$$P_{\text{out}(D)} = 1 - \exp\left(-\xi^D\left(\frac{d_{R,S}^{\tau_{R,S}}\sigma_R^2}{(1-\theta)P_S} + \frac{d_{D,R}^{\tau_{D,R}}\sigma_D^2}{P_R^{PSR}}\right)\right). \tag{4.45}$$

Proof: See Appendix B.2 for details. ■

4.6.2 Outage Probability of TSR

Using the capacity expression for PR_j in (4.24), the OP of PR_j in the TSR protocol can be written as

$$\begin{aligned} P_{\text{out}(j)}^{[\iota]} &= \Pr\left[J^{[\iota]}\log_2(1+\gamma_j^{[\iota]}) < \mathcal{R}_{\text{th}}^j\right] = \Pr\left[J^{[\iota]}\log_2\left(1 + \frac{P_j|h_{j,j}^{[\iota]}|^2}{d_{j,j}^{\tau_{j,j}}\sigma_{\tilde{n}_j}^{[\iota]2}}\right) < \mathcal{R}_{\text{th}}^j\right] \\ &= \Pr\left[\left|h_{j,j}^{[\iota]}\right|^2 < \frac{\left(2^{\frac{\mathcal{R}_{\text{th}}^j}{J^{[\iota]}}} - 1\right) d_{j,j}^{\tau_{j,j}}\sigma_{\tilde{n}_j}^{[\iota]2}}{P_j}\right]. \end{aligned} \tag{4.46}$$

Then, by following the same steps as in Appendix B.1, the closed-form expression for the OP of PR_j in the TSR, within the time slot ι, can be expressed by

$$P_{\text{out}(j)}^{[\iota]} = 1 - \exp\left(-\frac{\left(2^{\frac{\mathcal{R}_{\text{th}}^j}{J^{[\iota]}}} - 1\right) d_{j,j}^{\tau_{j,j}}\sigma_{\tilde{n}_j}^{[\iota]2}}{P_j}\right). \tag{4.47}$$

Furher, using (4.26) and (4.40), the OP of D for the TSR protocol can be executed as

$$P_{\text{out}(D)} = \Pr\left[\frac{1-\alpha}{2}\log_2\left(1+\min(\gamma_R,\gamma_D)\right) < \mathcal{R}_{\text{th}}^{D}\right]. \tag{4.48}$$

Then, following similar steps as in Appendix B.2, the OP in (4.48) can be written in its closed-form as

$$P_{\text{out}(D)} = 1 - \exp\left(-v_{\text{th}}^{D}\left(\frac{d_{R,S}^{\tau_{R,S}}\sigma_R^2}{P_S} + \frac{d_{D,R}^{\tau_{D,R}}\sigma_D^2}{P_R^{\text{TSR}}}\right)\right), \tag{4.49}$$

where $v_{\text{th}}^{D} = 2^{\frac{2\mathcal{R}_{\text{th}}^{D}}{1-\alpha}} - 1$.

4.6.3 Bit-Error Rate

The BER of the data decoded at the receiver m for a symbol-by-symbol hard detection of the BPSK constellation with the zero-forcing equalization is expressed by [122, 162]

$$\text{BER}_m = \int_0^{\infty} Q(\sqrt{2\gamma_m}) f_{\gamma_m}(\gamma_m)\text{d}\gamma_m, \ \forall m \in \mathcal{B}, \tag{4.50}$$

where $Q(x) = 1/\sqrt{2\pi}\int_x^{\infty}\exp(-t^2/2)dt$ and $f_{\gamma_m}(\gamma_m)$ denote the Gaussian-Q function and the PDF of γ_m, accordingly.

4.7 Simulation Results and Discussion

In this section of the chapter, the simulation results for the proposed system model is presented. For the sake of simplicity, it is considered that the network consists of two primary user pairs and one cooperative SN. The parameters of the network are set as the next (unless it is specified otherwise). Each transmit node, except R, transmits with the power of P, whereas R utilizes the harvested power for data transmission. The optimal α^* and θ^* values (for the case $\eta = 0.8$) for both TSR and PSR protocols over various CSI settings can be derived through differentiation, i.e., $\text{d}\mathcal{C}_D^{\text{TSR}}/\text{d}\alpha = 0$ and $\text{d}\mathcal{C}_D^{\text{PSR}}/\text{d}\theta = 0$. The number of antennas at each node is taken as $M = N = 4$ (due to symmetric networks scenario). Moreover, each receive node in the PN and the SN is considered to have an equal rate threshold. Furthermore, the Rayleigh block fading is assumed and the nodes are located in the equal distance from each other, i.e., $d = 3$ m [138], and the path loss exponent is taken to be $\tau = 2.7$ (for urban area environments). The CSI mismatch parameters given by (κ, ψ) are set as $(0, 0.001)$, $(0, 0.05)$, $(0.75, 10)$, $(1, 10)$ and $(1.5, 15)$.

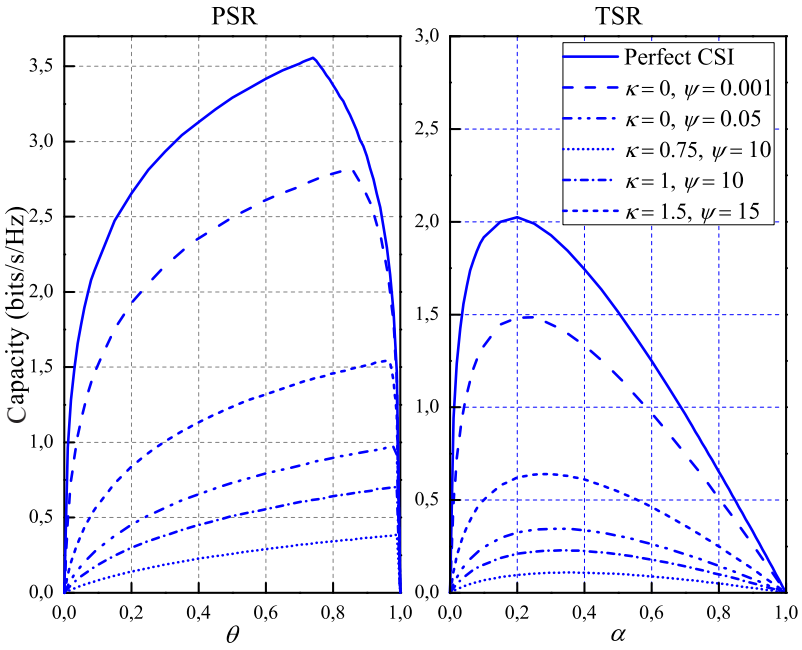

Figure 4.5. Average capacity versus the EH TS and PS coefficients for D in TSR and PSR protocols at 20 dB, respectively.

Fig. 4.5 illustrates the simulated results for the instantaneous capacity of the SN as a function of α and θ within various CSI settings at 20 dB. Eqs. (4.26) and (4.39) are taken for the capacity calculation of the TSR and PSR protocols, respectively. In the PSR protocol, when θ is too small, the capacity performance is low due to the fact that the less power of the obtained signal is devoted to the EH purpose which results in very low available transmit power at R. On the other hand, in the case of θ tends to 1, the capacity performance degrades because of the small power portion alloted for information decoding, whereas major fraction of power is inefficiently dedicated to the EH purpose. Similarly, the same performance pattern can be seen in α for the TSR-based system. From the plot it can be seen that, for the perfect CSI case, the optimal values of the TS fraction and the PS factor are considered to be as $\alpha^* = 0.2$ and $\theta^* = 0.75$, accordingly. For imperfect CSI, values of (α^*, θ^*) were determined as the next: for $\kappa = 0$, $\psi = 0.001 \rightarrow (0.25, 0.84)$; for $\kappa = 0$, $\psi = 0.05 \rightarrow (0.3, 0.97)$; for $\kappa = 0.75$, $\psi = 10 \rightarrow (0.35, 0.99)$; for $\kappa = 1$, $\psi = 10 \rightarrow (0.35, 0.97)$; for $\kappa = 1.5$, $\psi = 15 \rightarrow (0.3, 0.96)$.

Fig. 4.6 reveals the result of the CSI mismatch on the capacity performance of PR_j and D. It can be noted that the impact of ψ to capacity performance is significant when $\kappa = 0$. When SNR = 20 dB and $\psi = 0.001$, the capacity performance loss of PR_j is 1.82 bit/s/Hz whereas that of D for the PSR and TSR-based systems is observed to be as 0.66 and 0.57 bit/s/Hz, accordingly. These capacity losses of PR_j and D is effected by CSI mismatch due to the higher level of interference from primary and secondary transmit nodes. Overall, the capacity losses of the TSR is smaller than that of the PSR case, nevertheless, the PSR provides more bits/s/Hz than the TSR. On the other hand,

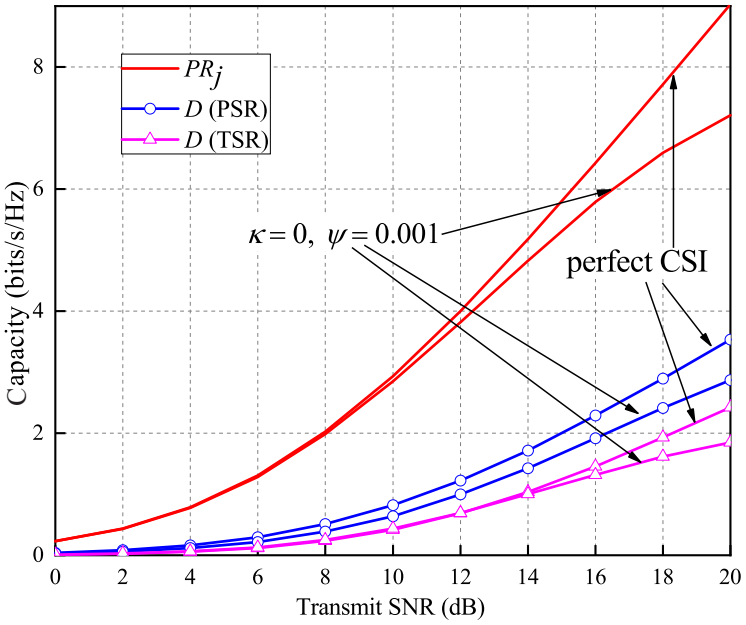

(a)

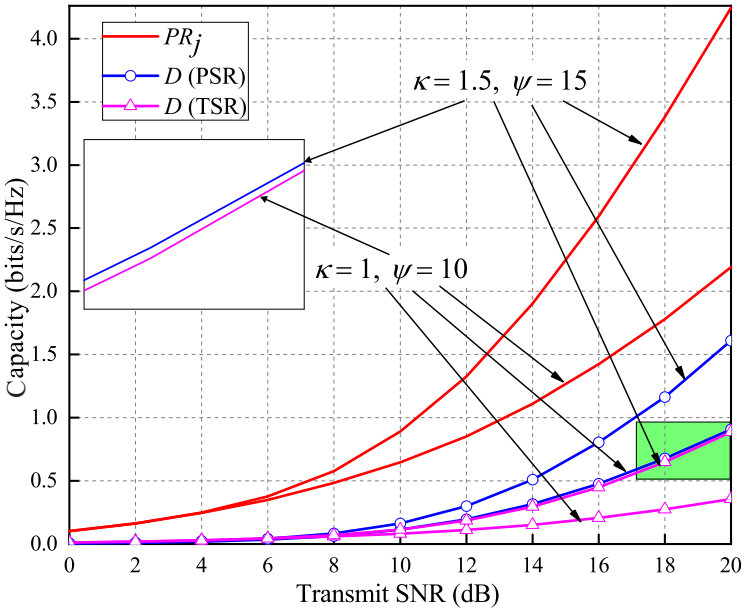

(b)

Figure 4.6. Average capacity versus SNR of PR_j and D operating in the TSR and PSR protocols under different CSI scenarios: a) Perfect CSI versus CSI mismatch ($\kappa = 0,\ \psi = 0.001$). b) CSI mismatch: ($\kappa = 1.5,\ \psi = 15$) versus ($\kappa = 1,\ \psi = 10$).

when $\kappa \neq 0$, the capacity shows poorer performance in the low SNR region. It is worth to mention that the dependence on the SNR results in the capacity growth when the SNR increases. In addition, it is noticed that the capacity performance improves as κ grows.

The impact of imperfect CSI parameters on the BER performance[3] of the PR_j and

[3]For the sake of brevity, the BER performance of PR_j only in the 1^{st} time slot is illustrated. The BER results of PR_j in the 2^{nd} time slot will perform better than those of PR_j in the 1^{st} time slot due to the

the SUs is shown in Fig. 4.7. When $\kappa = 0$, it is noticed that the channel error variance becomes SNR-independent and the BER performance degrades while the value of ψ is increased. Moreover, the BER performance of PR_j and SUs start their saturations at 23 dB and 27 dB, respectively, when $\psi = 0.001$. In addition, when $\psi = 0.05$, the BER curves of PR_j and SUs start to saturate after 17 dB and 24 dB, respectively (see Fig. 4.7a). Furthermore, it is worth to mention that ψ does not cause any impact on the BER performance at lower SNRs, i.e., the effect of ψ on the BER performance of PR_j and D starts at 3 dB and 4 dB, respectively. It can be explained by the fact that, the CSI quality approaches the perfect CSI when ψ tends to 0. From here, it means that the small value of ψ does not cause much effect on the error performance at lower SNRs. On the other hand, when $\kappa \neq 0$, no BER performance saturation is observed as the channel error variance becomes SNR-dependent (see Fig. 4.7b). It is noticed that, when the value of κ is increased, it leads to the better performance of the BER curves. Hence, when transmit SNR is set to be equal to 30 dB, the BER performance results of PR_j, R and D for $(\kappa = 0.75, \psi = 10)$, $(\kappa = 1, \psi = 10)$ and $(\kappa = 1.5, \psi = 15)$ are equal to $(0.0371, 0.0373$ and $0.1)$, $(0.0073, 0.0076$ and $0.024)$, $(0.00035, 0.0005$ and $0.0013)$, accordingly. In overall, results showed that the BER performance of PR_j performs better compared to those of the SUs. This happens due to the signal's power coefficient of $(1-\theta)$ dedicated to data detection at R. In other words, the lower fraction of the allocated power for data detection at R causes a higher probability of the incorrect data detection. Now, by comparing the BER performance of the SN users, it can be seen that R shows outperformance over D. It is due to the fact that R relays the decoded data to D with a certain number of errors, which in turn, affects and degrades the error rate of D. In addition, the BER performance of D additionally degrades due to mismatched CSI caused by the SN and the PNs. Finally, it can be noticed that, in imperfect CSI cases, the BER performance of R shows almost the same result as that of PR_j at higher SNRs.[4]

A deeper analysis of the effect of κ and ψ on the BER in the PSR-based system at 20 dB is illustrated in Fig. 4.8. It is clearly seen from the plot that an increase of κ leads to the improvement of the BER performance. Contrary, an increase of the value of ψ results in the degradation of the BER curves. In the first sub-figure of Fig. 4.8, it can be seen that the BER performance of various settings of ψ approach 0.0019 at certain κ values. When the second sub-figure shows how the BER performance for various values of κ degrades

simple fact that, during the 2^{nd} time slot which is R-D transmission phase, PR_j obtains interference from R with transmit power P_R^{PSR}. As it will be shown later in Fig. 4.10, for the considered network parameters, the harvested power P_R^{PSR} is always less than P.

[4]This can be explained due to the error variance λ of the mismatched channel. The SINRs of R and PR_j can be approximately expressed as $\text{SINR}_R = \frac{(1-\theta)\rho}{\frac{\lambda}{1+\lambda}(1-\theta)\rho(1+L)+1}$ and $\text{SINR}_j^{[1]} = \frac{\rho}{\frac{\lambda}{1+\lambda}\rho(1+L)+1}$, respectively, where $\rho = \frac{P}{\sigma_n^2}$ indicates the nominal transmit SNR. Therefore, at higher transmit power level, the SINR of R approaches the SINR of PR_j, i.e., $\lim_{\rho\to\infty} \Delta \to 0$, where $\Delta = \left|\text{SINR}_R - \text{SINR}_j^{[1]}\right|$

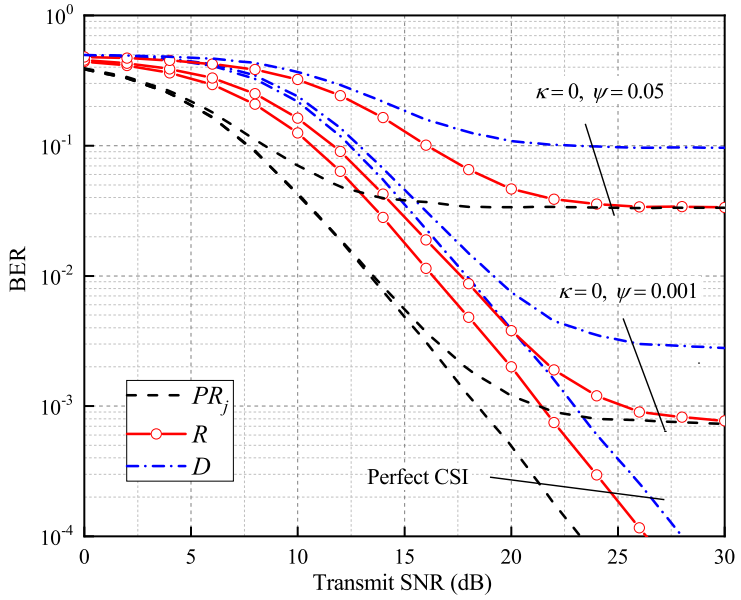

(a)

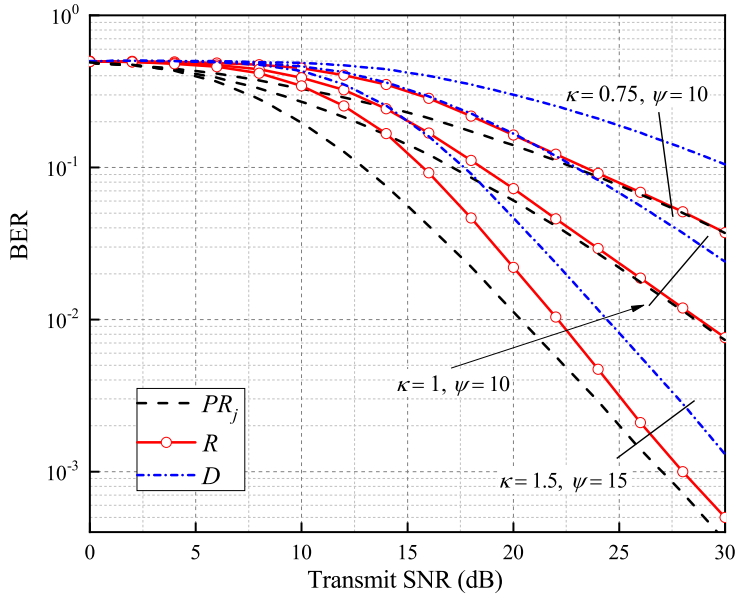

(b)

Figure 4.7. BER versus SNR for the PSR protocol under different CSI scenarios:
a) BER performance for perfect CSI and SNR-independent CSI mismatch cases $((0,\ 0.001)$ and $(0,\ 0.005))$.
b) BER performance for SNR-dependent CSI mismatch cases $((0.75,\ 10),\ (1,\ 10)$ and $(1.5,\ 15))$.

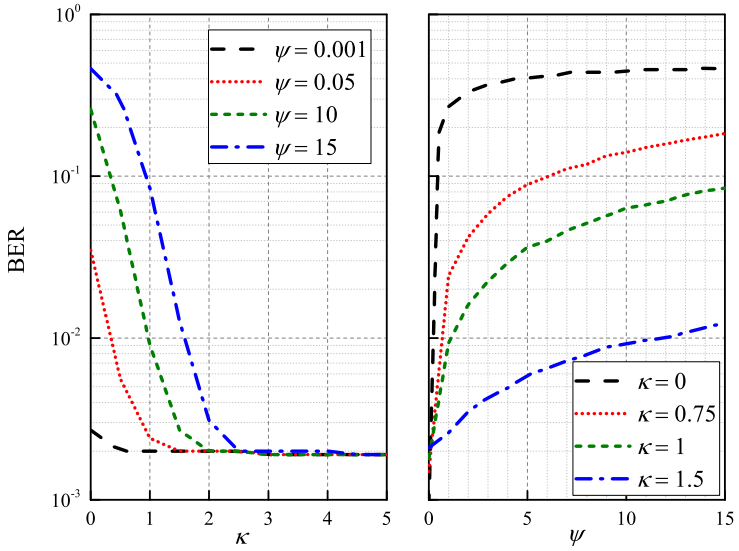

Figure 4.8. BER versus CSI mismatch parameters κ and ψ of D at 20 dB in the PSR mode.

as the value of ψ raises. Besides, it is noticed that, when the values of κ are small, the BER performance degrades more sharply.

Fig. 4.9 depicts analytical values of the OP for PR_j and D in Section 4.6 and their simulated results. The channel settings consider perfect CSI and $d = 1$ m and $d = 3$ m at 25 dB. It can be noted from the plot that the OP degrades by raising the rate threshold. Moreover, D attains worse OP compared with PR_j. Moreover, the simulation results verify the analytical ones by showing the same results, which proves the correctness of the derived analytical results. In Fig. 4.9a, the OP results for the PSR-based system is illustrated. As it is seen from there, the OP of PR_j in the 1^{st} and 2^{nd} time slots show perfect match as both time slots have equal time fractions of $T/2$. Furthermore, when $d = 1$ m, PR_j and D approach the outage at 5.4 and 5 bits/s/Hz, accordingly. On the other hand, when $d = 3$ m, PR_j is in the outage at 3.4 bits/s/Hz, whereas D obtains that at 2 bits/s/Hz. From here, it can be concluded that the increase in the distance between nodes leads to the degradation of the OP due to the channel path loss effect. Moreover, the comparison between the OP of PR_j and D shows that the OP performance of D corrupts more as the distance increases due to the fact that the effect of the distance on the OP is doubled in the two-hop communication of the SN. (see Eq. (4.45)). In Fig. 4.9b, the OP results obtained for the TSR-based system is plotted. When $d = 1$ m, during the 1^{st} time slot, PR_j obtains the outage at 5.8 bits/s/Hz, while PR_j reaches the outage at 5 bits/s/Hz within the 2^{nd} time slot. This phenomenon can be explained by the simple fact that, PR_j is allocated with a time portion of $(1+\alpha)T/2$ for the signal reception in the 1^{st} time slot, whereas the time portion of $(1-\alpha)T/2$ is allocated for PR_j within the 2^{nd} time slot for the same purpose (see Fig. 4.3). In addition, D experiences the outage at 4.8 bits/s/Hz,

which is lower for 0.2 bits/s/Hz rate compared with the OP of the PSR-based system.

Now, using settings of $L = 5$, the impact of primary interference on the EH performance at R is studied. Thus, Fig. 4.10 illustrates the harvested power at R in means of various distances between PR_j and R. The distance between S and R is set as $d = 3$ m,

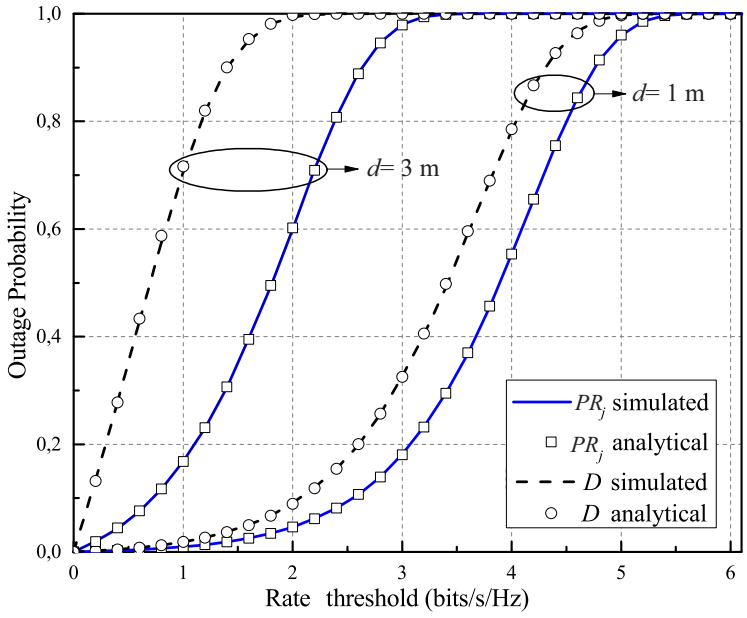

(a)

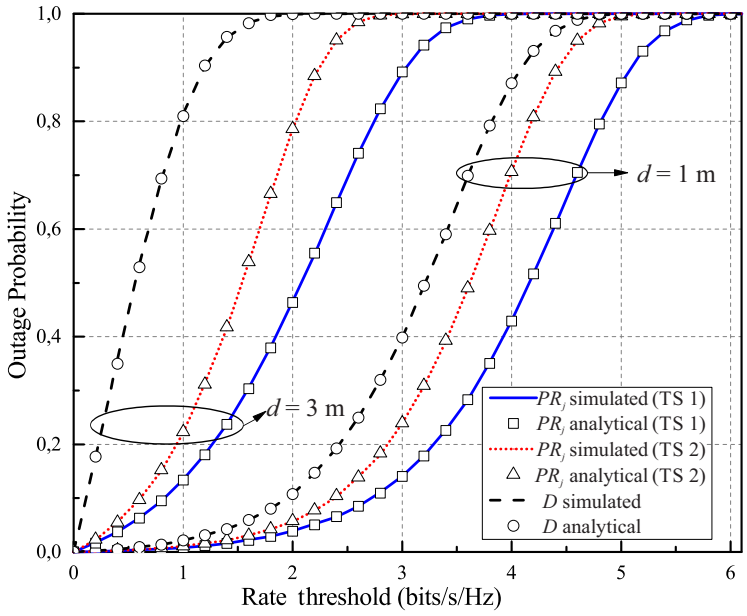

(b)

Figure 4.9. The OP of the PN and the SN with different values of data rate threshold at 25 dB with the perfect CSI case: a) The OP of the system in the PSR protocol. b) The OP of the system in the TSR protocol.

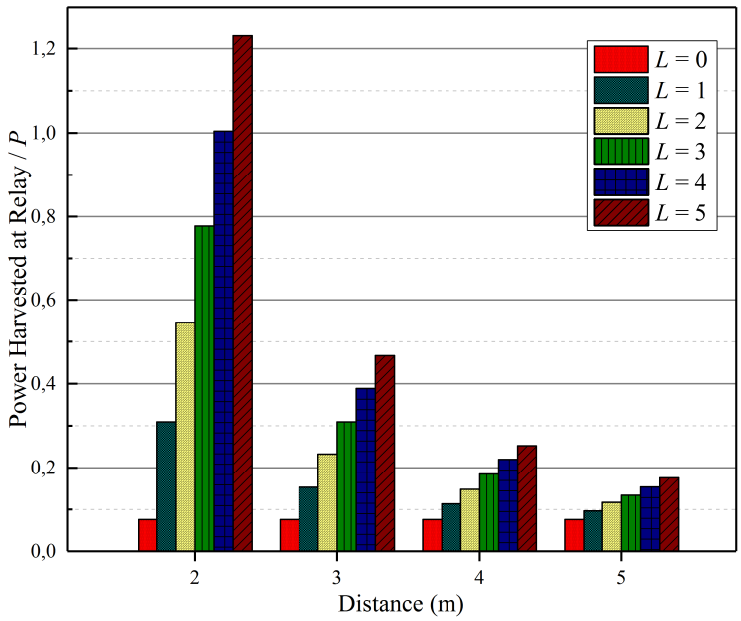

(a)

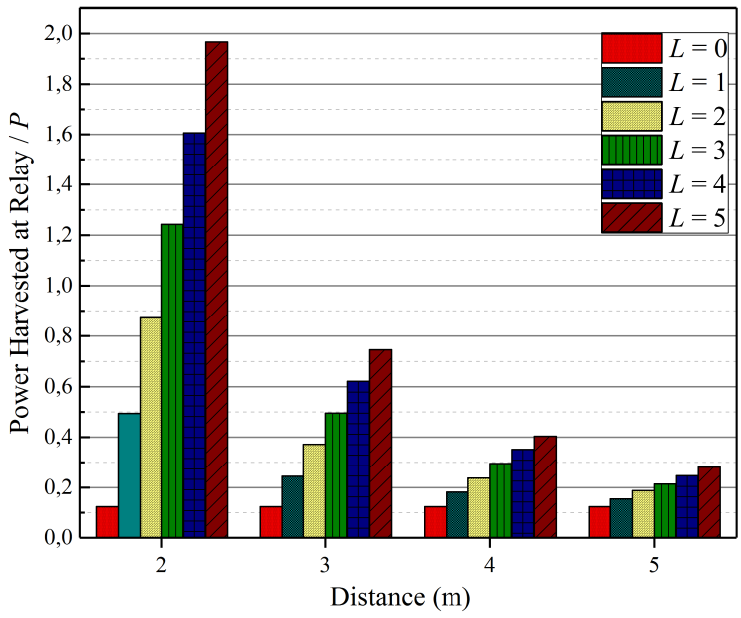

(b)

Figure 4.10. Average harvested power versus distance for the TSR and PSR protocols at 20 dB: a) The TSR protocol. b) The PSR protocol.

while the distance between PR_j to R differs from 2 m to 5 m. The harvested energy is prorated with regard to the transmit power P. From the plot, it is noted that when $L = 5$, the harvested power is the highest. In other words, R harvest more power when the number of coming interference sources is higher. Furthermore, it is also seen that the most power is harvested from S and the power harvested from primary interference becomes lower when PR_j is located further from R. It can be explained by the fact that, in longer distances, the effect of the path-loss on the signal quality is stronger. Finally, the

comparison of the EH performance for optimal TSR and optimal PSR protocols shows that R harvests more power in the latter protocol than in the former one.

4.8 Chapter Summary

This Chapter investigated the CRN consisting of L pairs of PUs and one SN, which composes S, the energy-restricted R and D. The interference received at the PUs and the SN was managed using the IA technique by applying precoding and interference suppression BF matrices. Furthermore, the capacity and BER performance of the EH-based DF CRN by deploying the TSR and PSR protocols were analyzed. In addition, along with perfect CSI, five sets of imperfect CSI parameters (κ, ψ) given by $(0, 0.001)$, $(0, 0.05)$, $(0.75, 10)$, $(1, 10)$ and $(1.5, 15)$ were considered to investigate the effect of the CSI quality on the performance of the system capacity and the BER. The simulated results showed that the system performance can be improved by increasing the values of κ, while an increase of ψ degraded the system performance. Moreover, an optimal selection of the EH time fraction in the TSR protocol and the PS fraction in the PSR protocol were found to be important in achieving the best system performance. From the results, it can be concluded that the optimized PSR protocol obtained better performance over the optimized TSR scheme in terms of capacity and BER performance. In addition, it was observed that an increase in the distance between nodes results in an outage degradation. Then, the derived closed-form expressions for the OP analysis of the SN showed that the PSR protocol outperformed the TSR protocol which validity was confirmed by good agreement with simulation results. Finally, it was shown that the increase in the number of interfering primary nodes allows R to harvest more power, while the increase of interfering nodes' distance results in lower harvested power.

The contributions of this Chapter can be categorized into two main parts:

- We showed that by using the IA technique in underlay cooperative CR networks, interference at the primary receivers can be efficiently canceled as a result secondary transmit nodes are not required to limit their transmit power. Consequently, SNs can obtain better system performance in terms of the OP and the BER.

- Not similar to many works related to interference managing where unwanted interference has been canceled or removed, we used intra- and inter-network interference for EH purpose to feed the power-limited relay node.

Chapter 5

Cognitive Radio Non-Orthogonal Multiple Access Networks

NOMA is considered to be one of the promising multiple access techniques for 5G networks. This Chapter studies a dual-hop underlay CR-NOMA networks. Closed-form expressions for the OP of NOMA secondary destination users are evaluated for DF and AF relaying techniques. Furthermore, power allocation factors for different distances of secondary NOMA users are found to satisfy OP fairness for all users. Moreover, the OP for NOMA is compared with that for conventional orthogonal MA (OMA) to show the supremacy of the former MA technique. All derived analytical expressions are validated with Monte Carlo simulations.

5.1 Introduction

5.1.1 Cooperative NOMA

In NOMA, stronger users, by having preliminary information about messages of the other users, can act as relays. Hence, a cooperative NOMA was presented in [61], where users with stronger channel gains were assigned relay roles to forward the signals to the users with weaker channel gains. The results showed that the cooperative NOMA outperforms both the conventional cooperative OMA and non-cooperative NOMA. Moreover, the cooperative NOMA with a dedicated relay was studied in [163, 164]. Further, in [163], the OP results showed that the cooperative NOMA outperforms the cooperative OMA regarding a coding gain while, in [164], a NOMA scheme with a two-way relay that supports both uplink and downlink was proposed, where the results showed that the proposed system achieves better sum rate compared to the OMA scheme. Furthermore, in [165], the PA scheme in cooperative NOMA systems for fixed and adaptive relaying cases was studied. In addition, the benefits of cooperative NOMA networks were widely studied in various network scenarios [166, 167].

It is already known that due to the distinct characteristic of the underlay CR paradigm, the SN transmissions should not interfere with the PN communication. This fact makes the power control at secondary transmit nodes more critical and due to that traditional underlay CR is often limited to short-range communications [168]. To address these challenges, a cooperative underlay NOMA architecture has been proposed [84, 87, 169], where a relay helps to improve the radio coverage and minimize an outage for underlay NOMA networks.

5.2 Contribution of the Chapter

The main contribution of the Chapter can be concluded as

- The synergy of cooperative underlay CR and NOMA is studied in terms of the outage performance of NOMA users applying both DF and AF relaying methods over Rayleigh and Nakagami-m fading channels.
- The power allocation factors are found for NOMA secondary users in order to guarantee outage fairness (OF) among NOMA users.
- Considering the effect of imperfect CSI on the outage performance, we derived a general closed-form solution for the OP when the number of secondary NOMA nodes is extended to K users.
- The comparison between the proposed cooperative CR-NOMA and the conventional cooperative CR-OMA shows the supremacy of the former.

5.3 Organization of the Chapter

This Chapter studies a downlink dual-hop CR-NOMA model with the imposed ITC at PR. The chapter considers several different scenarios for the proposed system model. In Section 5.4, we propose a system model where only one secondary node is limited (Case 1) by maximum transmit power. The OP is investigated as a performance metric for the considered system model applying DF and AF relaying methods over Rayleigh and Nakagami-m fading channels. Here, the closed-form OP expression is derived for two NOMA secondary users. Then, in Section 5.5, the scenario where PR applies the ITC to both S and R (Case 2) is considered. By considering the effect of the imperfect CSI on the outage performance, we derive a general closed-form solution for the OP when the number of secondary NOMA nodes is extended to K users. All derived analytical results are verified by Monte-Carlo simulations. Furthermore, in order to obtain OF among NOMA users, the power allocation factors are found depending on the distance

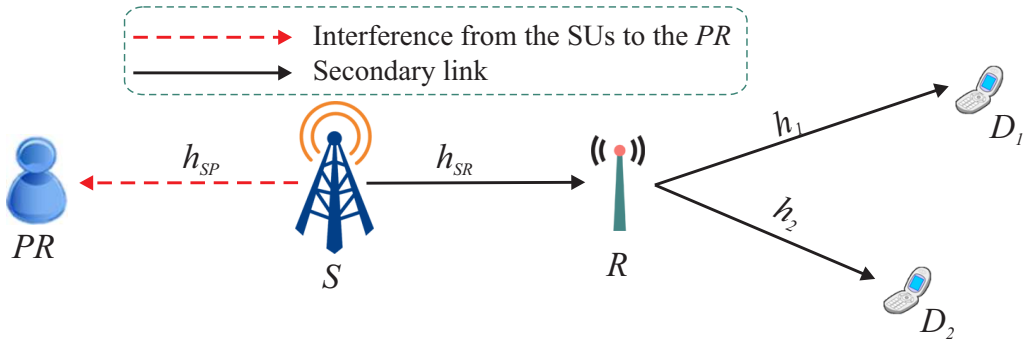

Figure 5.1. A system model of the downlink dual-hop underlay CR-NOMA network with transmit power constraint at the secondary source.

between the relay and secondary NOMA users. Finally, the obtained OP performance for NOMA is compared to that for conventional cooperative OMA to show the supremacy of the former.

5.4 Outage analysis of dual-hop CR-NOMA: Case 1

In this part, the outage performance will be evaluated for CR-NOMA by assuming just only one secondary transmit node is constrained from the maximum allowable transmit power due to its close location to PR.

5.4.1 CR-NOMA with two secondary NOMA users

5.4.1.1 System Model

Consider the scenario with a downlink dual-hop underlay CR-NOMA network shown in Fig. 5.1. The network consists of S, R, two destination users (D_1 and D_2) and PR. It is assumed that the direct S-to-D_1 and S-to-D_2 links do not exist. Another assumption is that all nodes are equipped with a single antenna and operate in a half-duplex mode. Fading-channel gains, i.e., h_{SP}, h_{SR}, h_1 and h_2, follow the i.n.i.d. Rayleigh block fading model. Moreover, it is assumed that perfect CSI is available at each node. Furthermore, the corresponding distances between nodes are expressed by d_{SP}, d_{SR}, d_1 and d_2. According to the system model, S causes interference to PR, whereas R, which operates in DF and AF modes, cannot interfere with the PN due to its remote location from PR (see Fig. 5.1). Another assumption is that the SN can communicate only if PR does not receive harmful interference from S. Hence, S is restricted by transmit power as [161]

$$P_S \leq \min\left(\frac{I d_{SP}^{\tau}}{|h_{SP}|^2}, \bar{P}_S\right), \tag{5.1}$$

where τ is the path-loss exponent, $\bar{P}_S$ and I indicate maximum average transmit power available at S and the ITC at PR, accordingly. By considering this power restriction, S transmits the next superimposed signal to D_1 and D_2 through the aid of R in two-time slots

$$x_S = \sqrt{\alpha_1 P_S} x_1 + \sqrt{\alpha_2 P_S} x_2, \tag{5.2}$$

where x_1 and x_2, with $\mathbb{E}(|x_i|^2) = 1$, $i \in \{1, 2\}$, denotes the intended data to D_1 and D_2, respectively, α_1 and α_2 stand for the PA factors for corresponding users, with $\alpha_1 + \alpha_2 =$ 1. Further, during the 1^{st} time slot, the signal received at R can be written as

$$y_R = h_{SR} \left(\sqrt{\frac{\alpha_1 P_S}{d_{SR}^{\tau}}} x_1 + \sqrt{\frac{\alpha_2 P_S}{d_{SR}^{\tau}}} x_2 \right) + n_R, \tag{5.3}$$

where $n_{(\cdot)} \sim \mathcal{CN}(0, \sigma_{(\cdot)}^2)$ denotes the AWGN at each receiving node[1]. Moreover, channels and the PA factors are ordered as $h_1 < h_2$ and $\alpha_1 > \alpha_2$, which means that D_1 is allocated with the higher power portion due to its channel weaknesses.

5.4.1.2 Decode-and-Forward Relaying Scheme

Here, it is considered the case when R employed the DF relaying scheme. Saying so, in the 2^{nd} time slot, R decodes and removes x_1 from the received signal in (5.3) before detecting x_2, according to the principle of NOMA [61]. Thus, at R, the SINR of decoding x_1 is derived as

$$\gamma_{R,1} = \frac{|h_{SR}|^2 \frac{\alpha_1 P_S}{d_{SR}^{\tau}}}{|h_{SR}|^2 \frac{\alpha_2 P_S}{d_{SR}^{\tau}} + \sigma^2} = \frac{|h_{SR}|^2 \alpha_1 \rho_S}{|h_{SR}|^2 \alpha_2 \rho_S + d_{SR}^{\tau}}, \tag{5.4}$$

where $\rho_S = \frac{P_S}{\sigma^2}$ is the source transmit SNR. Further, on the condition[2] that $\gamma_{R,1} \geq \xi_1$, where $\xi_{(\cdot)}$ denotes the predefined SNR threshold at $D_{(\cdot)}$, the data detected in (5.4) is removed from the remaining signal and the SNR to detect x_2 at R can be written as

$$\gamma_{R,2} = \frac{|h_{SR}|^2 \alpha_2 \rho_S}{d_{SR}^{\tau}}. \tag{5.5}$$

Further, R relays the detected superimposed signal x_R to D_1 and D_2

$$x_R = \sqrt{\beta_1 P_R} \tilde{x}_1 + \sqrt{\beta_2 P_R} \tilde{x}_2, \tag{5.6}$$

[1]For mathematical tractability and without loss of generality, it is assumed that the noise power at each receiving node is equal to σ^2, i.e., $\sigma_P^2 = \sigma_R^2 = \sigma_1^2 = \sigma_2^2 = \sigma^2$ throughout the paper.

[2]This condition provides succesfull implemantation of the SIC at R to remove x_1.

where P_R stands for the relay transmit power, $\tilde{x}_1$ and $\tilde{x}_2$ indicate decoded and forwarded data to corresponding receivers whereas β_1 and β_2, with β_1 + β_2 = 1, satisfying $\beta_1 > \beta_2$, represent the PA factors at R. Hence, the received signal at D_1 and D_2 can be respectively written as

$$y_1 = h_1 \left(\sqrt{\frac{\beta_1 P_R}{d_1^\tau}} \tilde{x}_1 + \sqrt{\frac{\beta_2 P_R}{d_1^\tau}} \tilde{x}_2 \right) + n_1 \tag{5.7}$$

and

$$y_2 = h_2 \left(\sqrt{\frac{\beta_1 P_R}{d_2^\tau}} \tilde{x}_1 + \sqrt{\frac{\beta_2 P_R}{d_2^\tau}} \tilde{x}_2 \right) + n_2, \tag{5.8}$$

where n_1 and n_2 denote the AWGN noise terms at D_1 and D_2, accordingly. Moreover, D_2 applies the SIC by detecting $\tilde{x}_1$ at the same time considering its own data $\tilde{x}_2$ as a background noise. Thus, the SINR of detecting x_1 at D_2 can be formulated as follows

$$\gamma_{2,1} = \frac{|h_2|^2 \beta_1 \rho_R}{|h_2|^2 \beta_2 \rho_R + d_2^\tau}, \tag{5.9}$$

where $\rho_R = \frac{P_R}{\sigma^2}$ stands for the transmit SNR at R. Further, on the condition that $\gamma_{2,1} \geq \xi_1$, i.e., the SIC is successfully implemented at D_2 to remove x_1, the data detected in (5.9) is removed from the remaining signal and the SNR to detect x_2 at D_2 can be written as

$$\gamma_{2,2} = \frac{|h_2|^2 \beta_2 \rho_R}{d_2^\tau}. \tag{5.10}$$

Due to the channel ordering, D_1 is allocated with higher power fraction. Thus, D_1 detects $\tilde{x}_1$ by treating $\tilde{x}_2$ as a background noise with the next SINR

$$\gamma_1 = \frac{|h_1|^2 \beta_1 \rho_R}{|h_1|^2 \beta_2 \rho_R + d_1^\tau}. \tag{5.11}$$

Then, the achievable rates of x_1 and x_2 can be written as [170]

$$\mathcal{R}_1 = \frac{1}{2} \log_2 \left(1 + \min \left(\gamma_{R,1}, \gamma_{2,1}, \gamma_1\right)\right) \tag{5.12}$$

and

$$\mathcal{R}_2 = \frac{1}{2} \log_2 \left(1 + \min \left(\gamma_{R,2}, \gamma_{2,2}\right)\right), \tag{5.13}$$

accordingly, where all SNR values involved in each $\min$ function are independent RVs.

5.4.1.3 Amplify-and-Forward Relaying Scheme

Not similar to the DF relaying, where R detects and forwards the signal from S to secondary destinations, in the AF protocol, R amplifies the signal received from S and forwards to both secondary destinations. Hence, D_1 and D_2 respectively receive the following signals

$$y_1^{\text{AF}} = \sqrt{\frac{P_R}{d_1^\tau}} h_1 G y_R + n_1 = \sqrt{\frac{P_S P_R}{d_{SR}^\tau d_1^\tau}} h_{SR} h_1 \sum_{i=1}^{2} \sqrt{\alpha_i} x_i G + \sqrt{\frac{P_R}{d_1^\tau}} h_1 n_R G + n_1 \quad (5.14)$$

and

$$y_2^{\text{AF}} = \sqrt{\frac{P_R}{d_2^\tau}} h_2 G y_R + n_2 = \sqrt{\frac{P_S P_R}{d_{SR}^\tau d_2^\tau}} h_{SR} h_2 \sum_{i=1}^{2} \sqrt{\alpha_i} x_i G + \sqrt{\frac{P_R}{d_2^\tau}} h_2 n_R G + n_2, \quad (5.15)$$

where G denotes the amplification factor at R which can be formulated as

$$G = \sqrt{\frac{1}{\frac{P_S}{d_{SR}^\tau}|h_{SR}|^2 + \sigma^2}}. \quad (5.16)$$

Then, due to higher value of α_1, D_1 can treat x_2 as a background noise and detect x_1 by the following SINR

$$\begin{aligned}
\gamma_1^{\text{AF}} &= \frac{\frac{P_S}{d_{SR}^\tau}|h_{SR}|^2 \frac{P_R}{d_1^\tau}|h_1|^2 G^2 \alpha_1}{\frac{P_S}{d_{SR}^\tau}|h_{SR}|^2 \frac{P_R}{d_1^\tau}|h_1|^2 G^2 \alpha_2 + \frac{P_R}{d_1^\tau}|h_1|^2 G^2 \sigma^2 + \sigma^2} \\
&= \frac{\frac{\rho_S}{d_{SR}^\tau}|h_{SR}|^2 \frac{\rho_R}{d_1^\tau}|h_1|^2 \alpha_1}{\frac{\rho_S}{d_{SR}^\tau}|h_{SR}|^2 \frac{\rho_R}{d_1^\tau}|h_1|^2 \alpha_2 + \frac{\rho_R}{d_1^\tau}|h_1|^2 + \frac{\rho_S}{d_{SR}^\tau}|h_{SR}|^2 + 1} \\
&= \frac{n_s Y n_1 X \alpha_1}{n_s Y n_1 X \alpha_2 + n_1 X + n_s Y + 1},
\end{aligned} \quad (5.17)$$

where $n_s = \frac{\rho_S}{d_{SR}^\tau}$, $n_1 = \frac{\rho_R}{d_1^\tau}$, $X = |h_1|^2$ and $Y = |h_{SR}|^2$. Then, according to the principle of NOMA, D_2 detects x_1 by treating its own signal as a background noise, which SINR can be derived as

$$\gamma_{2,1}^{\text{AF}} = \frac{n_s Y n_2 Q \alpha_1}{n_s Y n_2 Q \alpha_2 + n_2 Q + n_s Y + 1}, \quad (5.18)$$

where $n_2 = \frac{\rho_R}{d_2^\tau}$ and $Q = |h_2|^2$ is an exponential distribution. Further, on the condition that $\gamma_{2,1} \geq \xi_1$, the detected x_1 in (5.18) is removed and D_2 detects its own data from the remaining signal, which SNR can be written as

$$\gamma_2^{\text{AF}} = \frac{n_s Y n_2 Q \alpha_2}{n_2 Q + n_s Y + 1}. \quad (5.19)$$

Furthermore, the achievable rates[3] of D_1 and D_2 can be respectively derived by

$$\mathcal{R}_1^{\text{AF}} = \frac{1}{2}\log_2\left(1+\gamma_1^{\text{AF}}\right), \tag{5.20}$$

$$\mathcal{R}_2^{\text{AF}} = \frac{1}{2}\log_2\left(1+\gamma_2^{\text{AF}}\right). \tag{5.21}$$

5.4.1.4 Outage Performance Analysis

5.4.1.5 Outage for the Decode-and-Forward Relaying Mode

The OP of x_1 for DF mode can be formulated as

$$\begin{aligned} P_{\text{out},1}(\xi_1) =& 1-\Pr\left[\min\left(\gamma_{R,1},\gamma_{2,1},\gamma_1\right)>\xi_1\right] \\ =& 1-\Pr\left[\gamma_{R,1}>\xi_1\right]\Pr\left[\gamma_{2,1}>\xi_1\right]\Pr\left[\gamma_1>\xi_1\right] \\ =& F_{\gamma_{2,1}}(\xi_1)+\left(1-F_{\gamma_{2,1}}(\xi_1)\right)\left(F_{\gamma_1}(\xi_1)+F_{\gamma_{R,1}}(\xi_1)-F_{\gamma_1}(\xi_1)F_{\gamma_{R,1}}(\xi_1)\right). \end{aligned} \tag{5.22}$$

Proposition 5 The closed-form OP expression for x_1 is written as

$$P_{\text{out},1}(\xi_1) = 1-e^{-\frac{\xi_1\left(\psi\bar{\rho}_S\left(d_1^{\tau}+d_2^{\tau}\right)+\kappa\rho_R d_{SR}^{\tau}\right)}{2\kappa\psi\bar{\rho}_S\rho_R}} + \frac{\xi_1 d_{SR}^{\tau} e^{-\frac{\kappa\rho_R\left(\psi\rho_I d_{SP}^{\tau}+\xi_1 d_{SR}^{\tau}\right)+\xi_1\psi\bar{\rho}_S\left(d_1^{\tau}+d_2^{\tau}\right)}{2\kappa\psi\bar{\rho}_S\rho_R}}}{\psi\rho_I d_{SP}^{\tau}+\xi_1 d_{SR}^{\tau}}, \tag{5.23}$$

where, $\xi_1 < \frac{\alpha_1}{\alpha_2}$ and $\xi_1 < \frac{\beta_1}{\beta_2}$, otherwise, $P_{\text{out},1}(\xi_1)=1$.

Proof: See Appendix C.1 for details. ■

The OP of the signal x_2 can be written as

$$\begin{aligned} P_{\text{out},2}(\xi_2) &= 1-\Pr\left[\min\left(\gamma_{R,2},\gamma_{2,2}\right)>\xi_2\right] = 1-\Pr\left[\gamma_{R,2}>\xi_2\right]\Pr\left[\gamma_{2,2}>\xi_2\right] \\ &= F_{\gamma_{2,2}}(\xi_2)+F_{\gamma_{R,2}}(\xi_2)-F_{\gamma_{2,2}}(\xi_2)F_{\gamma_{R,2}}(\xi_2). \end{aligned} \tag{5.24}$$

Proposition 6 The closed-form OP expression for x_2 is written as

$$P_{\text{out},2}(\xi_2) = 1-e^{-\frac{\xi_2\left(\bar{\rho}_S\alpha_2 d_2^{\tau}+\rho_R\beta_2 d_{SR}^{\tau}\right)}{2\bar{\rho}_S\rho_R\alpha_2\beta_2}} + \frac{\xi_2 d_{SR}^{\tau} e^{-\frac{\rho_R\beta_2\left(\rho_I\alpha_2 d_{SP}^{\tau}+\xi_2 d_{SR}^{\tau}\right)+\bar{\rho}_S\alpha_2\xi_2 d_2^{\tau}}{2\alpha_2\beta_2\bar{\rho}_S\rho_R}}}{\alpha_2\rho_I d_{SP}^{\tau}+\xi_2 d_{SR}^{\tau}}. \tag{5.25}$$

Proof: See Appendix C.2 for details. ■

[3] In the DF mode, we considered the achievable rate of the messages in order to derive the OP. However, in the AF mode, RVs γ_1^{AF} and $\gamma_{2,1}^{\text{AF}}$ are correlated to each other, which makes the derivation of a closed-form solution for the OP of x_1 very complex or even intractable. Thus, we concentrate on the OP derivation of D_1 and D_2 for the AF scenario.

5.4.1.6 Outage for the Amplify-and-Forward Relaying Mode

Not similar to the DF relaying, the intended data in the AF relaying is detected only at the final destination, i.e., D_1 and D_2. Therefore, the OP for D_1 can be expressed as

$$P_{\text{out},1}^{\text{AF}}(\xi_1) = 1 - \Pr\left[\gamma_1^{\text{AF}} > \xi_1\right] = 1 - \left(1 - F_{\gamma_1}^{\text{AF}}(\xi_1)\right) \triangleq F_{\gamma_1}^{\text{AF}}(\xi_1). \tag{5.26}$$

Proposition 7 The exact OP expression of D_1 can be written as

$$\begin{aligned} P_{out,1}^{\text{AF}}(\xi_1) =& 1 - e^{-\frac{u_1(n_1+n_s)}{n_1}} 2\sqrt{r} K_1\left(2\sqrt{r}\right)\left(1 - e^{-c}\right) - \frac{n_1 e^{-\frac{cn_1(\bar{u}_1+1)+n_p\bar{u}_1}{n_1}}}{\bar{u}_1(n_p\bar{u}_1+1)} \\ &\times \sum_{k=0}^{\infty} \frac{\left(-\frac{c\bar{u}_1(n_p\bar{u}_1+1)}{n_1}\right)^k}{k!} G_{3\ 2}^{1\ 3}\left(\frac{n_1(\bar{u}_1+1)}{\bar{u}_1(n_p\bar{u}_1+1)}\middle| \begin{matrix} 0,\ k-1,\ k \\ 0,\ k \end{matrix}\right), \end{aligned} \tag{5.27}$$

where $\xi_1 < \frac{\alpha_1}{\alpha_2}$, otherwise, $\mathcal{P}_1(\xi_1) \sim 1$.

Proof: See Appendix C.3 for details. ■

Furthermore, the OP of D_2 can be expressed by

$$P_{\text{out},2}^{\text{AF}}(\xi_2) = 1 - \Pr\left[\gamma_2^{\text{AF}} > \xi_2\right] = 1 - \left(1 - F_{\gamma_2}^{\text{AF}}(\xi_2)\right) \triangleq F_{\gamma_2}^{\text{AF}}(\xi_2). \tag{5.28}$$

Proposition 8 The exact OP of D_2 can be written as

$$\begin{aligned} P_{out,2}^{\text{AF}}(\xi_2) =& 1 - e^{-\frac{u_2(n_2+n_s)}{n_2}} 2\sqrt{r_2} K_1\left(2\sqrt{r_2}\right)\left(1 - e^{-c}\right) - \frac{n_2 e^{-\frac{cn_2(\bar{u}_2+1)+n_p\bar{u}_2}{n_2}}}{\bar{u}_2(n_p\bar{u}_2+1)} \\ &\times \sum_{k=0}^{\infty} \frac{\left(-\frac{c\bar{u}_2(n_p\bar{u}_2+1)}{n_2}\right)^k}{k!} G_{3\ 2}^{1\ 3}\left(\frac{n_2(\bar{u}_2+1)}{\bar{u}_2(n_p\bar{u}_2+1)}\middle| \begin{matrix} 0,\ k-1,\ k \\ 0,\ k \end{matrix}\right), \end{aligned} \tag{5.29}$$

where $r_2 = \frac{u_2(n_s u_2+1)}{n_2}$.

Proof: See Appendix C.4 for details. ■

5.4.1.7 Numerical Results

This part of the Chapter represents numerical and simulation results for the OP over Rayleigh fading channels. The adopted system parameters for numerical and simulation results are taken as (unless otherwise stated): $d_1 = \{1.5d, 2d, 3d, 4d, 5d\}$[3], $d_{SP} =$

[3] d is assumed to be a unity in order to focus on OP results.

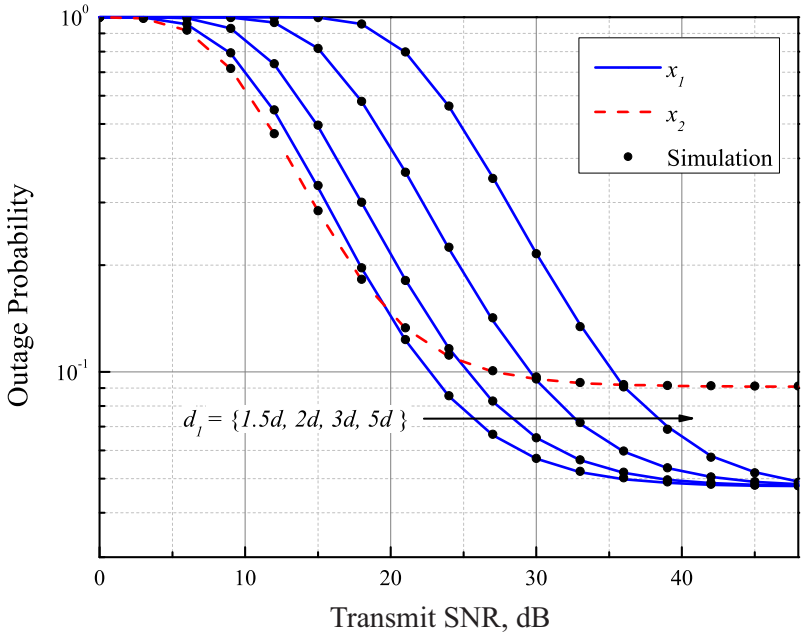

Figure 5.2. The OP of x_1 and x_2 versus SNR performance when $d_1 = \{1.5d, 2d, 3d, 5d\}$, $\alpha_1 = 0.8$ and $\alpha_2 = 0.2$.

$d_{SR} = d_2 = d$, $\tau = 2.7$, $I = 20$ dB, $\alpha_1 = \beta_2 = 0.8$, $\alpha_2 = \beta_2 = 0.2$, and $\xi = \xi_1 = \xi_2 = 3$ dB.

Numerical Results for the Decode-and-Forward Relaying mode

In Fig. 5.2, the OP results for x_1 and x_2 obtained using (5.23) and (5.25), accordingly, are illustrated. One observation is that the outage of x_2 shows better performance than that of x_1 at lower SNR values (until 20 dB). The latter is due to the fact that D_2 cancels interference from D_1 by applying the SIC, while D_1 detects the desired signal without canceling interference from D_2 which increases the probability of error in data detection. Another observation is that the OP x_1 in different d_1 cases outperforms that of x_2 at higher SNR. This can be explained as follows: at higher SNR values, D_1 receives a stronger signal to detect the desired data which, in turn, provides less possibility for an outage. To compare the OP performance of x_1 at different d_1, it is seen that the increase of d_1 leads to the rise of the outage curve. Moreover, the simulation results match with the analytical ones, which proves the correctness of the derived closed-form OP expressions of x_1 and x_2.

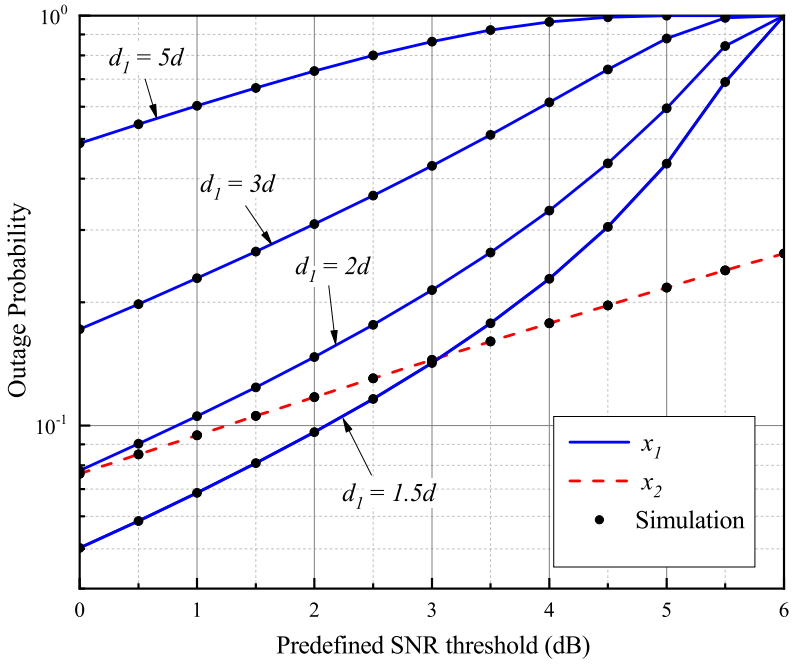

Figure 5.3. The OP of x_1 and x_2 versus the SNR threshold at 20 dB when $d_1 = \{1.5d, 2d, 3d, 5d\}$, $\alpha_1 = 0.8$ and $\alpha_2 = 0.2$.

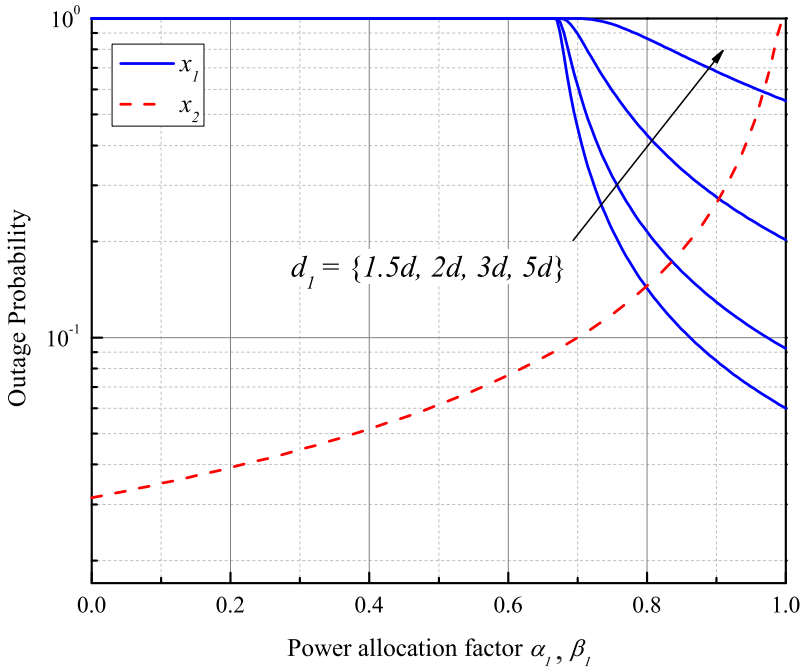

Figure 5.4. The OP of x_1 and x_2 versus PA factors at 20 dB when $d_1 = \{1.5d, 2d, 3d, 5d\}$.

The analytical values of the OP for x_1 and x_2 with various d_1 distances and SNR threshold values are shown in Fig. 5.3. It is observed that curves of the OP raise by increasing the SNR threshold. When $d_1 \geq 2d$, x_1 shows worse outage performance compared to x_2. When $d_1 = 1.5d$ and $\xi < 3$ dB, the OP of x_1 achieves better performance

Table 5.1. OF-based PA factors for different d_1 for the DF mode.

d_1	$1.5d$	$2d$	$3d$	$5d$
α_1^*, β_1^*	0.8	0.83	0.91	0.97
α_2^*, β_2^*	0.2	0.17	0.09	0.03

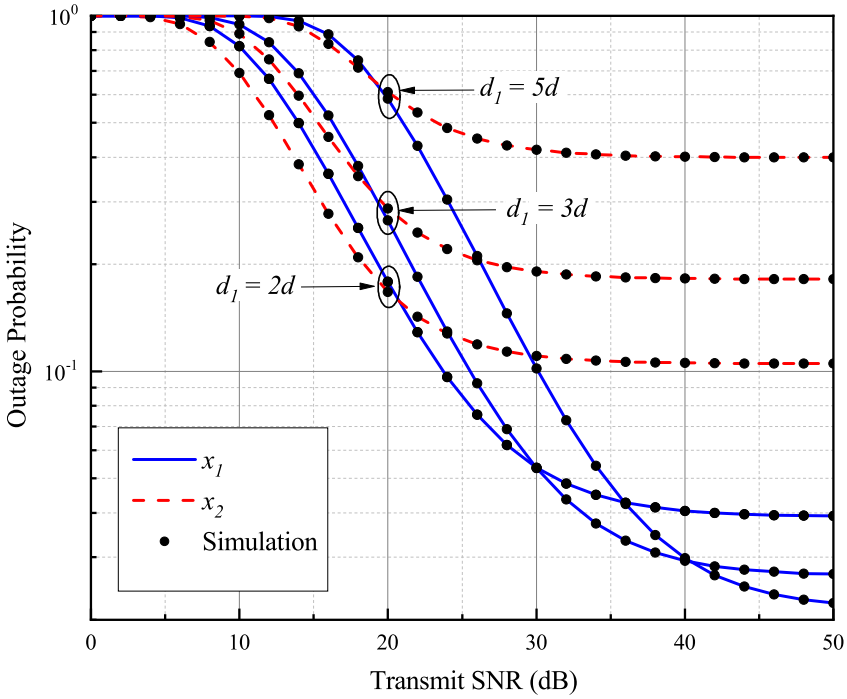

Figure 5.5. The OP of x_1 and x_2 versus the transmit SNR performance with OF-based PA factors when $d_1 = \{2d, 3d, 5d\}$.

than that of x_2. It is due to the fact that higher value of power allocated to D_1 compare to D_2. However, when $\xi > 3$ dB, the OP curve of x_1 dramatically increases reaching an outage at 6 dB.

The OF-based PA factors α_1^* and β_1^* at 20 dB is shown in Fig. 5.4. It is clearly seen that, when $\xi > \frac{\alpha_1}{\alpha_2}$, signal x_1 is in outage for all values of d_1. However, when $\xi < \frac{\alpha_1}{\alpha_2}$, the increase of α_1 leads to an improvement of the outage performance of x_1 at the same time decreasing that of x_2. The observed OF-based PA factors for different d_1 values are given in Table 5.1.

Fig. 5.5 illustrates the outage performance results with OF-based α_1^*, β_1^* and α_2^*, β_2^* values in the case of different d_1. It is observed that, in all d_1 cases, the outage performance of x_2 outperforms that of x_1 at values of SNR lower than 20 dB. At other SNR values, the OP of x_1 is stronger than that of x_2. Moreover, when d_1 is increased, the saturation of outage curve of x_1 starts at higher SNRs due to the fact that larger α_1 is needed when D_1 is located far away from R.

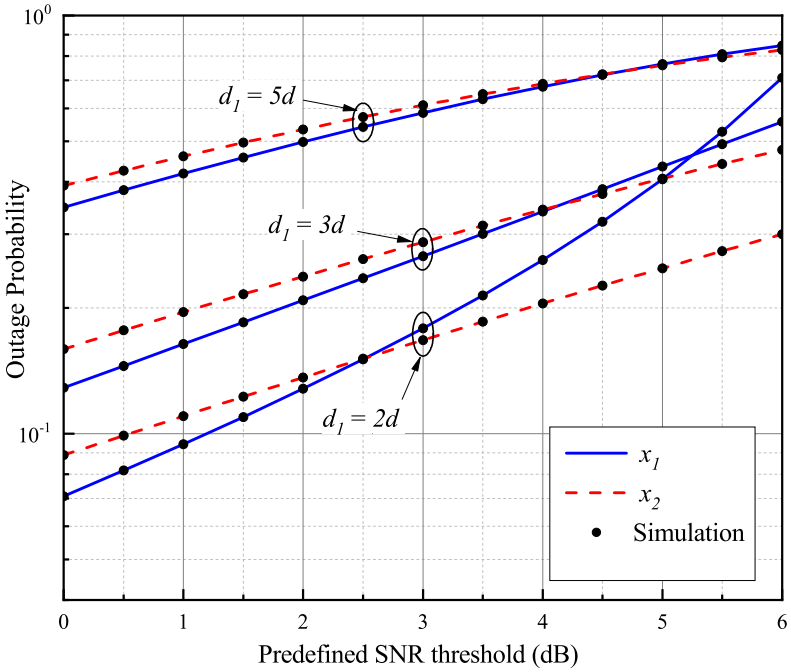

Figure 5.6. The OP versus SNR threshold with OF-based PA factors at 20 dB, when $d_1 = \{2d, 3d, 5d\}$.

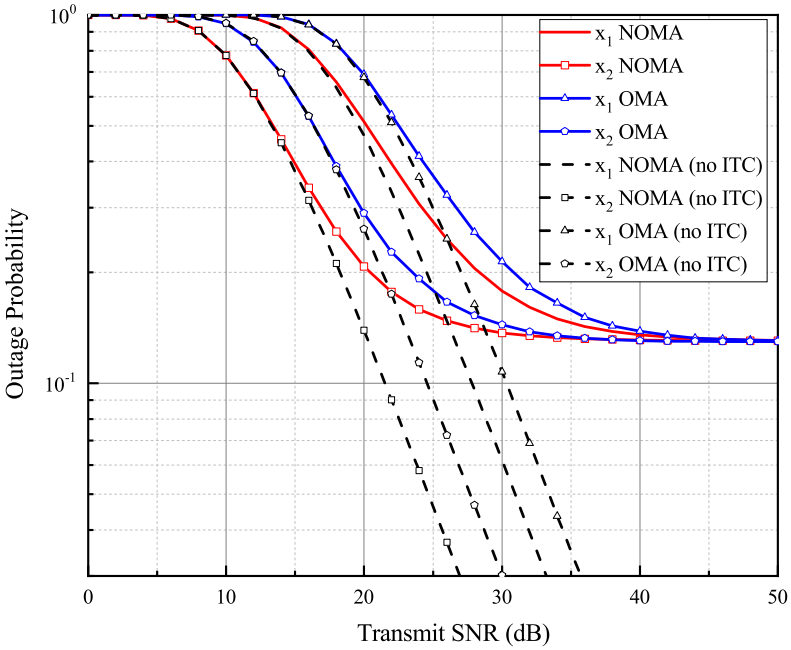

Figure 5.7. The OP versus the transmit SNR performance for NOMA and OMA users with $\alpha_1 = 0.8$, $d_1 = 2d$ and $u = 4.7$ dB.

Fig. 5.6 shows the results of the OP versus the SNR threshold with OF-based PA factors for d_1. It is observed that the OF-based PA factors improved the OP performance of x_1 in all d_1 cases providing fairness for both users.

The comparison of the OP for cooperative NOMA to that for cooperative OMA is illustrated in Fig. 5.7. We consider two cases, with no ITC, e.g., $I = \infty$ and when $I = 20$ dB. In the proposed system model, the cooperative NOMA requires two-time slots to deliver the intended messages to D_1 and D_2, whereas four time periods are needed for cooperative OMA to serve two destination users. Hence, the data requirements for cooperative OMA is set as 2-fold of that for cooperative NOMA for a fair comparison of two MA techniques. Moreover, it is assumed that transmit power levels at S and R are equal and normalized to P, e.g, $P_S = P_R = P$. Therefore, in the OMA case, the power allocated for each data transmission at S and R is equal to $\frac{1}{2}P$. The other parameters of the OMA system are identical with those of the NOMA system. As it is seen from Fig. 5.7, both messages of cooperative NOMA outperform the OMA ones for all SNR regimes when no ITC implemented. When $I = 25$ dB, the OP curves for NOMA messages start to saturate at lower SNR regimes compared to those for the OMA ones. This phenomenon can be explained by using the simple fact that in the OMA case, the transmitted power $\frac{1}{2}P$ increases the ITC at PR regarding (5.1).

Numerical Results for the Amplify-and-Forward Relaying mode

The OP results for D_1 and D_2 of AF CR-NOMA are shown in Fig. 5.8. It is observed that the OP for D_2 performs better than that for D_1 in all d_1 distances. It is due to the fact that D_2 removes the unwanted message of D_1 by applying the SIC technique which improves the probability of errors in the data detection. On the other hand, the OP saturation for D_2 starts at lower SNRs compared with that for D_2. Moreover, it is noticed that the OP of D_1 degrades as d_1 increases. However, a saturation of the outage curve of D_1 starts at higher SNRs when the value of d_1 increases. This phenomenon can be explained by the fact that higher α_1 is required when D_1 is located farther from R. Moreover, Fig. 5.8 also compares the OP results derived for NOMA with simulated results for OMA in the cases without ITC, i.e., $P_I = \infty$, and when $P_I = 20$ dB. As it is seen in no ITC regime, both NOMA users outperform the OMA users in terms of the OP for all SNR values. However, when the ITC is applied ($P_I = 20$ dB), OMA users' OP curves start their saturation at higher SNR levels compared to those for the NOMA users.

In Fig. 5.9, the OP is plotted versus the transmit SNR for D_1 and D_2 when $d_1 = 3d$. We compare the OP of the proposed AF mode with that of the DF mode. Moreover, we plot high SNR approximation using $e^{-t} = 1 - t$ and $K_1(\omega) \sim 1/\omega$ for both AF and DF modes. It can be observed from the plot that the DF relaying performs better than the AF one. Furthermore, the OP of the high SNR approximation of the AF mode is consistent with that of the DF mode, which means that the maximum optimal OP of the AF cannot exceed the outage performance of the DF mode. In addition, Monte Carlo simulations results are consistent with the derived analytical results, which confirm the accuracy of

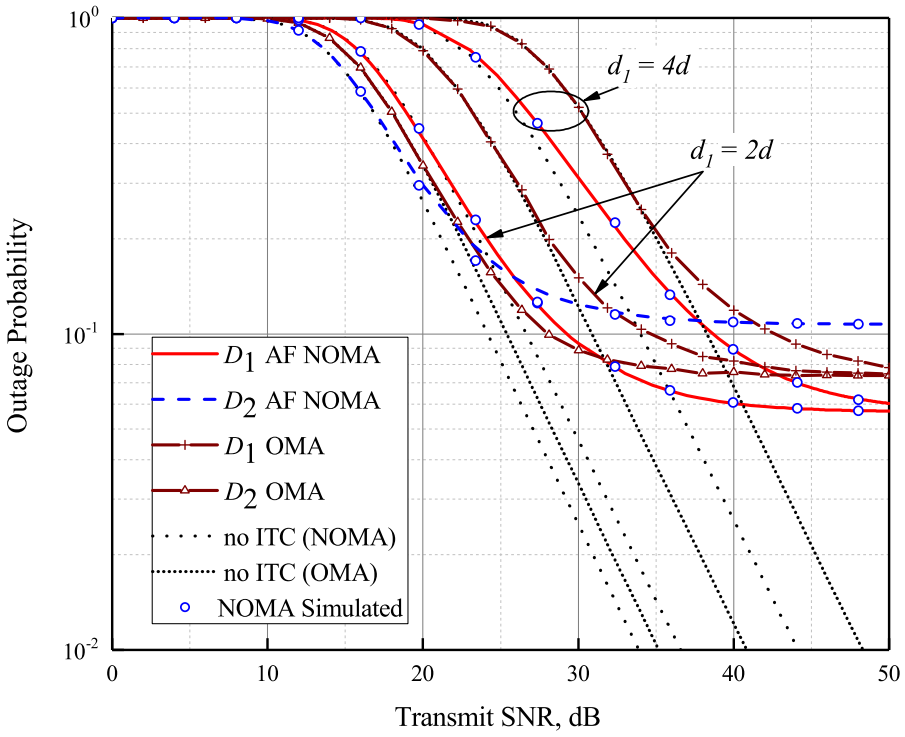

Figure 5.8. The OP of D_1 and D_2 versus the transmit SNR when $d_1 = \{2d, 4d\}$, $\alpha_1 = 0.8$, $\alpha_2 = 0.2$ and $\tau = 0$.

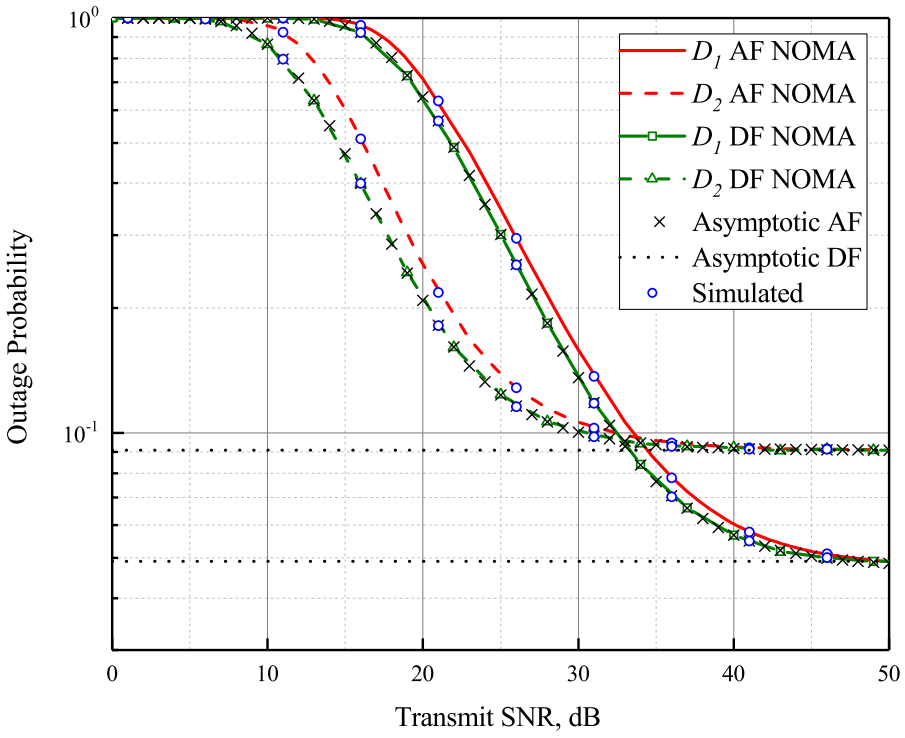

Figure 5.9. The OP of D_1 and D_2 versus the transmit SNR when $d_1 = 3d$, $\alpha_1 = 0.8$, $\alpha_2 = 0.2$ and $\tau = 0$.

Table 5.2. The observed OF-based PA factors for the AF mode.

d_1	$1.5d$	$2d$	$4d$
α_1^*	0.79	0.84	0.945
α_2^*	0.21	0.16	0.055

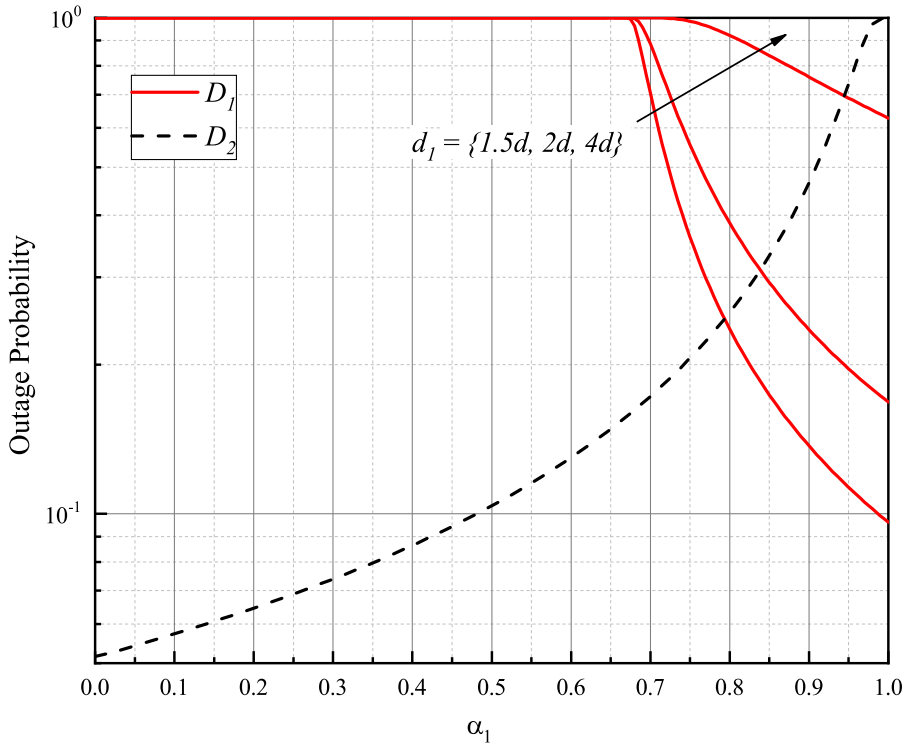

Figure 5.10. The OP of D_1 and D_2 versus the PA factors at 20 dB when $d_1 = \{1.5d, 2d, 4d\}$ and $\tau = 0$.

the derived exact and approximated OP expressions.

The numerical results on the OF-based PA factors for D_1 and D_2 are shown in Fig. 5.10. Hence, all observed values of OF-based α_1^* and α_2^* for different d_1 distances are illustrated in Table 5.2.

Fig. 5.11 shows the OP versus the transmit SNR with OF-based α_1^* and α_2^* regarding different d_1. It is observed from the figure that, for all d_1 values, D_2 shows better outage performance compared to D_1 at lower SNRs (< 22) dB. However, at higher SNR levels, D_1 is superior to D_2 in terms of the outage performance. Furthermore, when the value of d_1 rises, the OP saturation of D_1 commences at higher SNR levels. This phenomenon can be explained by using the simple fact that D_1 requires a larger value of α_1 when it is located farther from R. Finally, at about 22 dB, the OP performance of both users are the same, which confirms that OF-based PA factors provide OP fairness for users.

Fig. 5.12 illustrates the results on the OP versus the predefined SNR threshold considering OF-based α_1^* and α_2^* for various d_1 at 20 dB transmit SNR. It is worth mentioning that the OF-based PA factors improve the outage performance of D_1 (for all d_1 values)

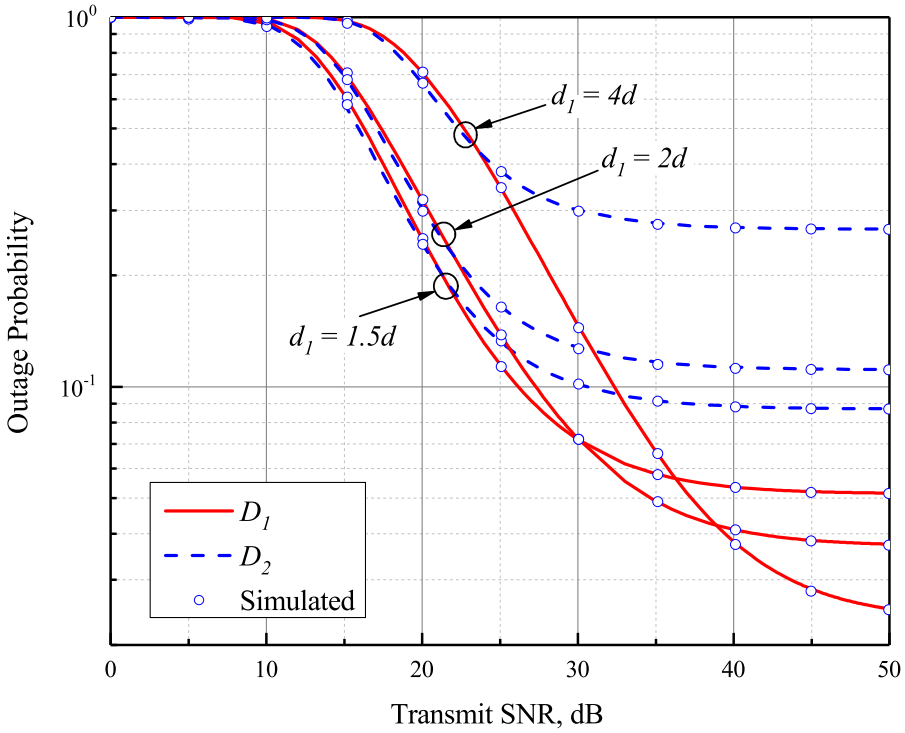

Figure 5.11. The OP of D_1 and D_2 versus the transmit SNR with OF-based PA factors when $d_1 = \{1.5d, 2d, 4d\}$ and $\tau = 0$.

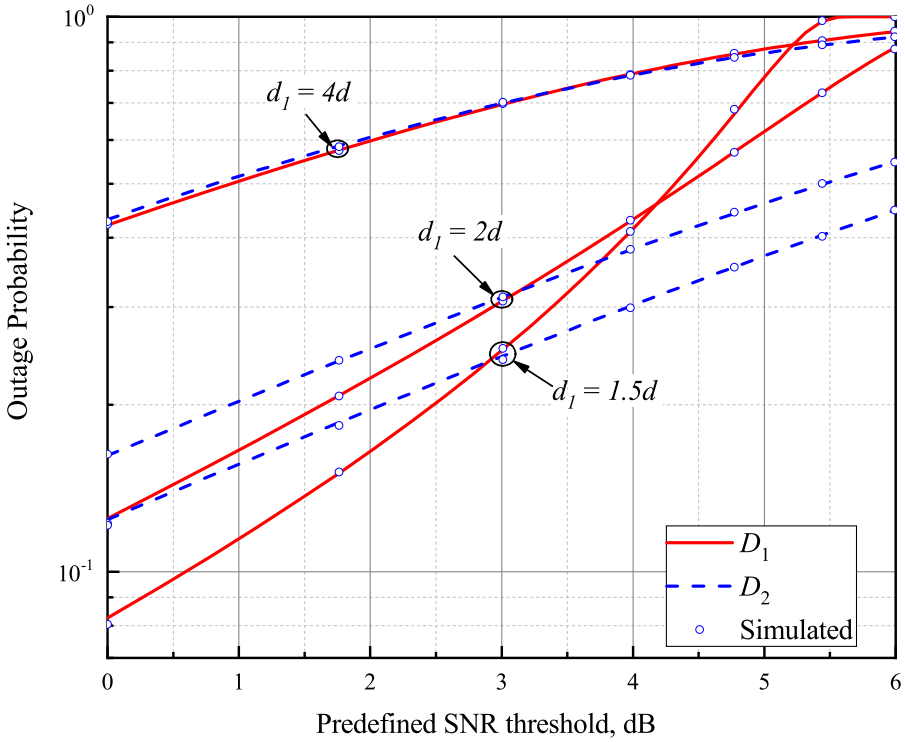

Figure 5.12. The OP of D_1 and D_2 versus the predefined SNR threshold with OF-based PA factors at 20 dB when $d_1 = \{1.5d, 2d, 4d\}$ and $\tau = 0$.

and provide fairness among NOMA users, especially, at the predefined SNR threshold of 3 dB.

5.4.2 CR-NOMA over Nakagami-m distribution

In the wireless communication, the received signal strength or power fluctuate due to the fading effect. It occurs due to multiple copies of the same transmitted signal reaching the receiver over various paths. Accordingly, the received signal power becomes RV, which can be described through different distributions, e.g., Rayleigh, Rician, Nakagami-m, etc. The Nakagami-m distribution has been broadly used for theoretical modeling of the channel fading, particularly in the wireless environment after the legendary work by Nakagami was published in [171]. The Nakagami-m is an empirical model covering a wide range of multipath fading models through the introduction of the parameter m. Thus, this channel model can give more precise results for representing the channel when it is used to model the communication systems [172, 173].

In this part, a downlink dual-hop underlay CR-NOMA network is studied for the Nakagami-m distribution. The considered system model is the same as in the previous sub-chapter despite the transmit power constraint is applied at the DF based R instead of S (see Fig. 5.13). Thus, it is assumed that S does not interfere with PR due its sufficient remoteness. Moreover, channel coefficients, i.e., h_t, $\forall t \in \{SR, RP, 1, 2\}$, experience quasi-static non - independent and identically distributed Nakagami-m fading which PDF can be written as

$$f_{h_t}(r) = \frac{2\lambda_t^{m_t}}{\Gamma(m_t)} r^{2m_t-1} \exp\left(-\lambda_t r^2\right), \ \lambda_t = \frac{m_t}{\hat{r}_t}, \tag{5.30}$$

It worth to mention that the Nakagami-m fading can describe different multipath channels by using the fading parameter m. For example, the one-sided Gaussian fading and the Rayleigh fading can be described by setting $m = \frac{1}{2}$ and $m = 1$, respectively. Additionally, the Nakagami-m fading frequently used to describe the indoor [174] and urban [175] multipath environments. According to the proposed system model, R is restricted from maximum transmit power as the secondary transmission is only permitted if PR receive a tolerable level of interference caused by the SN. Therefore, the transmit power restriction at R can be written as [161]

$$P_R \leq \min\left(\frac{Id_{RP}^{\tau}}{|h_{RP}|^2}, \bar{P}_R\right), \tag{5.31}$$

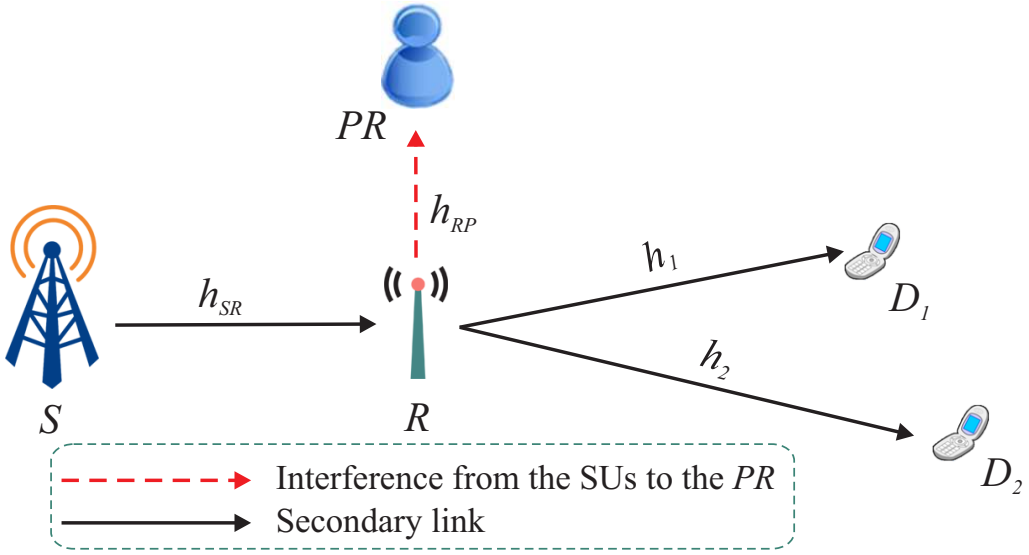

Figure 5.13. A dual-hop underlay dual-hop CR-NOMA network.

where $\bar{P}_R$ is the maximum allowed transmit power at R. Then, S broadcasts the superimposed signal to R, which can be written as followings

$$y_R = \sqrt{\frac{P_S}{d_{SR}^{\tau}}} h_{SR} \left(\sqrt{a_1} x_1 + \sqrt{a_2} x_2\right) + n_R. \tag{5.32}$$

In this system model, the power allocation factors are assumed to be as $a_1 < a_2$ and channel ordering as $h_1 > h_2$, which means that the channel of D_1 is stronger than that of D_2. Hence, D_2 is allocated with higher power portion. After R receives the signal from S, it implements the SIC scheme first to decode x_2 with the SINR of

$$\gamma_{R,2} = \frac{|h_{SR}|^2 a_2 P_S}{|h_{SR}|^2 a_1 P_S + \sigma_R^2 d_{SR}^{\tau}}. \tag{5.33}$$

Further, on the condition that $\gamma_{R,2} \geq \xi_2$, i.e., the SIC is successfully implemented at R to remove x_2. Then, the data detected in (5.4) is removed from the remaining signal and the SNR to detect x_1 at R can be written as

$$\gamma_{R,1} = \frac{|h_{SR}|^2 a_1 P_S}{\sigma_R^2 d_{SR}^{\tau}}. \tag{5.34}$$

Furthermore, R forwards the detected superimposed signal of $x_R = \sum_{i=1}^{2} \sqrt{b_i P_R} \tilde{x}_i$ to both secondary users, where $b_1 < b_2$. Thus, in the 2^{nd} time slot, the received signals at D_1 and D_2 are respectively expressed by followings

$$y_1 = \sqrt{\frac{P_R}{d_1^{\tau}}} h_1 \left(\sqrt{b_1} \tilde{x}_1 + \sqrt{b_2} \tilde{x}_2\right) + n_1 \tag{5.35}$$

and

$$y_2 = \sqrt{\frac{P_R}{d_2^\tau}} h_2 \left(\sqrt{b_1}\tilde{x}_1 + \sqrt{b_2}\tilde{x}_2 \right) + n_2. \tag{5.36}$$

Further, D_1 applies the SIC technique to detect $\tilde{x}_2$ whereas treating its own signal $\tilde{x}_1$ as a background noise. Therefore, the SNR of detecting $\tilde{x}_2$ can be written by

$$\gamma_{1,2} = \frac{|h_1|^2 b_2 \rho_R}{|h_1|^2 b_1 \rho_R + d_1^\tau}. \tag{5.37}$$

Then, on the condition that $\gamma_{1,2} \geq \xi_2$, i.e., the SIC is successfully implemented at D_1 to remove x_2, the data detected in (5.37) is removed from the remaining signal and the SNR to detect $\tilde{x}_1$ at D_1 can be written as

$$\gamma_{1,1} = \frac{|h_1|^2 b_1 \rho_R}{d_1^\tau}. \tag{5.38}$$

Regarding D_2, it decodes $\tilde{x}_2$ while $\tilde{x}_1$ is treated as a background noise, which SINR can be expressed as

$$\gamma_{2,2} = \frac{|h_2|^2 b_2 \rho_R}{|h_2|^2 b_1 \rho_R + \ d_2^\tau}. \tag{5.39}$$

Now, the achievable rates for x_1 and x_2 are derived by [170]

$$\mathcal{R}_1 = \frac{1}{2} \log_2 \left(1 + \min \left(\gamma_{R,1}, \gamma_{1,1}\right)\right) \tag{5.40}$$

and

$$\mathcal{R}_2 = \frac{1}{2} \log_2 \left(1 + \min \left(\gamma_{R,2}, \gamma_{1,2}, \gamma_{2,2}\right)\right), \tag{5.41}$$

respectively.

5.4.2.1 Outage Performance Analysis

This section will evaluate the OP for x_1 and x_2 for Nakagami-m distribution. The OP of x_1 can be expressed by followings

$$\begin{aligned} P_{\text{out},1}(\xi_1) &= 1 - \Pr\left[\min\left(\gamma_{R,1}, \gamma_{1,1}\right) > \xi_1\right] = 1 - \Pr\left[\gamma_{1,1} > \xi_1\right] \Pr\left[\gamma_{R,1} > \xi_1\right] \\ &= F_{\gamma_{1,1}}(\xi_1) + F_{\gamma_{R,1}}(\xi_1) - F_{\gamma_{1,1}}(\xi_1) F_{\gamma_{R,1}}(\xi_1). \end{aligned} \tag{5.42}$$

Proposition 9 The closed-form OP expression for x_1 can be written as

$$P_{\text{out},1}(\xi_1) = 1 - \frac{\Gamma\left(m_{SR}, \frac{\lambda_{SR}\xi_1 d_{SR}^{\tau}}{a_1\rho_S}\right)}{\Gamma\left(m_{SR}\right)}\left[\frac{\Gamma\left(m_1, \frac{\lambda_1\xi_1 d_1^{\tau}}{b_1\bar{\rho}_R}\right)}{\Gamma\left(m_1\right)}\left(1 - \frac{\Gamma\left(m_{RP}, \frac{\lambda_{RP}\rho_I d_{RP}^{\tau}}{\bar{\rho}_R}\right)}{\Gamma\left(m_{RP}\right)}\right)\right.$$
$$\left. + \frac{\lambda_{RP}^{m_{RP}}}{\Gamma(m_{RP})}\sum_{i=0}^{m_1-1}\frac{\left(\frac{\lambda_1\xi_1 d_1^{\tau}}{b_1\rho_I d_{RP}^{\tau}}\right)^i}{i!}c_1^{-(m_{RP}+i)}\Gamma\left(m_{RP}+i, \frac{\rho_I d_{RP}^{\tau}}{\bar{\rho}_R}c_1\right)\right] \quad (5.43)$$

Proof: See Appendix C.5 for details. ■

Similarly as x_1, the OP of x_2 is expressed by

$$\begin{aligned} P_{\text{out},2}(\xi_2) =& 1 - \Pr\left[\min\left(\gamma_{R,2}, \gamma_{1,2}, \gamma_{2,2}\right) > \xi_2\right] \\ =& 1 - \Pr\left[\gamma_{R,2} > \xi_2\right]\Pr\left[\gamma_{1,2} > \xi_2\right]\Pr\left[\gamma_{2,2} > \xi_2\right] \\ =& F_{\gamma_{1,2}}(\xi_2) + \left(1 - F_{\gamma_{1,2}}(\xi_2)\right)\left(F_{\gamma_{2,2}}(\xi_2) + F_{\gamma_{R,2}}(\xi_2) - F_{\gamma_{2,2}}(\xi_2)F_{\gamma_{R,2}}(\xi_2)\right). \end{aligned} \quad (5.44)$$

Proposition 10 The closed-form OP expression for x_2 is given in C.6.

Proof: See Appendix C.6 for details. ■

5.4.2.2 Numerical Results

In this section, numerical and simulation results of the OP expressions for Nakagami-m fading will be presented. The system parameters are adopted as follows: d_{RP} = d_{SR} = d_1 = d, d_2 = $2d, 4d, 6d$, τ = 3, I = 25 dB and the corresponding SNR threshold $\xi = \xi_1 = \xi_2$ = 1 dB. Moreover, parameters of Nakagami-m distribution are taken as $m = m_{RP} = m_{SR} = m_1 = m_2 = 1$, $\hat{r} = \hat{r}_{RP} = \hat{r}_{SR} = \hat{r}_1 = \hat{r}_2 = \sqrt{2}$.

Fig. 5.14 illustrates the OP versus the transmit SNR for both messages of NOMA users. Here, it is assumed that $a_2 = b_2 = 0.8$. It is clearly seen from the plot that the OP of x_1 shows better performance compared to that of x_2 for low SNR levels (below 30 dB). On the other hand, after 30 dB, the OP of x_2 perform better. This can be explained by the fact that D_1 implements the SIC method in order to decode the desired message (which intuitively provides us with higher SNR value) whereas D_2 decodes x_2 by treating $x_1$as a background noise. The OP curve of x_1 starts saturating at 25 dB and then, after 35 dB, it becomes flat due to the fact that the OP of x_1 in (5.43) cannot outperform that of x_1 observed at R (as the relay transmit power is constrained). Moreover, it can be seen that the OP of x_2 remains its improvement till it reaches the best performance defined by the OP of x_2 attainable at R. Furthermore, it is noticed that the increase of d_2 results in the

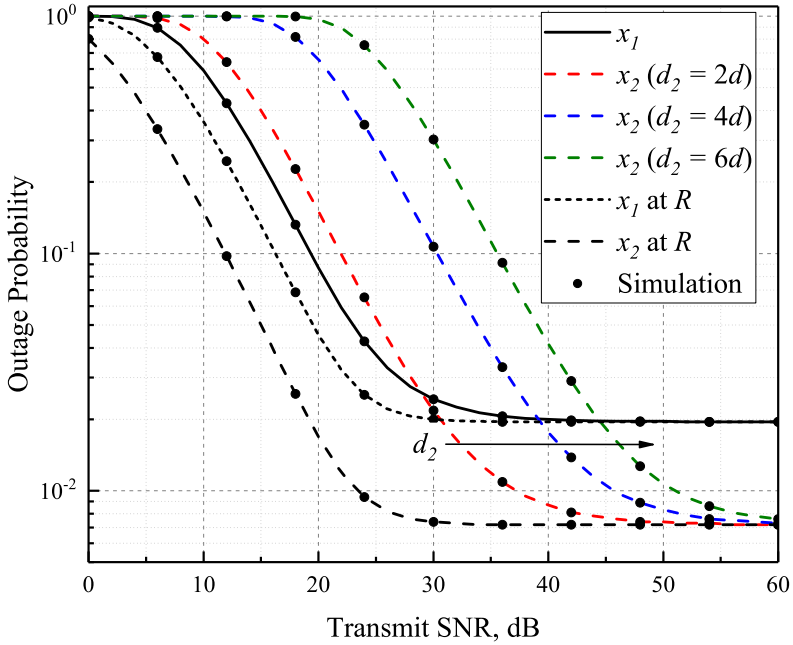

Figure 5.14. The OP versus the transmit SNR for x_1 and x_2 when d_2 = {2 m, 4 m, 6 m}, $a_1 = b_1 = 0.2$ and $a_2 = b_2 = 0.8$.

degradation of the OP performance. However, the saturation of the OP curves happens at higher SNR levels when the value of d_2 is higher.

In the previous results, it was assumed that $a_1 = b_1 = 0.2$ and $a_2 = b_2 = 0.8$. According to the NOMA concept, different PA coefficients are applied to the user terminals located at the different distances from the transmitter, i.e., $R \rightarrow D_1$ and $R \rightarrow D_2$. However, this is not valid for the $S \rightarrow R$ link and thus we can find OF-based PA coefficients a_1 and a_2 to provide equal outage performance for x_1 and x_2 since we found that at high SNR the OP curves of x_1 and x_2 saturate at the OP values defined by the outage observed at R. Therefore, in Fig. 5.15, we plot the OP of x_1 and x_2 as a function of a_1 attainable at D_1 and D_2, respectively. The following system parameters are adopted: $d_{RP} = d_1 = 2d$, $d_2 = 2d$ and $d_{SR} = \{d; 2d\}$. The observation SNR point is 30 dB. The increase of a_1 results in the OP improvement of x_1 while deteriorating the performance of the message x_2. For both distances, each pair of the corresponding OP curves can be characterized by the same intersection point which can be simply determined using Mathematica software. For the defined system parameters, the OF-based power coefficient a_1^* equals 0.307 which provides the equal OP for both users (will be used for the next results discussion).

In Fig. 5.16, the OF-based OP results for $a_1^* = 0.307$ and $a_2^* = 0.693$ are depicted. It is noted that, compared with the results in Fig. 5.14, the saturation of the OP curves starts at 0.0128 for both x_1 and x_2 observed at the corresponding destination users for $b_1^* = 0.089$ and $b_2^* = 0.911$, i.e., the OP of x_1 improves while the OP of x_2 degrades. In the case when d_{SR} is increased, the saturation starts at higher SNR levels. It can be explained by

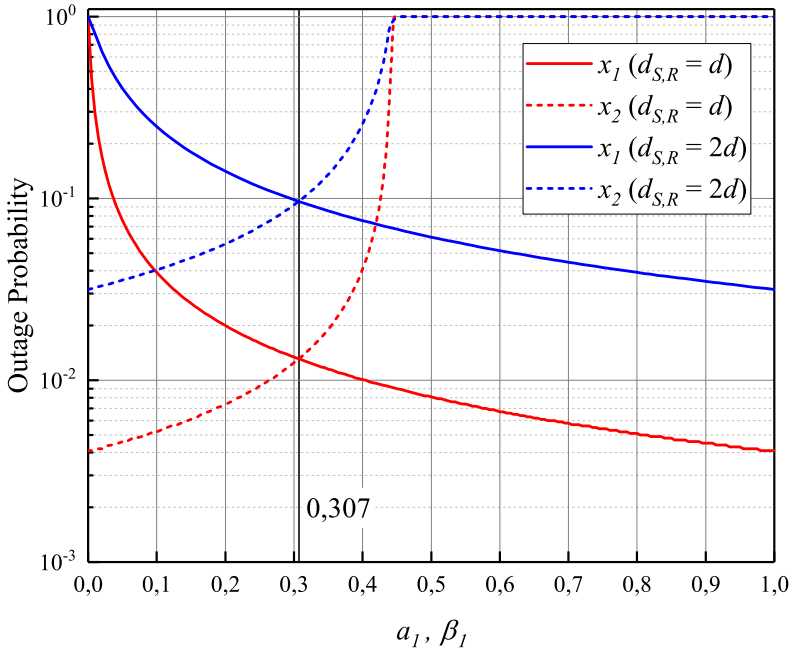

Figure 5.15. The OP versus a_1 for x_1 and x_2 at 30 dB when d_{SR} = {d, 2d}.

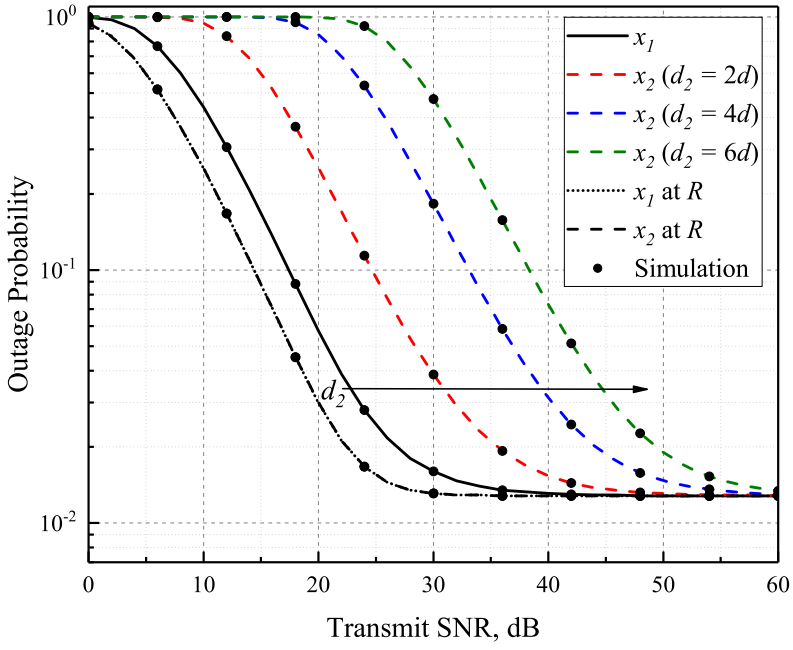

Figure 5.16. The optimized OP versus the transmit SNR for x_1 and x_2 when d_2 = {2d, 4d, 6d}.

the simple fact that more transmit power is required to overcome the path-loss attenuation and support the required performance.

5.5 Outage analysis of dual-hop CR-NOMA: Case 2

In this part, we consider a dowlink underlay CR-NOMA model consisting of K NOMA secondary destination users. It is assumed that both S and R are restricted by the maximum transmit power. This assumption is practical and provides extra useful insights into the system performance. Besides, considering the ITC results in the appearance of the additional RVs, which, in turn, significantly complicates the already complex analysis. Moreover, we consider imperfect CSI conditions and applied interference from primary transmitters to secondary receive nodes. The exact generalized closed-form expressions for the OP of the secondary destination users are derived and verified by Monte-Carlo simulations.

5.5.1 DF CR-NOMA with K secondary NOMA users

5.5.1.1 System Model

A downlink dual-hop DF underlay CR-NOMA network is shown in Fig. 5.17, where the system model consists of the PR and the SN with S, R and K NOMA secondary destination users $(D_1, ..., D_{K-1}, D_K)$. Fading-channel gains, i.e., h_{SP}, h_{SR}, h_{RP}, h_1,..., h_{K-1} and h_K, follow i.n.i.d. Rayleigh block fading model. In all previous system models in this chapter, it is assumed perfect CSI. However, due to the unpredictable characteristics of the wireless medium, in practice, the wireless CSI becomes imperfect. Considering this, the real channels, by assuming imperfect CSI and minimum mean square estimation error model, can be written by [68, 176]

$$h_t = \hat{h}_t + \tilde{h}_t, \ \forall t \in \{SP, SR, 1, ..., K-1, K\}, \tag{5.45}$$

where $\hat{h}_t$ denotes the estimated channel coefficient with $\mathcal{CN}(0, \sigma^2_{\hat{h}_t})$ while $\tilde{h}_t$ stands for the error term, which is modeled as a complex Gaussian distributed RV with $\mathcal{CN}(0, \sigma^2_{\tilde{h}_t})$, where $\sigma^2_{\tilde{h}_t}$ is the variance. The distances between nodes are expressed by d_{SP}, d_{SR} and $d_1, ..., d_{K-1}, d_K$. Moreover, the PN interference[4] received at the SN users can be indicated by P_I. It is assumed that S and R can interfere with PR. Hence, the transmit power level

[4]In general, CSI of primary transmitters is not available at secondary receivers. Thus, with regard to the central limit theorem [177], secondary receivers can manage all interference signals coming from primary transmitters as the AWGN noise with $\mathcal{CN}(0, \nu\sigma^2)$, where ν is the scaling coefficient of P_I. For instance, considering HetNet systems, when the receiver obtains interference from many sources, the total interference signals from these N interfering nodes can be approximated as a sum of n terms, which, with the respect to the CLT, can be further approximated by a complex Gaussian distribution [178], [179, §3.9.2].

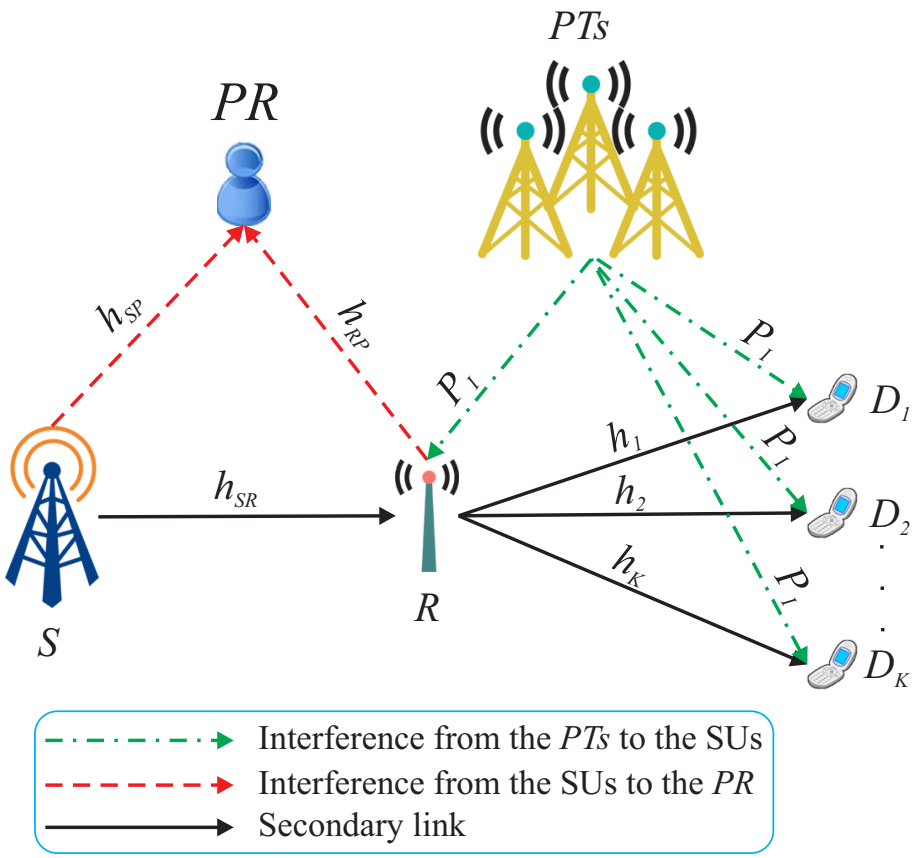

Figure 5.17. A downlink underlay dual-hop CR-NOMA network.

at the secondary transmit node L, $\forall L \in \{S, R\}$, is restricted as

$$P_L \leq \min\left(\frac{Id_{LP}^{\tau}}{|h_{LP}|^2}, \bar{P}_L\right), \tag{5.46}$$

where $\bar{P}_L$ denotes the maximum average allowed transmit power level at L.

Now, by considering the aforementioned power restrictions, S conveys the superimposed signal to K secondary NOMA destination users with the help of R in two-time slots, which can be written as

$$x_S = \sum_{p=1}^{K} \sqrt{\alpha_p P_S} x_p, \tag{5.47}$$

where x_p, with $\mathbb{E}(|x_p|^2) = 1$, is the intended message to D_p while α_p denotes the PA factor, with $\sum_{p=1}^{K} \alpha_p = 1$. Furthermore, regarding the system model, the channel gains of destination NOMA users are ordered as $h_1 < ... < h_{K-1} < h_K$, while $\alpha_1 > ... > \alpha_{K-1} > \alpha_K$, which means that the channel of D_1 is weaker than the channel of D_{K-1}. Accordingly, a higher power portion is allotted to D_1.

In the 1^{st} time slot, R obtains the superimposed NOMA signal as follows

$$\begin{aligned} y_R &= \left(\hat{h}_{SR} + \tilde{h}_{SR}\right) \sqrt{\frac{P_S}{d_{SR}^{\tau}}} \sum_{p=1}^{K} \sqrt{\alpha_p} x_p + P_I + n_R \\ &= \hat{h}_{SR} \sqrt{\frac{P_S}{d_{SR}^{\tau}}} \sum_{p=1}^{K} \sqrt{\alpha_p} x_p + \underbrace{\tilde{h}_{SR} \sqrt{\frac{P_S}{d_{SR}^{\tau}}} \sum_{p=1}^{K} \sqrt{\alpha_p} x_p + P_I + n_R}_{\text{effective noise}}. \end{aligned} \tag{5.48}$$

For mathematical tractability and without loss of generality, it is assumed that each SN receive node obtains the same P_I from the primary transmitters.

Further, R applies the SIC with the following decoding order of the users' messages: first of all, the message of the user 1 ($j = 1$) is decoded at the same time treating the other messages ($j = 2, ..., K$) as a background noise. Further, R removes the decoded message from the obtained signal. In the next phase, R decodes the message of the user 2 by treating the remained messages ($j = 3, .., K$) as a background noise, and so on and so forth. In the final stage, the message of the user K can be decoded at R without any inter-user interference. Therefore, the SINR at R to decode x_j is derived by

$$\gamma_{R,j} = \frac{|\hat{h}_{SR}|^2 \alpha_j \rho_S}{|\hat{h}_{SR}|^2 \rho_S \Theta + \zeta_R d_{SR}^{\tau}}, \tag{5.49}$$

where $\zeta_R = \frac{\rho_S \sigma_{\tilde{h}_{SR}}^2}{d_{SR}^{\tau}} + \nu + 1$ and $\Theta = \sum_{p=j+1}^{K} \alpha_p$. Then, on the condition that $\gamma_{R,j} \geq \xi_j$, i.e., the SIC is successfully implemented at R to remove x_j, the messages detected in (5.49) are removed from the received signal and the SNR to detect x_K at R can be written as

$$\gamma_{R,K} = \frac{|\hat{h}_{SR}|^2 \alpha_K \rho_S}{\zeta_R d_{SR}^{\tau}}. \tag{5.50}$$

Then, within the 2^{nd} time slot, the detected superimposed signal at R is further forwarded to all secondary NOMA destination users, which is shown by

$$x_R = \sum_{p=1}^{K} \sqrt{P_R \beta_p} \tilde{x}_p, \tag{5.51}$$

where $\tilde{x}_p$ is the detected message of the corresponding NOMA user at R; β_p, with $\sum_{p=1}^{K} \beta_p =$

1, satisfying $\beta_1 > ... > \beta_{K-1} > \beta_K$, denotes the relay PA factor. Then, the received superimposed signal at D_j can be written as

$$y_j = \hat{h}_j \sqrt{\frac{P_R}{d_j^\tau}} \sum_{p=1}^{K} \sqrt{\beta_p} \tilde{x}_p + \underbrace{\tilde{h}_j \sqrt{\frac{P_R}{d_j^\tau}} \sum_{p=1}^{K} \sqrt{\beta_p} \tilde{x}_p + P_I + n_j}_{\text{effective noise}}, \ \forall j \in \{1, ..., K-1, K\}. \tag{5.52}$$

Moreover, D_k uses the SIC in order to decode the undesired signal of D_j ($1 \leq j \leq k \leq K$) by following the same method as in R. Hence, the SINR of decoding the message j at D_k can be expressed as

$$\gamma_{k,j} = \frac{|\hat{h}_k|^2 \beta_j \rho_R}{|\hat{h}_k|^2 \rho_R \Phi + \zeta_k d_k^\tau}, \ \forall k \in \{1, ..., K\}, \tag{5.53}$$

where $\Phi = \sum_{p=j+1}^{K} \beta_p$ and $\zeta_k = \frac{\rho_R \sigma_{\tilde{h}_k}^2}{d_k^\tau} + \nu + 1$. Finally, if the messages of $K-1$ users are detected successfully, the D_K can detect its own message K without any inter-user interference, which SNR is written by

$$\gamma_K = \frac{|\hat{h}_K|^2 \beta_K \rho_R}{\zeta_K d_K^\tau}, \tag{5.54}$$

where $\zeta_K = \frac{\rho_R \sigma_{\tilde{h}_K}^2}{d_K^\tau} + \nu + 1$. The achievable rates for the messages dedicated to D_j ($1 \leq j \leq k < K$) and D_K can be expressed by [170]

$$\mathcal{R}_j = \frac{1}{2} \log_2 \left(1 + \min \left(\gamma_{R,j} \gamma_{k,j}\right)\right) \tag{5.55}$$

and

$$\mathcal{R}_K = \frac{1}{2} \log_2 \left(1 + \min \left(\gamma_{R,K}, \gamma_K\right)\right), \tag{5.56}$$

respectively.

5.5.1.2 Outage Performance Analysis

The OP for the proposed system model is investigated in this part. The message x_j is considered to be in an outage if the achievable rate of x_j is below a predefined target rate $\mathcal{R}_{\text{th}j}$ (which corresponding receive SNR threshold is $\xi_j = 2^{2\mathcal{R}_{\text{th}j}} - 1$), i.e., $P_{\text{out}} =$

$\Pr\left[\mathcal{R}_j < \mathcal{R}_{\text{th}j}\right]$. Hence, the OP of x_j is derived by followings

$$\begin{aligned} P_{\text{out},j}(\xi_j) =& 1 - \Pr\left[\min\left(\gamma_{R,j}, \gamma_{k,j}\right) > \xi_j\right] \\ =& F_{\gamma_{R,j}}(\xi_j) + \left(1 - F_{\gamma_{R,j}}(\xi_j)\right)\left((-1)^n \sum_{\forall j} \prod_{\forall t} F_{\gamma_{t,j}}(\xi_j)\right), \end{aligned} \tag{5.57}$$

where $t = \{m^{(0)}, m^{(1)}, ..., m^{(n)}\}$, $n = K - j$, $m^{(0)} = j, j+1, ..., K$, $m^{(1)} = j+1, ..., K$, $m^{(n)} = j+n, ..., K$ and $m^{(n)} \neq m^{(n+1)}$. For instance, if $K = 3$, the OP of x_2 $(j = 2)$ is derived from (5.57) as follows: $n = 1$, $m^{(0)} = 2, 3$ and $m^{(1)} = 3$ $(m^{(0)} \neq m^{(1)})$. Hence, firstly, the CDFs of $F_{\gamma_{2,2}}$ and $F_{\gamma_{3,2}}$ are summed, then the product of the both CDFs are subtracted (since $m^{(0)} \neq m^{(1)} \rightarrow m^{(0)} = 2$ and $m^{(1)} = 3$), and te resulted equation can be written by followings

$$\begin{aligned} P_{\text{out},2}(\xi_2) =& 1 - \Pr\left[\min\left(\gamma_{R,2}, \gamma_{3,2}, \gamma_{2,2}\right) > \xi_2\right] \\ =& 1 - \Pr\left[\gamma_{R,2} > \xi_2\right]\Pr\left[\gamma_{3,2} > \xi_2\right]\Pr\left[\gamma_{2,2} > \xi_2\right] \\ =& F_{\gamma_{R,2}}(\xi_2) + \left(1 - F_{\gamma_{R,2}}(\xi_2)\right)\left(F_{\gamma_{2,2}}(\xi_2) + F_{\gamma_{3,2}}(\xi_2) - F_{\gamma_{2,2}}(\xi_2)F_{\gamma_{3,2}}(\xi_2)\right). \end{aligned} \tag{5.58}$$

Proposition 11 The closed-form expression for the CDF of the RV $\gamma_{R,j}$ in (5.49) is expressed as

$$F_{\gamma_{R,j}}(\xi_j) = \begin{cases} 1 - \underbrace{\left(e^{-\frac{\xi_j \zeta_R d_{SR}^{\tau}}{2\mu\bar{\rho}_S}} - \frac{\mathcal{G}_{R,j} e^{-\frac{\mu\rho_I d_{SP}^{\tau} + \xi_j \zeta_R d_{SR}^{\tau}}{2\mu\bar{\rho}_S}}}{\mu + \mathcal{G}_{R,j}}\right)}_{\Lambda_{R,j}}, & \xi_j < \frac{\alpha_j}{\Theta}, \\ 1, & \text{otherwise.} \end{cases} \tag{5.59}$$

Proof: See Appendix C.7 for details. ■

Proposition 12 The closed-form expression for the CDF of the RV $\gamma_{k,j}$ in (5.53) is expressed as

$$\begin{aligned} F_{\gamma_{k,j}}(\xi_j) =& \underbrace{\frac{K!}{(K-k)!(k-1)!}\sum_{i=0}^{K-k}\frac{(-1)^i}{k+i}\binom{K-k}{i}}_{L_k(i)}\underbrace{\sum_{n=0}^{k+i}(-1)^n\binom{k+i}{n}}_{\mathcal{V}_k(n)} \\ &\times\left[\underbrace{\left(1 - e^{-\frac{\rho_I d_{RP}^{\tau}}{2\bar{\rho}_R}}\right)}_{\mathcal{I}} e^{-\frac{\xi_j \zeta_k d_k^{\tau} n}{2\epsilon\bar{\rho}_R}} + \frac{\epsilon e^{-\frac{\rho_I d_{RP}^{\tau}\left(\epsilon + \mathcal{G}_{k,j} n\right) + \mathcal{O}_{k,j}\bar{\rho}_R n}{2\epsilon\bar{\rho}_R}}}{\epsilon + \mathcal{G}_{k,j} n}\right] \end{aligned} \tag{5.60}$$

Proof: See Appendix C.8 for details. ■

Now, using (5.59) and (C.51), the OP expression in the example shown in (5.58) can be expressed in its closed form as

$$P_{\text{out},2}(\xi_2) = 1-\Lambda_{R,2}+\Lambda_{R,2}\times\left(\sum_{p=2}^{3} L_p(i)\mathcal{V}_p(n)\left[\mathcal{I}e^{-\frac{\xi_2\zeta_p d_p^{\tau} n}{2\epsilon\bar{\rho}_R}} + \frac{\epsilon e^{-\frac{\rho_I d_{RP}^{\tau}\left(\epsilon+\mathcal{G}_{p,2}n\right)+\mathcal{O}_{p,2}\bar{\rho}_R n}{2\epsilon\bar{\rho}_R}}}{\epsilon+\mathcal{G}_{p,2}n}\right]\right.$$
$$\left. - \prod_{p=2}^{3} L_p(i)\mathcal{V}_p(n)\left[\mathcal{I}e^{-\frac{\xi_2\zeta_p d_p^{\tau} n}{2\epsilon\bar{\rho}_R}} + \frac{\epsilon e^{-\frac{\rho_I d_{RP}^{\tau}\left(\epsilon+\mathcal{G}_{p,2}n\right)+\mathcal{O}_{p,2}\bar{\rho}_R n}{2\epsilon\bar{\rho}_R}}}{\epsilon+\mathcal{G}_{p,2}n}\right]\right), \quad (5.61)$$

where $\xi_2 < \frac{\alpha_2}{\alpha_3}$ and $\xi_2 < \frac{\beta_2}{\beta_3}$, otherwise, $P_{\text{out},2}(\xi_2) = 1$.

The OP of x_K, similar to x_j, can be written as follows

$$\begin{aligned} P_{\text{out},K}(\xi_K) =& 1 - \Pr\left[\min\left(\gamma_{R,K}, \gamma_K\right) > \xi_K\right] \\ =& F_{\gamma_K}(\xi_K) + F_{\gamma_{R,K}}(\xi_K) - F_{\gamma_K}(\xi_K)F_{\gamma_{R,K}}(\xi_K), \end{aligned} \quad (5.62)$$

where ξ_K is the receive SNR threshold at D_K. Now, following the same steps as in Appendix C.7, the CDF of $\gamma_{R,K}$ can be written in a closed-form as

$$F_{\gamma_{R,K}}(\xi_K) = 1 - \underbrace{\left(e^{-\frac{\xi_K\zeta_R d_{SR}^{\tau}}{2\alpha_K\bar{\rho}_S}} - \frac{\mathcal{G}_{R,K}e^{-\frac{\alpha_K\rho_I d_{SP}^{\tau}+\xi_K\zeta_R d_{SR}^{\tau}}{2\alpha_K\bar{\rho}_S}}}{\alpha_K+\mathcal{G}_{R,K}}\right)}_{\Lambda_{R,K}}. \quad (5.63)$$

In addition, by applying order statistics for the strongest channel [180, Eq. (19)], the CDF of the ordered RV $|\hat{h}_K|^2$ can be expressed by

$$F_{|\hat{h}_K|^2}(\xi_K) \triangleq F_{\gamma_K}(\xi_K) = \left[1 - e^{-\frac{\xi_K\zeta_K d_K^{\tau}}{2\beta_K\rho_R}}\right]^K. \quad (5.64)$$

Then, following the same steps as in Appendix C.8, the CDF of γ_K can be written in a closed-form as

$$F_{\gamma_K}(\xi_K) = \mathcal{V}_K(m)\left(\mathcal{I}e^{-\frac{\xi_K\zeta_K d_K^{\tau} m}{2\beta_K\bar{\rho}_R}} + \frac{\beta_K e^{-\frac{\rho_I d_{RP}^{\tau}(\beta_K+\mathcal{G}_K m)+\mathcal{O}_K\bar{\rho}_R m}{2\beta_K\bar{\rho}_R}}}{\beta_K+\mathcal{G}_K m}\right), \quad (5.65)$$

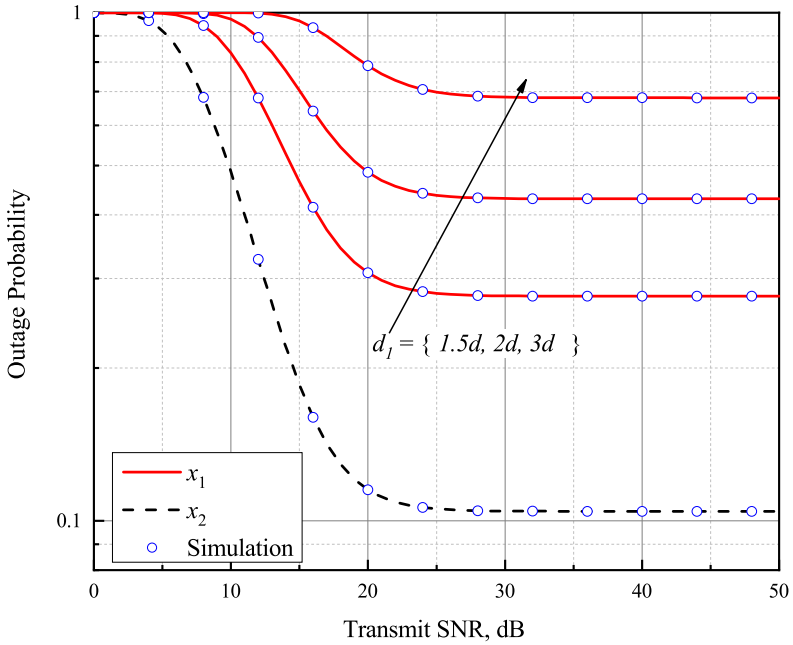

Figure 5.18. The OP of messages x_1 and x_2 versus the transmit SNR when $d_1 = \{1.5d, 2d, 3d\}$, $\alpha_1 = 0.8$, $\alpha_2 = 0.2$, $\nu = 0$ and $\sigma^2_{\tilde{h}_\iota} = 0$.

where $\mathcal{V}_K(m) = \sum_{m=0}^{K} \binom{K}{m}(-1)^m$. Finally, substituting (5.63) and (5.65) into (5.62), the OP of x_K can be written in its closed-form as

$$\mathcal{P}_{\text{out},K} = 1 - \Lambda_{R,K}\left[1 - \mathcal{V}_K(m)\left(\mathcal{I}e^{-\frac{\xi_K \zeta_K d_K^{\tau} m}{2\beta_K \bar{\rho}_R}} + \frac{\beta_K e^{-\frac{\rho_I d_{RP}^{\tau}(\beta_K + \mathcal{G}_K m) + \mathcal{O}_K \bar{\rho}_R m}{2\beta_K \bar{\rho}_R}}}{\beta_K + \mathcal{G}_K m}\right)\right]. \tag{5.66}$$

Now, using (5.55) and (5.56), the average throughput of the messages devoted to D_j $(j < \forall k \leq K)$ and D_K are respectively written as

$$\mathcal{C}_j = \mathcal{R}_j\left(1 - \mathcal{P}_{\text{out},j}\right), \tag{5.67}$$

$$\mathcal{C}_K = \mathcal{R}_K\left(1 - \mathcal{P}_{\text{out},K}\right). \tag{5.68}$$

5.5.1.3 Numerical Results

In this section, numerical results on the OP over thhe Rayleigh fading is presented. As a special case, it is considered that the system model consists of two secondary NOMA destination users ($K = 2$), i.e., D_1 and D_2. Similarly in the previous system models, the next system parameters are considered: $d_1 = \{1.5d, 2d, 3d\}$, $d_{SP} = d_{SR} = d_{RP} = d_2 = d$, equal source and relay transmit power, i.e., $P_S = P_R = P$, $I = 20$ dB, $\alpha_i =$

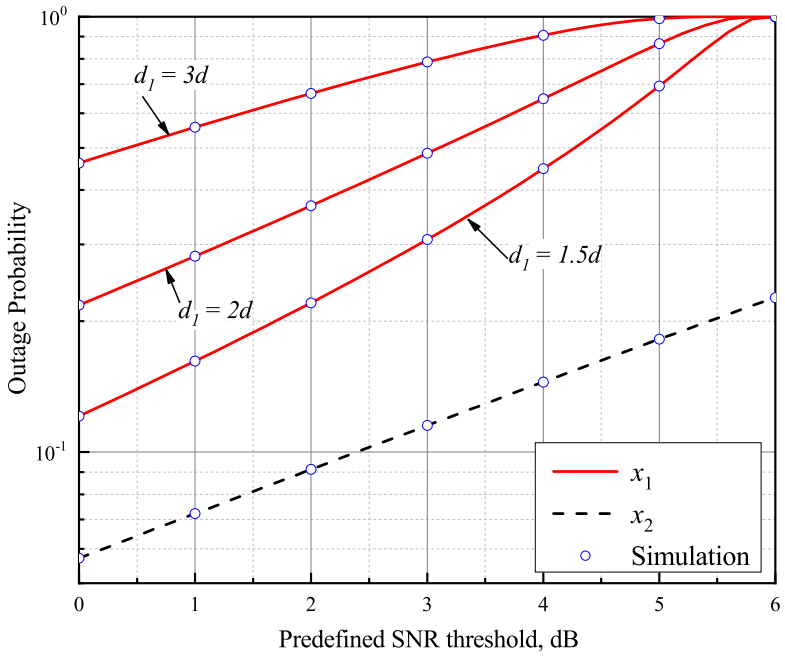

Figure 5.19. The OP of messages x_1 and x_2 versus the SNR threshold at 20 dB when $d_1 = \{1.5d, 2d, 3d\}$, $\alpha_1 = 0.8$, $\alpha_2 = 0.2$, $\nu = 0$ and $\sigma^2_{\tilde{h}_\iota} = 0$.

β_i, $\forall i \in \{1, 2\}$, $\nu = 0.5$, $\xi = \xi_1 = \xi_2 = 3$ dB, $\sigma^2_{\tilde{h}_\iota} = \{0.001, 0.005\}$, with $\forall \iota \in \{SP, SR, RP, 1, 2\}$, and $\tau = 2.7$ (for urban area).

Fig. 5.18 illustrates the OP results for messages x_1 and x_2 obtained using (5.57) and (5.66), respectively. The PA factors are taken as $\alpha_1 = \beta_1 = 0.8$ and $\alpha_2 = \beta_2 = 0.2$. It is observed that the OP of x_2 performs better than that of x_1 at all SNR values. This phenomenon is explained by the fact that D_2 applies the SIC to remove the message of D_1, whereas D_1 detects its message without eliminating the message of D_2. The comparison of the OP performance of message x_1 at different d_1 shows that the outage performance degrades as the distance d_1 increases. In addition, Monte Carlo simulations show a consistency with the analytical ones, which confirms the correctness of the derived closed-form expressions for the OP of messages x_1 and x_2.

In Fig. 5.19, we demonstrate the OP performance versus the SNR threshold for messages x_1 and x_2 with different values of d_1. From the plot, it is seen that the OP of both messages degrades by increasing the SNR threshold value. It is noticed that the increase of the distance d_1 degrades the OP of message x_1. For example, when $d = 1.5d$ and $d = 3d$, message x_1 reaches an outage at 6 dB and 5.6 dB, respectively. The message x_2 shows the best result by reaching the OP of 0.23 at 6 dB.

Fig. 5.20 shows the simulated results on the OF-based PA factors for messages x_1 and

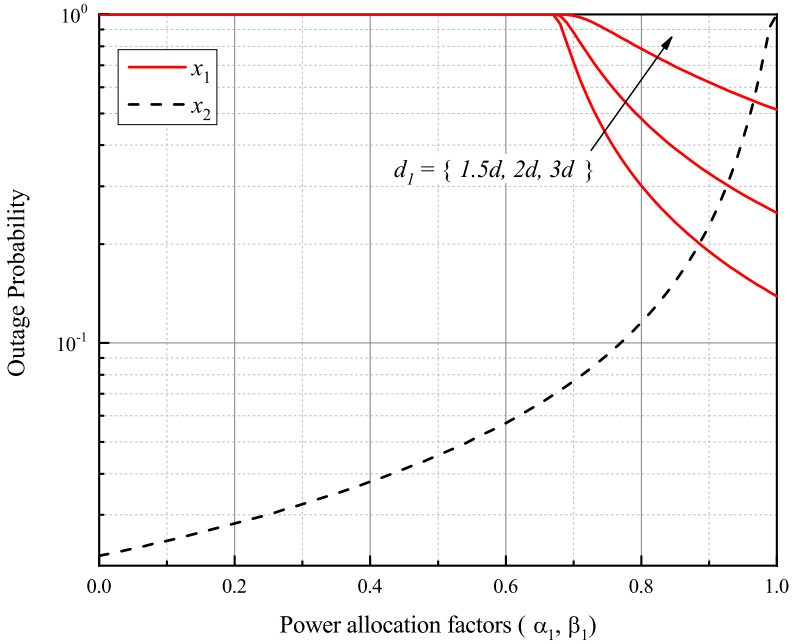

Figure 5.20. The OP of messages x_1 and x_2 versus PA factors at 20 dB when $d_1 = \{1.5d, 2d, 3d\}$, $\nu = 0$ and $\sigma^2_{\tilde{h}_\iota} = 0$.

Table 5.3. The observed OF-based PA factors (K users).

d_1	$1.5d$	$2d$	$3d$
α_1^*, β_1^*	0.885	0.93	0.965
α_2^*, β_2^*	0.115	0.07	0.035

x_2 at 20 dB. It is seen from the plot that, for all d_1 values, the OP of message x_1 is equal to 1 when $\psi > \frac{\alpha_1}{\alpha_2}$. On the other hand, when $\psi < \frac{\alpha_1}{\alpha_2}$, an increase of the value of α_1 leads to an improvement of the OP of message x_1, by the same time, decreasing that of message x_2. The observed OF-based PA factors for different d_1 values are illustrated in Table 5.3.

Fig. 5.21 demonstrates the outage performance versus the transmit SNR with OF-based α_1^*, β_1^* and α_2^*, β_2^* considering various d_1. From the plot, we observe that for all values of d_1, message x_2 shows an outperformance over message x_1 in terms of the OP at SNR levels higher than 17 dB. However, at lower SNR levels, the OP difference of both messages is not considerable, which shows that OF-based PA factors provide OP fairness for both messages.

The results on the outage performance versus the SNR threshold using OF-based α_1^*, β_1^* and α_2^*, β_2^* for different d_1 at the transmit SNR of 20 dB are illustrated in Fig. 5.22. It is observed that the OF-based PA factors improve the OP of x_1 in all d_1 values providing fairness for both messages.

In Fig. 5.23, the comparison of the CR-NOMA with CR-OMA in terms of the outage performance is demonstrated. In order to show the impact of the ITC on the OP of messages x_1 and x_2, two scenarios are considered: with no ITC, i.e., $I = \infty$ and when

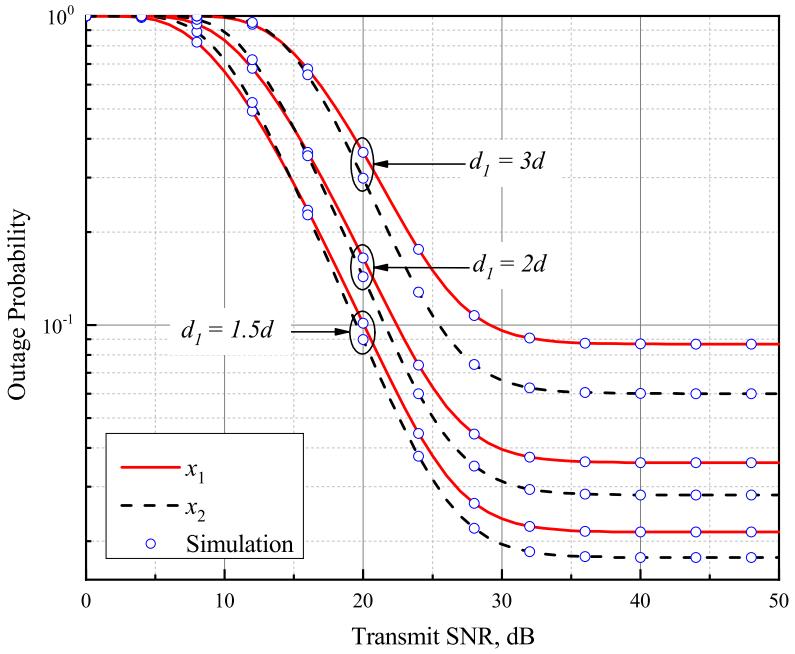

Figure 5.21. The OP of messages x_1 and x_2 versus the transmit SNR with OF-based PA factors when $d_1 = \{1.5d, 2d, 3d\}$, $\nu = 0$ and $\sigma^2_{\tilde{h}_\iota} = 0$.

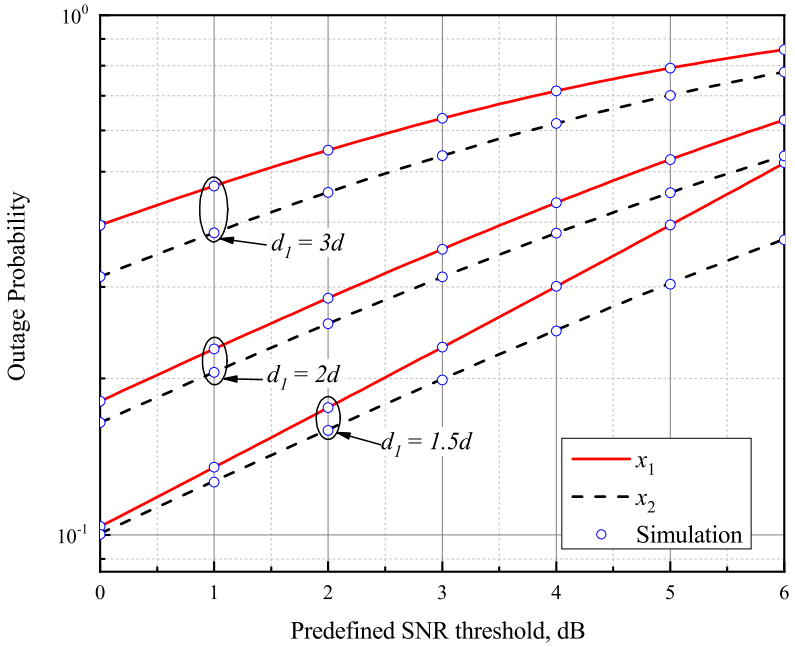

Figure 5.22. The OP of messages x_1 and x_2 versus the SNR threshold with OF-based PA factors at 20 dB when $d_1 = \{1.5d, 2d, 3d\}$, $\nu = 0$ and $\sigma^2_{\tilde{h}_\iota} = 0$.

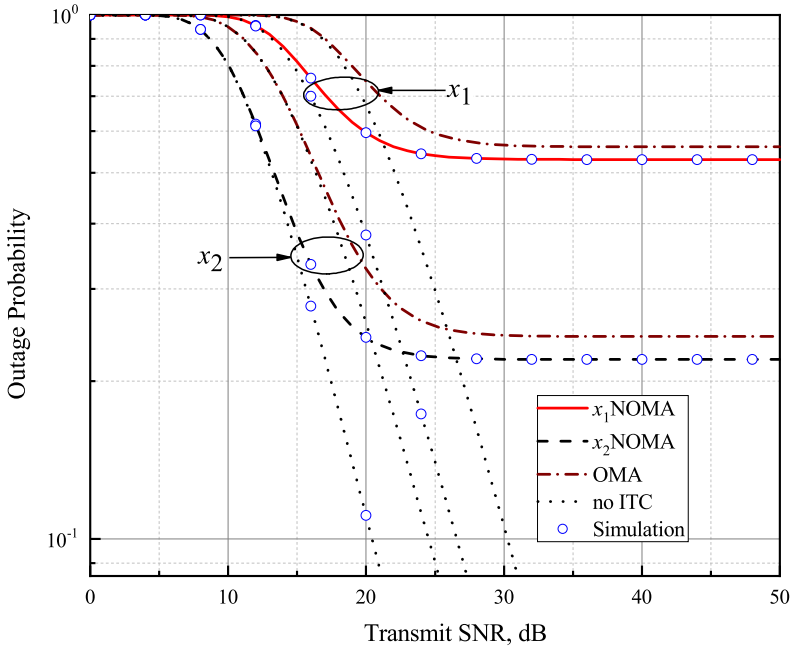

Figure 5.23. The OP of messages x_1 and x_2 versus the transmit SNR for NOMA and OMA scenarios with $\alpha_1 = 0.8$, $d_1 = 2d$, $\nu = 0$ and $\sigma^2_{\tilde{h}_\iota} = 0$.

$I = 20$ dB. It is obvious from Fig. 5.23 that both messages of CR-NOMA obtain better outage performance compared to those messages of the CR-OMA for all SNR levels. It is also noticed that saturation of outage curves for CR-NOMA starts at lower SNR regimes compared to those for the CR-OMA. This phenomenon can be explained by the fact that, regarding (5.46), the source and relay transmit power of $\frac{1}{2}P$ in the CR-OMA network increases the level of the ITC at PR, which consequently raises the SNR value where the OP saturation starts.

Fig. 5.24 illustrates the effect of the imperfect CSI and PN interference on the OP performance of NOMA messages. Here, we consider the case when $I = \infty$. It can be seen from the plot that the OP of both messages degrades when imperfect CSI and PN interference exist. When the PN interference is inserted, the OP of both messages degrades linearly. It is also noticed that when $\sigma^2_{\tilde{h}_l} = 0.001$, the effect of the channel error variance on the outage performance is insignificant at SNR levels below 15 dB. However, the impact of the imperfect channel on the OP curves of both messages becomes more significant at moderate SNRs. Moreover, due to the impact of the channel error variance, the OP becomes SNR-independent at higher SNR levels and starts saturating at 48 dB for message x_1 and at 45 dB for message x_2. In addition, when $\sigma^2_{\tilde{h}_l} = 0.005$, the channel error variance starts to degrade the OP of messages x_1 and x_2 at 17 dB and 12 dB, respectively, while, the OP saturation for the same messages begins at 45 dB and 40 dB, accordingly.

Fig. 5.25 shows the results on the average throughput obtained from (5.67) and (5.68). It is clearly shown that the message x_2 outperforms the message x_1 in terms of the average

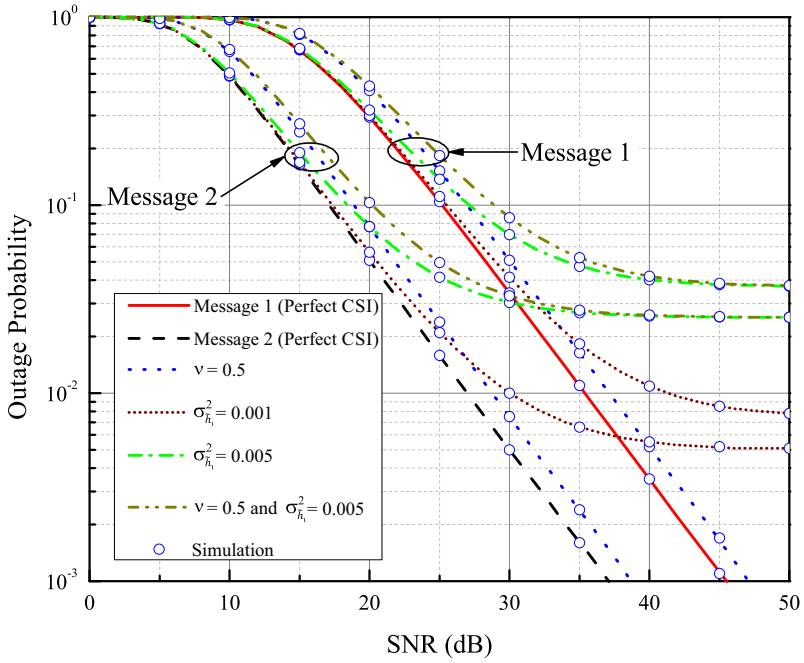

Figure 5.24. The OP of messages x_1 and x_2 versus the transmit SNR with imperfect CSI and PN's interference when $\alpha_1 = 0.8$ and $d_1 = 2d$.

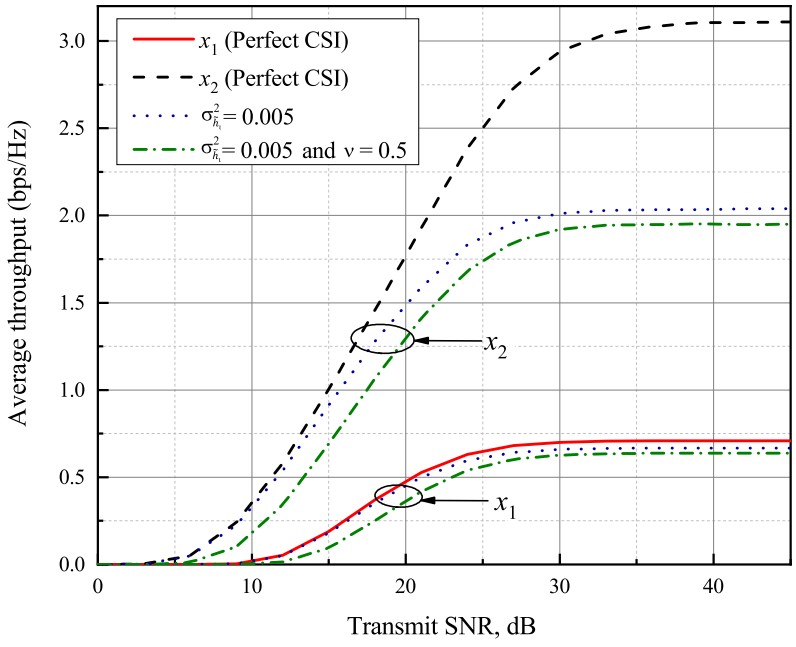

Figure 5.25. The average throughput versus the transmit SNR for NOMA messages with $\alpha_1 = 0.8$ and $d_1 = 2d$.

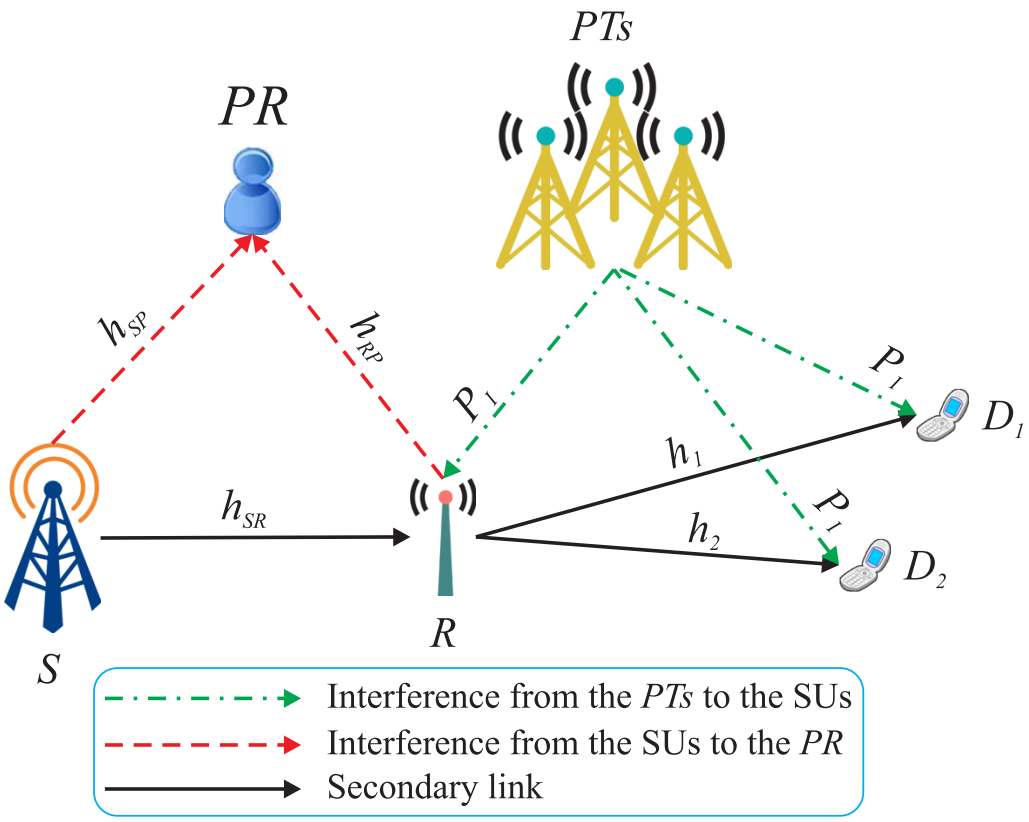

Figure 5.26. A system model of the downlink dual-hop underlay CR-NOMA network with the AF relaying.

throughput performance. The message x_2 achieves the maximum average throughput of 3.1 bps/Hz and 2.04 bps/Hz at 39 dB for the perfect CSI and when $\sigma^2_{\tilde{h}_l} = 0.005$, respectively. After that, the curves of the average throughput start saturating because of the ITC. Hence, it shows that imperfect CSI degrades the average throughput by 1.06 bps/Hz at 39 dB. On the other hand, the saturation of the average throughput of the message x_1 begins at 30 dB by achieving 0.71 bps/Hz.

5.5.2 System Model for AF CR-NOMA

The proposed system model in this section is the extension of Fig. 5.1, where only S was restricted by the maximum transmit power. Now, it is assumed that PR applies the ITC to both secondary transmit nodes S and R as they cause interference to the PN. Moreover, PTs cause interference to the SN (See Fig. 5.26). The channel between R and PR is denoted by h_{RP}, which also follow i.n.i.d. Rayleigh block fading model.

During the 1^{st} time slot, R obtains the following signal

$$y_R^{\text{AF}} = \sqrt{\frac{P_S}{d_{SR}^{\tau}}} h_{SR} \sum_{i=1}^{2} \sqrt{\alpha_i} x_j + P_I + n_R, \tag{5.69}$$

In the 2^{nd} time slot, based on the AF protocol, first, R amplifies the received signal with an amplification factor $G = 1/\sqrt{\frac{P_S}{d_{SR}^{\tau}}|h_{SR}|^2 + \sigma^2}$ and, then, forwards it to U_j, $j \in \{1, 2\}$. Thus, the received signal at U_j can be written as

$$y_j^{\text{AF}} = \sqrt{\frac{P_S P_R}{d_{SR}^{\tau} d_j^{\tau}}} h_{SR} h_j \sum_{i=1}^{2} \sqrt{\alpha_i} x_j G + \underbrace{\sqrt{\frac{P_S}{d_{SR}^{\tau}}} h_j n_R G + \sqrt{\frac{P_S}{d_{SR}^{\tau}}} h_j P_I G + P_I + n_j}_{\text{effective noise}}, \quad (5.70)$$

Then, as due to higher value of α_1, D_1 detects its own signal by treating x_2 as a background noise, which SINR can be written as

$$\begin{aligned} \gamma_1^{\text{AF}} =& \frac{\frac{\rho_S}{d_{SR}^{\tau}}|h_{SR}|^2 \frac{\rho_R}{d_1^{\tau}}|h_1|^2 \alpha_1}{\frac{\rho_S}{d_{SR}^{\tau}}|h_{SR}|^2 \frac{\rho_R}{d_1^{\tau}}|h_1|^2 \alpha_2 + \frac{\rho_R}{d_1^{\tau}}|h_1|^2 \bar{\nu} + \frac{\rho_S}{d_{SR}^{\tau}}|h_{SR}|^2 \bar{\nu} + \bar{\nu}} \\ =& \frac{n_s Y n_1 X \alpha_1}{n_s Y n_1 X \alpha_2 + n_1 X \bar{\nu} + n_s Y \bar{\nu} + \bar{\nu}}, \end{aligned} \quad (5.71)$$

where $\bar{\nu} = \nu + 1$. Then, D_2 treats its own signal as a noise when detects x_1 by the SINR

$$\gamma_{2,1}^{\text{AF}} = \frac{n_s Y n_2 Q \alpha_1}{n_s Y n_2 Q \alpha_2 + n_2 Q \bar{\nu} + n_s Y \bar{\nu} + \bar{\nu}}. \quad (5.72)$$

After successfully removing x_1 using the SIC, d_2 detects its own message x_2 from the remaining signal with the SINR

$$\gamma_2^{\text{AF}} = \frac{n_s Y n_2 Q \alpha_2}{n_2 Q \bar{\nu} + n_s Y \bar{\nu} + \bar{\nu}}. \quad (5.73)$$

5.5.3 Outage Analysis

The OP of D_1 can be written as

$$P_{\text{out},1}^{\text{AF}}(\xi_1) = 1 - \Pr\left[\gamma_1^{\text{AF}} > \xi_1\right] = 1 - \left(1 - F_{\gamma_1}^{\text{AF}}(\xi_1)\right). \quad (5.74)$$

Proposition 13 The exact OP expression of D_1 can be written as

$$
\begin{aligned}
P_{\text{out},1}^{\text{AF}}(\xi_1) &= \left(1-e^{-C_S}\right)\left(1-e^{-C_R}\right)\left(1-e^{-\frac{u_{s,1}(n_1+n_s)}{n_1}}2\sqrt{r_1}K_1\left(2\sqrt{r_1}\right)\right) \\
&+ \left(1-e^{-C_R}\right)\left(e^{-C_S}-e^{-\frac{C_S n_1\left(u_{p,1}+1\right)+n_p u_{p,1}}{n_1}}\Omega_{B_2}\right)+\left(1-e^{-C_S}\right)\left(e^{-C_R}\left(1-e^{-u_{s,1}}\right)\right. \\
&\left.+\frac{e^{-C_R(u_{s,1}+1)}}{u_{s,1}+1}-e^{-\frac{C_R\left(m_1+n_s u_{s,1}\right)+m_1 u_{s,1}}{m_1}}\frac{C_R}{\Upsilon_C}\sum_{k=0}^{\infty}\frac{\left(-\Upsilon_C\right)^k}{k!}G_{3\ 2}^{1\ 3}\left(\frac{C_R\Theta_C}{\Upsilon_C}\middle|\begin{matrix}0,\ k-1,\ k\\ 0,\ k\end{matrix}\right)\right) \\
&+ e^{-C_R-C_S}-\Theta_{D_1}\times\Psi(0)\frac{\pi}{C_R}MG_{2\ 2:0\ 1:2\ 3}^{1\ 1:1\ 0:3\ 1}\left(\frac{\Upsilon_{D_2}}{M},\frac{\zeta}{M}\middle|\begin{matrix}0 & -\frac{1}{2}\\ 0 & -\frac{1}{2}\end{matrix}\middle|\begin{matrix}-\\ 0\end{matrix}\middle|\begin{matrix}1\ 1\\ 1\ 2\ 1\end{matrix}\right) \\
&+ \Theta_{D_1}\sum_{k=1}^{\infty}\Psi(k)C_R^{k-1}\sum_{n=0}^{k-1}\binom{k-1}{n}\left(\frac{1}{C_R\zeta}\right)^n\sum_{m=0}^{\infty}\frac{\left(-\zeta C_R r\right)^m}{m!} \\
&\times G_{4\ 4}^{2\ 4}\left(\frac{\Upsilon_{D_2}}{\zeta}\middle|\begin{matrix}-n,\ m-n-1,\ 2m-n-2,\ 2m-n-1\\ 0,\ m-n-1,\ 2m-n-1,\ m-n\end{matrix}\right),
\end{aligned}
\tag{5.75}
$$

where $\theta_1 < \frac{\alpha_1}{\alpha_2}$, otherwise, $\mathcal{P}_1(\theta_1) \sim 1$.

Proof: See Appendix C.9 for details. ■

The OP derivation of D_2 can be found by following the similar approach as in Appendix C.9.

5.5.4 Numerical Results

We adopt the following system parameters to present the results for the above investigation: $P_I = 20$ dB, $\alpha_1 = 0.8$, $\alpha_2 = 0.2$, $\theta_1 = \theta_2 = 3$ dB, $\eta = 2.7$, $d_1 = 2d$, $d_{SP} = d_{SR} = d_2 = d$, $\alpha_1 = 0.8$, $\alpha_2 = 0.2$. Without loss of generality, d is assumed to be unity in order to focus on the OP results.

Fig. 5.27 shows the OP results for D_1 and D_2. It is observed that the OP for D_2 performs better than that for D_1. It is due to the fact that D_2 removes the unwanted message of D_1 by applying the SIC technique which results in an improvement of the error probability in the message detection. Moreover, the OP results for both users in the NOMA system show better performance compared to the same users in the OMA scenario. Finally, it is noticed that primary interference ($\nu = 0.2$) considerably degrades the OP of secondary nodes.

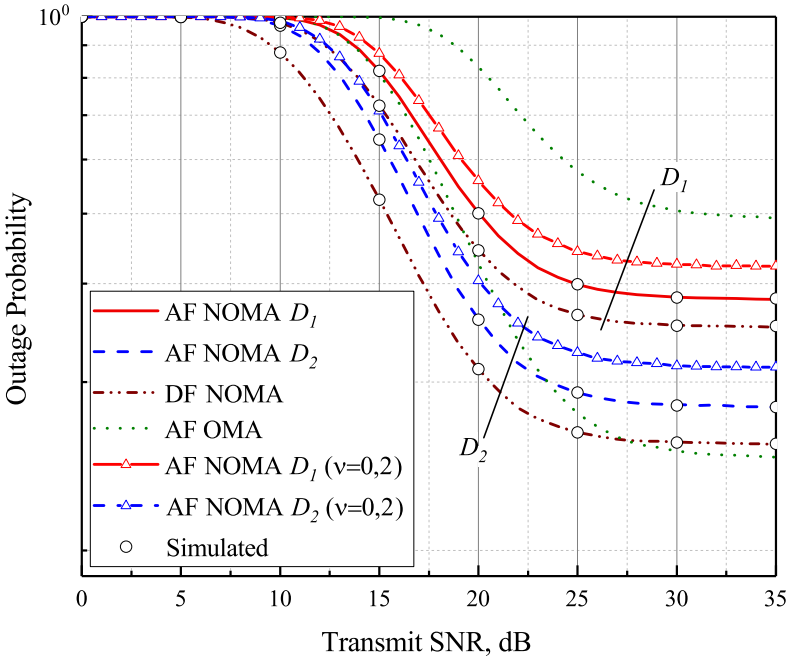

Figure 5.27. The OP of Users 1 and 2 versus the transmit SNR when $d_1 = \{2d, 4d\}$, $\alpha_1 = 0.8$, $\alpha_2 = 0.2$ and $\tau = 0$.

5.6 Chapter Summary

This Chapter proposed the dual-hop underlay CR-NOMA networks with the imposed ITC at PR for different system model scenarios. The OP was investigated as the main performance metric for the considered system model applying DF and AF relaying methods over Rayleigh and Nakagami-m fading channels. First, the OP performance was evaluated to the scenario with two NOMA secondary users and the OF-based PA factors were found for both users to guarantee OP fairness between NOMA users. Then, considering the effect of the imperfect CSI on the outage performance, we derived a general closed-form OP expression of SUs when the number of secondary NOMA nodes was extended to K users. In addition, the obtained OP performance for CR-NOMA was compared to that for conventional CR-OMA to show the supremacy of the former. Finally, all derived analytical results were verified by Monte-Carlo simulations, which validated the accuracy of the performance analysis.

Chapter 6

Wireless Powered CR-NOMA

In this chapter, we study the OP of the dual-hop underlay CR network consisted of a secondary relay node with energy harvesting and two NOMA secondary destination users (D_1 and D_2). Moreover, the OF-based power allocation factors are found for different distances of D_1 in order to satisfy OP fairness for both D_1 and D_2. Additionally, the CR-NOMA is compared with CR-OMA in terms of the OP. Finally, the obtained analytical expressions are corroborated by Monte Carlo simulations.

6.1 Introduction

CR-NOMA is a promising technique that can not only improve the spectral efficiency but also can increase user connectivity in wireless communication networks [59]. Aside from the spectrum, another key objective of future 5G networks is to maximize energy efficiency. Hence, one of the promising methods to enhance energy efficiency is wireless EH [132]. In the EH-enabled networks, energy-limited nodes can harvest RF signals, then convert them into the DC [140]. The motivation for the application of SWIPT to NOMA can be illustrated in works [181–183]. In these works, SWIPT is applied for NOMA uplink transmission, where users harvest energy from the base station and then send their information to the base station simultaneously by utilizing the NOMA policy. The authors in [184] studied resource allocation for uplink SWIPT - NOMA transmission, where PA and the durations for power and information transfer are jointly designed to eliminate the doubly near-far effect.

Note that SWIPT is also can be applied to cooperative NOMA communication [185]. As it was already mentioned before, cooperative NOMA can cause effective aid to the users with weak channel conditions, by using the strong users as relay nodes. But, in real time communications, these users may not desire to perform as relay nodes, considering the fact that the procedure can consume a considerable amount of power which shorten their battery life. On the other hand, by implementing SWIPT, the strong users can harvest energy from signals conveyed by the base station and use that harvested energy to further forward signals of weak users. Thus, the authors in [185] studied SWIPT in cooperative

NOMA, where users are spatially randomly located and NOMA users which are located near to the source act as EH relays to assist far NOMA users. Moreover, inspired by the idea in [185], the authors in [186] investigated cooperative SWIPT-NOMA in terms of a transmitter beamforming design, a power splitting ratio optimization and a receiver filter design in order to maximize the rate of the relay node. Moreover, the authors in [187] studied the NOMA system with a wireless powered near user with the TS, the PS and generalized schemes, where the achievable rate regions of the TS and PS were derived in closed-form expressions. Furthermore, the OP of cooperative relaying transmissions in two-user SWIPT-NOMA networks was studied in [188], where the authors proposed a best-near best-far user selection scheme to use the EH-based near users as relay nodes. The authors in [189] proposed antenna selection method to study the OP for EH-based NOMA relaying networks over Nakagami-m fading. In addition, the authors in [140] studied the EH-based cooperative CRN with multiple primary users and one secondary network, where interference at receive nodes is canceled with the IA technique. The derived outage performance results showed that the PS protocol outperforms the TS one.

6.2 Contributions of the Chapter

The main contributions of the Chapter are as follows:

- We study the OP for the cooperative underlay CR-NOMA networks with enabled the SWIPT technology.
- The OP for the proposed system model with EH-enabled R calculated numerically. In addition, the OF-based PA factors are calculated depending on NOMA users' channel quality. Thus, the proper evaluated PA factors can guarantee fairness among NOMA users in terms of the OP.
- We investigate how the PA factor in the PS mode and the distance of nodes affect on the harvested power level.
- Cooperative CR-OMA networks are taken as a benchmark to illustrate the better performance of the cooperative CR-NOMA.

The remainder of this chapter is organized as follows. Section 6.3 describes the system model with evaluated achievable rates. In Section 6.4, the OP analysis of both secondary destination users are presented. Moreover, in Section 6.5, numerical results are presented and discussed. Finally, Section 6.6 concludes the Chapter.

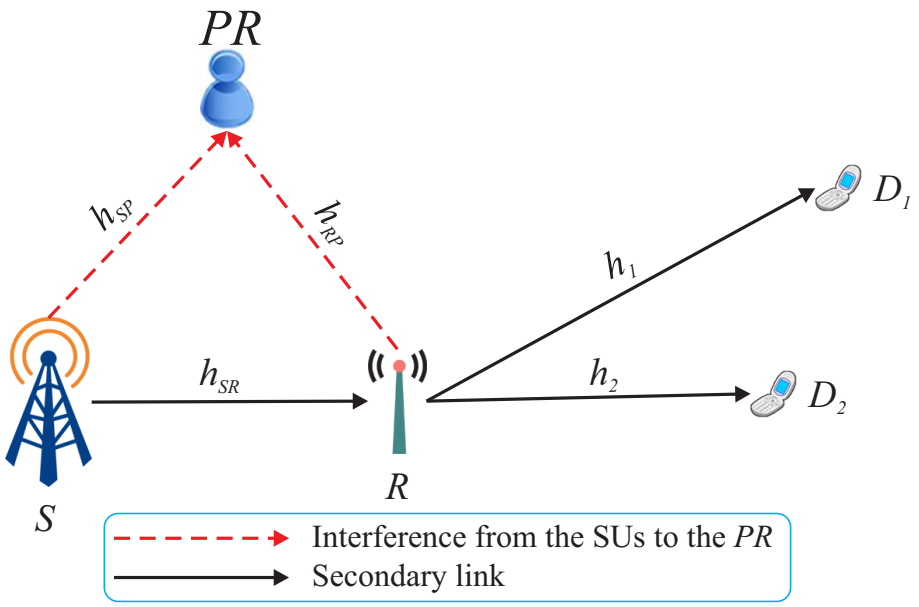

Figure 6.1. A downlink dual-hop underlay CR-NOMA network.

6.3 System Model

We consider a downlink dual-hop DF underlay CR-NOMA network consisting of PR and a SN with S, an energy-constrained R operating in a half-duplex mode and two destination NOMA users (D_1 and D_2) as shown in Fig. 6.1. Channels between nodes, i.e., h_{SP}, h_{SR}, h_1 and h_2, are assumed to follow an i.n.i.d. Rayleigh block fading model with $\mathcal{CN}(0,1)$. Moreover, a global CSI is assumed to be available at each node. The corresponding distances between nodes are denoted by d_{SP}, d_{SR}, d_1 and d_2. Regarding the system model, S and R cause interference to PR, Thus, the SN communication is available only if PR does not receive harmful interference from the SN. Hence, the transmit power constraints are imposed at S and R regarding (5.46). Hence, considering the transmit power restriction, the superimposed signal $\sqrt{P_S\alpha_1}x_1 + \sqrt{P_S\alpha_2}x_2$ is conveyed from S to D_1 and D_2 via the assistance of R within two time slots. Without loss of generality, we assume that the channels of destination NOMA users are ordered as $h_1 < h_2$. Based on the ordering of the users' channels, the corresponding PA factors are ordered as $\alpha_1 > \alpha_2$.

6.3.1 Power-Splitting Relaying

The PSR protocol is illustrated in Fig. 6.2, where, during the 1^{st} time slot, a coefficient θ, with $(0 < \theta < 1)$, of the received signal power at R is utilized for the EH purpose, while the remaining signal $(1-\theta)$ is used for the data detection at R. Hence, the signal received

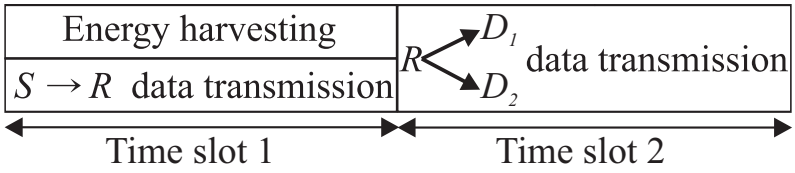

Figure 6.2. The time frame structure of the PSR protocol.

at R for the EH purpose can be written as

$$y_R^{EH} = h_{SR}\left(\sqrt{\frac{\alpha_1 \theta P_S}{d_{SR}^{\tau}}}x_1 + \sqrt{\frac{\alpha_2 \theta P_S}{d_{SR}^{\tau}}}x_2\right) + \sqrt{\theta}n_R, \tag{6.1}$$

where $n_R \sim \mathcal{CN}(0, \sigma_R^2)$ stands for the AWGN at R. Therefore, neglecting the relatively small power harvested from the noise, the harvested energy at R can be derived by [140]

$$E_H = \frac{\eta\theta T}{2}|h_{SR}|^2\left(\frac{\alpha_1 P_S}{d_{SR}^{\tau}} + \frac{\alpha_2 P_S}{d_{SR}^{\tau}}\right) = \frac{\eta\theta T|h_{SR}|^2 P_S}{2d_{SR}^{\tau}}, \tag{6.2}$$

where η denotes the EH conversion efficiency, with $(0 < \eta < 1)$ and T is the total time required for the end-to-end transmission. Regarding the fact that transmit power at R relates to the EH as $P_R = 2E_H/T$, the transmit power at R can be expressed as [127]

$$P_R = \frac{\eta\theta|h_{SR}|^2 P_S}{d_{SR}^{\tau}}. \tag{6.3}$$

Moreover, the signal received for the $S - R$ information transmission can be written as

$$y_R^{IT} = \sqrt{1-\theta}h_{SR}\left(\sqrt{\frac{\alpha_1 P_S}{d_{SR}^{\tau}}}x_1 + \sqrt{\frac{\alpha_2 P_S}{d_{SR}^{\tau}}}x_2\right) + n_R. \tag{6.4}$$

Furthermore, R decodes and removes x_1 from (6.4), and x_2 can be detected from the remained signal. The SINR and SNR to decode x_1 and x_2 at R can be derived as

$$\gamma_{R,1} = \frac{(1-\theta)\alpha_1\rho_S|h_{SR}|^2}{(1-\theta)\alpha_2\rho_S|h_{SR}|^2 + d_{SR}^{\tau}} \tag{6.5}$$

and

$$\gamma_{R,2} = \frac{(1-\theta)\alpha_2\rho_S|h_{SR}|^2}{d_{SR}^{\tau}}, \tag{6.6}$$

respectively.

Furthermore, during the 2^{nd} time slot, R forwards the detected superimposed signal $\sqrt{P_R\beta_1}\tilde{x}_1 + \sqrt{P_R\beta_2}\tilde{x}_2$ to D_1 and D_2. Therefore, D_1 and D_2 receive the following signals

$$y_1 = h_1\left(\sqrt{\frac{\beta_1 P_R}{d_1^\tau}}\tilde{x}_1 + \sqrt{\frac{\beta_2 P_R}{d_1^\tau}}\tilde{x}_2\right) + n_1 \tag{6.7}$$

and

$$y_2 = h_2\left(\sqrt{\frac{\beta_1 P_R}{d_2^\tau}}\tilde{x}_1 + \sqrt{\frac{\beta_2 P_R}{d_2^\tau}}\tilde{x}_2\right) + n_2, \tag{6.8}$$

respectively, where n_1 and n_2 stand for the AWGN noise terms at D_1 and D_2, respectively. Furthermore, D_2 implements SIC by detecting $\tilde{x}_1$ while considering its own data $\tilde{x}_2$ as a noise. The SINR of which can be written as

$$\gamma_{2,1} = \frac{\eta\theta\beta_1\rho_S|h_2|^2|h_{SR}|^2}{\eta\theta\beta_2\rho_S|h_2|^2|h_{SR}|^2 + d_2^\tau d_{SR}^\tau}. \tag{6.9}$$

Furthermore, D_2 extracts the detected data in (6.9) from the received signal. Then, D_2 detects its own signal from the remaining signal by the following SNR

$$\gamma_{2,2} = \frac{\eta\theta\beta_2\rho_S|h_2|^2|h_{SR}|^2}{d_2^\tau d_{SR}^\tau}. \tag{6.10}$$

Now, as D_1 is allocated with higher PA factors, it can detect its message by treating $\tilde{x}_2$ as a background noise with the following SINR

$$\gamma_1 = \frac{\eta\theta\beta_1\rho_S|h_1|^2|h_{SR}|^2}{\eta\theta\beta_2\rho_S|h_1|^2|h_{SR}|^2 + d_1^\tau d_{SR}^\tau}. \tag{6.11}$$

Then, the end-to-end achievable rates of x_1 and x_2 can be respectively written as the followings

$$\mathcal{R}_1 = \frac{1}{2}\log_2\left(1 + \min\left(\gamma_{R,1}, \gamma_{2,1}, \gamma_1\right)\right) \tag{6.12}$$

and

$$\mathcal{R}_2 = \frac{1}{2}\log_2\left(1 + \min\left(\gamma_{R,2}, \gamma_{2,2}\right)\right). \tag{6.13}$$

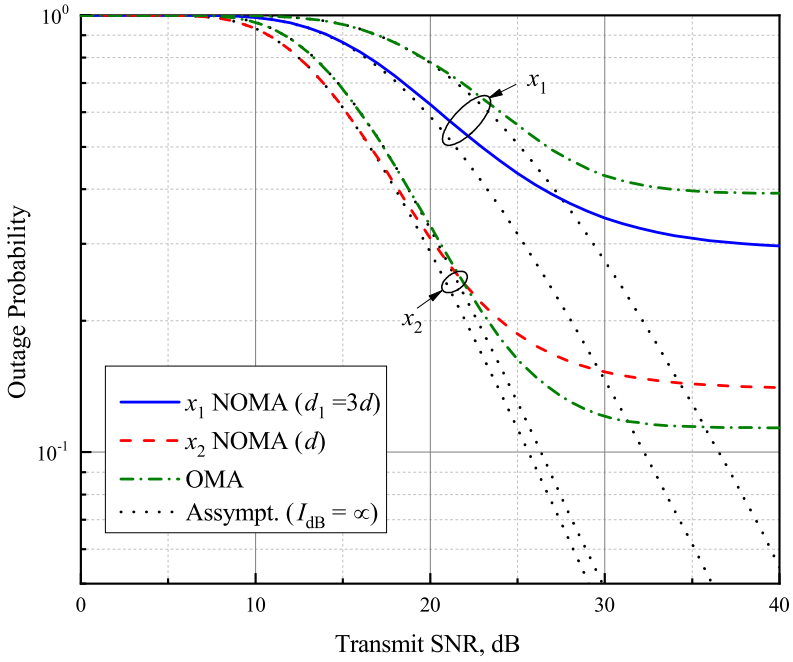

Figure 6.3. The OP of x_1 and x_2 versus the ransmit SNR threshold at 25 dB when $d_1 = 3d$, $\alpha_1 = 0.8$ and $\alpha_2 = 0.2$.

6.4 Outage Probability

This section investigates the OP for x_1 and x_2. Therefore, the OP of x_1 can be derived as

$$P_{\text{out},1}(\xi_1) = 1 - \Pr\left[\min\left(\gamma_{R,1}, \gamma_{2,1}, \gamma_1\right) > \xi_1\right], \tag{6.14}$$

where RVs $\gamma_{R,1}$, $\gamma_{2,1}$ and γ_1 are dependent to each other. Similarly, the OP of x_2 can be expressed as

$$P_{\text{out},2}(\xi_2) = 1 - \Pr\left[\min\left(\gamma_{R,2}, \gamma_{2,2}\right) > \xi_2\right], \tag{6.15}$$

where RVs $\gamma_{R,2}$ and $\gamma_{2,2}$ are dependent to each other.

Due to the dependence of RVs to each other in (6.14) and (6.15), the analytical derivation of the OP becomes very complicated which is the out of the scope of this Chapter. Hence, the OP for x_1 and x_2 will be investigated only numerically.

6.5 Numerical Results

In this section, the OP of the proposed system model is evaluated over Rayleigh fading channels. We adopt the following system parameters, unless stated otherwise: $\alpha_j = \beta_j$, $\xi_j = 3$ dB $\forall j \in \{1, 2\}$, $\eta = 0.8$, $\theta = 0.75$, $d_1 = \{1.5d, 3d, 4d\}$, $d_{SP} = d_{SR} = d_2 = d$, $\tau = 2.7$.

Table 6.1. OF-based PA factors for different d_1 with EH.

d_1	$1.5d$	$3d$	$4d$
α_1^*, β_1^*	0.792	0.885	0.927
α_2^*, β_2^*	0.208	0.115	0.073

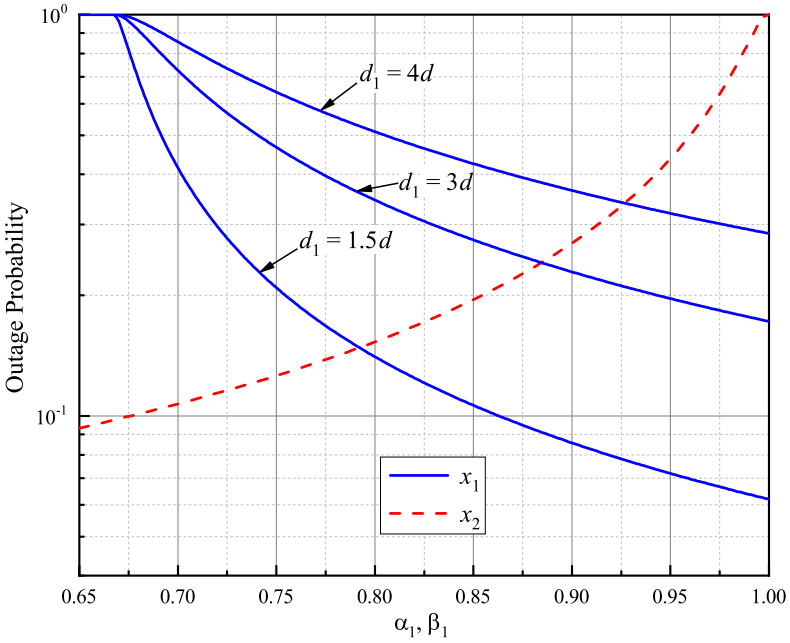

Figure 6.4. The OP of x_1 and x_2 versus PA factors at 20 dB when $d_1 = \{1.5d, 3d, 5d\}$.

In Fig. 6.3, the OP results of x_1 and x_2 are illustrated. It is considered that $\alpha_1 = \beta_1 = 0.8$, $\alpha_2 = \beta_2 = 0.2$, $d_1 = 3d$. Additionally, the asymptotic case without ITC ($I = \infty$) is also plotted to analyze the OP when SUs can transmit with a maximum transmit power. Moreover, the OP results of the conventional cooperative CR-OMA are plotted to compare that of the proposed cooperative CR-NOMA model. From the plotted results, it is clearly seen that x_2 outperforms x_1 in terms of the OP results. It can be explained by the fact that D_2 implements the SIC to remove the interference from D_1, while D_1 detects its data without canceling the interference which results in worse the OP results. Moreover, in no ITC case, both messages of the cooperative CR-NOMA obtain better OP compared to that of cooperative CR-OMA for all SNR values. When $I = 30$ dB, a saturation of OP curves for NOMA users began at lower SNRs compared with those of the OMA ones. It is due to the fact that, the transmitted power of $\frac{1}{2}P_S$ at S results in an increase of the ITC value at PR.

Fig. 6.4 shows the OF-based values of PA factors for x_1 and x_2 at 20 dB for different values of d_1. It is noted that x_1 is in outage for all values of d_1 when $u > \frac{\alpha_1}{\alpha_2}$. When $u < \frac{\alpha_1}{\alpha_2}$, an increase of the value of α_1 improves the OP of x_1 and decrease that of x_2. Moreover, it is noticed that when d_1 is larger, the OP results get worse. Finally, the obser-

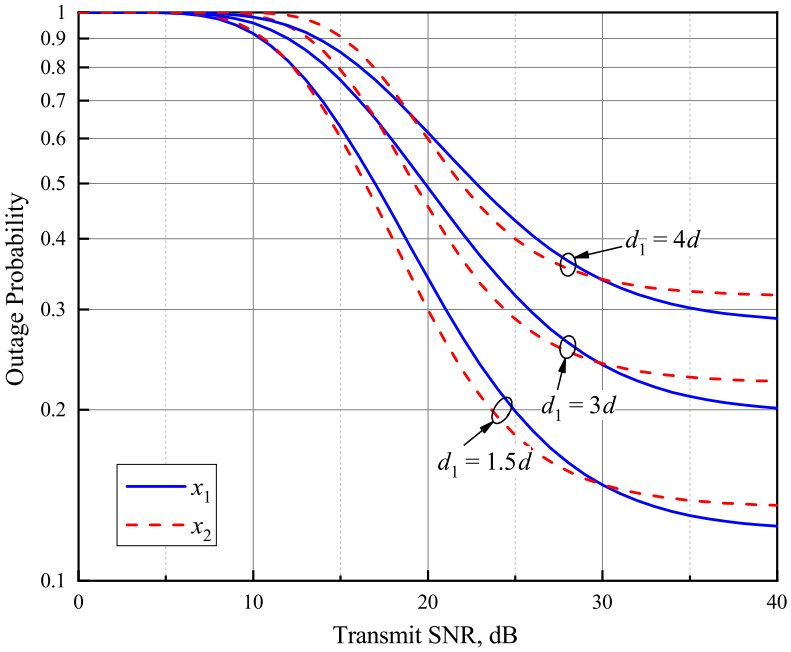

Figure 6.5. The OP of x_1 and x_2 versus the transmit SNR performance with OF-based PA factors when $d_1 = \{1.5d, 3d, 4d\}$.

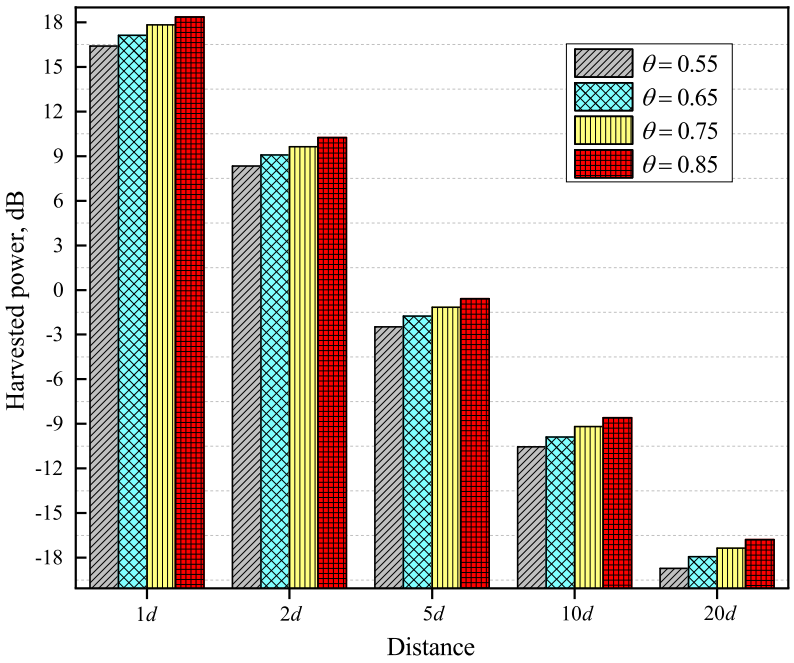

Figure 6.6. Harvested power versus the S-R distance performance with various θ values.

ved OF-based PA factors for various values of d_1 are illustrated in Table 6.1.

Fig. 6.5 plots results for the OP with OF-based PA factors when $d_1 = \{1.5d, 3d, 4d\}$. Noticeably, in all d_1 cases, the OP of x_2 performs better than that of x_1 at SNR levels below 27 dB. However, the OP of x_1 obtains better results than that of x_2 at higher SNRs.

Moreover, the saturation of the OP curve of x_1 starts at higher SNRs when d_1 is larger. It is due to the fact that larger α_1 is needed when D_1 is located far away from R. Finally, it can be deduced that the OF-based PA factors improved the OP performance of x_1 in all d_1 cases providing fairness for both users.

Fig. 6.6 illustrates the harvested power at R regarding various distances between S - R, i.e., $d_{SR} = \{1d, 2d, 5d, 10d, 20d\}$. It is noted that R harvest less power when the value of d_{SR} is higher. It can be explained by the simple fact that the path-loss effect in longer distances degrades the signal power more intensively. Moreover, it is noted that the increase of θ allows harvesting much power.

6.6 Conclusion

The SWIPT is another candidate technology for the future 5G networks which can maximize energy efficiency. Hence, this chapter studied the SWIPT in dual-hop underlay CR-NOMA networks with the DF relaying over the Rayleigh distribution. The OP for cooperative DF underlay CR-NOMA networks with EH-enabled R calculated numerically. Moreover, we found OF-based PA factors depending on NOMA users' channel quality. Thus, numerical results showed that the proper evaluated PA factors can guarantee fairness of both NOMA destination users in terms of the OP. Furthermore, cooperative CR-OMA networks were used as a benchmark to illustrate the better performance of the cooperative CR-NOMA. The comparison of two EH modes, i.e, TS and PS, in Section 3, showed that the PS mode is superior. Therefore, in this Chapter, we studied the PS mode, where it is shown that the increase of θ allows harvesting more power, while the increase of d_{SR} results in less harvested power.

Chapter 7

Conclusions and Future Work

5G is the next major evolution of cellular communication systems with performance improvements of several orders of magnitude over 4G. Hence, the main set of 5G requirements is recognized in the industry as follows: higher spectral and energy efficiency, lower end-to-end latency, massive connectivity, etc. [154]. Due to these high demands on performance improvements in mobile communications, the candidate technologies that can be implemented in 5G are still under consideration. The techniques that jointly studied in this thesis are the potential candidates for 5G. For example, IA-embedded networks can improve the spectral efficiency by mitigating the interference while the CR and NOMA can improve spectrum scarcity and provide massive connectivity. Furthermore, 5G networks can become more energy efficient by applying the SWIPT with different EH protocols.

In this thesis, we investigated the CR networks with EH and NOMA techniques. This concluding chapter summarizes all the key contributions from different chapters and suggests several interesting future research directions.

7.1 Conclusions

Emerging cellular technologies proposed for use in 5G communications will accommodate a wide range of usage scenarios with diverse link requirements. This will necessitate operation over a versatile set of wireless channels, i.e., indoor, outdoor, line-of-sight (LOS) and non-LOS. To bridge the gap between practical and theory channels, Chapter 3 considered the generalized $\alpha-\mu$ fading distribution, which includes several other distributions as special cases, i.e., Rayleigh, Gamma, Exponential, Nakagami-m, One-sided Gaussian, and Weibull. This Chapter studied the underlay CR network over generalized $\alpha-\mu$ fading distribution, where the primary receiver applies interference temperature constraint to secondary transmit nodes. Based on the used dual-hop CR network model, the closed-form OP expression for secondary destination node was derived analytically. Furthermore, the impact of the interference temperature constraint on the system outage and SER performance were investigated. From the derived results, we showed that the applied interference constraint degrades the outage and SER performances, which could

be clearly seen from the outage saturation. In addition, Monte Carlo simulations show a consistency with the analytical results, which confirms the correctness of the derived closed-form expression.

Chapter 4 investigated a dual-hop DF wireless powered CR network with IA over Rayleigh fading channels. An introducing CR networks presents two new types of interference, i.e., inter-network interference and intra-network interference. In order to mitigate the negative effect of intra- and inter-network interference terms at the primary and secondary receivers, we used an IA technique by applying precoding and interference suppression beamforming matrices. Here we showed that by using IA technique in underlay cooperative CR networks, interference at primary receivers can be efficiently canceled, and, as a result, secondary transmit nodes are not required to limit their transmit power. Consequently, SNs obtained better system performance in terms of the OP and BER. Moreover, unlike many works in the current literature related to the interference management where unwanted interference has been canceled or removed, we used inter- and intra-network interference for EH purposes to feed the power-limited relay node. In addition, an optimal selection of the EH time fraction in the TSR protocol and the PS fraction in the PSR protocol was found to be important in achieving the best system performance. Moreover, the derived closed-form expressions for the OP of the SN in different CSI mismatch scenarios showed that the PSR protocol outperformed the TSR protocol which validity was confirmed by good agreement with simulation results. Finally, it was shown that the increase in the number of interfering primary nodes allows R to harvest more power, while the increase of interfering nodes' distance results in lower harvested power.

CR and NOMA will provide more efficient utilization of wireless spectrum in the future. Moreover, the design principle of CR-NOMA networks is perfectly aligned to functional requirements of 5G networks. Thus, Chapter 5 focused on a downlink CR-NOMA model with an imposed interference constraint at the primary receiver. The outage probability was investigated as the main performance metric for the considered system model applying DF and AF relaying methods over Rayleigh and Nakagami-m fading channels. First, the OP was evaluated for the scenario with two secondary users and the OF-based power allocation factors were found for both users to guarantee OP fairness between NOMA users. Then, to attain more practical insight, we considered the effect of the imperfect CSI on the outage performance and derived a general closed-form solution for the outage performance when the number of secondary non-orthogonal nodes was extended to K users. Hence, in this chapter, we showed that CR-NOMA networks not only achieve massive connectivity, but also obtain better outage performance compared to the conventional CR-OMA. Finally, all derived analytical results were verified by Monte-Carlo

simulations, which validated the accuracy of the performance analysis.

Finally, in Chapter 6, we studied the wireless energy EH in underlay CR-NOMA networks with the DF relaying. The OP for cooperative DF underlay CR-NOMA networks with EH-enabled relay calculated numerically. Moreover, we optimized the power allocation factors depending on the NOMA users' channel quality. Thus, numerical results showed that the properly evaluated power allocation factors can guarantee fairness among NOMA destination users in terms of the OP. Furthermore, cooperative CR-OMA networks were used as a benchmark to illustrate the better performance of the cooperative CR-NOMA. The PS mode showed that the increase of power splitting coefficient allows harvesting more power, while the increase of the source-relay distance results in less harvested power.

7.2 Future Work

Here we suggest some possible research extensions to the work in this thesis as follows.

- In Chapter 3, we studied the outage and SER performance of the underlay CR network considering an ideal transceiver hardware. However, physical transceiver hardware introduces impairments that distort the emitted and received signals in any communication system. Hence, in practice, hardware suffers from various types of impairments, i.e, I/Q imbalance, phase noise and high power amplifier (HPA) nonlinearities [190]. The authors in [191] showed how I/Q imbalance attenuates the amplitude and rotates the phase of the desired constellation, which lead to an SER floor. Hence, as hardware impairments have a deleterious impact on the achievable performance, it would be worthwhile to consider the proposed system model with the aforementioned hardware impairments scenarios.

- Chapter 4 and 6 studied SWIPT technique in CR networks considering linear RF harvesting, which exhibit a linear relationship between input RF and output harvested power. However, rectennas, due to the presence of diodes, exhibit highly nonlinear behavior with limited sensitivity due to the need for bias [192]. Thus, it would be worthwhile to evaluate the RF harvesting model in the thesis considering nonlinearity, sensitivity and saturation of the RF harvesting circuits as well as other facts from the relevant microwave literature.

- In Chapter 5, we investigated CR-NOMA networks assuming that users are able to perform the perfect SIC, and thus completely remove the inter-user interference from the weaker signals. However, in practical systems, the decoding error might be inevitable during the procedure of the SIC, as a result, the interference that are not

removed completely decreases the quality of the received signal [193]. Hence, imperfect SIC has a great impact on the performance of NOMA, especially in massive access systems [194]. Imperfect SIC in NOMA systems has attracted the attention, but is still an open issue. Therefore, studying the proposed CR-NOMA with imperfect SIC is very promising as it can provide extra useful practical insights.

Appendix A

Appendix for Chapter 3

A.1 Proof of Proposition 1

Here, the derivation of (3.21) is provided. Since $|h_{SR}|^2$ and $|h_{SP}|^2$ in (3.14) are independent from each other, (3.14) can be further reformulated by

$$\Lambda_1 = F_{|h_{SR}|^2}\left(\frac{\xi\sigma_R^2}{\bar{P}_S}\right) F_{|h_{SP}|^2}\left(\frac{I}{\bar{P}_S}\right) = \left(1 - e^{-\frac{\lambda\xi\sigma_R^2}{\bar{P}_S}}\right)\left(1 - e^{-\frac{\lambda I}{\bar{P}_S}}\right). \tag{A.1}$$

Then, Ψ in (3.15) can be derived as follows

$$\begin{aligned}\Psi_1 &= \int_{\frac{I}{\bar{P}_S}}^{\infty} f_{|h_{SP}|^2}(y) \int_0^{\frac{y\xi\sigma_R^2}{I}} f_{|h_{SR}|^2}(z)\, \mathrm{d}z\mathrm{d}y = \int_{\frac{I}{\bar{P}_S}}^{\infty} \lambda e^{-\lambda y}\left(1 - e^{-\frac{y\lambda\xi\sigma_R^2}{I}}\right)\mathrm{d}y \\ &= \int_{\frac{I}{\bar{P}_S}}^{\infty} \lambda e^{-\lambda y}\mathrm{d}y - \int_{\frac{I}{\bar{P}_S}}^{\infty} \lambda e^{-\frac{\lambda y\left(I+\xi\sigma_R^2\right)}{I}}\mathrm{d}y = e^{-\frac{\lambda I}{\bar{P}_S}} - \frac{I e^{-\frac{\lambda\left(I+\xi\sigma_R^2\right)}{\bar{P}_S}}}{I+\xi\sigma_R^2}.\end{aligned} \tag{A.2}$$

Then, by substituting (A.1) and (A.2) into (3.13), the CDF of $\eth_S$ can be derived in a closed form as

$$F_{\eth_S}(\xi) = 1 - e^{-\frac{\lambda\xi\sigma_R^2}{\bar{P}_S}} + \frac{\xi\sigma_R^2 e^{-\frac{\lambda\left(I+\xi\sigma_R^2\right)}{\bar{P}_S}}}{I+\xi\sigma_R^2}. \tag{A.3}$$

Similarly to $F_{\eth_S}(\xi)$, the closed-form expression for $F_{\eth_R}(\xi)$ can be derived by following the same steps as in (3.13) - (A.2) and written as

$$F_{\eth_R}(\xi) = 1 - e^{-\frac{\lambda\xi\sigma_D^2}{\bar{P}_R}} + \frac{\xi\sigma_D^2 e^{-\frac{\lambda\left(I+\xi\sigma_D^2\right)}{\bar{P}_R}}}{I+\xi\sigma_D^2}. \tag{A.4}$$

Finally, by using (A.3) and (A.4) and after some mathematical manipulations, the closed-form expression for the OP of D can be computed as in (3.21). ■

A.2 Proof of Proposition 2

From (3.14), the CDFs of $|h_{SR}|^2$ and $|h_{SP}|^2$ can be respectively derived as followings

$$F_{|h_{SR}|^2}(\xi) = \int_0^{\frac{\xi\sigma_R^2}{P_S}} \frac{\alpha_{SR}\mu_{SR}{}^{\mu_{SR}}\gamma^{\frac{\alpha_{SR}\mu_{SR}}{2}-1}}{2\Gamma(\mu_{SR})\bar{\gamma}^{\frac{\alpha_{SR}\mu_{SR}}{2}}} e^{-\mu_{SR}\left(\frac{\gamma}{\bar{\gamma}}\right)^{\frac{\alpha_{SR}}{2}}} \mathrm{d}x = \frac{\gamma_{\text{inc}}\left(\mu_{SR}, \mu_{SR}\left(\frac{\xi\sigma_R^2}{\bar{\gamma}P_S}\right)^{\frac{\alpha_{SR}}{2}}\right)}{\Gamma(\mu_{SR})} \tag{A.5}$$

and

$$F_{|h_{SP}|^2} = \int_0^{\frac{I}{P_S}} \frac{\alpha_{SP}\mu_{SP}{}^{\mu_{SP}}\gamma^{\frac{\alpha_{SP}\mu_{SP}}{2}-1}}{2\Gamma(\mu_{SP})\bar{\gamma}^{\frac{\alpha_{SP}\mu_{SP}}{2}}} e^{-\mu_{SP}\left(\frac{\gamma}{\bar{\gamma}}\right)^{\frac{\alpha_{SP}}{2}}} \mathrm{d}x = \frac{\gamma_{\text{inc}}\left(\mu_{SP}, \mu_{SP}\left(\frac{I}{\bar{\gamma}P_S}\right)^{\frac{\alpha_{SP}}{2}}\right)}{\Gamma(\mu_{SP})}. \tag{A.6}$$

Then, by using (A.5) and (A.6), (3.14) can be further rewritten as

$$\Lambda_2 = \frac{\gamma_{\text{inc}}\left(\mu_{SR}, \mu_{SR}\left(\frac{\xi\sigma_R^2}{\bar{\gamma}P_S}\right)^{\frac{\alpha_{SR}}{2}}\right)}{\Gamma(\mu_{SR})} \frac{\gamma_{\text{inc}}\left(\mu_{SP}, \mu_{SP}\left(\frac{I}{\bar{\gamma}P_S}\right)^{\frac{\alpha_{SP}}{2}}\right)}{\Gamma(\mu_{SP})}. \tag{A.7}$$

Further, Ψ in (3.15) can be computed by

$$\begin{aligned}\Psi_2 = &\int_{\frac{I}{P_S}}^{\infty} f_{|h_{SP}|^2}(y) \int_0^{\frac{\xi y\sigma_R^2}{I}} f_{|h_{SR}|^2}(z)\, \mathrm{d}z\mathrm{d}y = \int_{\frac{I}{P_S}}^{\infty} \frac{\alpha_{SP}\mu_{SP}{}^{\mu_{SP}}\gamma^{\frac{\alpha_{SP}\mu_{SP}}{2}-1}}{2\Gamma(\mu_{SP})\bar{\gamma}^{\frac{\alpha_{SP}\mu_{SP}}{2}}} e^{-\mu_{SP}\left(\frac{\gamma}{\bar{\gamma}}\right)^{\frac{\alpha_{SP}}{2}}} \\ &\times \int_0^{\frac{\xi y\sigma_R^2}{I}} \frac{\alpha_{SR}\mu_{SR}{}^{\mu_{SR}}\gamma^{\frac{\alpha_{SR}\mu_{SR}}{2}-1}}{2\Gamma(\mu_{SR})\bar{\gamma}^{\frac{\alpha_{SR}\mu_{SR}}{2}}} e^{-\mu_{SR}\left(\frac{\gamma}{\bar{\gamma}}\right)^{\frac{\alpha_{SR}}{2}}} \mathrm{d}z\mathrm{d}y = \frac{\alpha_{SP}\mu_{SP}{}^{\mu_{SP}}}{2\Gamma(\mu_{SP})\Gamma(\mu_{SR})\bar{\gamma}^{\frac{\alpha_{SP}\mu_{SP}}{2}}} \\ &\times \int_{\frac{I}{P_S}}^{\infty} \gamma^{\frac{\alpha_{SP}\mu_{SP}}{2}-1} e^{-\mu_{SP}\left(\frac{\gamma}{\bar{\gamma}}\right)^{\frac{\alpha_{SP}}{2}}} \gamma_{\text{inc}}\left(\mu_{SR}, \mu_{SR}\left(\frac{\xi y\sigma_R^2}{\bar{\gamma}I}\right)^{\frac{\alpha_{SR}}{2}}\right) \mathrm{d}y. \end{aligned} \tag{A.8}$$

Now, by applying the series expansion of an incomplete gamma function [110]

$$\gamma_{\text{inc}}(n, x) = \Gamma(n) - \Gamma(n)e^{-x}\sum_{m=0}^{n-1}\frac{x^m}{m!} \tag{A.9}$$

Ψ_2 can be re-expressed in a closed form as

$$\Psi_2 = \frac{\Gamma\left(\mu_{SP}, \mu_{SP}\left(\frac{I}{\bar{\gamma}\bar{P}_S}\right)^{\frac{\alpha_{SP}}{2}}\right)}{\Gamma(\mu_{SP})} - \frac{\mu_{SP}^{\mu_{SP}}}{\Gamma\left(\mu_{SP}\bar{\gamma}^{\frac{\alpha_{SP}\mu_{SP}}{2}}\right)} \times \sum_{i=0}^{\mu_{SR}-1} \frac{\left(\mu_{SR}\left(\frac{\xi\sigma_R^2}{\bar{\gamma}I}\right)^{\frac{\alpha_{SR}}{2}}\right)^i}{i!\left(\frac{\mu_{SP}}{\bar{\gamma}^{\alpha_{SP}/2}} + \mu_{SR}\left(\frac{\xi\sigma_R^2}{\bar{\gamma}I}\right)^{\frac{\alpha_{SR}}{2}}\right)^{\mu_{SP}+i}} \times \Gamma\left(\mu_{SP}+1, \left(\frac{I}{\bar{P}_S}\right)^{\frac{\alpha_{SR}}{2}}\left[\frac{\mu_{SP}}{\bar{\gamma}^{\alpha_{SP}/2}} + \mu_{SR}\left(\frac{\xi\sigma_R^2}{\bar{\gamma}I}\right)^{\frac{\alpha_{SR}}{2}}\right]\right), \tag{A.10}$$

where $\Gamma(s,x) = \int_x^\infty t^{s-1}e^{-t}\mathrm{d}t$ denotes the upper incomplete gamma function. Further, by summing (A.7) and (A.10), the CDF of $\eth_S$ for the $\alpha-\mu$ distribution can be written in a closed form as in (3.26) Then, by following the similar approach as in deriving the CDF of $\eth_S$, the closed-form expression for the CDF of $\eth_R$ for the $\alpha-\mu$ distribution can be expressed as in (3.27) ■

Appendix B

Appendices for Chapter 4

B.1 Proof of Proposition 3

Eq. (4.41) can be extended as

$$P_{\text{out}(j)}^{[\iota]} = \Pr\left[\frac{1}{2}\log_2\left(1+\frac{P_j|h_{j,j}^{[\iota]}|^2}{d_{j,j}^{\tau_{j,j}}\sigma_{\tilde{n}_j}^{[\iota]2}}\right) < \mathcal{R}_{\text{th}}^{j}\right] = \Pr\left[\left|h_{j,j}^{[\iota]}\right|^2 < \frac{\xi^j d_{j,j}^{\tau_{j,j}}\sigma_{\tilde{n}_j}^{[\iota]2}}{P_j}\right]. \tag{B.1}$$

By setting the rate threshold $\mathcal{R}_{\text{th}}$ to positive value, the OP of $|h_{j,j}^{[\iota]}|^2$ can be found from the following cumulative distribution function (CDF)

$$\Pr\left[\left|h_{j,j}^{[\iota]}\right|^2 \leq r_j^{[\iota]}\right] = 1 - e^{-r_j^{[\iota]}}, \quad r_j^{[\iota]} \geq 0, \tag{B.2}$$

where $r_j^{[\iota]} = \frac{\xi^j d_{j,j}^{\tau_{j,j}}\sigma_{\tilde{n}_j}^{[\iota]2}}{P_j}$.

Finally, the OP of PR_j can be derived from (B.2) as (4.43). ■

B.2 Proof of Proposition 4

The OP for relaying SN can be found by using the end-to-end capacity at D. Thus, (4.44) can be further extended as

$$\begin{aligned}
P_{\text{out}(D)} =& \Pr\left[\min(\gamma_R,\gamma_D) < \xi^D\right] = 1 - \Pr\left[\min(\gamma_R,\gamma_D) > \xi^D\right] \\
=& 1 - \Pr\left[\gamma_R > \xi^D\right]\Pr\left[\gamma_R > \xi^D\right] \\
=& 1 - \Pr\left[\frac{(1-\rho)P_S\,|h_{R,S}|^2}{d_{R,S}^{\tau_{R,S}}\sigma_{\tilde{n}_R}^2} > \xi^D\right]\Pr\left[\frac{P_R^{PSR}\,|h_{D,R}|^2}{d_{D,R}^{\tau_{D,R}}\sigma_{\tilde{n}_D}^2} > \xi^D\right] \\
=& 1 - \Pr\left[|h_{R,S}|^2 > \frac{\xi^D d_{R,S}^{\tau_{R,S}}\sigma_{\tilde{n}_R}^2}{(1-\rho)P_S}\right]\Pr\left[|h_{D,R}|^2 > \frac{\xi^D d_{D,R}^{\tau_{D,R}}\sigma_{\tilde{n}_D}^2}{P_R^{PSR}}\right],
\end{aligned} \tag{B.3}$$

where $\xi^D = 2^{2\mathcal{R}_{\text{th}}^D} - 1$ is the corresponding SNR threshold at D while P_R^{PSR} is the harvested energy at R given in (4.30). As $\left|h_{j,j}^{[l]}\right|^2$ in Appendix B.1, $|h_{R,S}|^2$ and $|h_{D,R}|^2$ also follow exponential distribution with CDFs

$$\Pr\left[|h_{R,S}|^2 \leq r_R\right] = 1 - e^{-r_R}, \quad r_R \geq 0, \tag{B.4a}$$

$$\Pr\left[|h_{D,R}|^2 \leq r_D\right] = 1 - e^{-r_D}, \quad r_D \geq 0, \tag{B.4b}$$

respectively, where $r_R = \frac{\xi^D d_{R,S}^{\tau_{R,S}} \sigma_{\tilde{n}_R}^2}{(1-\rho)P_S}$ and $r_D = \frac{\xi^D d_{D,R}^{\tau_{D,R}} \sigma_{\tilde{n}_D}^2}{P_R^{PSR}}$. Hence, inserting (B.4) into (B.3) gives the OP of D as (4.45). ■

Appendix C

Appendices for Chapter 5

C.1 Proof of Proposition 5

The CDFs of $\gamma_{2,1}$ and γ_1 are derived using (5.9) and (5.11) as

$$F_{\gamma_{2,1}}(\xi_1) = \Pr\left[|h_2|^2 < \frac{\xi_1 d_2^\tau}{\kappa\rho_R}\right] = \begin{cases} 1 - e^{-\frac{\xi_1 d_2^\tau}{2\kappa\rho_R}}, & \xi_1 < \frac{\beta_1}{\beta_2}, \\ 1, & \text{otherwise}, \end{cases} \tag{C.1}$$

and

$$F_{\gamma_1}(\xi_1) = \Pr\left[|h_1|^2 < \frac{\xi_1 d_1^\tau}{\kappa\rho_R}\right] = \begin{cases} 1 - e^{-\frac{\xi_1 d_1^\tau}{2\kappa\rho_R}}, & \xi_1 < \frac{\beta_1}{\beta_2}, \\ 1, & \text{otherwise}, \end{cases} \tag{C.2}$$

where $\kappa = \beta_1 - \beta_2\xi_1$ while $|h_1|^2$ and $|h_2|^2$ follow exponential distribution. Then, the CDF of the RV $\gamma_{R,1}$ can be derived as

$$\begin{aligned} F_{R,1}(\xi_1) =& \Pr\left[\frac{|h_{SR}|^2\alpha_1\bar{\rho}_S}{|h_{SR}|^2\alpha_2\bar{\rho}_S + d_{SR}^\tau} < \xi_1, \bar{\rho}_S < \frac{\rho_I d_{SP}^\tau}{|h_{SP}|^2}\right] \\ &+ \Pr\left[\frac{|h_{SR}|^2\alpha_1\frac{\rho_I}{|h_{SP}|^2}}{|h_{SR}|^2\alpha_2\frac{\rho_I}{|h_{SP}|^2} + d_{SR}^\tau} < \xi_1, \bar{\rho}_S > \frac{\rho_I d_{SP}^\tau}{|h_{SP}|^2}\right] \\ =& \underbrace{\Pr\left[|h_{SR}|^2 < \frac{\xi_1 d_{SR}^\tau}{\psi\bar{\rho}_S}, |h_{SP}|^2 < \frac{\rho_I d_{SP}^\tau}{\bar{\rho}_S}\right]}_{A_1} \\ &+ \underbrace{\Pr\left[\frac{|h_{SR}|^2}{|h_{SP}|^2} < \frac{\xi_1 d_{SR}^\tau}{\psi\rho_I}, |h_{SP}|^2 > \frac{\rho_I d_{SP}^\tau}{\bar{\rho}_S}\right]}_{B_1}, \end{aligned} \tag{C.3}$$

where $|h_{SP}|^2$ and $|h_{SR}|^2$ also follow exponential distributions, $\psi = \alpha_1 - \alpha_2\xi_1$, $\bar{\rho}_S = \frac{\bar{P}_S}{\sigma^2}$ stands for the maximum allowed transmit SNR at S and $\rho_I = \frac{I}{\sigma^2}$ denotes the temperature-constraint-to-noise ratio at PR. Now, in the term A_1 of (C.3), $|h_{SP}|^2$ and $|h_{SR}|^2$ are

independent from each other, thus, the term A_1 might be reformulated as

$$A_1 = F_{|h_{SR}|^2}\left(\frac{\xi_1 d_{SR}^{\tau}}{\psi\bar{\rho}_S}\right) F_{|h_{SP}|^2}\left(\frac{\rho_I d_{SP}^{\tau}}{\bar{\rho}_S}\right) = \left(1 - e^{-\frac{\xi_1 d_{SR}^{\tau}}{2\psi\bar{\rho}_S}}\right)\left(1 - e^{-\frac{\rho_I d_{SP}^{\tau}}{2\bar{\rho}_S}}\right). \quad \text{(C.4)}$$

Regarding the term B_1 in (C.3), it can be further extended as

$$\begin{aligned} B_1 &= \int_{\frac{\rho_I d_{SP}^{\tau}}{\bar{\rho}_S}}^{\infty} f_{|h_{SP}|^2}(y) \int_0^{\frac{\xi_1 d_{SR}^{\tau} y}{\psi\rho_I d_{SP}^{\tau}}} f_{|h_{SR}|^2}(z)\mathrm{d}z\mathrm{d}y = \int_{\frac{\rho_I d_{SP}^{\tau}}{\bar{\rho}_S}}^{\infty} \frac{1}{2} e^{\frac{y}{2}} \left(1 - e^{-\frac{y\xi_1 d_{SR}^{\tau}}{2\psi\rho_I d_{SP}^{\tau}}}\right) \mathrm{d}y \\ &= e^{-\frac{\rho_I d_{SP}^{\tau}}{2\bar{\rho}_S}} - \frac{\psi\rho_I d_{SP}^{\tau} e^{-\frac{\psi\rho_I d_{SP}^{\tau} + \xi_1 d_{SR}^{\tau}}{2\psi\bar{\rho}_S}}}{\psi\rho_I d_{SP}^{\tau} + \xi_1 d_{SR}^{\tau}}. \end{aligned} \quad \text{(C.5)}$$

Then, after substituting (C.4) and (C.5) into (C.3) and after some algebraic manipulations, the closed-form expression for (C.3) can be written as

$$F_{\gamma_{R,1}}(\xi_1) = \begin{cases} 1 - e^{-\frac{\xi_1 d_{SR}^{\tau}}{2\psi\bar{\rho}_S}} + \frac{\xi_1 d_{SR}^{\tau} e^{-\frac{\psi\rho_I d_{SP}^{\tau} + \xi_1 d_{SR}^{\tau}}{2\psi\bar{\rho}_S}}}{\psi\rho_I d_{SP}^{\tau} + \xi_1 d_{SR}^{\tau}}, & \xi_1 < \frac{\alpha_1}{\alpha_2}, \\ 1, & \text{otherwise.} \end{cases} \quad \text{(C.6)}$$

Finally, the closed-form expression for the OP of x_1 can be derived by substituting (C.1), (C.2) and (C.6) into (5.22), which can be written as in (5.23) ■

C.2 Proof of Proposition 6

The CDF of the RV $\gamma_{2,2}$ by using (5.10) is further expressed by

$$F_{\gamma_{2,2}}(\xi_2) \triangleq F_{|h_2|^2}(\xi_2) = \Pr\left[\frac{|h_2|^2\beta_2\rho_R}{d_2^{\tau}} < \xi_2\right] = \Pr\left[|h_2|^2 < \frac{\xi_2 d_2^{\tau}}{\beta_2\rho_R}\right] = 1 - e^{-\frac{\xi_2 d_2^{\tau}}{2\beta_2\rho_R}}. \quad \text{(C.7)}$$

Furthermore, the CDF of the RV $\gamma_{R,2}$ is expressed by

$$\begin{aligned} F_{\gamma_{R,2}}(\xi_2) =& \Pr\left[\frac{|h_{SR}|^2\alpha_2\bar{\rho}_S}{d_{SR}^{\tau}} < \xi_2, \bar{\rho}_S < \frac{\rho_I d_{SP}^{\tau}}{|h_{SP}|^2}\right] \\ &+ \Pr\left[\frac{|h_{SR}|^2\alpha_2\rho_I}{|h_{SP}|^2 d_{SR}^{\tau}} < \xi_2, \bar{\rho}_S > \frac{\rho_I d_{SP}^{\tau}}{|h_{SP}|^2}\right] \\ =& \underbrace{\Pr\left[|h_{SR}|^2 < \frac{\xi_2 d_{SR}^{\tau}}{\alpha_2\bar{\rho}_S}, |h_{SP}|^2 < \frac{\rho_I d_{SP}^{\tau}}{\bar{\rho}_S}\right]}_{C_1} \\ &+ \underbrace{\Pr\left[\frac{|h_{SR}|^2}{|h_{SP}|^2} < \frac{\xi_2 d_{SR}^{\tau}}{\alpha_2\rho_I}, |h_{SP}|^2 > \frac{\rho_I d_{SP}^{\tau}}{\bar{\rho}_S}\right]}_{D_1}, \end{aligned} \quad \text{(C.8)}$$

where the term C_1 can be reformulated as followings

$$C_1 = F_{|h_{SR}|^2}\left(\frac{\xi_2 d_{SR}^{\tau}}{\alpha_2 \bar{\rho}_S}\right) F_{|h_{SP}|^2}\left(\frac{\rho_I d_{SP}^{\tau}}{\bar{\rho}_S}\right) = \left(1 - e^{-\frac{\xi_2 d_{SR}^{\tau}}{2\alpha_2 \bar{\rho}_S}}\right)\left(1 - e^{-\frac{\rho_I d_{SP}^{\tau}}{2\bar{\rho}_S}}\right). \quad \text{(C.9)}$$

Then, the term D_1 in (C.8) is extended as follows

$$\begin{aligned} D_1 &= \int_{\frac{\rho_I d_{SP}^{\tau}}{\bar{\rho}_S}}^{\infty} f_{|h_{SP}|^2}(y) \int_0^{\frac{\xi_2 d_{SR}^{\tau} y}{\alpha_2 \rho_I d_{SP}^{\tau}}} f_{|h_{SR}|^2}(z)\mathrm{d}z\mathrm{d}y = \int_{\frac{\rho_I d_{SP}^{\tau}}{\bar{\rho}_S}}^{\infty} \frac{1}{2} e^{\frac{y}{2}} \left(1 - e^{-\frac{y\xi_2 d_{SR}^{\tau}}{2\alpha_2 \rho_I d_{SP}^{\tau}}}\right) \mathrm{d}y \\ &= e^{-\frac{\rho_I d_{SP}^{\tau}}{2\bar{\rho}_S}} - \frac{\alpha_2 \rho_I d_{SP}^{\tau} e^{-\frac{\alpha_2 \rho_I d_{SP}^{\tau} + \xi_2 d_{SR}^{\tau}}{2\alpha_2 \bar{\rho}_S}}}{\alpha_2 \rho_I d_{SP}^{\tau} + \xi_2 d_{SR}^{\tau}}. \end{aligned} \quad \text{(C.10)}$$

Now, (C.9) and (C.10) can be substituted into (C.8), then after some algebraic manipulations, (C.8) can be written by

$$F_{\gamma_{R,2}}(\xi_2) = 1 - e^{-\frac{\xi_2 d_{SR}^{\tau}}{2\alpha_2 \bar{\rho}_S}} + \frac{\xi_2 d_{SR}^{\tau} e^{-\frac{\alpha_2 \rho_I d_{SP}^{\tau} + \xi_2 d_{SR}^{\tau}}{2\alpha_2 \bar{\rho}_S}}}{\alpha_2 \rho_I d_{SP}^{\tau} + \xi_2 d_{SR}^{\tau}}. \quad \text{(C.11)}$$

Finally, the OP in (5.24), after inserting (C.7) and (C.11), can be written in a closed-form as in (5.25).

C.3 Proof of Proposition 7

Considering the ITC, the CDF in (5.26), which is also the OP of D_1, can be derived as

$$\begin{aligned} P_{\text{out},1}^{\text{AF}}(\xi_1) =& \Pr\left[\frac{n_s Y n_1 X \alpha_1}{n_s Y n_1 X \alpha_2 + n_1 X + n_s Y + 1} < \xi_1, \bar{\rho}_S < \frac{\rho_I d_{SP}^{\eta}}{Z}\right] \\ &+ \Pr\left[\frac{\frac{n_p}{Z} Y n_1 X \alpha_1}{\frac{n_p}{Z} Y n_1 X \alpha_2 + n_1 X + \frac{n_p}{Z} Y + 1} < \xi_1, \bar{\rho}_S > \frac{\rho_I d_{SP}^{\eta}}{Z}\right] \\ \overset{\varepsilon}{=}& \Pr\left[n_1 X \left(n_s Y \left(\alpha_1 - \alpha_2 \xi_1\right) - \xi_1\right) < n_s Y \xi_1 + \xi_1, Z < \frac{\rho_I d_{SP}^{\eta}}{\bar{\rho}_S}\right] \\ &+ \Pr\left[n_1 X \left(\frac{n_p}{Z} Y \left(\alpha_1 - \alpha_2 \xi_1\right) - \xi_1\right) < \frac{n_p}{Z} Y \xi_1 + \xi_1, Z > \frac{\rho_I d_{SP}^{\eta}}{\bar{\rho}_S}\right] \\ =& \underbrace{\Pr\left[Y < \frac{\xi_1}{n_s \psi} \triangleq u_1, X < \frac{Y n_s u_1 + u_1}{n_1 (Y - u_1)}, Z < c\right]}_{A} \\ &+ \underbrace{\Pr\left[Y < \frac{Z \xi_1}{n_p \psi} \triangleq Z \bar{u}_1, X < \frac{Y n_P \bar{u}_1 + Z \bar{u}_1}{n_1 (Y - Z \bar{u}_1)}, Z > c\right]}_{B}, \end{aligned} \quad \text{(C.12)}$$

where $n_p = \frac{\rho_I d_{SP}^{\eta}}{d_{SR}^{\eta}}$, $c = \frac{\rho_I d_{SP}^{\eta}}{\bar{\rho}_S}$, $\rho_I = \frac{P_I}{\sigma^2}$ and $Z = |h_{SP}|^2$. Moreover, the step ε in (C.12) relies on $\alpha_1 > \alpha_2 \xi_1$, otherwise, $P_{\text{out},1}^{\text{AF}}(\xi_1) = 1$ regardless of the system SNR. Then, we

can further rewrite the term A in (C.12) as

$$A = \underbrace{\int_0^c f_Z(z)\mathrm{d}z \int_0^{u_1} f_Y(y)\mathrm{d}y}_{A_1} + \underbrace{\int_0^c f_Z(z)\mathrm{d}z}_{A_2} \underbrace{\int_{u_1}^{\infty} F_X\left(\frac{yn_s u_1 + u_1}{n_1(y-u_1)}\right) f_Y(y)\mathrm{d}y}_{A_3}. \tag{C.13}$$

As the PDFs in the term A_1 are independent from each other, we can write it as

$$A_1 = \int_0^c f_Z(z)\mathrm{d}z \int_0^{u_1} f_Y(y)\mathrm{d}y = \left(1 - e^{-c}\right)\left(1 - e^{-u_1}\right), \tag{C.14}$$

and A_2 is written as

$$A_2 = \int_0^c f_Z(z)\mathrm{d}z = \left(1 - e^{-c}\right). \tag{C.15}$$

Then, the term A_3 can be further extended as

$$A_3 = \underbrace{\int_{u_1}^{\infty} e^{-y}\mathrm{d}y}_{A_{31}} - \underbrace{\int_{u_1}^{\infty} e^{-\frac{yn_s u_1 + u_1}{n_1(y-u_1)} - y}\,\mathrm{d}y}_{A_{32}}, \tag{C.16}$$

The term A_{31} in (C.16) can be further rewritten as

$$A_{31} = \int_{u_1}^{\infty} e^{-y}\mathrm{d}y = e^{-u_1}. \tag{C.17}$$

Moreover, by using a substitution of $t_1 = y - u_1$, A_{32} in (C.16) can be reformulated by

$$A_{32} = \int_0^{\infty} e^{-\frac{t_1 n_s u_1 + n_s u_1^2 + u_1}{n_1 t_1} - t_1 - u_1}\mathrm{d}t_1 = e^{-\frac{u_1(n_1+n_s)}{n_1}} \int_0^{\infty} e^{-\frac{u_1(n_s u_1+1)}{n_1}\frac{1}{t_1} - t_1}\mathrm{d}t_1. \tag{C.18}$$

Then, using [121, Eq. (3.324.1)], A_{32} can be further derived as

$$A_{32} = e^{-\frac{u_1(n_1+n_s)}{n_1}} 2\sqrt{\frac{u_1(n_s u_1+1)}{n_1}} K_1\left(2\sqrt{\frac{u_1(n_s u_1+1)}{n_1}}\right), \tag{C.19}$$

where $K_1(\cdot)$ is the modified Bessel function of the second kind of order 1. Further, the term A, after substituting (C.14), (C.15), (C.17) and (C.19) into (C.13) is reformulated as

$$\begin{aligned} A =& \left(1-e^{-c}\right)\left(1-e^{-u_1}\right)+\left(1-e^{-c}\right) \\ &\times\left(e^{-u_1}-e^{-\frac{u_1(n_1+n_s)}{n_1}}2\sqrt{\frac{u_1(n_su_1+1)}{n_1}}K_1\left(2\sqrt{\frac{u_1(n_su_1+1)}{n_1}}\right)\right) \\ =& \left(1-e^{-c}\right)\left(1-e^{-\frac{u_1(n_1+n_s)}{n_1}}2\sqrt{r_1}K_1\left(2\sqrt{r_1}\right)\right), \end{aligned} \tag{C.20}$$

where $r_1=\frac{u_1(n_su_1+1)}{n_1}$.

Now, the term B in (C.12) can be further extended as

$$B=\underbrace{\int_c^\infty f_Z(z)\int_0^{z\bar{u}_1} f_Y(y)\mathrm{d}y\mathrm{d}z}_{B_1}+\underbrace{\int_c^\infty f_Z(z)\int_{z\bar{u}_1}^\infty f_Y(y)F_X\left(\frac{n_py\bar{u}_1+z\bar{u}_1}{n_1\left(y-z\bar{u}_1\right)}\right)\mathrm{d}y\mathrm{d}z}_{B_2}. \tag{C.21}$$

The term B_1 can be derived as

$$\begin{aligned} B_1 =& \int_c^\infty e^{-z}\int_0^{z\bar{u}_1} e^{-y}\mathrm{d}y\mathrm{d}z=\int_c^\infty e^{-z}\left(1-e^{-z\bar{u}_1}\right)\mathrm{d}z \\ =& \int_c^\infty e^{-z}\mathrm{d}z-\int_c^\infty e^{-z(\bar{u}_1+1)}\mathrm{d}z=e^{-c}-\frac{e^{-c(\bar{u}_1+1)}}{\bar{u}_1+1}. \end{aligned} \tag{C.22}$$

Further, the term B_2 can be rewritten as

$$B_2=\int_c^\infty e^{-z}\left(\int_{z\bar{u}_1}^\infty e^{-y}\mathrm{d}y-\underbrace{\int_{z\bar{u}_1}^\infty e^{-\frac{n_py\bar{u}_1+z\bar{u}_1}{n_1(y-z\bar{u}_1)}-y}\mathrm{d}y}_{B_{21}}\right)\mathrm{d}z. \tag{C.23}$$

Then, by using $p_1=y-z\bar{u}_1$ and [121, Eq. (3.324.1)], the term B_{21} in (C.23) is written as

$$\begin{aligned} B_{21} =& \int_0^\infty e^{-\frac{n_p\bar{u}_1p_1+n_p\bar{u}_1^2z+z\bar{u}_1}{n_1p_1}-p_1-z\bar{u}_1}\mathrm{d}p_1=e^{-\frac{\bar{u}_1(n_p+zn_1)}{n_1}}\int_0^\infty e^{-\frac{z\bar{u}_1(n_p\bar{u}_1+1)}{n_1p_1}-p_1}\mathrm{d}p_1 \\ =& e^{-\frac{\bar{u}_1(n_p+zn_1)}{n_1}}2\sqrt{s_1}K_1\left(2\sqrt{s_1}\right), \end{aligned} \tag{C.24}$$

where $s_1 = \frac{z\bar{u}_1(n_p\bar{u}_1+1)}{n_1}$. Now, we rewrite (C.23) using (C.24) as

$$\begin{aligned} B_2 =& \int_c^\infty e^{-\bar{u}_1 z - z} \mathrm{d}z - \int_c^\infty e^{-\frac{\bar{u}_1(n_p+zn_1)}{n_1} - z} \mathrm{d}z \\ =& \frac{e^{-c(\bar{u}_1+1)}}{\bar{u}_1+1} - \underbrace{\int_c^\infty e^{-\frac{zn_1(\bar{u}_1+1)+n_p\bar{u}_1}{n_1}} 2\sqrt{s_1}K_1(2\sqrt{s_1})\mathrm{d}z}_{B_{22}}. \end{aligned} \tag{C.25}$$

Then, substituting $q = z - c$ and after some algebraic manipulations, the term B_{22} in (C.25) can be rewritten as

$$B_{22} = e^{-\frac{cn_1(\bar{u}_1+1)+n_p\bar{u}_1}{n_1}} \underbrace{\int_0^\infty e^{-q(\bar{u}_1+1)} 2\sqrt{l_1}K_1\left(2\sqrt{l_1}\right) \mathrm{d}q}_{\Lambda}. \tag{C.26}$$

where $l_1 = \frac{q\bar{u}_1(n_p\bar{u}_1+1)+c\bar{u}_1(n_p\bar{u}_1+1)}{n_1}$. Further, after applying [195, Eqs. (12) and (14)] and [196, Eq. (2.24.1.3)] to Λ in (C.26) and by substituting (C.22) - (C.25) into (C.21), the term B can be written in a closed-form expression as

$$B = e^{-c} - \frac{n_1 e^{-\frac{cn_1(\bar{u}_1+1)+n_p\bar{u}_1}{n_1}}}{\bar{u}_1(n_p\bar{u}_1+1)} \sum_{k=0}^{\infty} \frac{\left(-\frac{c\bar{u}_1(n_p\bar{u}_1+1)}{n_1}\right)^k}{k!} G_{3\,2}^{1\,3}\left(\frac{n_1(\bar{u}_1+1)}{\bar{u}_1(n_p\bar{u}_1+1)} \middle| \begin{matrix} 0,\ k-1,\ k \\ 0,\ k \end{matrix}\right) \tag{C.27}$$

Finally, by substituting (C.20) and (C.27) into (C.12), the exact OP for D_1 can be written as in (5.27). ■

C.4 Proof of Proposition 8

Using (5.19), the OP for D_2 can be further rewritten as

$$\begin{aligned} P_{\text{out},2}^{\text{AF}}(\xi_2) =& \Pr\left[\frac{n_s Y n_2 Q \alpha_2}{n_2 Q + n_s Y + 1} < \xi_2, \bar{\rho}_S < \frac{\rho_I d_{SP}^{\eta}}{Z}\right] \\ &+ \Pr\left[\frac{\frac{n_p}{Z} Y n_2 Q \alpha_2}{n_2 Q + \frac{n_p}{Z} Y + 1} < \xi_2, \bar{\rho}_S > \frac{\rho_I d_{SP}^{\eta}}{Z}\right] \\ =& \Pr\left[n_2 Q\left(n_s Y \alpha_2 - \xi_2\right) < n_s Y \xi_2 + \xi_2, Z < c\right] \\ &+ \Pr\left[n_2 Q\left(\frac{n_p}{Z} Y \alpha_2 - \xi_2\right) < \frac{n_p}{Z} Y \xi_2 + \xi_2, Z > c\right] \\ =& \underbrace{\Pr\left[Y < \frac{\xi_2}{n_s \alpha_2} \triangleq u_2, Q < \frac{Y n_s u_2 + u_2}{n_2(Y - u_2)}, Z < c\right]}_{C} \end{aligned}$$

$$+\underbrace{\Pr\left[Y<\frac{Z\bar{\theta}_2}{n_p\alpha_2}\triangleq Z\bar{u}_2, Q<\frac{Yn_P\bar{u}_2+Z\bar{u}_2}{n_2(Y-Z\bar{u}_2)}, Z>c\right]}_{D}. \tag{C.28}$$

The OP derivation of D_2 from (C.28) can be derived by following the same step as in (C.13) - (C.27) shown in Appendix (C.3), which is omitted for the sake of brevity. Hence, the OP expression for D_2 is written as in (5.29). ■

C.5 Proof of Proposition 9

First, by using the *"change of variable"* method [115, Eq. (14)], we re-express (5.30) as

$$f_{|h_t|^2}(r)=\frac{\lambda_t^{m_t}}{\Gamma(m_t)}r^{m_t-1}\exp\left(-\lambda_t r\right),\ g_t>0, \tag{C.29}$$

where $m_t\geq\frac{1}{2}$ and $\hat{r}_t$ stand for the Nakagami-m fading shaping parameter and average channel power gain, accordingly. Now, the CDF from (C.29) can be derived by

$$F_{|h_t|^2}(r)=1-\frac{\Gamma\left(m_t,\lambda_t r\right)}{\Gamma\left(m_t\right)},\ \forall t\in\{SR,RP,1,2\}. \tag{C.30}$$

Then, using (C.30), the CDF of $\gamma_{R,1}$ can be derived as follows

$$F_{\gamma_{R,1}}(\xi_1)=\Pr\left[|h_{SR}|^2<\frac{\xi_1 d_{SR}^{\tau}}{a_1\rho_S}\right]\triangleq F_{|h_{SR}|^2}(\xi_1)=1-\frac{\Gamma\left(m_{SR},\frac{\lambda_{SR}\xi_1 d_{SR}^{\tau}}{a_1\rho_S}\right)}{\Gamma\left(m_{SR}\right)}. \tag{C.31}$$

Further, the CDF of $\gamma_{1,1}$ can be written as

$$\begin{aligned}F_{\gamma_{1,1}}(\xi_1)=&\Pr\left[\frac{|h_1|^2b_1\bar{\rho}_R}{d_1^{\tau}}<\xi_1,\bar{\rho}_R<\frac{\rho_I d_{RP}^{\tau}}{|h_{RP}|^2}\right]\\&+\Pr\left[\frac{|h_1|^2b_1\rho_I d_{RP}^{\tau}}{|h_{RP}|^2d_1^{\tau}}<\xi_1,\bar{\rho}_R>\frac{\rho_I d_{RP}^{\tau}}{|h_{RP}|^2}\right]\\=&\underbrace{\Pr\left[|h_1|^2<\frac{\xi_1 d_1^{\tau}}{b_1\bar{\rho}_R},|h_{RP}|^2<\frac{\rho_I d_{RP}^{\tau}}{\bar{\rho}_R}\right]}_{N_1}\\&+\underbrace{\Pr\left[\frac{|h_1|^2}{|h_{RP}|^2}<\frac{\xi_1 d_1^{\tau}}{b_1\rho_I d_{RP}^{\tau}},|h_{RP}|^2>\frac{\rho_I d_{RP}^{\tau}}{\bar{\rho}_R}\right]}_{N_2},\end{aligned} \tag{C.32}$$

where $\bar{\rho}_R = \frac{\bar{P}_R}{\sigma_2}$. Now, as $|h_1|^2$ and $|h_{RP}|^2$ in N_1 of (C.32) are independent RVs, N_1 can be recalculated by

$$\begin{aligned} N_1 &= \int_0^{\frac{\rho_I d_{RP}^{\tau}}{\bar{\rho}_R}} f_{|h_{RP}|^2}(x)\mathrm{d}x \int_0^{\frac{\xi_1 d_1^{\tau}}{b_1 \bar{\rho}_R}} f_{|h_1|^2}(y)\mathrm{d}y \\ &= \left(1 - \frac{\Gamma\left(m_{RP}, \frac{\lambda_{RP}\rho_I d_{RP}^{\tau}}{\bar{\rho}_R}\right)}{\Gamma\left(m_{RP}\right)}\right)\left(1 - \frac{\Gamma\left(m_1, \frac{\lambda_1 \xi_1 d_1^{\tau}}{b_1 \bar{\rho}_R}\right)}{\Gamma\left(m_1\right)}\right). \end{aligned} \tag{C.33}$$

Then, N_2 in (C.32) using (C.30) can be further extended as

$$\begin{aligned} N_2 &= \int_{\frac{\rho_I d_{RP}^{\tau}}{\bar{\rho}_R}}^{\infty} f_{|h_{RP}|^2}(x) \int_0^{\frac{x\xi_1 d_1^{\tau}}{b_1 \rho_I d_{RP}^{\tau}}} f_{|h_1|^2}(y)\mathrm{d}y\, \mathrm{d}x \\ &= \int_{\frac{\rho_I d_{RP}^{\tau}}{\bar{P}_R}}^{\infty} \lambda_{RP}^{m_{RP}} x^{m_{RP}-1} \exp\left(-\lambda_{RP}x\right) \frac{\gamma_{\text{inc}}\left(m_1, \frac{\lambda_1 x \xi_1 d_1^{\tau}}{b_1 I d_{RP}^{\tau}}\right)}{\Gamma(m_{RP})\Gamma(m_1)}\mathrm{d}x, \end{aligned} \tag{C.34}$$

where $\gamma_{\text{inc}}(s,x) = \int_0^x t^{s-1}e^{-t}\mathrm{d}t$ denotes the lower incomplete Gamma function [121]. Then, applying the series expansion of the lower incomplete Gamma function $\gamma_{\text{inc}}(s,x) = \Gamma(s)\left(1 - e^{-x}\sum_{i=0}^{s-1}\frac{x^i}{i!}\right)$ as in [161] and after some algebraic manipulations, (C.34) can be further expressed by followings

$$N_2 = \frac{\Gamma\left(m_{RP}, \frac{\lambda_{RP}\rho_I d_{RP}^{\tau}}{\bar{\rho}_R}\right)}{\Gamma\left(m_{RP}\right)} - \frac{\lambda_{RP}^{m_{RP}}}{\Gamma(m_{RP})} \times \sum_{i=0}^{m_1-1} \frac{\left(\frac{\lambda_1 \xi_1 d_1^{\tau}}{b_1 \rho_I d_{RP}^{\tau}}\right)^i}{i! c_1^{m_{RP}+i}} \Gamma\left(m_{RP}+i, \frac{\rho_I d_{RP}^{\tau} c_1}{\bar{\rho}_R}\right), \tag{C.35}$$

where $c_1 = \lambda_{RP} + \frac{\lambda_1 \xi_1 d_1^{\tau}}{b_1 \rho_I d_{RP}^{\tau}}$. Hence, the CDF of $\gamma_{1,1}$ given in (C.32) can be rewritten in a closed-form as follows

$$\begin{aligned} F_{\gamma_{1,1}}(\xi_1) =& 1 - \left(1 - \frac{\Gamma\left(m_{RP}, \frac{\lambda_{RP}\rho_I d_{RP}^{\tau}}{\bar{\rho}_R}\right)}{\Gamma\left(m_{RP}\right)}\right)\frac{\Gamma\left(m_1, \frac{\lambda_1 \xi_1 d_1^{\tau}}{b_1 \bar{\rho}_R}\right)}{\Gamma\left(m_1\right)} \\ &- \sum_{i=0}^{m_1-1} \frac{\left(\frac{\lambda_1 \xi_1 d_1^{\tau}}{b_1 \rho_I d_{RP}^{\tau}}\right)^i}{i!\, c_1^{m_{RP}+i}} \frac{\lambda_{RP}^{m_{RP}}}{\Gamma(m_{RP})} \Gamma\left(m_{RP}+i, \frac{\rho_I d_{RP}^{\tau}}{\bar{\rho}_R} c_1\right). \end{aligned} \tag{C.36}$$

Finally, by substituting (C.31) and (C.36) into (5.42), a closed-form expression for the OP of x_1 can be expressed as in (5.43). ■

C.6 Proof of Proposition 10

By using (5.33), the CDF of $\gamma_{R,2}$ is derived as follows

$$\begin{aligned} F_{\gamma_{R,2}}(\xi_2) &= \Pr\left[|h_{SR}|^2 < \frac{\xi_2 d_{SR}^{\tau}}{\rho_S\left(a_2 - a_1\xi_2\right)}\right] \\ &\triangleq F_{|h_{SR}|^2}(\xi_2) = \begin{cases} 1 - \frac{\Gamma\left(m_{SR}, \frac{\lambda_{SR} u d_{SR}^{\tau}}{\rho_S(a_2 - a_1 u)}\right)}{\Gamma(m_{SR})}, & \text{if } u < \frac{a_2}{a_1}, \\ 1, & \text{otherwise.} \end{cases} \end{aligned} \tag{C.37}$$

Then, using (5.37), the CDF of $\gamma_{1,2}$ can be derived as

$$\begin{aligned} F_{\gamma_{1,2}}(\xi_2) =& \underbrace{\Pr\left[|h_1|^2 < \frac{\xi_2 d_1^{\tau}}{\bar{\rho}_R\left(b_2 - b_1\xi_2\right)},\ |h_{RP}|^2 < \frac{\rho_I d_{RP}^{\tau}}{\bar{\rho}_R}\right]}_{M_1} \\ &+ \underbrace{\Pr\left[\frac{|h_1|^2}{|h_{RP}|^2} < \frac{\xi_2 d_1^{\tau}}{\rho_I d_{RP}^{\tau}\left(b_2 - b_1\xi_2\right)},\ |h_{RP}|^2 > \frac{\rho_I d_{RP}^{\tau}}{\bar{\rho}_R}\right]}_{M_2}. \end{aligned} \tag{C.38}$$

Similar as in (C.33), the RVs $|h_1|^2$ and $|h_{RP}|^2$ in M_1 are independent from each other, thus, M_1 can be rewritten as follows

$$M_1 = \left(1 - \frac{\Gamma\left(m_{RP}, \frac{\lambda_{RP}\rho_I d_{RP}^{\tau}}{\bar{\rho}_R}\right)}{\Gamma\left(m_{RP}\right)}\right)\left(1 - \frac{\Gamma\left(m_1, \frac{\lambda_1\xi_2 d_1^{\tau}}{\bar{\rho}_R(b_2 - b_1\xi_2)}\right)}{\Gamma\left(m_1\right)}\right). \tag{C.39}$$

Now, the term M_2 in (C.38) can be further expressed by following the same steps as in the derivation of N_2 (shown in Appendix C.5)

$$\begin{aligned} M_2 =& \frac{\Gamma\left(m_{RP}, \frac{\lambda_{RP}\rho_I d_{RP}^{\tau}}{\bar{\rho}_R}\right)}{\Gamma\left(m_{RP}\right)} - \frac{\lambda_{RP}^{m_{RP}}}{\Gamma(m_{RP})}\sum_{i=0}^{m_1-1}\frac{\left(\frac{\lambda_1\xi_2 d_1^{\tau}}{\rho_I d_{RP}^{\tau}(b_2 - b_1\xi_2)}\right)^i}{i!} \\ &\times \Gamma\left(m_{RP} + i, \frac{\rho_I d_{RP}^{\tau}}{\bar{\rho}_R}c_2\right) c_2^{-(m_{RP}+i)}, \end{aligned} \tag{C.40}$$

where $c_2 = \lambda_{RP} + \frac{\lambda_1 \xi_2 d_1^\tau}{\rho_I d_{RP}^\tau (b_2 - b_1 \xi_2)}$. Further, by substituting (C.39) and (C.40) into (C.38), and after some algebraic manipulations, the CDF in (C.38) can be re-expressed as follows

$$F_{\gamma_{1,2}}(\xi_2) = 1 - \left(1 - \frac{\Gamma\left(m_{RP}, \frac{\lambda_{RP}\rho_I d_{RP}^\tau}{\bar{\rho}_R}\right)}{\Gamma(m_{RP})}\right) \frac{\Gamma\left(m_1, \frac{\lambda_1 \xi_2 d_1^\tau}{\bar{\rho}_R (b_2 - b_1 \xi_2)}\right)}{\Gamma(m_1)} - \frac{\lambda_{RP}^{m_{RP}}}{\Gamma(m_{RP})} \sum_{i=0}^{m_1 - 1} \Gamma\left(m_{RP} + i, \frac{\rho_I d_{RP}^\tau}{\bar{\rho}_R} c_2\right) \frac{\left(\frac{\lambda_1 \xi_2 d_1^\tau}{\rho_I d_{RP}^\tau (b_2 - b_1 \xi_2)}\right)^i}{i!\, c_2^{m_{RP}+i}}, \text{ if } \xi_2 < \frac{b_2}{b_1}. \tag{C.41}$$

Moreover, the CDF of the RV $\gamma_{2,2}$ can be derived using (5.39) and written as

$$F_{\gamma_{2,2}}(\xi_2) = \underbrace{\Pr\left[|h_2|^2 < \frac{\xi_2 d_2^\tau}{\bar{\rho}_R (b_2 - b_1 \xi_2)}, \; |h_{RP}|^2 < \frac{\rho_I d_{RP}^\tau}{\bar{\rho}_R}\right]}_{O_1} + \underbrace{\Pr\left[\frac{|h_2|^2}{|h_{RP}|^2} < \frac{\xi_2 d_2^\tau}{\rho_I d_{RP}^\tau (b_2 - b_1 \xi_2)}, \; |h_{RP}|^2 > \frac{\rho_I d_{RP}^\tau}{\bar{P}_R}\right]}_{O_2}. \tag{C.42}$$

Similar as in (C.33) and (C.39), $|h_2|^2$ and $|h_{RP}|^2$ in O_1 are independent from each other, thus, O_1 can be further expressed by

$$O_1 = 1 - \frac{\Gamma\left(m_{RP}, \frac{\lambda_{RP}\rho_I d_{RP}^\tau}{\bar{\rho}_R}\right)}{\Gamma(m_{RP})} - \frac{\Gamma\left(m_2, \frac{\lambda_2 \xi_2 d_2^\tau}{\bar{\rho}_R (b_2 - b_1 \xi_2)}\right)}{\Gamma(m_2)} \left(1 - \frac{\Gamma\left(m_{RP}, \frac{\lambda_{RP}\rho_I d_{RP}^\tau}{\bar{\rho}_R}\right)}{\Gamma(m_{RP})}\right). \tag{C.43}$$

Then, the term O_2 in (C.42) can be rewritten as

$$O_2 = \frac{\Gamma\left(m_{RP}, \frac{\lambda_{RP}\rho_I d_{RP}^\tau}{\bar{\rho}_R}\right)}{\Gamma(m_{RP})} - \frac{\lambda_{RP}^{m_{RP}}}{\Gamma(m_{RP})} \sum_{i=0}^{m_2 - 1} \frac{\left(\frac{\lambda_2 \xi_2 d_2^\tau}{\rho_I d_{RP}^\tau (b_2 - b_1 \xi_2)}\right)^i}{i!} c_3^{-(m_{RP}+i)} \times \Gamma\left(m_{RP} + i, \frac{I d_{RP}^\tau}{\bar{P}_R} c_3\right), \text{ if } \xi_2 < \frac{b_2}{b_1}, \tag{C.44}$$

where $c_3 = \lambda_{RP} + \frac{\lambda_2 v \sigma_2^2 d_2^\tau}{I d_{RP}^\tau (b_2 - b_1 v)}$. Then, by substituting (C.43) and (C.44) into (C.42), and after some algebraic manipulations, the CDF of $\gamma_{2,2}$ can be written in a closed-form as follows

$$F_{\gamma_{2,2}}(\xi_2) = 1 - \left(1 - \frac{\Gamma\left(m_{RP}, \frac{\lambda_{RP}\rho_I d_{RP}^\tau}{\bar{\rho}_R}\right)}{\Gamma(m_{RP})}\right) \frac{\Gamma\left(m_2, \frac{\lambda_2 \xi_2 d_2^\tau}{\bar{\rho}_R (b_2 - b_1 \xi_2)}\right)}{\Gamma(m_2)} - \frac{\lambda_{RP}^{m_{RP}}}{\Gamma(m_{RP})}$$

$$\times \sum_{i=0}^{m_2-1} \Gamma\left(m_{RP}+i, \frac{\rho_I d_{RP}^{\tau}}{\bar{\rho}_R} c_3\right) \frac{\left(\frac{\lambda_2 \xi_2 d_2^{\tau}}{\rho_I d_{RP}^{\tau}(b_2-b_1\xi_2)}\right)^i}{i!\, c_3^{m_{RP}+i}}, \text{ if } \xi_2 < \frac{b_2}{b_1}. \tag{C.45}$$

Finally, the OP of x_2 can be derived in a closed-form by substituting (C.37), (C.41) and (C.45) into (5.44). ■

C.7 Proof of Proposition 11

The CDF of the RV $\gamma_{R,j}$ in (5.49) can be further extended as

$$\begin{aligned} F_{\gamma_{R,j}}(\xi_j) =& \Pr\left[\frac{|\hat{h}_{SR}|^2 \alpha_j \bar{\rho}_S}{|\hat{h}_{SR}|^2 \bar{\rho}_S \Theta + \zeta_R d_{SR}^{\tau}} < \xi_j,\ \bar{\rho}_S < \frac{\rho_I d_{SP}^{\tau}}{|h_{SP}|^2}\right] \\ &+ \Pr\left[\frac{|\hat{h}_{SR}|^2 \alpha_1 \frac{\rho_I d_{SP}^{\tau}}{|h_{SP}|^2}}{|\hat{h}_{SR}|^2 \frac{\rho_I d_{SP}^{\tau}}{|h_{SP}|^2} \Theta + \bar{\zeta}_R d_{SR}^{\tau}} < \xi_j,\ \bar{\rho}_S > \frac{\rho_I d_{SP}^{\tau}}{|h_{SP}|^2}\right] \\ =& \underbrace{\Pr\left[|\hat{h}_{SR}|^2 < \frac{\xi_j \zeta_R d_{SR}^{\tau}}{\mu \bar{\rho}_S},\ |h_{SP}|^2 < \frac{\rho_I d_{SP}^{\tau}}{\bar{\rho}_S}\right]}_{A_3} \\ &+ \underbrace{\Pr\left[|\hat{h}_{SR}|^2 < \frac{|h_{SP}|^2 \mathcal{G}_{R,j} + \mathcal{O}_{R,j}}{\mu},\ |h_{SP}|^2 > \frac{\rho_I d_{SP}^{\tau}}{\bar{\rho}_S}\right]}_{B_3}, \end{aligned} \tag{C.46}$$

where $\mu = \alpha_j - \xi_j \Theta$, $\bar{\zeta}_R = \frac{\rho_I d_{SP}^{\tau} \sigma_{\hat{h}_{SR}}^2}{|h_{SP}|^2 d_{SR}^{\tau}} + \nu + 1$, $\mathcal{G}_{R,j} = \frac{\xi_j(\nu+1) d_{SR}^{\tau}}{\rho_I d_{SP}^{\tau}}$ and $\mathcal{O}_{R,j} = \xi_j \sigma_{\hat{h}_{SR}}^2$.

Further, as RVs $|h_{SP}|^2$ and $|\hat{h}_{SR}|^2$ in A_3 of (C.46) are independent from each other, the term A_3 can be re-expressed by follows

$$\begin{aligned} A_3 &= \left(1 - e^{-\frac{\xi_j \zeta_R d_{SR}^{\tau}}{2\mu \bar{\rho}_S}}\right)\left(1 - e^{-\frac{\rho_I d_{SP}^{\tau}}{2\bar{\rho}_S}}\right) \\ &= 1 - e^{-\frac{\xi_j \zeta_R d_{SR}^{\tau}}{2\mu \bar{\rho}_S}} - e^{-\frac{\rho_I d_{SP}^{\tau}}{2\bar{\rho}_S}} + e^{-\frac{\xi_j \zeta_R d_{SR}^{\tau} + \mu \rho_I d_{SP}^{\tau}}{2\mu \bar{\rho}_S}}. \end{aligned} \tag{C.47}$$

Then, the term B_3 in (C.46) can be further written as

$$\begin{aligned} B_3 &= \int_{\frac{\rho_I d_{SP}^{\tau}}{\bar{\rho}_S}}^{\infty} f_{|h_{SP}|^2}(y) \int_0^{\frac{y\mathcal{G}_{R,j} + \mathcal{O}_{R,j}}{\mu}} f_{|\hat{h}_{SR}|^2}(z) \mathrm{d}z \mathrm{d}y \\ &= \int_{\frac{\rho_I d_{SP}^{\tau}}{\bar{\rho}_S}}^{\infty} f_{|h_{SP}|^2}(y) \left(1 - e^{-\frac{y\mathcal{G}_{R,j} + \mathcal{O}_{R,j}}{2\mu}}\right) \mathrm{d}y = e^{-\frac{\rho_I d_{SP}^{\tau}}{2\bar{\rho}_S}} - \frac{\mu e^{-\frac{\rho_I d_{SP}^{\tau}(\mu + \mathcal{G}_{R,j}) + \mathcal{O}_{R,j}\bar{\rho}_S}{2\mu \bar{\rho}_S}}}{\mu + \mathcal{G}_{R,j}}. \end{aligned} \tag{C.48}$$

Finally, after substituting (C.47) and (C.48) into (C.46), and using some algebraic manipulations, the CDF of the RV $\gamma_{R,j}$ can be written in its closed form as in (5.59) ■

C.8 Proof of Proposition 12

Considering the relay power constraint, the CDF of the RV $\gamma_{k,j}$ is written as

$$\begin{aligned} F_{\gamma_{k,j}}(\xi_j) =& \Pr\left[\frac{|\hat{h}_k|^2\beta_i\bar{\rho}_R}{|\hat{h}_k|^2\bar{\rho}_R\Phi+\zeta_k d_k^\tau} < \xi_j,\ \bar{\rho}_R < \frac{\rho_I d_{RP}^\tau}{|h_{RP}|^2}\right] \\ &+ \Pr\left[\frac{|\hat{h}_k|^2\beta_i\frac{\rho_I d_{RP}^\tau}{|h_{RP}|^2}}{|\hat{h}_k|^2\frac{\rho_I d_{RP}^\tau}{|h_{RP}|^2}\Phi+\bar{\zeta}_k d_k^\tau} < \xi_j,\ \bar{\rho}_R > \frac{\rho_I d_{RP}^\tau}{|h_{RP}|^2}\right] \\ =& \underbrace{\Pr\left[|\hat{h}_k|^2 < \frac{\xi_j\zeta_k d_k^\tau}{\epsilon\bar{\rho}_R},\ |h_{RP}|^2 < \frac{\rho_I d_{RP}^\tau}{\bar{\rho}_R}\right]}_{\mathcal{D}_1} \\ &+ \underbrace{\Pr\left[|\hat{h}_k|^2 < \frac{|h_{RP}|^2\mathcal{G}_{k,j}+\mathcal{O}_{k,j}}{\epsilon},\ |h_{RP}|^2 > \frac{\rho_I d_{RP}^\tau}{\bar{\rho}_R}\right]}_{\mathcal{D}_2}, \end{aligned} \tag{C.49}$$

where $\bar{\zeta}_k = \frac{\rho_I d_{RP}^\tau \sigma_{\tilde{h}_k}^2}{|h_{RP}|^2 d_k^\tau} + \nu + 1$, $\epsilon = \beta_j - \xi_j\Phi$, $\mathcal{G}_{k,j} = \frac{\xi_j(\nu+1)d_k^\tau}{\rho_I d_{RP}^\tau}$ and $\mathcal{O}_{k,j} = \xi_j\sigma_{\tilde{h}_k}^2$. In the previous sections, channels of NOMA users have been ordered by their distance. However, in this system model, NOMA channels are ordered regarding order statistics [197]. First, let's write the CDFs of unordered NOMA channels $|\bar{h}_k|^2$ in (5.53), which follow an exponential distribution

$$F_{|\bar{h}_k|^2}(\xi_j) = \Pr\left[|\bar{h}_k|^2 < \frac{\xi_j\zeta_k d_k^\tau}{\epsilon\rho_R}\right] = \begin{cases} 1 - e^{-\frac{\xi_j\zeta_k d_k^\tau}{2\epsilon\rho_R}}, & \xi_j < \frac{\beta_j}{\Phi}, \\ 1, & \text{otherwise} \end{cases} \tag{C.50}$$

Then, by analyzing order statistics and using [180, Eq. (19)], the CDF of ordered RV $|\hat{h}_k|^2$ is expressed by

$$F_{|\hat{h}_k|^2}(\xi_j) = \underbrace{\frac{K!}{(K-k)!(k-1)!}\sum_{i=0}^{K-k}\frac{(-1)^i}{k+i}\binom{M-k}{i}}_{L_k(i)}\left[1 - e^{-\frac{\xi_j\zeta_k d_k^\tau}{2\epsilon\rho_R}}\right]^{k+i}. \tag{C.51}$$

Further, due to the independence of RVs $|\hat{h}_k|^2$ and $|h_{RP}|^2$ from each other, the term $\mathcal{D}_1$ in (C.49) can be extended using binomial expansion as

$$\mathcal{D}_1 = L_k(i)\left(1 - e^{-\frac{\xi_j\zeta_k d_k^\tau}{2\epsilon\bar{\rho}_R}}\right)^{k+i}\left(1 - e^{-\frac{\rho_I d_{RP}^\tau}{2\bar{\rho}_R}}\right)$$

$$= L_k(i) \sum_{n=0}^{k+i} (-1)^n \binom{k+i}{n} e^{-\frac{\xi_j \zeta_k d_k^{\tau} n}{2\epsilon \bar{\rho}_R}} \left(1 - e^{-\frac{\rho_I d_{RP}^{\tau}}{2\bar{\rho}_R}}\right). \tag{C.52}$$

Moreover, the term $\mathcal{D}_2$ in (C.49), using binomial expansion, can be further extended as

$$\begin{aligned}
\mathcal{D}_2 &= \int_{\frac{\rho_I d_{RP}^{\tau}}{\bar{\rho}_R}}^{\infty} f_{|h_{RP}|^2}(z) \left[L_k(i) \left(1 - e^{-\frac{z\mathcal{G}_{k,j} + \mathcal{O}_{k,j}}{2\epsilon}}\right)^{k+i} \right] \mathrm{d}z \\
&= L_k(i) \int_{\frac{\rho_I d_{RP}^{\tau}}{\bar{\rho}_R}}^{\infty} \frac{1}{2} e^{-\frac{z}{2}} \left(1 - e^{-\frac{z\mathcal{G}_{k,j} + \mathcal{O}_{k,j}}{2\epsilon}}\right)^{k+i} \mathrm{d}z \\
&= \frac{1}{2} L_k(i) \int_{\frac{\rho_I d_{RP}^{\tau}}{\bar{\rho}_R}}^{\infty} e^{-\frac{z}{2}} \sum_{n=0}^{k+i} (-1)^n \binom{k+i}{n} e^{-\frac{(z\mathcal{G}_{k,j} + \mathcal{O}_{k,j})n}{2\epsilon}} \mathrm{d}z \\
&= \frac{1}{2} L_k(i) \sum_{n=0}^{k+i} (-1)^n \binom{k+i}{n} \int_{\frac{\rho_I d_{RP}^{\tau}}{\bar{\rho}_R}}^{\infty} e^{-\frac{z\left(\epsilon + \mathcal{G}_{k,j} n\right) + \mathcal{O}_{k,j} n}{2\epsilon}} \\
&= L_k(i) \sum_{n=0}^{k+i} (-1)^n \binom{k+i}{n} \frac{\epsilon e^{-\frac{\rho_I d_{RP}^{\tau}\left(\epsilon + \mathcal{G}_{k,j} n\right) + \mathcal{O}_{k,j} \bar{\rho}_R n}{2\epsilon \bar{\rho}_R}}}{\epsilon + \mathcal{G}_{k,j} n}.
\end{aligned} \tag{C.53}$$

Then, after substituting (C.52) and (C.53) into (C.49), and some algebraic manipulations, a closed-form expression for the CDF of $\gamma_{k,j}$ is derived as in (5.60). ■

C.9 Proof of Proposition 13

Considering the source and relay power constraint, (5.74) can be further rewritten as

$$\begin{aligned}
P_{\text{out},1}^{\text{AF}}(\xi_1) &= \Pr\left[\frac{n_s Y n_1 X \alpha_1}{n_s Y n_1 X \alpha_2 + n_1 X \bar{\nu} + n_s Y \bar{\nu} + \bar{\nu}} < \xi_1, \bar{\rho}_S < \frac{\rho_I d_{SP}^{\tau}}{Z}, \bar{\rho}_R < \frac{\rho_I d_{RP}^{\tau}}{Q} \right] \\
&+ \Pr\left[\frac{\frac{n_p}{Z} Y n_1 X \alpha_1}{\frac{n_p}{Z} Y n_1 X \alpha_2 + n_1 X \bar{\nu} + \frac{n_p}{Z} Y \bar{\nu} + \bar{\nu}} < \xi_1, \bar{\rho}_S > \frac{\rho_I d_{SP}^{\tau}}{Z}, \bar{\rho}_R < \frac{\rho_I d_{RP}^{\tau}}{Q} \right] \\
&+ \Pr\left[\frac{n_s Y \frac{m_1}{Q} X \alpha_1}{n_s Y \frac{m_1}{Q} X \alpha_2 + \frac{m_1}{Q} X \bar{\nu} + n_s Y \bar{\nu} + \bar{\nu}} < \xi_1, \bar{\rho}_S < \frac{\rho_I d_{SP}^{\tau}}{Z}, \bar{\rho}_R > \frac{\rho_I d_{RP}^{\tau}}{Q} \right] \\
&+ \Pr\left[\frac{\frac{n_p}{Z} Y \frac{m_1}{Q} X \alpha_1}{\frac{n_p}{Z} Y \frac{m_1}{Q} X \alpha_2 + \frac{m_1}{Q} X \bar{\nu} + \frac{n_p}{Z} Y \bar{\nu} + \bar{\nu}} < \xi_1, \bar{\rho}_S > \frac{\rho_I d_{SP}^{\tau}}{Z}, \bar{\rho}_R > \frac{\rho_I d_{RP}^{\tau}}{Q} \right] \\
&\overset{a}{=} \Pr\left[n_1 X \left(n_s Y \psi - \bar{\xi}_1 \right) < n_s Y \bar{\xi}_1 + \bar{\xi}_1, Z < C_S, Q < C_R \right] \\
&+ \Pr\left[n_1 X \left(\frac{n_p}{Z} Y \psi - \bar{\xi}_1 \right) < \frac{n_p}{Z} Y \bar{\xi}_1 + \bar{\xi}_1, Z > C_S, Q < C_R \right] \\
&+ \Pr\left[\frac{m_1}{Q} X \left(n_s Y \psi - \bar{\xi}_1 \right) < n_s Y \bar{\xi}_1 + \bar{\xi}_1, Z < C_S, Q > C_R \right] \\
&+ \Pr\left[\frac{m_1}{Q} X \left(\frac{n_p}{Z} Y \psi - \bar{\xi}_1 \right) < \frac{n_p}{Z} Y \bar{\xi}_1 + \bar{\xi}_1, Z > C_S, Q > C_R \right]
\end{aligned}$$

$$
\begin{aligned}
&= \underbrace{\Pr\left[Y < u_{s,1}, X < \frac{\Delta_S}{n_1}, Z < C_S, Q < C_R\right]}_{A} \\
&+ \underbrace{\Pr\left[Y < Zu_{p,1}, X < \frac{\Delta_P}{n_1}, Z > C_S, Q < C_R\right]}_{B} \\
&+ \underbrace{\Pr\left[Y < u_{s,1}, X < \frac{Q\Delta_S}{m_1}, Z < C_S, Q > C_R\right]}_{C} \\
&+ \underbrace{\Pr\left[Y < Zu_{p,1}, X < \frac{Q\Delta_P}{m_1}, Z > C_S, Q > C_R\right]}_{D}
\end{aligned} \tag{C.54}
$$

where $u_{v,1} = \frac{\bar{\xi}_1}{n_v \psi}$, with $\forall v \in \{s, p\}$, $\bar{\xi}_1 = \bar{\nu}\xi_1$, $m_1 = \frac{\rho_I d_{RP}^{\tau}}{d_1^{\tau}}$, $Q = |h_{RP}|^2$, $C_L = \frac{\rho_I d_{LP}^{\tau}}{\rho_L}$, $\Delta_S = \frac{Y n_s u_{s,1} + u_{s,1}}{Y - u_{s,1}}$ and $\Delta_P = \frac{Y n_P u_{p,1} + Z u_{p,1}}{Y - Z u_{p,1}}$. Moreover, the step a in (C.54) relies on $\alpha_1 > \alpha_2 \xi_1$, otherwise, $\mathcal{P}_1(\xi_1) = 1$ regardless of the system SNR.

Now, we further extend the term A in (C.54) as

$$
\begin{aligned}
A = &\underbrace{\int_0^{C_S} f_Z(z)\mathrm{d}z \int_0^{C_R} f_Q(q)\mathrm{d}q \int_0^{u_{s,1}} f_Y(y)\mathrm{d}y}_{A_1} \\
&+ \underbrace{\int_0^{C_S} f_Z(z)\mathrm{d}z \int_0^{C_R} f_Q(q)\mathrm{d}q}_{A_2} \underbrace{\int_{u_{s,1}}^{\infty} F_X\left(\Delta_S\right) f_Y(y)\mathrm{d}y}_{A_3},
\end{aligned} \tag{C.55}
$$

Since the PDFs in the terms A_1 and A_2 are independent from each other, they can be rewritten as $A_1 = \left(1 - e^{-C_S}\right)\left(1 - e^{-C_R}\right)\left(1 - e^{-u_{s,1}}\right)$ and $A_2 = \left(1 - e^{-C_S}\right)\left(1 - e^{-C_R}\right)$. Then, the term A_3 can be further extended as

$$
A_3 = \underbrace{\int_{u_{s,1}}^{\infty} e^{-y}\mathrm{d}y}_{A_{31}} - \underbrace{\int_{u_{s,1}}^{\infty} e^{-\frac{y n_s u_{s,1} + u_{s,1}}{n_1 (y - u_{s,1})} - y}\,\mathrm{d}y}_{A_{32}}. \tag{C.56}
$$

The term A_{31} in (C.56) can be further rewritten as

$$
A_{31} = \int_{u_{s,1}}^{\infty} e^{-y}\mathrm{d}y = e^{-u_{s,1}}. \tag{C.57}
$$

Moreover, by substituting $t = y - u_{s,1}$, A_{32} in (C.56) can be rewritten as follows

$$
A_{32} = \int_0^{\infty} e^{-\frac{t n_s u_{s,1} + n_s u_1^2 + u_{s,1}}{n_1 t} - t - u_{s,1}}\mathrm{d}t = e^{-\frac{u_{s,1}(n_1 + n_s)}{n_1}} \int_0^{\infty} e^{-\frac{u_{s,1}(n_s u_{s,1} + 1)}{n_1}\frac{1}{t} - t}\mathrm{d}t. \tag{C.58}
$$

Then, using [121, Eq. (3.324.1)], A_{32} can be further derived as

$$A_{32} = e^{-\frac{u_{s,1}(n_1+n_s)}{n_1}} 2\sqrt{r_1} K_1\left(2\sqrt{r_1}\right), \tag{C.59}$$

where $r_1 = \frac{u_{s,1}(n_s u_{s,1}+1)}{n_1}$ and $K_1(\cdot)$ is the modified Bessel function of the second kind of order 1. Further, after substituting A_1, A_2, A_{31} and A_{32} into (C.55) and some mathematical manipulations, the term A can be written in its closed-form as

$$A = \left(1 - e^{-C_S}\right)\left(1 - e^{-C_R}\right)\left(1 - e^{-\frac{u_{s,1}(n_1+n_s)}{n_1}} 2\sqrt{r_1} K_1\left(2\sqrt{r_1}\right)\right). \tag{C.60}$$

Now, the term B in (C.54) can be further extended as

$$\begin{aligned} B = & \underbrace{\int_0^{C_R} f_Q(q)\mathrm{d}q \int_{C_S}^{\infty} f_Z(z) \int_0^{zu_{p,1}} f_Y(y)\mathrm{d}y\mathrm{d}z}_{B_1} \\ & + \underbrace{\int_0^{C_R} f_Q(q)\mathrm{d}q}_{B_{21}} \underbrace{\int_{C_S}^{\infty} f_Z(z) \int_{zu_{p,1}}^{\infty} f_Y(y) F_X\left(\frac{\Delta_P}{n_1}\right)\mathrm{d}y\mathrm{d}z}_{B_{22}}, \end{aligned} \tag{C.61}$$

where B_1 and B_{21} can be respectively derived as $B_1 = \left(1 - e^{-C_R}\right)\left(e^{-C_S} - \frac{e^{-C_S\left(u_{p,1}+1\right)}}{u_{p,1}+1}\right)$ and $B_{21} = \left(1 - e^{-C_R}\right)$ while B_{22} can be further extended as

$$B_{22} = \int_{C_S}^{\infty} e^{-z} \left[\int_{zu_{p,1}}^{\infty} e^{-y}\mathrm{d}y - \underbrace{\int_{zu_{p,1}}^{\infty} e^{-\frac{\Delta_P}{n_1}-y}\mathrm{d}y}_{\Omega_{B_1}}\right]\mathrm{d}z \tag{C.62}$$

Then, using $p = y - zu_{p,1}$ and [121, Eq. (3.324.1)], Ω_{B_1} can be formulated as

$$\Omega_{B_1} = e^{-\frac{n_p u_{p,1}}{n_1} - zu_{p,1}} 2\sqrt{b_1} K_1\left(2\sqrt{b_1}\right), \tag{C.63}$$

where $b_1 = \frac{zu_{p,1}(n_p u_{p,1}+1)}{n_1}$. Now, we rewrite B_{22} as follows

$$B_{22} = \frac{e^{-C_S(u_{p,1}+1)}}{u_{p,1}+1} - \int_{C_S}^{\infty} e^{-\frac{zn_1\left(u_{p,1}+1\right)+n_p u_{p,1}}{n_1}} 2\sqrt{b_1} K_1\left(2\sqrt{b_1}\right)\mathrm{d}z \tag{C.64}$$

Then, using $r = z - C_S$, B_{22} can be reformulated as

$$B_{22} = \frac{e^{-C_S(u_{p,1}+1)}}{u_{p,1}+1} - e^{-\frac{C_S n_1\left(u_{p,1}+1\right)+n_p u_{p,1}}{n_1}} \underbrace{\int_0^\infty e^{-\frac{r n_1\left(u_{p,1}+1\right)}{n_1}} 2\sqrt{b_2} K_1\left(2\sqrt{b_2}\right) \mathrm{d}r}_{\Omega_{B_2}}, \tag{C.65}$$

where $b_2 = \frac{u_{p,1}(r+C_S)(n_p u_{p,1}+1)}{n_1}$. Then, by applying [196, Eqs. (2.24.1.3) and (8.2.2.15), Ch. 3], Ω_{B_2} can be derived by follows

$$\Omega_{B_2} = \Upsilon_B \sum_{k=0}^{\infty} \frac{(-\Theta_B)^k}{k!} G_{3\,2}^{1\,3}\left(\frac{C_S \Lambda_B}{\Theta_B}\middle|\begin{matrix} 0,\ k-1,\ k \\ 0,\ k \end{matrix}\right), \tag{C.66}$$

where $\Lambda_B = u_{p,1}+1$, $\Upsilon_B = \frac{C_S}{\Theta_B}$, $\Theta_B = \frac{u_{p,1} C_S (n_p u_{p,1}+1)}{n_1}$. Thus, B can be written as

$$B = \left(1 - e^{-C_R}\right)\left(e^{-C_S} - e^{-\frac{C_S n_1\left(u_{p,1}+1\right)+n_p u_{p,1}}{n_1}} \Omega_{B_2}\right). \tag{C.67}$$

The term C in (C.54) can be further reformulated as

$$\begin{aligned} C = & \underbrace{\int_0^{C_S} f_Z(z)\mathrm{d}z \int_{C_R}^\infty f_Q(q)\mathrm{d}q \int_0^{u_{s,1}} f_Y(y)\mathrm{d}y}_{C_1} \\ & + \underbrace{\int_0^{C_S} f_Z(z)\mathrm{d}z}_{C_{21}} \underbrace{\int_{C_R}^\infty f_Q(q) \int_{u_{s,1}}^\infty f_Y(y) F_X\left(\frac{Q\Delta_S}{m_1}\right)\mathrm{d}y\mathrm{d}q}_{C_{22}}, \end{aligned} \tag{C.68}$$

where $C_1 = e^{-C_R}\left(1 - e^{-C_S}\right)\left(1 - e^{-u_{s,1}}\right)$ and $C_{21} = \left(1 - e^{-C_S}\right)$. Then, C_{22} can be further extended as

$$C_{22} = \int_{C_R}^\infty e^{-q} \left[\int_{u_{s,1}}^\infty e^{-y}\mathrm{d}y - \underbrace{\int_{u_{s,1}}^\infty e^{-\frac{q\Delta_S}{m_1}-y}\mathrm{d}y}_{\Omega_{C_1}}\right]\mathrm{d}q \tag{C.69}$$

Further, using $t = y - u_{s,1}$ and [121, Eq. (3.324.1)], Ω_{C_1} can be rewritten as

$$\beta = e^{-\frac{q n_s u_{s,1}}{m_1} - u_{s,1}} 2\sqrt{c_1} K_1\left(2\sqrt{c_1}\right), \tag{C.70}$$

where $c_1 = \frac{qu_{s,1}(n_s u_{s,1}+1)}{m_1}$. Then, we reformulate C_{22} as

$$C_{22} = \frac{e^{-C_R(u_{s,1}+1)}}{u_{s,1}+1} - \int_{C_R}^{\infty} \frac{e^{-\frac{q\left(m_1+n_s u_{s,1}\right)+m_1 u_{s,1}}{m_1}}}{\left(2\sqrt{c_1}K_1\left(2\sqrt{c_1}\right)\right)^{-1}} \mathrm{d}q \tag{C.71}$$

Then, applying $w = q - C_R$, C_{22} can be written as

$$C_{22} = \frac{e^{-C_R(u_{s,1}+1)}}{u_{s,1}+1} - e^{-\frac{C_R\left(m_1+n_s u_{s,1}\right)+m_1 u_{s,1}}{m_1}} \underbrace{\int_0^{\infty} e^{-\frac{w\left(m_1+n_s u_{s,1}\right)}{m_1}} 2\sqrt{c_2}K_1\left(2\sqrt{c_2}\right) \mathrm{d}w}_{\Omega_{C_2}}, \tag{C.72}$$

where $c_2 = \frac{(w+C_R)(n_s u_{s,1}+1)}{m_1}$. Further, Ω_{C_2} can be derived by

$$\Omega_{C_2} = \frac{C_R}{\Upsilon_C} \sum_{k=0}^{\infty} \frac{(-\Upsilon_C)^k}{k!} G_{3\ 2}^{1\ 3}\left(\frac{C_R \Theta_C}{\Upsilon_C} \middle| \begin{matrix} 0,\ k-1,\ k \\ 0,\ k \end{matrix} \right), \tag{C.73}$$

where $\Upsilon_C = \frac{C_R(n_s u_{s,1}+1)}{m_1}$ and $\Theta_C = \frac{m_1+n_s u_{s,1}}{m_1}$. Then, C can be written as

$$C = \left(1 - e^{-C_S}\right)\left(e^{-C_R}\left(1 - e^{-u_{s,1}}\right) + \frac{e^{-C_R(u_{s,1}+1)}}{u_{s,1}+1} - e^{-\frac{C_R\left(m_1+n_s u_{s,1}\right)+m_1 u_{s,1}}{m_1}} \Omega_{C_2} \right). \tag{C.74}$$

Now, the term D in (C.54) can be further extended as

$$\begin{aligned} D = & \underbrace{\int_{C_R}^{\infty} f_Q(q)\mathrm{d}q \int_{C_S}^{\infty} f_Z(z) \int_0^{z u_{p,1}} f_Y(y)\mathrm{d}y\mathrm{d}z}_{D_1} \\ & + \underbrace{\int_{C_R}^{\infty} f_Q(q) \int_{C_S}^{\infty} f_Z(z) \int_{z u_{p,1}}^{\infty} f_Y(y) F_X\left(\Delta_P\right) \mathrm{d}y\mathrm{d}z\mathrm{d}q}_{D_2}. \end{aligned} \tag{C.75}$$

The term D_1 can be derived as

$$D_1 = \int_{C_R}^{\infty} e^{-q}\mathrm{d}q \left(\int_{C_S}^{\infty} e^{-z}\mathrm{d}z - \int_c^{\infty} e^{-z(u_{p,1}+1)}\mathrm{d}z \right) = e^{-C_R}\left(e^{-C_S} - \frac{e^{-C_S(u_{p,1}+1)}}{u_{p,1}+1} \right). \tag{C.76}$$

Further, the term D_2 can be rewritten as

$$D_2 = \int_{C_R}^{\infty} e^{-q} \int_{C_S}^{\infty} e^{-z} \left(\int_{zu_{p,1}}^{\infty} e^{-y} \mathrm{d}y - \underbrace{\int_{zu_{p,1}}^{\infty} e^{-\frac{n_p y u_{p,1} + z u_{p,1}}{n_1 (y - z u_{p,1})} - y} \mathrm{d}y}_{D_{21}} \right) \mathrm{d}z \mathrm{d}q. \tag{C.77}$$

Then, by using substitution $t = y - zu_{p,1}$ and [121, Eq. (3.324.1)], the term D_{21} is derived by

$$D_{21} == e^{-\frac{q n_p u_{p,1}}{m_1} - z u_{p,1}} 2\sqrt{s} K_1\left(2\sqrt{s}\right), \tag{C.78}$$

where $s = \frac{q z u_{p,1}(n_p u_{p,1}+1)}{m_1}$. Now, we rewrite (C.77) using (C.78) as

$$D_2 = \int_{C_R}^{\infty} e^{-q} \left(\int_{C_S}^{\infty} e^{-u_{p,1} z - z} \mathrm{d}z - \underbrace{\int_{C_S}^{\infty} e^{-\frac{z m_1 (u_{p,1}+1) + q n_p u_{p,1}}{m_1}} 2\sqrt{s} K_1(2\sqrt{s}) \mathrm{d}z}_{\Omega_{D_1}} \right) \mathrm{d}q \tag{C.79}$$

Then, by using substituting $w = z - C_S$ in the term Ω_{D_1} and after some algebraic manipulations, D_2 can be reformulated as

$$D_2 = \frac{e^{-C_R - C_S(u_{p,1}+1)}}{u_{p,1}+1} - \underbrace{\int_{C_R}^{\infty} e^{-q} D_{22} \mathrm{d}q}_{\Omega_{D_2}}, \tag{C.80}$$

where $D_{22} = \int_0^{\infty} \frac{e^{-\frac{(w m_1 + C_S m_1)(u_{p,1}+1) + q n_p u_{p,1}}{m_1}}}{\left(2\sqrt{l} K_1\left(2\sqrt{l}\right)\right)^{-1}} \mathrm{d}w$ and $l = \frac{w q u_{p,1}(n_p u_{p,1}+1) + C_S q u_{p,1}(n_p u_{p,1}+1)}{m_1}$. Further, after applying [195, Eqs. (12) and (14)] and [196, Eq. (2.24.1.3)], D_{22} can be derived as

$$\begin{aligned} D_{22} =& \frac{m_1}{u_{p,1}\left(n_p u_{p,1}+1\right)} e^{-c_s(u_{p,1}+1)} q^{-1} e^{-\frac{n_p u_{p,1}}{m_1} q} \\ & \times \sum_{k=0}^{\infty} \frac{(-T)^k}{k!} G_{3\,2}^{1\,3} \left(\frac{(u_{p,1}+1) m_1}{(n_p u_{p,1}+1) u_{p,1}} q^{-1} \middle| \begin{matrix} 0,\ k-1,\ k \\ 0,\ k \end{matrix} \right), \end{aligned} \tag{C.81}$$

where $T = \frac{u_{p,1} c_s (n_p u_{p,1}+1)}{m_1} q$. Then, we write

$$\Omega_{D_2} = \Upsilon_{D_1} \sum_{k=0}^{\infty} \Psi(k) \int_{C_R}^{\infty} q^{k-1} e^{-q \Upsilon_{D_2}} G_{3\,2}^{1\,3} \left(\frac{(u_{p,1}+1) m_1}{(n_p u_{p,1}+1) u_{p,1}} q^{-1} \middle| \begin{matrix} 0,\ k-1,\ k \\ 0,\ k \end{matrix} \right) \mathrm{d}q, \tag{C.82}$$

where $\Upsilon_{D_1} = \frac{m_1 e^{-c_s\left(u_{p,1}+1\right)}}{u_{p,1}(n_p u_{p,1}+1)}$, $\Psi(k) = \frac{(-u_{p,1}c_3(n_p u_{p,1}+1))^k}{(m_1)^k k!}$ and $\Upsilon_{D_2} = \frac{n_p u_{p,1}}{m_1} + 1$. Assuming that $s = q - C_R$, (C.82) can be rewritten as

$$\begin{aligned}\Omega_{D_2} =&\Upsilon_{D_1} e^{-C_R\Upsilon_{D_2}} \sum_{k=0}^{\infty} \Psi(k) \int_0^{\infty} (s+C_R)^{k-1} e^{-s\Upsilon_{D_2}} \\ &\times G_{2\ 3}^{3\ 1}\left(\zeta(s+C_R)\middle|\begin{matrix}1,\ 1-k\\ 1,\ 2-k,\ 1-k\end{matrix}\right)\mathrm{d}s = \Theta_{D_1}\times\Psi(0) \\ &\times \underbrace{\int_0^{\infty}}_{M_1} (s+C_R)^{-1} e^{-s\Upsilon_{D_2}} G_{2\ 3}^{3\ 1}\left(\zeta(s+C_R)\middle|\begin{matrix}1,\ 1\\ 1,\ 2,\ 1\end{matrix}\right)\mathrm{d}s \\ &+ \Theta_{D_1}\sum_{k=1}^{\infty}\Psi(k)\underbrace{\int_0^{\infty}}_{M_2}(s+C_R)^{k-1}e^{-s\Upsilon_{D_2}}\Theta_{D_2}\mathrm{d}s, \end{aligned} \tag{C.83}$$

where $\Theta_{D_2} = G_{2\ 3}^{3\ 1}\left(\zeta(s+C_R)\middle|\begin{matrix}1,\ 1-k\\ 1,\ 2-k,\ 1-k\end{matrix}\right)$, $\Theta_{D_1} = \Upsilon_{D_1}e^{-C_R\Upsilon_{D_2}}$, $\Psi(0) = 1$ and $\zeta = \frac{(n_p u_{p,1}+1)u_{p,1}}{(u_{p,1}+1)m_1}$. Then, we have

$$\begin{aligned}M_1 =&\frac{\pi}{C_R}\int_0^{\infty} G_{2\ 2}^{1\ 1}\left(\underbrace{\left(-\frac{1}{C_R}\right)}_{M}s\middle|\begin{matrix}0,\ \frac{1}{2}\\ 0,\ \frac{1}{2}\end{matrix}\right) \\ &\times G_{0\ 1}^{1\ 0}\left(s\Upsilon_{D_2}\middle|\begin{matrix}-\\ 0\end{matrix}\right) G_{2\ 3}^{3\ 1}\left(\zeta s+\underbrace{\zeta C_R}_{E_1}\middle|\begin{matrix}1,\ 1\\ 1,\ 2,\ 1\end{matrix}\right)\mathrm{d}s, \end{aligned} \tag{C.84}$$

which has a closed-form solution only if $E_1 \to 0$. If it is true, then

$$M_1 = \frac{\pi}{C_R} M G_{2\ 2:0}^{1\ 1:1}{}_{1:2\ 3}^{0:3\ 1}\left(\frac{\Upsilon_{D_2}}{M},\frac{\zeta}{M}\middle|\begin{matrix}0 & -\frac{1}{2}\\ 0 & -\frac{1}{2}\end{matrix}\middle|\begin{matrix}-\\ 0\end{matrix}\middle|\begin{matrix}1\ 1\\ 1\ 2\ 1\end{matrix}\right). \tag{C.85}$$

Furthermore,

$$\begin{aligned}M_2 =&C_R^{k-1}\int_0^{\infty}\sum_{n=0}^{k-1}\binom{k-1}{n}\left(\frac{s}{C_R}\right)^n e^{-s\Upsilon_{D_2}} \\ &\times G_{2\ 3}^{3\ 1}\left(\zeta s+\zeta C_R\middle|\begin{matrix}1,\ 1-k\\ 1,\ 2-k,\ 1-k\end{matrix}\right)\mathrm{d}s \\ =&C_R^{k-1}\sum_{n=0}^{k-1}\binom{k-1}{n}\left(\frac{1}{C_R}\right)^n\int_0^{\infty}s^{n+1-1}e^{-s\Upsilon_{D_2}}\end{aligned}$$

$$\times G_{2\,3}^{3\,1}\left(\zeta s+\zeta C_R\middle|\begin{matrix}1,\ 1-k\\ 1,\ 2-k,\ 1-k\end{matrix}\right)\mathrm{d}s. \tag{C.86}$$

Assuming $a=\zeta s$ and $\mathrm{d}s=\frac{1}{\zeta}\mathrm{d}a$, M_2 can be derived as

$$\begin{aligned}M_2 =&C_R^{k-1}\sum_{n=0}^{k-1}\binom{k-1}{n}\left(\frac{1}{C_R\zeta}\right)^n\int_0^\infty a^{n+1-1}e^{-a\frac{\Upsilon_{D_2}}{\zeta}}\\ &\times G_{2\,3}^{3\,1}\left(a+\zeta C_R\middle|\begin{matrix}1,\ 1-k\\ 1,\ 2-k,\ 1-k\end{matrix}\right)\mathrm{d}s = C_R^{k-1}\sum_{n=0}^{k-1}\\ &\times\binom{k-1}{n}\left(\frac{1}{C_R\zeta}\right)^n\int_0^\infty a^{n+1-1}G_{0\,1}^{1\,0}\left(a\frac{\Upsilon_{D_2}}{\zeta}\middle|\begin{matrix}-\\ 0\end{matrix}\right)\\ &\times G_{2\,3}^{3\,1}\left(a+\zeta C_R\middle|\begin{matrix}1,\ 1-k\\ 1,\ 2-k,\ 1-k\end{matrix}\right)\mathrm{d}s\\ =&C_R^{k-1}\sum_{n=0}^{k-1}\binom{k-1}{n}\left(\frac{1}{C_R\zeta}\right)^n\sum_{m=0}^{\infty}\frac{(-\zeta C_R r)^m}{m!}\\ &\times G_{4\,4}^{2\,4}\left(\frac{\Upsilon_{D_2}}{\zeta}\middle|\begin{matrix}-n,\ m-n-1,\ 2m-n-2,\ 2m-n-1\\ 0,\ m-n-1,\ 2m-n-1,\ m-n\end{matrix}\right).\end{aligned} \tag{C.87}$$

Then, D can be written in its closed form as

$$D=e^{-C_R-C_S}-\Omega_{D_2}. \tag{C.88}$$

Finally, after substituting (C.60), (C.67), (C.74) and (C.88) into (C.54), the exact OP expression for D_1 can be written as in (5.75). ■

Bibliography

[1] "United states frequency allocations." https://www.ntia.doc.gov/files/ntia/publications/2003-allochrt.pdf. U.S. Department of Commerce, National Telecommunications and Information Administration, Office of Spectrum Management, Accessed: 2018-09-23.

[2] F. Zhou, Y. Wu, Y. Liang, Z. Li, Y. Wang, and K. Wong, "State of the art, taxonomy, and open issues on cognitive radio networks with NOMA," *CoRR*, vol. abs/1801.01997, 2018.

[3] Q. Zhao and B. M. Sadler, "A survey of dynamic spectrum access," *IEEE Signal Processing Magazine*, vol. 24, pp. 79–89, May 2007.

[4] S. Haykin, "Cognitive radio: brain-empowered wireless communications," *IEEE Journal on Selected Areas in Communications*, vol. 23, pp. 201–220, February 2005.

[5] A. Goldsmith, S. A. Jafar, I. Maric, and S. Srinivasa, "Breaking spectrum gridlock with cognitive radios: An information theoretic perspective," *Proceedings of the IEEE*, vol. 97, pp. 894–914, May 2009.

[6] F. Boccardi, R. W. Heath, A. Lozano, T. L. Marzetta, and P. Popovski, "Five disruptive technology directions for 5G," *IEEE Communications Magazine*, vol. 52, pp. 74–80, February 2014.

[7] M. H. Islam, C. L. Koh, S. W. Oh, X. Qing, Y. Y. Lai, C. Wang, Y.-C. Liang, B. E. Toh, F. Chin, G. L. Tan, and W. Toh, "Spectrum survey in singapore: Occupancy measurements and analysis," in *I3rd Int. Conf. CROWNCOM*, pp. 1–7, May 2008.

[8] D. Datla, A. M. Wyglinski, and G. J. Minden, "A spectrum surveying framework for dynamic spectrum access networks," *IEEE Trans. Veh. Technol.*, vol. 58, no. 8, pp. 4158–4168, October 2009.

[9] J. Mitola and G. Q. Maguire, "Cognitive radio: making software radios more personal," *IEEE Personal Communications*, vol. 6, pp. 13–18, August 1999.

[10] J. Mitola, "Cognitive radio for flexible mobile multimedia communications," in *Mobile Multimedia Communications, 1999. (MoMuC '99) 1999 IEEE International Workshop on*, pp. 3–10, 1999.

[11] "Report of the spectrum efficiency working group." http://www.fcc.gov/sptf/reports.html. FCC Spectrum Policy Task Force, Accessed: 2018-09-23.

[12] J. M. Peha, "Approaches to spectrum sharing," *IEEE Communications Magazine*, vol. 43, pp. 10–12, February 2005.

[13] T. C. Clancy, "Achievable capacity under the interference temperature model," in *IEEE INFOCOM 2007 - 26th IEEE International Conference on Computer Communications*, pp. 794–802, May 2007.

[14] J. Winters, "On the capacity of radio communication systems with diversity in a rayleigh fading environment," *IEEE Journal on Selected Areas in Communications*, vol. 5, pp. 871–878, June 1987.

[15] E. Telatar, "Capacity of multi-antenna Gaussian channels," *European Transactions on Telecommunications*, vol. 10, p. 585–595, November 1999.

[16] G. Nauryzbayev and E. Alsusa, "Identifying the maximum DoF region in the three-cell compounded MIMO network," in *2016 IEEE Wireless Communications and Networking Conference*, pp. 1–5, April 2016.

[17] G. J. Foschini, "Layered space-time architecture for wireless communication in a fading environment when using multi-element antennas," *Bell Labs Technical Journal*, vol. 1, pp. 41–59, Autumn 1996.

[18] G. G. Raleigh and J. M. Cioffi, "Spatio-temporal coding for wireless communication," *IEEE Transactions on Communications*, vol. 46, pp. 357–366, March 1998.

[19] V. Tarokh, N. Seshadri, and A. R. Calderbank, "Space-time codes for high data rate wireless communication: performance criterion and code construction," *IEEE Transactions on Information Theory*, vol. 44, pp. 744–765, March 1998.

[20] F. Rashid-Farrokhi, L. Tassiulas, and K. J. R. Liu, "Joint optimal power control and beamforming in wireless networks using antenna arrays," *IEEE Transactions on Communications*, vol. 46, pp. 1313–1324, October 1998.

[21] R. Zhang and Y. Liang, "Exploiting multi-antennas for opportunistic spectrum sharing in cognitive radio networks," *IEEE Journal of Selected Topics in Signal Processing*, vol. 2, pp. 88–102, February 2008.

[22] J.Mitola, *Cognitive radio*. PhD thesis, Royal Institute of Technology, Stockholm, Sweden, 1999.

[23] O. E. Ayach, S. W. Peters, and R. W. Heath, "The practical challenges of interference alignment," *IEEE Wireless Communications*, vol. 20, pp. 35–42, February 2013.

[24] D. Tse and P. Viswanath, *Fundamentals of Wireless Communication*. Cambridge, U.K.: Cambridge Univ. Press, 2005.

[25] V. R. Cadambe and S. A. Jafar, "Interference alignment and degrees of freedom of the k-user interference channel," *IEEE Transactions on Information Theory*, vol. 54, pp. 3425–3441, August 2008.

[26] X. Qu and C. G. Kang, "A closed-form solution to implement interference alignment and cancellation for a Gaussian interference multiple access channel," *IEEE Transactions on Wireless Communications*, vol. 13, pp. 710–723, February 2014.

[27] G. Bresler, D. Cartwright, and D. Tse, "Feasibility of interference alignment for the MIMO interference channel," *IEEE Transactions on Information Theory*, vol. 60, pp. 5573–5586, September 2014.

[28] E. G. Larsson, O. Edfors, F. Tufvesson, and T. L. Marzetta, "Massive MIMO for next generation wireless systems," *IEEE Communications Magazine*, vol. 52, pp. 186–195, February 2014.

[29] S. A. Jafar, *Interference Alignment:A New Look at Signal Dimensions in a Communication Network*. Now Foundations and Trends, 2011.

[30] G.Nauryzbayev, *Advanced Interference Alignment Techniques For Cellular Communication Networks*. PhD thesis, School of Electrical and Electronic Engineering, The University of Manchester, Manchester, UK, 2016.

[31] G. Nauryzbayev, S. Arzykulov, E. Alsusa, and T. A. Tsiftsis, "An alignment-based interference cancellation scheme for network-MIMO systems," in *2016 10th International Conference on Signal Processing and Communication Systems (ICSPCS)*, pp. 1–5, December 2016.

[32] G. Nauryzbayev, S. Arzykulov, E. Alsusa, and T. A. Tsiftsis, "A closed-form solution to implement interference alignment and cancellation scheme for the MIMO three-user X-channel model," in *2016 10th International Conference on Signal Processing and Communication Systems (ICSPCS)*, pp. 1–6, December 2016.

[33] C. M. Yetis, T. Gou, S. A. Jafar, and A. H. Kayran, "On feasibility of interference alignment in MIMO interference networks," *IEEE Transactions on Signal Processing*, vol. 58, pp. 4771–4782, September 2010.

[34] W. Shin, N. Lee, J. Lim, C. Shin, and K. Jang, "On the design of interference alignment scheme for two-cell MIMO interfering broadcast channels," *IEEE Transactions on Wireless Communications*, vol. 10, pp. 437–442, February 2011.

[35] C. Suh, M. Ho, and D. N. C. Tse, "Downlink interference alignment," *IEEE Transactions on Communications*, vol. 59, pp. 2616–2626, September 2011.

[36] V. R. Cadambe and S. A. Jafar, "Degrees of freedom of wireless networks with relays, feedback, cooperation, and full duplex operation," *IEEE Transactions on Information Theory*, vol. 55, pp. 2334–2344, May 2009.

[37] S. A. Jafar, "Blind interference alignment," *IEEE Journal of Selected Topics in Signal Processing*, vol. 6, pp. 216–227, June 2012.

[38] Y. Birk and T. Kol, "Informed-source coding-on-demand (ISCOD) over broadcast channels," in *Proceedings. IEEE INFOCOM '98, the Conference on Computer Communications. Seventeenth Annual Joint Conference of the IEEE Computer and Communications Societies. Gateway to the 21st Century (Cat. No.98*, vol. 3, pp. 1257–1264 vol.3, March 1998.

[39] H. Weingarten, "On the compound MIMO broadcast channel," in *in Proceedings of Annual Information Theory and Applications Workshop UCSD*, 2007.

[40] S. A. Jafar, "Interference alignment-a new look at signal dimemsions in a communication network," *Found. Trends Commun. Inf. Theory*, vol. 7, no. 1, p. 1–130, 2010.

[41] N. Zhao, F. R. Yu, and V. C. M. Leung, "Opportunistic communications in interference alignment networks with wireless power transfer," *IEEE Wireless Communications*, vol. 22, pp. 88–95, February 2015.

[42] H. Yu, "A review on interference alignment in multiuser interference channels," *Wireless Pers. Commun.*, vol. 83, p. 1751–1764, August 2015.

[43] N. Zhao, F. R. Yu, M. Jin, Q. Yan, and V. C. M. Leung, "Interference alignment and its applications: A survey, research issues, and challenges," *IEEE Communications Surveys Tutorials*, vol. 18, pp. 1779–1803, thirdquarter 2016.

[44] H. J. Visser and R. J. M. Vullers, "RF energy harvesting and transport for wireless sensor network applications: Principles and requirements," *Proceedings of the IEEE*, vol. 101, pp. 1410–1423, June 2013.

[45] X. Lu, P. Wang, D. Niyato, D. I. Kim, and Z. Han, "Wireless networks with RF energy harvesting: A contemporary survey," *IEEE Communications Surveys Tutorials*, vol. 17, pp. 757–789, Secondquarter 2015.

[46] K. Huang and X. Zhou, "Cutting the last wires for mobile communications by microwave power transfer," *IEEE Communications Magazine*, vol. 53, pp. 86–93, June 2015.

[47] Z. Popovic, "Cut the cord: Low-power far-field wireless powering," *IEEE Microwave Magazine*, vol. 14, pp. 55–62, March 2013.

[48] I. Krikidis, S. Timotheou, S. Nikolaou, G. Zheng, D. W. K. Ng, and R. Schober, "Simultaneous wireless information and power transfer in modern communication systems," *IEEE Communications Magazine*, vol. 52, pp. 104–110, November 2014.

[49] M. Agiwal, A. Roy, and N. Saxena, "Next generation 5G wireless networks: A comprehensive survey," *IEEE Communications Surveys Tutorials*, vol. 18, pp. 1617–1655, thirdquarter 2016.

[50] Z. Ding, C. Zhong, D. W. K. Ng, M. Peng, H. A. Suraweera, R. Schober, and H. V. Poor, "Application of smart antenna technologies in simultaneous wireless information and power transfer," *IEEE Communications Magazine*, vol. 53, pp. 86–93, April 2015.

[51] X. Chen, D. W. K. Ng, and H. H. Chen, "Secrecy wireless information and power transfer: challenges and opportunities," *IEEE Wireless Communications*, vol. 23, pp. 54–61, April 2016.

[52] S. Ulukus, A. Yener, E. Erkip, O. Simeone, M. Zorzi, P. Grover, and K. Huang, "Energy harvesting wireless communications: A review of recent advances," *IEEE Journal on Selected Areas in Communications*, vol. 33, pp. 360–381, March 2015.

[53] M. Amjad, F. Akhtar, M. H. Rehmani, M. Reisslein, and T. Umer, "Full-duplex communication in cognitive radio networks: A survey," *IEEE Communications Surveys Tutorials*, vol. 19, pp. 2158–2191, Fourthquarter 2017.

[54] X. Lu, P. Wang, D. Niyato, D. I. Kim, and Z. Han, "Wireless charging technologies: Fundamentals, standards, and network applications," *IEEE Communications Surveys Tutorials*, vol. 18, pp. 1413–1452, Secondquarter 2016.

[55] N. Zhao, S. Zhang, F. R. Yu, Y. Chen, A. Nallanathan, and V. C. M. Leung, "Exploiting interference for energy harvesting: A survey, research issues, and challenges," *IEEE Access*, vol. 5, pp. 10403–10421, 2017.

[56] O. Ozel, K. Tutuncuoglu, S. Ulukus, and A. Yener, "Fundamental limits of energy harvesting communications," *IEEE Communications Magazine*, vol. 53, pp. 126–132, April 2015.

[57] M. L. Ku, W. Li, Y. Chen, and K. J. R. Liu, "Advances in energy harvesting communications: Past, present, and future challenges," *IEEE Communications Surveys Tutorials*, vol. 18, pp. 1384–1412, Secondquarter 2016.

[58] F. Akhtar and M. H. Rehmani, "Energy harvesting for self-sustainable wireless body area networks," *IT Professional*, vol. 19, pp. 32–40, March 2017.

[59] Z. Ding, X. Lei, G. K. Karagiannidis, R. Schober, J. Yuan, and V. K. Bhargava, "A survey on non-orthogonal multiple access for 5G networks: Research challenges and future trends," *IEEE Journal on Selected Areas in Communications*, vol. 35, pp. 2181–2195, October 2017.

[60] S. M. R. Islam, M. Zeng, O. A. Dobre, and K. Kwak, "Resource allocation for downlink NOMA systems: Key techniques and open issues," *IEEE Wireless Communications*, vol. 25, pp. 40–47, April 2018.

[61] Z. Ding, M. Peng, and H. V. Poor, "Cooperative non-orthogonal multiple access in 5G systems," *IEEE Communications Letters*, vol. 19, pp. 1462–1465, August 2015.

[62] M. Moltafet, N. Mokari, M. R. Javan, H. Saeedi, and H. Pishro-Nik, "A new multiple access technique for 5G: Power domain sparse code multiple access (PSMA)," *IEEE Access*, vol. 6, pp. 747–759, 2018.

[63] D. Zhai, "Adaptive codebook design and assignment for energy saving in SCMA networks," *IEEE Access*, vol. 5, pp. 23550–23562, 2017.

[64] M. AL-Imari, M. A. Imran, R. Tafazolli, and D. Chen, "Performance evaluation of low density spreading multiple access," in *2012 8th International Wireless Communications and Mobile Computing Conference (IWCMC)*, pp. 383–388, August 2012.

[65] J. Zeng, D. Kong, X. Su, L. Rong, and X. Xu, "On the performance of pattern division multiple access in 5G systems," in *2016 8th International Conference on Wireless Communications Signal Processing (WCSP)*, pp. 1–5, October 2016.

[66] X. Dai, S. Chen, S. Sun, S. Kang, Y. Wang, Z. Shen, and J. Xu, "Successive interference cancelation amenable multiple access (SAMA) for future wireless communications," in *2014 IEEE International Conference on Communication Systems*, pp. 222–226, November 2014.

[67] D. Fang, Y. Huang, Z. Ding, G. Geraci, S. Shieh, and H. Claussen, "Lattice partition multiple access: A new method of downlink non-orthogonal multiuser transmissions," in *2016 IEEE Global Communications Conference (GLOBECOM)*, pp. 1–6, December 2016.

[68] Z. Yang, Z. Ding, P. Fan, and G. K. Karagiannidis, "On the performance of non-orthogonal multiple access systems with partial channel information," *IEEE Transactions on Communications*, vol. 64, pp. 654–667, February 2016.

[69] Z. Ding, Z. Yang, P. Fan, and H. V. Poor, "On the performance of non-orthogonal multiple access in 5G systems with randomly deployed users," *IEEE Signal Processing Letters*, vol. 21, pp. 1501–1505, December 2014.

[70] G. Nauryzbayev, M. Abdallah, and H. Elgala, "On the performance of noma-enabled spectrally and energy efficient OFDM (SEE-OFDM) for indoor visible light communications," in *2018 IEEE 87th Vehicular Technology Conference (VTC Spring)*, pp. 1–5, June 2018.

[71] Y. Saito, A. Benjebbour, Y. Kishiyama, and T. Nakamura, "System-level performance evaluation of downlink non-orthogonal multiple access (NOMA)," in *2013 IEEE 24th Annual International Symposium on Personal, Indoor, and Mobile Radio Communications (PIMRC)*, pp. 611–615, September 2013.

[72] Z. Ding, P. Fan, and H. V. Poor, "Impact of user pairing on 5G nonorthogonal multiple-access downlink transmissions," *IEEE Transactions on Vehicular Technology*, vol. 65, pp. 6010–6023, August 2016.

[73] "5G radio access: Requirements, concepts and technologies," *NTT DOCOMO, Inc.,Tokyo, Japan, 5G Whitepaper*, July 2014.

[74] "5G, a techology vision," *Shengzheng, China, 5G Whitepaper*, March 2015.

[75] S. Verdu, *Multiuser Detection*. Cambridge Press, 1998.

[76] X. Wang and H. V. Poor, *Wireless Communication Systems: Advanced Techniques for Signal Reception*. Prentice Hall, New York, US, 2004.

[77] T. S. Rappaport, *Wireless Communications: Principles and Practice*. Prentice Hall, New York, US, 1998.

[78] "Study on downlink multiuser superposition transmission for LTE, TSG RAN meeting 67," *3rd Generation Partnership Project(3GPP)*, vol. Tech. Rep. RP-150496, March 2015.

[79] S. Timotheou and I. Krikidis, "Fairness for non-orthogonal multiple access in 5G systems," *IEEE Signal Processing Letters*, vol. 22, pp. 1647–1651, October 2015.

[80] Z. Ding and H. V. Poor, "Cooperative energy harvesting networks with spatially random users," *IEEE Signal Processing Letters*, vol. 20, pp. 1211–1214, December 2013.

[81] Y. Zhang, Q. Yang, T. Zheng, H. Wang, Y. Ju, and Y. Meng, "Energy efficiency optimization in cognitive radio inspired non-orthogonal multiple access," in *2016 IEEE 27th Annual International Symposium on Personal, Indoor, and Mobile Radio Communications (PIMRC)*, pp. 1–6, September 2016.

[82] S. Arzykulov, G. Nauryzbayev, T. A. Tsiftsis, and M. Abdallah, "Outage performance of underlay CR-NOMA networks," in *2018 10th International Conference on Wireless Communications and Signal Processing (WCSP)*, pp. 1–6, October 2018.

[83] S. Arzykulov, T. A. Tsiftsis, G. Nauryzbayev, M. Abdallah, and G. Yang, "Outage performance of underlay CR-NOMA networks with detect-and-forward relaying," in *2018 IEEE Global Communications Conference (GLOBECOM)*, pp. 1–6, December 2018.

[84] L. Lv, J. Chen, and Q. Ni, "Cooperative non-orthogonal multiple access in cognitive radio," *IEEE Communications Letters*, vol. 20, pp. 2059–2062, October 2016.

[85] Y. Liu, Z. Ding, M. Elkashlan, and J. Yuan, "Nonorthogonal multiple access in large-scale underlay cognitive radio networks," *IEEE Transactions on Vehicular Technology*, vol. 65, pp. 10152–10157, December 2016.

[86] L. Lv, Q. Ni, Z. Ding, and J. Chen, "Application of non-orthogonal multiple access in cooperative spectrum-sharing networks over Nakagami- m fading channels," *IEEE Transactions on Vehicular Technology*, vol. 66, pp. 5506–5511, June 2017.

[87] L. Lv, J. Chen, Q. Ni, and Z. Ding, "Design of cooperative non-orthogonal multicast cognitive multiple access for 5G systems: User scheduling and performance analysis," *IEEE Transactions on Communications*, vol. 65, pp. 2641–2656, June 2017.

[88] Y. Chen, L. Wang, and B. Jiao, "Cooperative multicast non-orthogonal multiple access in cognitive radio," in *2017 IEEE International Conference on Communications (ICC)*, pp. 1–6, May 2017.

[89] G. Nauryzbayev and S. Seilov, "Impact of antenna correlation and imperfect CSI on interference alignment in compound MIMO BC," in *2016 International Conference on Information and Communication Technology Convergence (ICTC)*, pp. 544–548, October 2016.

[90] G. Nauryzbayev and S. Kaliyeva, "A non-iterative solution to implement interference alignment and cancellation scheme for the three-user MIMO X-channel model," in *2016 International Conference on Information and Communication Technology Convergence (ICTC)*, pp. 538–543, October 2016.

[91] G. Nauryzbayev and S. Kaliyeva, "Interference alignment cancellation scheme for network-MIMO systems," in *2016 International Conference on Information and Communication Technology Convergence (ICTC)*, pp. 237–240, October 2016.

[92] M. Yuksel and E. Erkip, "Multiple-antenna cooperative wireless systems: A diversity-multiplexing tradeoff perspective," *IEEE Transactions on Information Theory*, vol. 53, pp. 3371–3393, October 2007.

[93] Kwang-Chen and R. Prasad, *Cooperative Communications and Networks*. Wiley Telecom, 2009.

[94] J. N. Laneman, D. N. C. Tse, and G. W. Wornell, "Cooperative diversity in wireless networks: Efficient protocols and outage behavior," *IEEE Transactions on Information Theory*, vol. 50, pp. 3062–3080, December 2004.

[95] J. N. Laneman and G. W. Wornell, "Distributed space-time-coded protocols for exploiting cooperative diversity in wireless networks," *IEEE Transactions on Information Theory*, vol. 49, pp. 2415–2425, October 2003.

[96] A. Scaglione and Y.-W. Hong, "Opportunistic large arrays: cooperative transmission in wireless multihop ad hoc networks to reach far distances," *IEEE Transactions on Signal Processing*, vol. 51, pp. 2082–2092, August 2003.

[97] J. Al-khori, G. Nauryzbayev, M. Abdallah, and M. Hamdi, "Secrecy capacity of hybrid RF/VLC DF relaying networks with jamming," in *2019 International Conference on Computing, Networking and Communications (ICNC)*, pp. 67–72, Feb 2019.

[98] J. Al-Khori, G. Nauryzbayev, M. M. Abdallah, and M. Hamdi, "Secrecy performance of decode-and-forward based hybrid RF/VLC relaying systems," *IEEE Access*, vol. 7, pp. 10844–10856, 2019.

[99] J. Al-khori, G. Nauryzbayev, M. Abdallah, and M. Hamdi, "Physical layer security for hybrid RF/VLC DF relaying systems," in *2018 IEEE 88th Vehicular Technology Conference (VTC-Fall)*, pp. 1–6, August 2018.

[100] J. Al-Khori, G. Nauryzbayev, M. M. Abdallah, and M. Hamdi, "Joint beamforming design and power minimization for friendly jamming relaying hybrid RF/VLC systems," *IEEE Photonics Journal*, vol. 11, pp. 1–18, April 2019.

[101] J. N. Laneman, D. N. C. Tse, and G. W. Wornell, "Cooperative diversity in wireless networks: Efficient protocols and outage behavior," *IEEE Transactions on Information Theory*, vol. 50, pp. 3062–3080, December 2004.

[102] L. Dong, Z. Han, A. P. Petropulu, and H. V. Poor, "Improving wireless physical layer security via cooperating relays," *IEEE Transactions on Signal Processing*, vol. 58, pp. 1875–1888, March 2010.

[103] T. Wang, A. Cano, G. B. Giannakis, and J. N. Laneman, "High-performance cooperative demodulation with decode-and-forward relays," *IEEE Transactions on Communications*, vol. 55, pp. 1427–1438, July 2007.

[104] M. Janani, A. Hedayat, T. E. Hunter, and A. Nosratinia, "Coded cooperation in wireless communications: space-time transmission and iterative decoding," *IEEE Transactions on Signal Processing*, vol. 52, pp. 362–371, February 2004.

[105] G. Kramer, M. Gastpar, and P. Gupta, "Cooperative strategies and capacity theorems for relay networks," *IEEE Transactions on Information Theory*, vol. 51, pp. 3037–3063, September 2005.

[106] J. Si, Z. Li, X. Chen, B. Hao, and Z. Liu, "On the performance of cognitive relay networks under primary user's outage constraint," *IEEE Communications Letters*, vol. 15, pp. 422–424, April 2011.

[107] H. A. Suraweera, P. J. Smith, and N. A. Surobhi, "Exact outage probability of cooperative diversity with opportunistic spectrum access," in *ICC Workshops - 2008 IEEE International Conference on Communications Workshops*, pp. 79–84, May 2008.

[108] S. Kim, W. Choi, Y. Choi, J. Lee, Y. Han, and I. Lee, "Downlink performance analysis of cognitive radio based cellular relay networks," in *2008 3rd International*

Conference on Cognitive Radio Oriented Wireless Networks and Communications (CrownCom 2008), pp. 1–6, May 2008.

[109] J. Lee, H. Wang, J. G. Andrews, and D. Hong, "Outage probability of cognitive relay networks with interference constraints," *IEEE Transactions on Wireless Communications*, vol. 10, pp. 390–395, February 2011.

[110] C. Zhong, T. Ratnarajah, and K. K. Wong, "Outage analysis of decode-and-forward cognitive dual-hop systems with the interference constraint in Nakagami-m fading channels," *IEEE Transactions on Vehicular Technology*, vol. 60, pp. 2875–2879, July 2011.

[111] P. Bithas, G. Efthymogloi, and D. Kalivas, "Outage probability of cognitive relay networks over generalized fading channels with interference constraints," in *MoWNet'2014*, vol. 40, pp. 84–91, 2014.

[112] M. D. Yacoub, "The α- μ distribution: A physical fading model for the stacy distribution," *IEEE Transactions on Vehicular Technology*, vol. 56, pp. 27–34, January 2007.

[113] A. M. Magableh and M. M. Matalgah, "Moment generating function of the generalized α- μ distribution with applications," *IEEE Communications Letters*, vol. 13, pp. 411–413, June 2009.

[114] A. Papoulis and S. Pillai, *Probability, Random Variables and Stochastic Processes*. Fourth Edition, 2001.

[115] G. Nauryzbayev, K. M. Rabie, M. Abdallah, and B. Adebisi, "Ergodic capacity analysis of wireless powered AF relaying systems over $\alpha - \mu$ fading channels," in *GLOBECOM 2017 - 2017 IEEE Global Communications Conference*, pp. 1–6, December 2017.

[116] N. Zhao, F. R. Yu, H. Sun, and M. Li, "Adaptive power allocation schemes for spectrum sharing in interference-alignment-based cognitive radio networks," *IEEE Transactions on Vehicular Technology*, vol. 65, pp. 3700–3714, May 2016.

[117] G. Nauryzbayev, K. M. Rabie, M. Abdallah, and B. Adebisi, "On the performance analysis of WPT-based dual-hop AF relaying networks in $\alpha - \mu$ fading," *IEEE Access*, vol. 6, pp. 37138–37149, 2018.

[118] G. Nauryzbayev, M. Abdallah, and K. M. Rabie, "Outage probability of the EH-based full-duplex AF and DF relaying systems in $\alpha - \mu$ environment," in *2018 IEEE 88th Vehicular Technology Conference (VTC-Fall)*, pp. 1–6, August 2018.

[119] K. Dautov, S. Arzykulov, G. Nauryzbayev, and R. C. Kizilirmak, "On the performance of UAV-enabled multihop V2V FSO systems over generalized α - μ channels," in *2018 International Conference on Computing and Network Communications (CoCoNet)*, pp. 69–73, August 2018.

[120] O. S. Badarneh and F. S. Almehmadi, "Performance of multihop wireless networks in $alpha$-mu fading channels perturbed by an additive generalized Gaussian noise," *IEEE Communications Letters*, vol. 20, pp. 986–989, May 2016.

[121] I. S. Gradshteyn and I. M. Ryzhik, *Table of Integrals, Series, and Products*. A. Jeffrey, Ed. San Diego: Academic Press, 2000.

[122] M. K. Simon and M. Alouini, "A unified approach to the performance analysis of digital communication over generalized fading channels," *Proceedings of the IEEE*, vol. 86, pp. 1860–1877, September 1998.

[123] G. Nauryzbayev and E. Alsusa, "Enhanced multiplexing gain using interference alignment cancellation in multi-cell MIMO networks," *IEEE Transactions on Information Theory*, vol. 62, no. 1, pp. 357–369, January 2016.

[124] G. Nauryzbayev and E. Alsusa, "Interference alignment cancellation in compounded MIMO broadcast channels with general message sets," *IEEE Transactions on Communications*, vol. 63, pp. 3702–3712, October 2015.

[125] G. Nauryzbayev, E. Alsusa, and M. Abdallah, "On the feasibility of interference alignment in compounded MIMO broadcast channels with antenna correlation and mixed user classes," *IEEE Transactions on Vehicular Technology*, vol. 67, pp. 2130–2140, March 2018.

[126] G. Nauryzbayev, E. Alsusa, and J. Tang, "An alignment based interference cancellation scheme for multi-cell MIMO networks," in *2015 IEEE 81st Vehicular Technology Conference (VTC Spring)*, pp. 1–5, May 2015.

[127] A. A. Nasir, X. Zhou, S. Durrani, and R. A. Kennedy, "Relaying protocols for wireless energy harvesting and information processing," *IEEE Transactions on Wireless Communications*, vol. 12, pp. 3622–3636, July 2013.

[128] Y. Yi, J. Zhang, Q. Zhang, and T. Jiang, "Exploring frequency diversity with interference alignment in cognitive radio networks," in *2012 IEEE Global Communications Conference (GLOBECOM)*, pp. 5579–5583, December 2012.

[129] J. Tang, S. Lambotharan, and S. Pomeroy, "Interference cancellation and alignment techniques for multiple-input and multiple-output cognitive relay networks," *IET Signal Processing*, vol. 7, pp. 188–200, May 2013.

[130] T. Xu, L. Ma, and G. Sternberg, "Practical interference alignment and cancellation for MIMO underlay cognitive radio networks with multiple secondary users," in *2013 IEEE Global Communications Conference (GLOBECOM)*, pp. 1009–1014, December 2013.

[131] K. Rabie, B. Adebisi, G. Nauryzbayev, O. S. Badarneh, X. Li, and M. Alouini, "Full-duplex energy-harvesting enabled relay networks in generalized fading channels," *IEEE Wireless Communications Letters*, vol. 8, pp. 384–387, April 2019.

[132] X. Chen, Z. Zhang, H. Chen, and H. Zhang, "Enhancing wireless information and power transfer by exploiting multi-antenna techniques," *IEEE Communications Magazine*, vol. 53, pp. 133–141, April 2015.

[133] I. Krikidis, "Relay selection in wireless powered cooperative networks with energy storage," *IEEE Journal on Selected Areas in Communications*, vol. 33, pp. 2596–2610, December 2015.

[134] N. Zhao, F. R. Yu, and V. C. M. Leung, "Simultaneous wireless information and power transfer in interference alignment networks," in *2014 International Wireless Communications and Mobile Computing Conference (IWCMC)*, pp. 7–11, August 2014.

[135] C. Zhong, H. A. Suraweera, G. Zheng, I. Krikidis, and Z. Zhang, "Wireless information and power transfer with full duplex relaying," *IEEE Transactions on Communications*, vol. 62, pp. 3447–3461, October 2014.

[136] S. Park, H. Kim, and D. Hong, "Cognitive radio networks with energy harvesting," *IEEE Transactions on Wireless Communications*, vol. 12, pp. 1386–1397, March 2013.

[137] G. Zheng, Z. Ho, E. A. Jorswieck, and B. Ottersten, "Information and energy cooperation in cognitive radio networks," *IEEE Transactions on Signal Processing*, vol. 62, pp. 2290–2303, May 2014.

[138] K. M. Rabie, A. Salem, E. Alsusa, and M. Alouini, "Energy-harvesting in cooperative AF relaying networks over log-normal fading channels," in *2016 IEEE International Conference on Communications (ICC)*, pp. 1–7, May 2016.

[139] S. Arzykulov, G. Nauryzbayev, T. A. Tsiftsis, and M. Abdallah, "Error performance of wireless powered cognitive relay networks with interference alignment," in *2017 IEEE 28th Annual International Symposium on Personal, Indoor, and Mobile Radio Communications (PIMRC)*, pp. 1–5, October 2017.

[140] S. Arzykulov, G. Nauryzbayev, T. A. Tsiftsis, and M. Abdallah, "On the performance of wireless powered cognitive relay network with interference alignment," *IEEE Transactions on Communications*, vol. 66, pp. 3825–3836, September 2018.

[141] S. Arzykulov, G. Nauryzbayev, T. A. Tsiftsis, and M. Abdallah, "On the capacity of wireless powered cognitive relay network with interference alignment," in *GLOBECOM 2017 - 2017 IEEE Global Communications Conference*, pp. 1–6, December 2017.

[142] M. Amir, A. El-Keyi, and M. Nafie, "Constrained interference alignment and the spatial degrees of freedom of MIMO cognitive networks," *IEEE Transactions on Information Theory*, vol. 57, pp. 2994–3004, May 2011.

[143] F. Wang and X. Zhang, "Resource allocation for multiuser cooperative overlay cognitive radio networks with RF energy harvesting capability," in *2016 IEEE Global Communications Conference (GLOBECOM)*, pp. 1–6, December 2016.

[144] F. Wang and X. Zhang, "Joint resource allocation and admission control for energy harvesting based cooperative overlay cognitive radio networks," in *2016 IEEE Conference on Computer Communications Workshops (INFOCOM WKSHPS)*, pp. 796–801, April 2016.

[145] B. Xie, Y. Li, H. Minn, and A. Nosratinia, "Adaptive interference alignment with CSI uncertainty," *IEEE Transactions on Communications*, vol. 61, pp. 792–801, February 2013.

[146] N. Zhao, F. R. Yu, H. Sun, A. Nallanathan, and H. Yin, "A novel interference alignment scheme based on sequential antenna switching in wireless networks," *IEEE Transactions on Wireless Communications*, vol. 12, pp. 5008–5021, October 2013.

[147] X. Rao and V. K. N. Lau, "Minimization of CSI feedback dimension for interference alignment in MIMO interference multicast networks," *IEEE Transactions on Information Theory*, vol. 61, pp. 1218–1246, March 2015.

[148] K. Gomadam, V. R. Cadambe, and S. A. Jafar, "A distributed numerical approach to interference alignment and applications to wireless interference networks," *IEEE Transactions on Information Theory*, vol. 57, pp. 3309–3322, June 2011.

[149] O. E. Ayach, S. W. Peters, and R. W. Heath, "The feasibility of interference alignment over measured MIMO-OFDM channels," *IEEE Transactions on Vehicular Technology*, vol. 59, pp. 4309–4321, November 2010.

[150] M. El-Absi, S. Galih, M. Hoffmann, M. El-Hadidy, and T. Kaiser, "Antenna selection for reliable MIMO-OFDM interference alignment systems: Measurement-based evaluation," *IEEE Transactions on Vehicular Technology*, vol. 65, pp. 2965–2977, May 2016.

[151] S. Kim, R. Vyas, J. Bito, K. Niotaki, A. Collado, A. Georgiadis, and M. M. Tentzeris, "Ambient RF energy-harvesting technologies for self-sustainable standalone wireless sensor platforms," *Proceedings of the IEEE*, vol. 102, pp. 1649–1666, November 2014.

[152] *CROSS: Cognitive Radio Open Source System*. Available: http://cornet.wireless.vt.edu/trac/wiki/Cross.

[153] L. Yang, Z. Zhang, W. Hou, B. Y. Zhao, and H. Zheng, "Papyrus: a software platform for distributed dynamic spectrum sharing using SDRs," *ACM SIGCOMM Comput. Commun.*, vol. 41, p. 31–37, January 20141.

[154] R. Vannithamby and S. Talwar, *Towards 5G Applications, Requirements and Candidate Technologies*. Intel Corporation, USA, 2017.

[155] X. Yongjun and Z. Xiaohui, "Optimal power allocation for multiuser underlay cognitive radio networks under QoS and interference temperature constraints," *China Communications*, vol. 10, pp. 91–100, October 2013.

[156] K. Furutsu and T. Ishida, "On the theory of amplitude distribution of impulsive random noise," *IEEE Transactions on Wireless Communications*, vol. 32, no. 7, 1961.

[157] S. K. Jayaweera, *Signal Processing for Cognitive Radios*. Hoboken, NJ, USA: Wiley, 2014.

[158] N. I. Miridakis, T. A. Tsiftsis, G. C. Alexandropoulos, and M. Debbah, "Simultaneous spectrum sensing and data reception for cognitive spatial multiplexing distributed systems," *IEEE Transactions on Wireless Communications*, vol. 16, pp. 3313–3327, May 2017.

[159] S. Kay, *Fundamentals of statistical signal processing: Estimation theory*. Englewood Cliffs NJ: Prentice-Hall, 1993.

[160] J. Tang and S. Lambotharan, "Interference alignment techniques for MIMO multi-cell interfering broadcast channels," *IEEE Transactions on Communications*, vol. 61, pp. 164–175, January 2013.

[161] S. Arzykulov, G. Nauryzbayev, and T. A. Tsiftsis, "Underlay cognitive relaying system over $\alpha - \mu$ fading channels," *IEEE Communications Letters*, vol. 21, pp. 216–219, January 2017.

[162] C. Wang, E. K. S. Au, R. D. Murch, and V. K. N. Lau, "Closed-form outage probability and BER of MIMO zero-forcing receiver in the presence of imperfect CSI," in *2006 IEEE 7th Workshop on Signal Processing Advances in Wireless Communications*, pp. 1–5, July 2006.

[163] X. Liang, Y. Wu, D. W. K. Ng, Y. Zuo, S. Jin, and H. Zhu, "Outage performance for cooperative NOMA transmission with an AF relay," *IEEE Communications Letters*, vol. 21, pp. 2428–2431, November 2017.

[164] C. Y. Ho and C. Y. Leow, "Cooperative non-orthogonal multiple access using two-way relay," in *2017 IEEE International Conference on Signal and Image Processing Applications (ICSIPA)*, pp. 459–463, September 2017.

[165] X. Chen, G. Liu, Z. Ding, F. R. Yu, and P. Fan, "Power allocation for full-duplex cooperative non-orthogonal multiple access systems," in *GLOBECOM 2017 - 2017 IEEE Global Communications Conference*, pp. 1–6, December 2017.

[166] Z. Wei, D. W. K. Ng, and J. Yuan, "Power-efficient resource allocation for MC-NOMA with statistical channel state information," in *2016 IEEE Global Communications Conference (GLOBECOM)*, pp. 1–7, December 2016.

[167] G. Nauryzbayev, S. Arzykulov, T. A. Tsiftsis, and M. Abdallah, "Performance of cooperative underlay cr-noma networks over Nakagami-m channels," in *2018 IEEE International Conference on Communications Workshops (ICC Workshops)*, pp. 1–6, May 2018.

[168] G. I. Tsiropoulos, O. A. Dobre, M. H. Ahmed, and K. E. Baddour, "Radio resource allocation techniques for efficient spectrum access in cognitive radio networks," *IEEE Communications Surveys Tutorials*, vol. 18, pp. 824–847, Firstquarter 2016.

[169] L. Lv, J. Chen, Q. Ni, Z. Ding, and H. Jiang, "Cognitive non-orthogonal multiple access with cooperative relaying: A new wireless frontier for 5G spectrum sharing," *IEEE Communications Magazine*, vol. 56, pp. 188–195, April 2018.

[170] D. Wan, M. Wen, H. Yu, Y. Liu, F. Ji, and F. Chen, "Non-orthogonal multiple access for dual-hop decode-and-forward relaying," in *2016 IEEE Global Communications Conference (GLOBECOM)*, pp. 1–6, December 2016.

[171] M. Nakagami, "The m-distribution–a general formula for intensity distribution of rapid fading," in *Statistical Methods in Radio Wave Propagation*, 1960.

[172] P. Dharmawansa, N. Rajatheva, and K. Ahmed, "On the distribution of the sum of Nakagami-m random variables," *IEEE Transactions on Communications*, vol. 55, no. 7, pp. 1407–1416, 2007.

[173] M. D. Yacoub, C. R. C. M. da Silva, and J. E. V. Bautista, "Second-order statistics for diversity-combining techniques in Nakagami-fading channels," *IEEE Transactions on Vehicular Technology*, vol. 50, pp. 1464–1470, November 2001.

[174] A. U. Sheikh, M. Abdi, and M. Handforth, "Indoor mobile radio channel at 946 MHz: Measurements and modeling," in *IEEE 43rd Vehicular Technology Conference*, pp. 73–76, May 1993.

[175] H. Suzuki, "A statistical model for urban radio propogation," *IEEE Transactions on Communications*, vol. 25, pp. 673–680, July 1977.

[176] S. Arzykulov, T. A. Tsiftsis, G. Nauryzbayev, and M. Abdallah, "Outage performance of cooperative underlay CR-NOMA with imperfect CSI," *IEEE Communications Letters*, vol. 23, pp. 176–179, January 2019.

[177] I. Barany and V. H. Vu, "Central limit theorems for Gaussian polytopes," *arXiv:math/0610192v1 [math.CO]*, November 2006.

[178] A. Kammoun, M. Kharouf, W. Hachem, and J. Najim, "A central limit theorem for the SINR at the LMMSE estimator output for large-dimensional signals," *IEEE Transactions on Information Theory*, vol. 55, pp. 5048–5063, November 2009.

[179] T. Q. S. Quek, G. Roche, I. Guvenc, and M. Kountouris, *Deployment, PHY Techniques, and Resource Management*. Cambridge University Press, UK, 2013.

[180] J. Men, J. Ge, and C. Zhang, "Performance analysis of nonorthogonal multiple access for relaying networks over nakagami-m fading channels," *IEEE Transactions on Vehicular Technology*, vol. 66, pp. 1200–1208, February 2017.

[181] P. D. Diamantoulakis, K. N. Pappi, Z. Ding, and G. K. Karagiannidis, "Wireless-powered communications with non-orthogonal multiple access," *IEEE Transactions on Wireless Communications*, vol. 15, pp. 8422–8436, December 2016.

[182] P. D. Diamantoulakis, K. N. Pappi, Z. Ding, and G. K. Karagiannidis, "Optimal design of non-orthogonal multiple access with wireless power transfer," in *2016 IEEE International Conference on Communications (ICC)*, pp. 1–6, May 2016.

[183] Y. Yuan and Z. Ding, "The application of non-orthogonal multiple access in wireless powered communication networks," in *2016 IEEE 17th International Workshop on Signal Processing Advances in Wireless Communications (SPAWC)*, pp. 1–5, July 2016.

[184] H. Chingoska, Z. Hadzi-Velkov, I. Nikoloska, and N. Zlatanov, "Resource allocation in wireless powered communication networks with non-orthogonal multiple access," *IEEE Wireless Communications Letters*, vol. 5, pp. 684–687, December 2016.

[185] Y. Liu, Z. Ding, M. Elkashlan, and H. V. Poor, "Cooperative non-orthogonal multiple access with simultaneous wireless information and power transfer," *IEEE Journal on Selected Areas in Communications*, vol. 34, pp. 938–953, April 2016.

[186] R. Sun, Y. Wang, X. Wang, and Y. Zhang, "Transceiver design for cooperative non-orthogonal multiple access systems with wireless energy transfer," *IET Communications*, vol. 10, no. 15, pp. 1947–1955, 2016.

[187] J. Gong and X. Chen, "Achievable rate region of non-orthogonal multiple access systems with wireless powered decoder," *IEEE Journal on Selected Areas in Communications*, vol. 35, pp. 2846–2859, December 2017.

[188] N. T. Do, D. B. D. Costa, T. Q. Duong, and B. An, "A BNBF user selection scheme for NOMA-based cooperative relaying systems with SWIPT," *IEEE Communications Letters*, vol. 21, pp. 664–667, March 2017.

[189] W. Han, J. Ge, and J. Men, "Performance analysis for NOMA energy harvesting relaying networks with transmit antenna selection and maximal-ratio combining over Nakagami-m fading," *IET Communications*, vol. 10, no. 18, pp. 2687–2693, 2016.

[190] E. Bjornson, M. Matthaiou, and M. Debbah, "A new look at dual-hop relaying: Performance limits with hardware impairments," *IEEE Transactions on Communications*, vol. 61, pp. 4512–4525, November 2013.

[191] T. C. W. Schenk, E. R. Fledderus, and P. F. M. Smulders, "Performance analysis of zero-IF MIMO OFDM transceivers with IQ imbalance," *Journal of Communications*, vol. 2, pp. 9–19, December 2007.

[192] P. N. Alevizos and A. Bletsas, "Sensitive and nonlinear far-field RF energy harvesting in wireless communications," *IEEE Transactions on Wireless Communications*, vol. 17, pp. 3670–3685, June 2018.

[193] P. Li, R. C. de Lamare, and R. Fa, "Multiple feedback successive interference cancellation detection for multiuser MIMO systems," *IEEE Transactions on Wireless Communications*, vol. 10, pp. 2434–2439, August 2011.

[194] X. Chen, R. Jia, and D. W. K. Ng, "On the design of massive non-orthogonal multiple access with imperfect successive interference cancellation," *IEEE Transactions on Communications*, pp. 1–1, 2018.

[195] V. S. Adamchik and O. I. Marichev, "The algorithm for calculating integrals of hypergeometric type functions and its realization in REDUCE system," in *International Conference on Symbolic and Algebraic Computation*, pp. 212–224, 1990.

[196] A. P. Prudnikov, Y. A. Brychkov, and O. I. Marichev, *Integrals and Series, Vol. 3: More Special Functions*. Gordon and Breach, New York, 1990.

[197] H. A. David and H. N. Nagaraja, *Order Statistics*. 3rd ed., New York, USA: Wiley, 2003.